PASJ: Publ. Astron. Soc. Japan **65**, 23, 2013 February 25

Survey of Period Variations of Superhumps in SU UMa-Type Dwarf Novae. IV. The Fourth Year (2011–2012)

Taichi KATO,[1*] Franz-Josef HAMBSCH,[2,3,4] Hiroyuki MAEHARA,[5] Gianluca MASI,[6] Ian MILLER,[7] Ryo NOGUCHI,[8] Chihiro AKASAKA,[8] Tomoya AOKI,[8] Hiroshi KOBAYASHI,[8] Katsura MATSUMOTO,[8] Shinichi NAKAGAWA,[8] Takuma NAKAZATO,[8] Takashi NOMOTO,[8] Kazuyuki OGURA,[8] Rikako ONO,[8] Keisuke TANIUCHI,[8] William STEIN,[9] Arne HENDEN,[10] Enrique de MIGUEL,[11,12] Seiichiro KIYOTA,[13] Pavol A. DUBOVSKY,[14] Igor KUDZEJ,[14] Kazuyoshi IMAMURA,[15] Hidehiko AKAZAWA,[15] Ryosuke TAKAGI,[15] Yuya WAKABAYASHI,[15] Minako OGI,[15] Kenji TANABE,[15] Joseph ULOWETZ,[16] Etienne MORELLE,[17] Roger D. PICKARD,[18,19] Tomohito OHSHIMA,[1] Kiyoshi KASAI,[20] Elena P. PAVLENKO,[21] Oksana I. ANTONYUK,[21] Aleksei V. BAKLANOV,[21] Kirill ANTONYUK,[21] Denis SAMSONOV,[21] Nikolaj PIT,[21] Aleksei SOSNOVSKIJ,[21] Colin LITTLEFIELD,[22] Richard SABO,[23] Javier RUIZ,[24,25] Thomas KRAJCI,[26] Shawn DVORAK,[27] Arto OKSANEN,[28] Kenji HIROSAWA,[29] William N. GOFF,[30] Berto MONARD,[31] Jeremy SHEARS,[32] David BOYD,[33] Irina B. VOLOSHINA,[34] Sergey Yu. SHUGAROV,[34,35] Drahomir CHOCHOL,[35] Atsushi MIYASHITA,[36] Jochen PIETZ,[37] Natalia KATYSHEVA,[34] Hiroshi ITOH,[38] Greg BOLT,[39] Maksim V. ANDREEV,[40,41] Nikolai PARAKHIN,[40] Viktor MALANUSHENKO,[42] Fabio MARTINELLI,[43] Denis DENISENKO,[44] Chris STOCKDALE,[45] Peter STARR,[46] Mike SIMONSEN,[10] Paul J. TRISTRAM,[47] Akihiko FUKUI,[48] Tamas TORDAI,[49] Robert FIDRICH,[49] Kevin B. PAXSON,[50] Koh-ichi ITAGAKI,[51] Youichirou NAKASHIMA,[52] Seiichi YOSHIDA,[53] Hideo NISHIMURA,[54] Timur V. KRYACHKO,[55] Andrey V. SAMOKHVALOV,[55] Stanislav A. KOROTKIY,[55] Boris L. SATOVSKI,[55] Rod STUBBINGS,[56] Gary POYNER,[57] Eddy MUYLLAERT,[58] Vladimir GERKE,[59] Walter MACDONALD II,[60] Michael LINNOLT,[10] Yutaka MAEDA,[61] and Hubert HAUTECLER[58]

[1] *Department of Astronomy, Kyoto University, Kitashirakawa-Oiwake-cho, Sakyo-ku, Kyoto 606-8502*
[*] *tkato@kusastro.kyoto-u.ac.jp*
[2] *Groupe Européen d'Observations Stellaires (GEOS), 23 Parc de Levesville, 28300 Bailleau l'Evêque, France*
[3] *Bundesdeutsche Arbeitsgemeinschaft für Veränderliche Sterne (BAV), Munsterdamm 90, 12169 Berlin, Germany*
[4] *Vereniging Voor Sterrenkunde (VVS), Oude Bleken 12, 2400 Mol, Belgium*
[5] *Kwasan and Hida Observatories, Kyoto University, Kitakazan-Ohmine-cho, Yamashina-ku, Kyoto 607-8471*
[6] *The Virtual Telescope Project, Via Madonna del Loco 47, 03023 Ceccano (FR), Italy*
[7] *Furzehill House, Ilston, Swansea, SA2 7LE, UK*
[8] *Osaka Kyoiku University, 4-698-1 Asahigaoka, Kashiwara, Osaka 582-8582*
[9] *6025 Calle Paraiso, Las Cruces, NM 88012, USA*
[10] *American Association of Variable Star Observers (AAVSO), 49 Bay State Rd., Cambridge, MA 02138, USA*
[11] *Departamento de Física Aplicada, Facultad de Ciencias Experimentales, Universidad de Huelva, 21071 Huelva, Spain*
[12] *Center for Backyard Astrophysics, Observatorio del CIECEM, Parque Dunar, Matalascañas, 21760 Almonte, Huelva, Spain*
[13] *Variable Star Observers League in Japan (VSOLJ), 405-1003 Matsushiro, Tsukuba, Ibaraki 305-0035*
[14] *Vihorlat Observatory, Mierova 4, Humenne, Slovakia*
[15] *Department of Biosphere-Geosphere System Science, Faculty of Informatics, Okayama University of Science, 1-1 Ridai-cho, Okayama, Okayama 700-0005*
[16] *Center for Backyard Astrophysics Illinois, Northbrook Meadow Observatory, 855 Fair Ln, Northbrook, IL 60062, USA*
[17] *9 rue Vasco de GAMA, 59553 Lauwin Planque, France*
[18] *The British Astronomical Association, Variable Star Section (BAA VSS), Burlington House, Piccadilly, London, W1J 0DU, UK*
[19] *3 The Birches, Shobdon, Leominster, Herefordshire, HR6 9NG, UK*
[20] *Baselstrasse 133D, CH-4132 Muttenz, Switzerland*
[21] *Crimean Astrophysical Observatory, 98409, Nauchny, Crimea, Ukraine*
[22] *Department of Physics, University of Notre Dame, Notre Dame, IN 46556, USA*
[23] *2336 Trailcrest Dr., Bozeman, MT 59718, USA*
[24] *Observatorio de Cántabria, Ctra. de Rocamundo s/n, Valderredible, Cantabria, Spain*
[25] *Agrupación Astronómica Cántabra, Apartado 573, 39080-Santander, Spain*
[26] *Astrokolkhoz Observatory, Center for Backyard Astrophysics New Mexico, PO Box 1351 Cloudcroft, NM 83117, USA*
[27] *Rolling Hills Observatory, 1643 Nightfall Drive, Clermont, FL 34711, USA*
[28] *Nyrola Observatory, Jyvaskylan Sirius ry, Vertaalantie 419, FI-40270 Palokka, Finland*
[29] *216-4 Maeda, Inazawa-cho, Inazawa, Aichi 492-8217*
[30] *13508 Monitor Ln., Sutter Creek, CA 95685, USA*
[31] *Bronberg Observatory, Center for Backyard Astronomy Pretoria, PO Box 11426, Tiegerpoort 0056, South Africa*
[32] *"Pemberton," School Lane, Bunbury, Tarporley, Cheshire, CW6 9NR, UK*
[33] *Silver Lane, West Challow, Wantage, OX12 9TX, UK*

[34] *Sternberg Astronomical Institute, Lomonosov Moscow University, Universitetskiy ave. 13, Moscow 119992, Russia*
[35] *Astronomical Institute of the Slovak Academy of Sciences, 05960, Tatranska Lomnica, The Slovak Republic*
[36] *Seikei Meteorological Observatory, Seikei High School, 3-3-1 Kichijoji-Kita-machi, Musashino, Tokyo 180-8633*
[37] *Nollenweg 6, 65510 Idstein, Germany*
[38] *VSOLJ, 1001-105 Nishiterakata-machi, Hachioji, Tokyo 192-0153*
[39] *Camberwarra Drive, Craigie, Western Australia 6025, Australia*
[40] *Institute of Astronomy, Russian Academy of Sciences, 361605 Peak Terskol, Kabardino-Balkaria, Russia*
[41] *International Center for Astronomical, Medical and Ecological Research of NASU, 27 Akademika Zabolotnoho Str., 03680 Kiev, Ukraine*
[42] *Apache Point Observatory, New Mexico State University, 2001 Apache Point Road, PO Box 59, Sunspot, NM 88349-0059, USA*
[43] *Palareta, 18-56040 Montecatini, Val Di Cecina, Italy*
[44] *Space Research Institute (IKI), Russian Academy of Sciences, Moscow, Russia*
[45] *8 Matta Drive, Churchill, Victoria 3842, Australia*
[46] *Warrumbungle Observatory, Tenby, 841 Timor Rd, Coonabarabran NSW 2357, Australia*
[47] *Mt. John Observatory, PO Box 56, Lake Tekapo 8770, New Zealand*
[48] *Okayama Astrophysical Observatory, National Astronomical Observatory of Japan, Kamogata-cho, Asakuchi, Okayama 719-0232*
[49] *Polaris Observatory, Hungarian Astronomical Association, Laborc utca 2/c, 1037 Budapest, Hungary*
[50] *20219 Eden Pines, Spring, TX 77379, USA*
[51] *Itagaki Astronomical Observatory, Teppo-cho, Yamagata, Yamagata 990-2492*
[52] *968-4 Yamadanoshou, Oku-cho, Setouchi, Okayama 701-4246*
[53] *2-4-10-708 Tsunashima-Nishi, Kohoku-ku, Yokohama 223-0053*
[54] *302-6 Miyawaki, Kakegawa, Shizuoka 436-0086*
[55] *Astrotel-Caucasus Observatory, 41 Lenin Street, village Zelenchukskaya Karachay-Cherkessiya, 369140, Russia*
[56] *Tetoora Observatory, Tetoora Road, Victoria, Australia*
[57] *BAA Variable Star Section, 67 Ellerton Road, Kingstanding, Birmingham, B44 0QE, UK*
[58] *Vereniging Voor Sterrenkunde (VVS), Moffelstraat 13, 3370 Boutersem, Belgium*
[59] *39-28 Razvilka, Moscow region, 142717, Russia*
[60] *Winchester Observatory, PO Box 142, Winchester, ON K0C 2K0, Canada*
[61] *12-14 Kaminishiyama-machi, Nagasaki, Nagasaki 850-0006*

(Received 2012 July 17; accepted 2012 October 1)

Abstract

Continuing the project described by Kato et al. (2009, PASJ, 61, S395), we collected times of superhump maxima for 86 SU UMa-type dwarf novae, mainly observed during the 2011–2012 season. We confirmed general trends recorded in our previous studies, such as the relation between period derivatives and orbital periods. There are some systems showing positive period derivatives despite the long orbital period. We observed the 2011 outburst of the WZ Sge-type dwarf nova BW Scl, and recorded an $O - C$ diagram similar to those of previously known WZ Sge-type dwarf novae. The WZ Sge-type dwarf nova OT J184228.1+483742 showed an unusual pattern of double outbursts composed of an outburst with early superhumps and one with ordinary superhumps. We propose an interpretation that a very small growth rate of the 3:1 resonance due to an extremely low mass-ratio led to quenching the superoutburst before the ordinary superhump appeared. We systematically studied ER UMa-type dwarf novae, and found that V1159 Ori showed positive superhumps similar to ER UMa in the 1990s. The recently recognized ER UMa-type object BK Lyn dominantly showed negative superhumps, and its behavior was very similar to the present-day state of ER UMa. The pattern of period variations in AM CVn-type objects was very similar to that of short-period hydrogen-rich SU UMa-type dwarf novae, making them a helium analogue of hydrogen-rich SU UMa-type dwarf novae. SBS 1108+574, a peculiar hydrogen-rich dwarf nova below the period minimum, showed a very similar pattern of period variations to those of short-period SU UMa-type dwarf novae. The mass-ratio derived from the detected orbital period suggests that this secondary is a somewhat evolved star whose hydrogen envelope was mostly stripped during the mass-exchange. CC Scl, MASTER OT J072948.66+593824.4, and OT J173516.9+154708 showed only low-amplitude superhumps with complex profiles. These superhumps are likely to be a combination of two closely separated periods.

Key words: accretion, accretion disks — stars: dwarf novae — stars: novae, cataclysmic variables

1. Introduction

In Kato et al. (2009, 2010, 2012a), we systematically surveyed period variations of superhumps in SU UMa-type dwarf novae (for general information of SU UMa-type dwarf novae and superhumps, see, e.g., Warner 1995). The period variation of superhumps in many SU UMa-type dwarf novae is generally composed of three distinct stages: an early

Table 1. List of superoutbursts.

Subsection	Object	Year	Observers or references*	ID†
3.1	V725 Aql	2012	AKz	
3.2	EG Aqr	2011	LCO, Kis, KU	
3.3	SV Ari	2011	KU, HaC, OKU, MEV, Mhh, OUS, Mas, DPV, SRI, AAVSO, Kis, PKV	
3.4	TT Boo	2012	IMi, OUS, Mhh, PXR	
3.5	CR Boo	2012	AAVSO, UJH, Nyr, MEV, DPV, GFB, SRI, HMB	
	CR Boo	2012b	UJH, SWI, AAVSO, MEV, Nyr, HMB, DKS	
3.6	NN Cam	2011	OKU, Mhh, SWI, IMi	
3.7	SY Cap	2011	Mhh, OUS	
3.8	GZ Cet	2011	Mhh, IMi, Hsk	
3.9	AK Cnc	2012	OUS	
3.10	CC Cnc	2011	SWI, OKU, KU, Mhh	
3.11	GO Com	2012	DPV, OKU, Mhh, PXR, IMi, Pol	
3.12	TU Crt	2011	Kis	
3.13	V503 Cyg	2011	Ter, LCO, KU, CRI, OKU, DPV, IMi, HMB	
	V503 Cyg	2011b	CRI	
3.14	V1454 Cyg	2012	IMi	
3.15	AQ Eri	2011	HMB, SWI	
3.16	UV Gem	2011	MEV, AAVSO	
3.17	NY Her	2011	AKz	
3.18	PR Her	2011	Kai, OUS, OKU, JSh, DPV, deM, SXN, IMi, Ioh, SAc, PXR	
3.19	V611 Her	2012	Mas	
3.20	V844 Her	2012	OUS, Vol, DPV, PXR, HMB, Hsk	
3.21	MM Hya	2012	HMB, Mhh, IMi, AAVSO	
3.22	VW Hyi	2011	HaC, AAVSO	
3.23	RZ LMi	2012	MEV, HMB	
	RZ LMi	2012b	HMB, DKS, AAVSO	
	RZ LMi	2012c	HMB, AAVSO	
3.24	BK Lyn	2012	HMB, AAVSO, MEV, DKS, Boy, UJH, Mhh, GFB, Kai, SRI	
	BK Lyn	2012b	UJH, Nyr, AAVSO, DKS, Boy, SRI	
3.25	V585 Lyr	2012	Mhh	
3.26	FQ Mon	2011	Kis	
3.27	V1032 Oph	2012	Kai, Mhh	
3.28	V2051 Oph	2012	Mhh	
3.29	V1159 Ori	2012	UJH, SWI	
3.30	AR Pic	2011	HaC	
3.31	GV Psc	2011	SWI, IMi, Mas, OKU	
3.32	BW Scl	2011	HaC, MLF, Mhh, SPE, Kis, Sto, DKS, KU, MOA, Hsk, Nyr, AAVSO	
3.33	CC Scl	2011	HaC	
3.34	V1208 Tau	2011	SWI, IMi, OKU	
3.35	V1212 Tau	2011b	MEV, IMi	
3.36	DI UMa	2007	Rutkowski et al. (2009)	
	DI UMa	2007b	Rutkowski et al. (2009)	
3.37	IY UMa	2011	OUS	
3.38	KS UMa	2012	OUS	
3.39	MR UMa	2012	DPV	

Table 1. (Continued)

Subsection	Object	Year	Observers or references*	ID†
3.40	PU UMa	2012	IMi, Kai, LCO, CRI, Mhh, PXR, OKU, JSh	
3.41	SS UMi	2012	HMB, AKz, AAVSO, Kai, UJH	
3.42	1RXS J231935	2011	MEV, Rui, PIE, OKU, PXR, deM, Mhh, AAVSO, Mtc	
3.43	ASAS J224349	2011	IMi	
3.44	DDE 19	2011	SWI	
3.45	MASTER J072948	2012	deM, SWI, Shu, IMi, Mhh	Balanutsa et al. (2012c)
3.46	MASTER J174305	2012	Kra	Balanutsa et al. (2012a)
3.47	MASTER J182201	2012	Mas	Balanutsa et al. (2012b)
3.48	MisV 1446	2012	GBo, MLF, Kis, Kai, KU, deM, HaC	
3.49	SBS 1108	2012	Kai, deM, Vol, LCO, APO, GFB, Mhh, NKa, CRI, OKU, Kis, Shu	
3.50	SDSS J073208	2012	SRI, PXR	Wils et al. (2010)
3.51	SDSS J080303	2011	deM, OKU, Rui, IMi	
3.52	SDSS J165359	2012	IMi, Mhh, PXR, OKU, deM	
3.53	SDSS J170213	2011	MEV, OKU, IMi, DPV, Mas, LCO, Boy, HMB	
3.54	SDSS J172102	2012	GFB, Mas	Rau et al. (2010)
3.55	SDSS J210449	2011	IMi	
3.56	SDSS J220553	2011	SWI, Mhh, NKa	
3.57	OT J001952	2012	deM	CSS 120131:001952+433901
3.58	OT J011516	2012	Mas	CSS 101008:011517+245530
3.59	OT J050716	2012	Mas	CSS 081221:050716+125314
3.60	OT J055721	2011	HaC, Mhh	SSS 111229:055722−363055
3.61	OT J064608	2011	SWI, Mas, Rui	CSS 080512:064608+403305
3.62	OT J081117	2011	Rui, Mhh	CSS 111030:081117+152003
3.63	OT J084127	2012	Mas, OKU, PXR	CSS 090525:084127+210054
3.64	OT J094854	2012	HMB, SWI, Mas	CSS 120315:094854+014911
3.65	OT J102842	2012	OKU, Kis, UJH, SWI, deM, HMB	CSS 090331:102843−081927
3.66	OT J105122	2012	SWI, CRI	CSS 120101:105123+672528
3.67	OT J125905	2012	Mas	CSS 120424:125906+242634
3.68	OT J131625	2012	Mas	CSS 080427:131626−151313
3.69	OT J142548	2011	Mas	CSS 110628:142548+151502
3.70	OT J144252	2012	MLF, HaC, LCO	CSS 120417:144252−225040
3.71	OT J144453	2012	Mhh, HaC	CSS 120424:144453−131118
3.72	OT J145921	2011	Kra, Mas, PIE	CSS 110613:145922+354806
3.73	OT J155631	2012	GBo, HMB	CSS 090321:155631−080440
3.74	OT J160410	2012	Mas	CSS 120326:160411+145618
3.75	OT J162806	2011	Mas, Mhh	CSS 110611:162806+065316
3.76	OT J163942	2012	IMi	CSS 080131:163943+122414
3.77	OT J170609	2011	Mas	CSS 090205:170610+143452
3.78	OT J173516	2011	OKU, Mas, Mhh, DPV, KU, HMB, Kis	CSS110623:173517+154708
3.79	OT J184228	2011	Mas, Mhh, OKU, DPV, OUS, Ioh, deM, SRI, UJH, KU, AAVSO, HMB, LCO, CRI, Hsk, IMi	Nishimura (Nakano et al. 2011)
3.80	OT J210950	2011	DKS, Rui, DPV, OUS, Kis, SRI, IMi, LCO, Mhh, AAVSO	Itagaki (Yamaoka et al. 2011)
3.81	OT J214738	2011	Mas, SWI, deM, HMB, OKU, Nyr, UJH, CRI	CSS 111004:214738+244554

Table 1. (Continued)

Subsection	Object	Year	Observers or references*	ID†
3.82	OT J215818	2011	SWI, Rui, JSh, deM, OKU, SRI, IMi, UJH, Mas, MEV	PNV J21581852+2419246
3.83	OT J221232	2011	SWI, Kai, Mas, CRI, SAc	CSS 090911:221232+160140
3.84	OT J224736	2012	Mas	CSS 120616:224736+250436
3.85	TCP J084616	2012	deM, Mas	TCP J08461690+3115554
3.86	TCP J231308	2011	Rui, Mas, Mhh, Kra, Kis	TCP J23130812+2337018

* Key to observers: AKz (Astrokolkhoz Obs.), APO (Apache Point Obs.), Boy‡(D. Boyd), CRI (Crimean Astrophys. Obs.), deM (E. de Miguel), DKS‡(S. Dvorak), DPV (P. A. Dubovsky), GBo (G. Bolt), GFB‡(W. N. Goff), HaC (F.-J. Hambsch, remote obs. in Chile), HMB (F.-J. Hambsch), Hsk (K. Hirosawa), IMi‡(I. Miller), Ioh (H. Itoh), JSh‡(J. Shears), Kai (K. Kasai), Kis (S. Kiyota), Kra (T. Krajci), KU (Kyoto Univ., Campus Obs.), LCO‡(C. Littlefield), Mas (G. Masi), MEV‡(E. Morelle), Mhh (H. Maehara), MLF‡(B. Monard), MOA (MOA Team), Mtc (Montecatini Obs.), NKa (N. Katysheva), Nyr (Nyrola and Hankasalmi Obs.), OKU (Osaka Kyoiku Univ.), OUS (Okayama Univ. of Science), PIE (J. Pietz), PKV‡(K. B. Paxson), Pol (Polaris Obs.), PXR‡(R. D. Pickard), Rui (J. Ruiz), SAc (Seikei High School), Shu (S. Yu. Shugarov), SPE‡(P. Starr), SRI‡(R. Sabo), Sto (C. Stockdale), SWI‡(W. Stein), SXN‡(M. Simonsen), Ter (Terskol Obs.), UJH‡(J. Ulowetz), Vol (I. B. Voloshina).

† Original identifications or discoverers.

‡ Inclusive of observations from the AAVSO database.

evolutionary stage with a longer superhump period ($P_{\rm SH}$) (stage A), a middle stage with a systematically varying period (stage B), and a final stage with a shorter, stable superhump period (stage C). These stages of objects with a short orbital period ($P_{\rm orb}$) are most distinct. Objects with a longer orbital period tend to show more gradual changes around the transition from stage B to C. It was also shown that the period derivative ($P_{\rm dot} = \dot{P}/P$) during stage B can be correlated with $P_{\rm SH}$, or binary mass-ratios ($q = M_2/M_1$). In Kato et al. (2012a), we also studied global trends in amplitudes of superhumps, and found that they are strongly correlated with orbital periods, and the dependence on the inclination is weak in non-eclipsing systems.

In the present study, we extended the survey to newly recorded objects and superoutbursts after the publication of Kato et al. (2012a).

2. Observation and Analysis

Data were obtained under campaigns led by the VSNET Collaboration (Kato et al. 2004b). In some objects, we used public data from the American Association of Variable Star Observers (AAVSO) international database.[1] The majority of the data were acquired by time-resolved CCD photometry by using telescopes in the 30 cm class, whose observational details on individual objects will be presented in future papers about their analysis and discussion. A list of outbursts and observers is summarized in table 1. The data analysis was conducted in just the same way as described in Kato et al. (2009, 2012a). We particularly refer to Phase Dispersion Minimization (PDM: Stellingwerf 1978). We also used the Least Absolute Shrinkage and Selection Operator (Lasso) method (Kato & Uemura 2012) for separating closely spaced periods. The time of all observations is expressed in Barycentric Julian Date (BJD). We also use the following abbreviations: $P_{\rm orb}$ for the orbital period and $\epsilon = (P_{\rm SH}/P_{\rm orb}) - 1$ for the fractional superhump excess.

[1] ⟨http://www.aavso.org/data-download⟩.

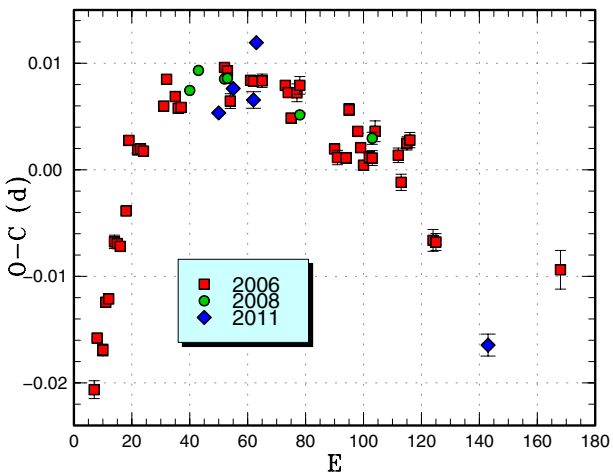

Fig. 1. Comparison of different superoutbursts of EG Aqr in the $O - C$ diagram. A period of 0.07885 d was used to draw this figure. Approximate cycle counts (E) after the start of the superoutburst were used. Since the starts of the 2008 and 2011 superoutbursts were not well constrained, we shifted the $O - C$ diagrams so as to best fit them to the best-recorded 2006 one.

The derived $P_{\rm SH}$, $P_{\rm dot}$, and other parameters are listed in table 2 in the same format as in Kato et al. (2009). The definitions of parameters P_1, P_2, E_1, E_2, and $P_{\rm dot}$ are the same as in Kato et al. (2009); P_1, P_2, E_1, E_2, and $P_{\rm dot}$ mean the superhump periods during stage B and stage C, the ranges of cycle count (E) during stage B and stage C, and the period derivative, respectively. We also present comparisons of different superoutbursts in the $O - C$ diagram because they have been one of the motivations for these surveys (cf. Uemura et al. 2005).

We use the terminology of superhumps summarized in Kato et al. (2012a). We especially call the reader's attention to the term "late superhumps." We only use "traditional" late superhumps when an $\sim$0.5-phase shift has been confirmed. Early superhumps are superhumps seen during the early stages of

Table 2. Superhump periods and period derivatives.

Object	Year	P_1 (d)*	Error*	E_1†	$P_{\rm dot}$‡	Error‡	P_2 (d)*	Error*	E_2†	$P_{\rm orb}$ (d)	Q§
EG Aqr	2011	0.078577	0.000055	0 93	−17.6	7.2	—	—	— —	—	CGM
SV Ari	2011	0.055524	0.000014	19 311	4.0	0.2	0.055350	0.000052	307 366	—	A
TT Boo	2012	0.078083	0.000015	0 113	1.6	0.8	—	—	— —	—	C
CR Boo	2012	0.017265	0.000002	0 247	2.0	0.2	0.017193	0.000006	237 395	0.017029	B
CR Boo	2012b	0.017257	0.000002	0 245	1.9	0.2	—	—	— —	0.017029	B
NN Cam	2011	0.074197	0.000023	0 57	7.1	3.8	0.073843	0.000013	54 109	0.0717	B
SY Cap	2011	0.063750	0.000026	0 31	—	—	—	—	— —	—	CG
AK Cnc	2012	0.067239	0.000123	0 46	—	—	—	—	— —	0.0651	C
CC Cnc	2011	0.075887	0.000001	0 27	—	—	0.075456	0.000028	42 103	0.07352	C
GO Com	2012	0.063016	0.000019	0 128	4.8	1.5	0.062492	0.000150	127 144	—	B
TU Crt	2011	—	—	— —	—	—	0.084962	0.000043	0 82	0.08209	C
V503 Cyg	2011	0.081309	0.000062	0 25	—	—	0.081046	0.000048	35 78	0.07777	B
V503 Cyg	2011b	0.081241	0.000057	0 87	−11.6	3.4	—	—	— —	0.07777	CGM
V1454 Cyg	2012	0.057494	0.000015	0 18	—	—	—	—	— —	—	C
AQ Eri	2011	—	—	— —	—	—	0.061648	0.000247	143 161	0.06094	CG
UV Gem	2011	0.092822	0.000094	0 13	—	—	—	—	— —	—	C
NY Her	2011	0.075802	0.000121	0 37	—	—	—	—	— —	—	CG
PR Her	2011	0.055022	0.000026	0 92	8.8	3.7	—	—	— —	0.05422	CE
V844 Her	2012	0.055901	0.000021	22 124	12.4	1.5	0.055873	0.000031	124 183	0.054643	B
MM Hya	2012	0.058872	0.000026	0 122	—	—	0.058625	0.000049	119 201	0.057590	C
VW Hyi	2011	0.076914	0.000026	25 68	8.2	5.8	0.076540	0.000019	77 146	0.074271	A
RZ LMi	2012	0.059441	0.000021	0 126	2.4	1.5	—	—	— —	—	C
RZ LMi	2012b	0.059472	0.000026	0 84	4.5	3.6	—	—	— —	—	C
RZ LMi	2012c	0.059408	0.000011	0 133	2.9	0.4	—	—	— —	—	B
BK Lyn	2012b	0.078510	0.000028	25 127	3.2	2.7	—	—	— —	0.07498	B
V585 Lyr	2012	0.060350	0.000038	0 19	—	—	—	—	— —	—	C
FQ Mon	2011	—	—	— —	—	—	0.072718	0.000180	0 14	—	C
V1032 Oph	2012	0.085965	0.000288	0 47	—	—	—	—	— —	0.081055	C
AR Pic	2011	—	—	— —	—	—	0.083154	0.000149	0 50	0.0801	CP
GV Psc	2011	0.094313	0.000018	0 62	−3.1	2.3	—	—	— —	—	C2
BW Scl	2011	0.055000	0.000008	25 210	4.4	0.3	—	—	— —	0.054323	A
CC Scl	2011	—	—	— —	—	—	0.060012	0.000028	0 152	0.05858	C
V1208 Tau	2011	—	—	— —	—	—	0.070481	0.000066	0 49	—	B
V1212 Tau	2011b	0.069692	0.000055	0 18	—	—	—	—	— —	—	C2
DI UMa	2007	0.055306	0.000015	18 182	4.1	0.8	—	—	— —	0.054566	B
DI UMa	2007b	0.055340	0.000040	0 126	9.3	4.3	—	—	— —	0.054566	B
MR UMa	2012	—	—	— —	—	—	0.064746	0.000021	0 48	—	C
PU UMa	2012	0.081090	0.000048	11 84	−14.3	2.6	0.080724	0.000100	84 121	0.077881	B
SS UMi	2012	0.070358	0.000128	0 33	—	—	—	—	— —	0.06778	C
1RXS J231935	2011	0.065989	0.000019	0 79	11.6	1.7	0.065528	0.000014	75 159	—	B
DDE 19	2011	—	—	— —	—	—	0.091210	0.000043	0 35	—	C
MisV 1446	2012	0.078072	0.000088	0 35	—	—	0.077304	0.000098	35 69	—	C
SBS 1108	2012	0.039118	0.000003	0 403	1.2	0.1	0.038869	0.000004	399 876	0.038449	CP
SDSS J073208	2012	0.079571	0.000021	0 72	—	—	—	—	— —	—	CG
SDSS J080303	2011	0.091949	0.000119	17 31	—	—	0.090393	0.000022	27 88	—	C
SDSS J165359	2012	—	—	— —	—	—	0.065105	0.000150	91 121	—	C
SDSS J170213	2011	0.105005	0.000056	32 117	17.0	2.8	—	—	— —	0.100082	B
SDSS J172102	2012	—	—	— —	—	—	0.026673	0.000008	0 463	—	C
SDSS J210449	2011	0.075315	0.000045	0 27	—	—	—	—	— —	—	C
SDSS J220553	2011	0.058151	0.000021	0 99	7.7	0.9	—	—	— —	0.05752	B
OT J001952	2012	0.056770	0.000039	0 18	—	—	—	—	— —	—	C
OT J050716	2012	0.065916	0.000080	0 15	—	—	—	—	— —	—	C
OT J055721	2011	0.059756	0.000017	0 153	4.6	0.9	—	—	— —	—	B
OT J064608	2011	0.061105	0.000023	0 82	11.1	2.6	—	—	— —	—	B
OT J081117	2011	0.058035	0.000027	0 63	—	—	—	—	— —	—	C
OT J084127	2012	0.087686	0.000252	0 4	—	—	—	—	— —	—	C

Table 2. (Continued)

Object	Year	P_1 (d)*	Error*	E_1†	$P_{\rm dot}$‡	Error‡	P_2 (d)*	Error*	E_2†	$P_{\rm orb}$ (d)	Q§
OT J094854	2012	0.057499	0.000021	0 77	8.3	2.8	—	—	— —	—	C
OT J102842	2012	0.038168	0.000008	70 151	—	—	—	—	— —	—	C
OT J105122	2012	0.061054	0.000109	0 30	—	—	—	—	— —	0.0596	C2
OT J144252	2012	0.065126	0.000028	0 59	13.6	4.3	0.064639	0.000054	59 107	—	B
OT J144453	2012	—	—	— —	—	—	0.082289	0.000060	0 58	—	C
OT J145921	2011	0.085114	0.000059	0 74	10.9	7.2	—	—	— —	—	C
OT J155631	2012	0.089309	0.000053	0 41	−21.3	5.8	—	—	— —	—	CG
OT J162806	2011	0.068847	0.000008	0 140	—	—	—	—	— —	—	CGM
OT J163942	2012	0.088585	0.000052	0 23	—	—	—	—	— —	—	C
OT J170609	2011	0.059460	0.000076	0 16	—	—	—	—	— —	—	C
OT J184228	2011	0.072342	0.000018	64 206	−0.9	1.5	—	—	— —	0.07168	BE
OT J210950	2011	0.060045	0.000026	34 188	8.5	0.6	0.059742	0.000022	187 289	0.05865	BP
OT J214738	2011	0.097147	0.000021	21 107	8.8	1.0	—	—	— —	0.09273	BP
OT J215818	2011	0.067397	0.000027	0 56	6.9	4.5	0.066852	0.000020	50 127	—	B
OT J221232	2011	0.090322	0.000097	0 29	—	—	0.090051	0.000028	29 106	—	B
OT J224736	2012	0.056673	0.000020	0 37	—	—	—	—	— —	—	C
TCP J084616	2012	0.096333	0.000106	0 12	—	—	—	—	— —	0.09139	C
TCP J231308	2011	0.071364	0.000044	0 24	—	—	0.071016	0.000033	28 85	—	C

* P_1, superhump period during stage B; Error, 1σ error; P_2, superhump period during stage C.
† Interval used for calculating the period (corresponding to E in section 3).
‡ In units of 10^{-5}.
§ Data quality and comments. A, excellent; B, partial coverage or slightly low quality; C, insufficient coverage or observations with large scatter; G, $P_{\rm dot}$ denotes global $P_{\rm dot}$; M, observational gap in middle stage; 2, late-stage coverage (the listed period may refer to P_2); E, $P_{\rm orb}$ refers to the period of early superhumps; P, $P_{\rm orb}$ refers to a shorter stable periodicity recorded in outburst.

Table 3. Superhump maxima of EG Aqr (2011).

E	Max*	Error	$O-C$†	N‡
0	55740.8707	0.0002	−0.0044	221
5	55741.2672	0.0004	−0.0007	119
12	55741.8181	0.0008	0.0001	88
13	55741.9023	0.0007	0.0058	78
93	55748.1819	0.0010	−0.0008	146

* BJD − 2400000.
† Against max = 2455740.8750 + 0.078577E.
‡ Number of points used to determine the maximum.

WZ Sge-type dwarf novae, and have periods close to the orbital periods (Kato et al. 1996a; Kato 2002a).

3. Individual Objects

3.1. V725 Aquilae

Y. Nakashima detected an outburst of this object on 2012 April 16 (vsnet-alert 14450). Subsequent observations confirmed that the outburst is indeed a superoutburst (vsnet-alert 14460). Due to short visibility in the morning, only observations on two nights were obtained. The PDM analysis yielded a period of 0.09047(5) d. We obtained a single superhump maximum of BJD 2456036.9734(8) ($N = 137$). It is noticeable that a likely superoutburst occurred in 2011 May (vsnet-alert 14460), and the interval between the two superoutbursts was only ~ 340 d, which is much shorter than the previously considered intervals (Uemura et al. 2001). The object faded quickly (unfiltered CCD magnitude of 17.6 on April 24),

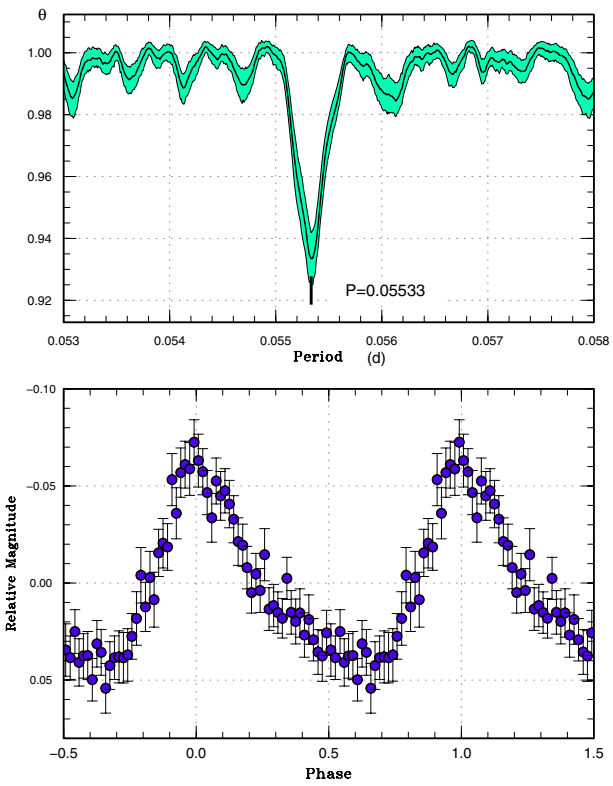

Fig. 2. Superhumps in SV Ari (2011). Upper: PDM analysis. Lower: Phase-averaged profile.

Table 4. Superhump maxima of SV Ari (2011).

E	Max*	Error	$O-C^{\dagger}$	$N^{\ddagger}$	E	Max*	Error	$O-C^{\dagger}$	$N^{\ddagger}$
0	55776.5824	0.0026	0.0059	66	103	55782.2838	0.0006	−0.0092	288
5	55776.8591	0.0010	0.0052	47	109	55782.6183	0.0006	−0.0077	44
7	55776.9722	0.0011	0.0072	99	113	55782.8402	0.0005	−0.0078	35
11	55777.1956	0.0009	0.0086	250	114	55782.8950	0.0006	−0.0085	35
12	55777.2464	0.0007	0.0039	358	127	55783.6165	0.0005	−0.0085	51
13	55777.3083	0.0014	0.0103	154	131	55783.8384	0.0008	−0.0086	35
16	55777.4748	0.0013	0.0104	41	132	55783.8941	0.0007	−0.0083	35
17	55777.5259	0.0015	0.0059	30	145	55784.6161	0.0007	−0.0079	51
18	55777.5860	0.0006	0.0106	49	150	55784.8916	0.0013	−0.0099	65
19	55777.6419	0.0003	0.0109	37	162	55785.5544	0.0037	−0.0131	26
23	55777.8629	0.0003	0.0099	53	163	55785.6194	0.0010	−0.0036	49
24	55777.9167	0.0004	0.0082	38	167	55785.8358	0.0019	−0.0092	30
30	55778.2477	0.0010	0.0062	84	168	55785.8944	0.0010	−0.0061	30
34	55778.4729	0.0014	0.0095	32	185	55786.8424	0.0035	−0.0016	28
35	55778.5252	0.0009	0.0063	31	186	55786.8891	0.0035	−0.0104	19
36	55778.5792	0.0003	0.0048	91	192	55787.2249	0.0039	−0.0076	105
37	55778.6356	0.0004	0.0056	50	203	55787.8394	0.0019	−0.0036	28
41	55778.8563	0.0006	0.0043	34	204	55787.8962	0.0024	−0.0023	28
43	55778.9637	0.0010	0.0008	28	222	55788.8967	0.0043	−0.0008	29
54	55779.5730	0.0003	−0.0004	38	240	55789.8813	0.0061	−0.0152	20
59	55779.8498	0.0005	−0.0012	36	252	55790.5667	0.0027	0.0042	51
60	55779.9032	0.0005	−0.0033	28	253	55790.5904	0.0023	−0.0276	51
66	55780.2370	0.0028	−0.0024	186	253	55790.6199	0.0007	0.0020	37
67	55780.2891	0.0016	−0.0059	167	257	55790.8503	0.0093	0.0103	19
77	55780.8425	0.0010	−0.0074	29	270	55791.5773	0.0049	0.0158	51
78	55780.9012	0.0010	−0.0043	75	272	55791.6554	0.0045	−0.0171	29
79	55780.9551	0.0008	−0.0059	70	307	55793.6346	0.0020	0.0196	22
83	55781.1839	0.0031	0.0009	100	310	55793.7952	0.0024	0.0137	30
84	55781.2324	0.0012	−0.0060	224	311	55793.8603	0.0009	0.0233	40
85	55781.2897	0.0008	−0.0043	252	364	55796.7895	0.0039	0.0110	20
95	55781.8415	0.0005	−0.0074	36	365	55796.8452	0.0034	0.0112	20
96	55781.8981	0.0005	−0.0064	32	366	55796.8987	0.0016	0.0092	16
102	55782.2312	0.0010	−0.0063	238					

* BJD − 2400000.
† Against max = 2455776.5764 + 0.055500E.
‡ Number of points used to determine the maximum.

and we probably observed the final stage of the superoutburst. There was a visual detection at a magnitude of 14.6 on April 27. The object may have shown a rebrightening, as observed in the 1999 one (Uemura et al. 2001).

3.2. *EG Aquarii*

The 2011 June superoutburst of this object was detected by R. Stubbings at a visual magnitude of 12.5 (vsnet-alert 13460). The object was under rather unfavorable conditions, and the observation was more limited than in the past studies (Imada et al. 2008b; Kato et al. 2009). The times of superhump maxima are listed in table 3. Although there was a likely stage B–C transition between $E = 13$ and $E = 93$, observations were not carried out over the epoch of this transition. We refer to the global $P_{\rm dot}$ as $P_{\rm dot}$ in table 2. A comparison of different superoutbursts of EG Aqr in the $O - C$ diagram is shown in figure 1.

3.3. *SV Arietis*

SV Ari was discovered by Wolf and Wolf (1905), who recorded the object at a magnitude of 12 on three Heidelberg plates taken on 1905 November 6. The object was not detected on November 1, and it quickly faded to 13.5 mag on November 21. According to Duerbeck (1987), there was a possible detection of its brightening with a magnitude of 15.7 on 1943 September 2 by K. Himpel and E. Jansch. Although Duerbeck (1987) even suggested an intergalactic nova, many observers, mostly amateur observers, intensively monitored the object while suspecting that it was a dwarf nova. Robertson et al. (1998) identified a $B = 22.1$ mag quiescent counterpart [see also Robertson et al. (2000); Duerbeck (1987) also proposed the same 22nd mag counterpart]. After a long period

Table 5. Superhump maxima of TT Boo (2012).

E	Max*	Error	$O-C^{\dagger}$	$N^{\ddagger}$
0	56016.4443	0.0002	−0.0010	81
1	56016.5239	0.0002	0.0005	83
2	56016.6011	0.0002	−0.0003	83
35	56019.1732	0.0039	−0.0034	30
36	56019.2549	0.0011	0.0002	56
37	56019.3315	0.0014	−0.0012	42
38	56019.4122	0.0005	0.0015	73
39	56019.4881	0.0005	−0.0007	78
40	56019.5673	0.0005	0.0005	82
60	56021.1277	0.0032	0.0001	44
61	56021.2069	0.0023	0.0013	58
62	56021.2861	0.0013	0.0024	54
113	56025.2689	0.0007	0.0054	56
139	56027.2870	0.0016	−0.0054	55

* BJD − 2400000.
† Against max = 2456016.4454 + 0.078036E.
‡ Number of points used to determine the maximum.

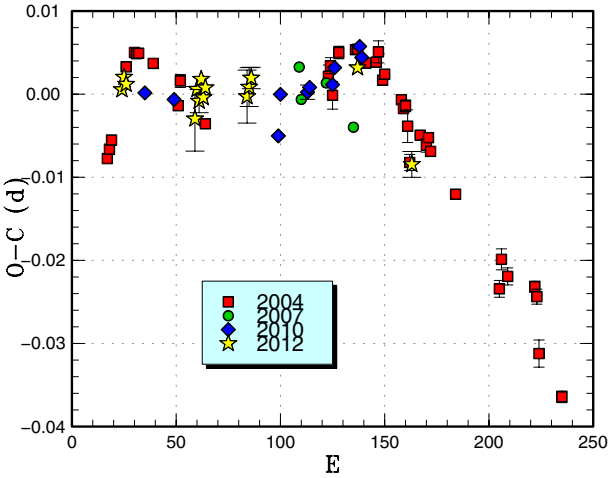

Fig. 3. Comparison of different superoutbursts of TT Boo in the $O-C$ diagram. A period of 0.07807 d was used to draw this figure. Approximate cycle counts (E) after the start of the superoutburst were used.

of unsuccessful detection of an outburst, R. Stubbings finally detected an outburst at a visual magnitude of 15.0 on 2011 August 2 (vsnet-outburst 13091). The outburst was immediately confirmed by T. Tordai and G. Masi, who detected superhumps (vsnet-alert 13541, 13552; figure 2).

The times of superhump maxima are listed in table 4. The early–middle portion of the $O-C$ diagram shows clear stages of A and B. During the period of BJD 2455789–2477912, there were sometimes two hump maxima, and humps with phases different from the main humps (E = 240, 253, 272) were also included in the table. There was some indication of stage C around the terminal stage ($E \geq 364$). The values given in table 2 were determined after rejecting humps at E = 240, 253, 272. The resultant $P_{\rm dot}$ for stage-B superhumps was $+4.0(0.2) \times 10^{-5}$, comparable to those of extreme WZ Sge-type dwarf novae.

The 2011 outburst was much fainter than that of 1905. This difference can be understood as a combination of two effects: (1) the magnitude scale in Wolf and Wolf (1905) was $\sim$2 mag brighter than the present scale, which is confirmed from a comparison of magnitudes of the comparison stars, and (2) the brightness maximum of the 2011 outburst was missed because there were no observations before Stubbings' detection. The lack of a stage of early superhumps, which is expected for such a WZ Sge-type dwarf nova, can also be understood for the same reason. No post-superoutburst rebrightening was recorded.

3.4. TT Bootis

We observed the early part of the 2012 superoutburst. The times of superhump maxima are listed in table 5. There were no detectable superhumps 0.8 d prior to the initial epoch of the superhump maximum. The resultant $P_{\rm dot}$ for stage B was smaller than those in 2004 and 2010, which is probably a result of the limited observation of stage B, and possibly due to contamination of stage A or C superhumps (figure 3).

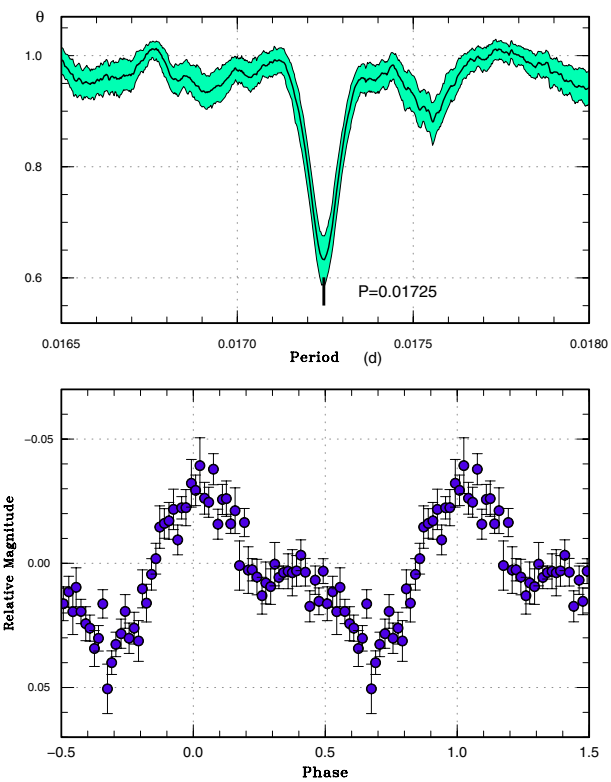

Fig. 4. Superhumps in CR Boo (2012 March) before the oscillatory phase. Upper: PDM analysis. Lower: Phase-averaged profile.

Table 6. Superhump maxima of CR Boo (2012 March).

E	Max*	Error	$O-C^{\dagger}$	$N^{\ddagger}$	E	Max*	Error	$O-C^{\dagger}$	$N^{\ddagger}$
0	55990.7536	0.0001	−0.0006	5	119	55992.8061	0.0004	−0.0007	13
1	55990.7724	0.0004	0.0010	6	120	55992.8238	0.0008	−0.0002	15
2	55990.7893	0.0005	0.0006	6	121	55992.8413	0.0004	0.0000	16
3	55990.8066	0.0009	0.0006	5	122	55992.8585	0.0012	−0.0001	15
4	55990.8237	0.0007	0.0006	6	124	55992.8925	0.0005	−0.0005	15
5	55990.8416	0.0009	0.0011	6	125	55992.9103	0.0009	0.0000	15
6	55990.8583	0.0005	0.0006	8	126	55992.9277	0.0006	0.0002	12
39	55991.4270	0.0005	0.0001	14	237	55994.8466	0.0010	0.0045	16
40	55991.4433	0.0003	−0.0008	17	239	55994.8783	0.0011	0.0017	15
41	55991.4613	0.0006	−0.0001	16	240	55994.8970	0.0006	0.0031	16
42	55991.4779	0.0005	−0.0008	16	241	55994.9154	0.0005	0.0043	16
43	55991.4946	0.0003	−0.0013	16	242	55994.9310	0.0011	0.0026	14
44	55991.5125	0.0006	−0.0006	12	243	55994.9502	0.0011	0.0046	25
45	55991.5295	0.0003	−0.0009	14	244	55994.9671	0.0013	0.0042	24
46	55991.5479	0.0006	0.0003	13	245	55994.9834	0.0007	0.0032	25
47	55991.5641	0.0004	−0.0007	8	246	55995.0009	0.0011	0.0035	25
48	55991.5819	0.0005	−0.0003	12	247	55995.0181	0.0011	0.0034	13
49	55991.5985	0.0003	−0.0009	15	284	55995.6566	0.0024	0.0037	21
50	55991.6161	0.0004	−0.0006	16	285	55995.6713	0.0016	0.0012	21
51	55991.6341	0.0005	0.0002	15	286	55995.6920	0.0013	0.0046	21
52	55991.6503	0.0007	−0.0008	17	287	55995.7075	0.0014	0.0029	22
53	55991.6677	0.0009	−0.0007	14	293	55995.8095	0.0012	0.0015	6
59	55991.7716	0.0006	−0.0003	7	295	55995.8402	0.0009	−0.0024	11
60	55991.7888	0.0003	−0.0003	6	297	55995.8804	0.0010	0.0033	14
61	55991.8053	0.0005	−0.0011	6	298	55995.8967	0.0014	0.0024	15
62	55991.8235	0.0002	−0.0002	5	299	55995.9126	0.0017	0.0011	14
63	55991.8403	0.0002	−0.0006	6	301	55995.9454	0.0016	−0.0007	24
64	55991.8569	0.0004	−0.0012	7	305	55996.0184	0.0019	0.0034	9
65	55991.8746	0.0002	−0.0007	7	306	55996.0329	0.0011	0.0005	9
66	55991.8921	0.0003	−0.0005	6	336	55996.5481	0.0017	−0.0017	22
96	55992.4093	0.0008	−0.0007	28	341	55996.6316	0.0008	−0.0044	17
97	55992.4267	0.0006	−0.0006	33	344	55996.6866	0.0010	−0.0011	37
98	55992.4445	0.0004	−0.0001	30	345	55996.7029	0.0017	−0.0022	36
99	55992.4615	0.0004	−0.0004	30	353	55996.8396	0.0008	−0.0034	10
100	55992.4778	0.0004	−0.0013	22	359	55996.9414	0.0007	−0.0051	12
101	55992.4952	0.0011	−0.0012	21	360	55996.9606	0.0010	−0.0032	7
102	55992.5129	0.0008	−0.0007	20	361	55996.9767	0.0028	−0.0043	15
103	55992.5302	0.0006	−0.0006	24	363	55997.0128	0.0014	−0.0026	9
104	55992.5472	0.0011	−0.0009	19	364	55997.0306	0.0021	−0.0021	8
105	55992.5626	0.0007	−0.0027	17	394	55997.5462	0.0020	−0.0039	16
106	55992.5814	0.0006	−0.0012	18	395	55997.5658	0.0032	−0.0016	18
118	55992.7889	0.0012	−0.0006	15					

* BJD − 2400000.
† Against max = 2455990.7542 + 0.017249E.
‡ Number of points used to determine the maximum.

3.5. *CR Bootis*

CR Boo is one of the prototypical "helium dwarf novae" (Patterson et al. 1997; Provencal et al. 1997; Kato et al. 2000b; for representative theoretical analyses, see Tsugawa & Osaki 1997 and Kotko et al. 2012; for recent observational reviews of AM CVn stars, see Solheim 2010 and Ramsay et al. 2011, 2012). Although superhumps of this object were well established in the past, published observations were either obtained in an anomalous state (Patterson et al. 1997) or not very ideally sampled (Kato et al. 2000b). The object was in a state of regular pattern of outbursts (cf. Kato et al. 2000b) with a supercycle of $\sim$50 d in 2011–2012. It is ideal for studying the behavior of superhumps in helium dwarf novae.

We present here an analysis of a superoutburst in 2012 March, mainly using the AAVSO observations. The

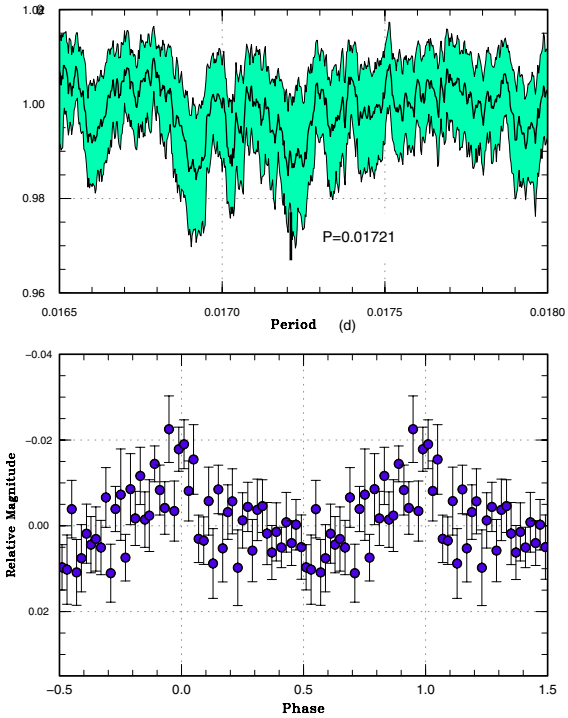

Fig. 5. Superhumps in CR Boo (2012 March) during the oscillatory phase. Upper: PDM analysis. Lower: Phase-averaged profile.

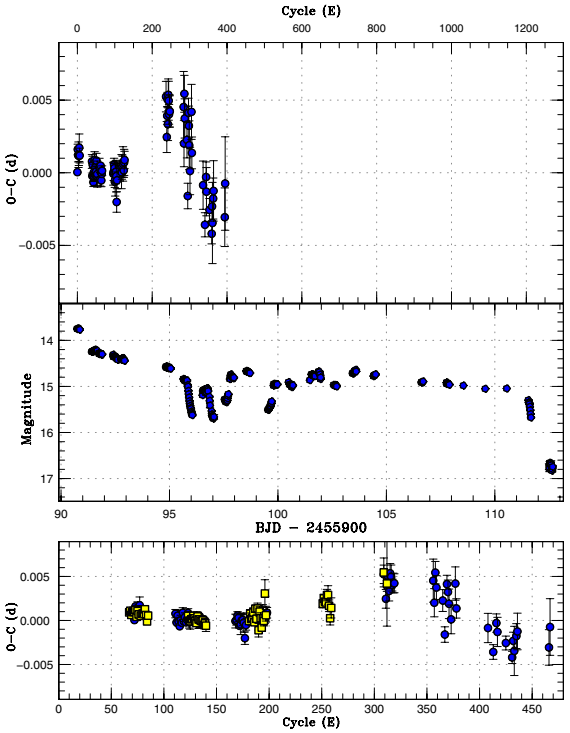

Fig. 6. $O-C$ diagram of superhumps in CR Boo. Upper: $O-C$ during the 2012 March superoutburst. We used a period of 0.017249 d for calculating the $O-C$ residuals. Middle: Light curve during the 2012 March superoutburst. Lower: Comparison of two superoutbursts in 2012 March (filled circles) and April (filled squares) in the $O-C$ diagram. Approximate cycle counts (E) after the start of the superoutburst were used.

superoutburst was first detected by G. Gualdoni on March 3 at $V = 13.61$ (AAVSO data). The existence of superhumps was soon recognized (vsnet-alert 14305). Although the object stayed in its plateau phase for six days, it started oscillations with a quasi-period of 1.0 d similar to that of Patterson et al. (1997); this state lasted for six days. The object apparently reached a more stable state, and finally started to fade rapidly on March 25. Although the overall behavior of the superoutburst was similar to those of hydrogen-rich SU UMa-type dwarf novae, the presence of an oscillatory state is different. The relatively large scatter in the supercycle-phase-folded light curve (figure 4 of Kato et al. 2000b) may have been a result of these oscillations.

The times of superhump maxima until the early stage of the oscillatory state are given in table 6. The $O-C$ diagram shows a pattern very similar to stages B and C in hydrogen-rich SU UMa-type dwarf novae. The $P_{\rm dot}$ for stage B was $+2.0(0.2) \times 10^{-5}$; ϵ values for stage-B and stage-C superhumps (figures 4 and 5) were 1.39(1)% and 0.97(4)%, respectively, similar to those of WZ Sge-type dwarf novae, but are larger than what is expected only from the mass-ratio. The stage B–C transition occurred when the oscillation started (figure 6). This may be analogous to WZ Sge-type dwarf novae, which usually do not show stage-C superhumps by the end of the plateau phase (Kato et al. 2009, 2010, 2012a). The oscillatory phase in CR Boo may correspond to a post-superoutburst stage in WZ Sge-type dwarf novae, when these objects tend to show various kinds of rebrightenings (cf. Kato et al. 2009). We might recall past examples of V803 Cen (Kato et al. 2004a) and V406 Hya (Nogami et al. 2004), both of which showed rebrightenings similar to WZ Sge-type dwarf novae. Ramsay et al. (2011) also noted the presence of a "dip" during the period of superoutbursts in short-$P_{\rm orb}$ AM CVn-type objects (see also Levitan et al. 2011; Kotko et al. 2012). Such phenomena may be more prevalent than what has been thought.

Although the superhumps in the later stage were not readily recognizable, we were able to detect the period by the PDM method: 0.017183(5) d during BJD 2455997.8–2456002.0 (oscillatory phase) and 0.017265(3) d during BJD 2456002.0–2456009.0 (second stable plateau). These periods indicate the persistence of superhumps until the end of the superoutburst.

One supercycle after, CR Boo underwent another superoutburst in 2012 April. The times of superhump maxima are listed in table 7. Although the object started oscillatory behavior as observed in the 2012 March superoutburst, the later part of the superoutburst was not so much observed as that in the March one. The resultant period and period derivative were quite similar to those of the March superoutburst. The $O-C$ diagram of stage B in April very well reproduced that of the March superoutburst (figure 6, lower panel).

3.6. NN Camelopardalis

We observed a superoutburst in 2011 December. The times of superhump maxima are listed in table 8. Although stage A

Table 7. Superhump maxima of CR Boo (2012 April).

E	Max*	Error	$O-C^{\dagger}$	$N^{\ddagger}$	E	Max*	Error	$O-C^{\dagger}$	$N^{\ddagger}$
0	56039.6483	0.0002	0.0009	21	70	56040.8548	0.0005	−0.0006	15
1	56039.6657	0.0002	0.0011	33	71	56040.8715	0.0003	−0.0011	13
2	56039.6825	0.0001	0.0006	33	72	56040.8890	0.0006	−0.0009	13
3	56039.7001	0.0003	0.0009	33	73	56040.9059	0.0007	−0.0012	15
4	56039.7175	0.0001	0.0010	34	114	56041.6136	0.0004	−0.0011	16
5	56039.7346	0.0002	0.0009	34	115	56041.6317	0.0005	−0.0003	16
6	56039.7521	0.0002	0.0011	34	116	56041.6483	0.0007	−0.0009	16
7	56039.7685	0.0002	0.0003	34	117	56041.6657	0.0009	−0.0007	13
8	56039.7865	0.0001	0.0010	33	118	56041.6836	0.0005	−0.0001	15
9	56039.8033	0.0002	0.0006	34	119	56041.6997	0.0004	−0.0013	15
11	56039.8376	0.0002	0.0004	24	120	56041.7185	0.0004	0.0003	15
12	56039.8551	0.0002	0.0006	32	121	56041.7346	0.0003	−0.0009	11
13	56039.8724	0.0002	0.0006	33	122	56041.7530	0.0006	0.0003	15
14	56039.8896	0.0003	0.0006	33	123	56041.7678	0.0008	−0.0022	14
15	56039.9074	0.0002	0.0011	33	124	56041.7872	0.0006	−0.0001	16
16	56039.9240	0.0002	0.0005	33	125	56041.8037	0.0006	−0.0008	15
17	56039.9405	0.0003	−0.0003	33	126	56041.8198	0.0004	−0.0019	12
18	56039.9584	0.0002	0.0004	33	127	56041.8381	0.0005	−0.0009	16
56	56040.6138	0.0005	0.0000	15	128	56041.8551	0.0006	−0.0012	15
57	56040.6305	0.0004	−0.0005	16	129	56041.8754	0.0016	0.0019	14
58	56040.6477	0.0003	−0.0006	16	130	56041.8902	0.0007	−0.0006	15
59	56040.6652	0.0004	−0.0004	15	184	56042.8229	0.0005	0.0003	15
60	56040.6825	0.0003	−0.0004	14	185	56042.8408	0.0005	0.0009	17
61	56040.7001	0.0004	−0.0000	16	186	56042.8577	0.0004	0.0005	18
62	56040.7170	0.0003	−0.0003	16	187	56042.8748	0.0003	0.0004	17
63	56040.7340	0.0005	−0.0006	14	188	56042.8929	0.0006	0.0012	18
64	56040.7510	0.0003	−0.0009	16	189	56042.9102	0.0010	0.0012	17
65	56040.7690	0.0005	−0.0001	13	190	56042.9262	0.0007	0.0000	18
66	56040.7859	0.0004	−0.0005	14	191	56042.9420	0.0008	−0.0014	18
67	56040.8031	0.0003	−0.0005	15	192	56042.9604	0.0011	−0.0003	18
68	56040.8202	0.0003	−0.0006	15	242	56043.8269	0.0016	0.0033	16
69	56040.8374	0.0003	−0.0007	14	245	56043.8774	0.0048	0.0021	15

* BJD − 2400000.
† Against max = 2456039.6474 + 0.017257E.
‡ Number of points used to determine the maximum.

and the early part of stage B were not observed, a clear pattern of stage B–C superhumps was detected.

A comparison of different superoutbursts in the $O-C$ diagram is shown in figure 7. The 2007 superoutburst, whose start of the main superoutburst was not observed, was shifted by 63 cycles so as to best match the others. This cycle count placed the initial epoch of superhump evolution around BJD 2454358.9, shortly after the precursor outburst. It was likely that superhumps started to grow just after the precursor outburst, and that the true start of the main superoutburst was not observed.

3.7. SY Capricorni

We observed a superoutburst in 2011 August–September. The times of superhump maxima are listed in table 9. Since only a limited fraction of the observation was obtained, we put the period analyzed by the PDM method into table 2.

3.8. GZ Ceti

This object (= SDSS J013701.06−091234.9) is an unusual short-$P_{\rm orb}$ dwarf nova with a massive secondary (Imada et al. 2006; Ishioka et al. 2007). We observed the 2011 superoutburst. We observed only the initial and final parts of the outburst. The times of superhump maxima are listed in table 10. Since amplitudes of superhumps on BJD 2455923 were still less than 0.1 mag, we must have caught the initial stage of the outburst. A comparison of different outbursts in the $O-C$ diagram is shown in figure 8. Despite its unusual properties, the $O-C$ curve is composed of stages B and C similar to those of ordinary SU UMa-type dwarf novae. The $P_{\rm dot}$ during stage B appears to be smaller than those of ordinary SU UMa-type dwarf novae with similar $P_{\rm SH}$, which is consistent with the result in Kato et al. (2009).

Table 8. Superhump maxima of NN Cam (2011).

E	Max*	Error	$O-C^{\dagger}$	$N^{\ddagger}$
0	55904.9897	0.0002	0.0015	254
1	55905.0612	0.0001	−0.0010	241
6	55905.4308	0.0005	−0.0017	75
7	55905.5044	0.0005	−0.0021	63
8	55905.5788	0.0004	−0.0017	68
9	55905.6526	0.0005	−0.0020	56
10	55905.7226	0.0010	−0.0060	42
11	55905.8007	0.0004	−0.0020	78
12	55905.8752	0.0004	−0.0016	78
13	55905.9501	0.0004	−0.0007	76
24	55906.7647	0.0005	−0.0007	77
25	55906.8392	0.0004	−0.0003	77
26	55906.9129	0.0005	−0.0006	78
29	55907.1393	0.0002	0.0037	294
30	55907.2091	0.0003	−0.0006	294
40	55907.9548	0.0003	0.0046	261
54	55908.9915	0.0002	0.0045	279
55	55909.0664	0.0003	0.0053	433
56	55909.1419	0.0005	0.0068	216
57	55909.2145	0.0004	0.0053	156
68	55910.0273	0.0004	0.0036	156
69	55910.1016	0.0005	0.0038	101
92	55911.7991	0.0005	−0.0019	79
93	55911.8731	0.0007	−0.0020	78
94	55911.9460	0.0003	−0.0031	307
95	55912.0212	0.0004	−0.0020	236
96	55912.0932	0.0006	−0.0040	159
109	55913.0546	0.0007	−0.0053	135

* BJD − 2400000.
† Against max = 2455904.9881 + 0.074053E.
‡ Number of points used to determine the maximum.

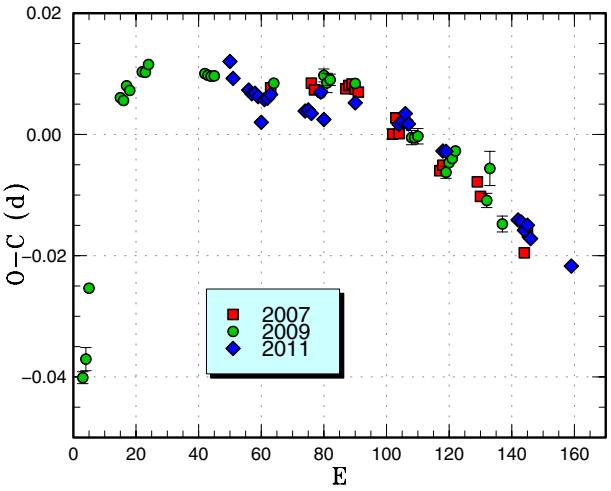

Fig. 7. Comparison of different superoutbursts of NN Cam in the $O-C$ diagram. A period of 0.0743 d was used to draw this figure. Approximate cycle counts (E) after the start of the superoutburst were used. The 2007 superoutburst was shifted by 63 cycles so as to best match the others.

Table 9. Superhump maxima of SY Cap (2011).

E	Max*	Error	$O-C^{\dagger}$	$N^{\ddagger}$
0	55803.0789	0.0005	0.0012	172
1	55803.1409	0.0006	−0.0005	154
16	55804.0964	0.0017	−0.0014	43
31	55805.0550	0.0007	0.0007	50

* BJD − 2400000.
† Against max = 2455803.0777 + 0.063761E.
‡ Number of points used to determine the maximum.

3.9. *AK Cancri*

We observed a superoutburst in 2012 January. Due to an observation of short duration, the recorded superhumps were limited in number (table 11). The resultant period suggests that we observed stage-B superhumps.

3.10. *CC Cancri*

We observed a superoutburst in 2011 December. The times of superhump maxima are listed in table 12. Although the data were rather sparse, stages B and C were recorded. The obtained periods were similar to those in 2001 (Kato et al. 2009).

A comparison of different superoutbursts in the $O-C$ diagram is shown in figure 9. An early-stage part of observations still is lacking for this object.

3.11. *GO Comae Berenices*

We observed the 2012 superoutburst of this object. The times of superhump maxima are listed in table 13. Both stages B and C can be identified as typical ones in GC Com. The $O-C$ variation during this outburst was similar to those in previous outbursts (figure 10).

3.12. *TU Crateris*

We observed the late stage of the 2011 superoutburst of TU Crt. The times of superhump maxima are listed in table 14. It is most likely that we observed only stage-C superhumps. The measured period is in agreement with that of stage-C superhumps recorded in 1998 (Mennickent et al. 1999) and analyzed in Kato et al. (2009). A comparison of different superoutbursts in the $O-C$ diagram is shown in figure 11.

3.13. *V503 Cygni*

Harvey et al. (1995) established the SU UMa-type nature of this object, and reported a mean $P_{\rm SH}$ of 0.08101(4) d. They also detected negative superhumps in quiescence. Although there may have been some evidence for hump corresponding to negative superhumps during superoutbursts, its presence was not well established.

We observed the 2011 July superoutburst, its subsequent phase with normal outbursts, and a 2011 October superoutburst. The times of superhump maxima during the July superoutburst are listed in table 15. There was a small hint of a break in the $O-C$ diagram for the superhumps during the period from $E = 25$ to $E = 35$, and we attributed this to a stage B–C

Table 10. Superhump maxima of GZ Cet (2011).

E	Max*	Error	$O-C$†	N‡
0	55924.2865	0.0011	0.0021	31
1	55924.3403	0.0003	−0.0007	54
2	55924.3963	0.0003	−0.0014	46
188	55934.9357	0.0003	0.0003	164
189	55934.9918	0.0002	−0.0003	165

* BJD − 2400000.
† Against max = 2455924.2844 + 0.056654E.
‡ Number of points used to determine the maximum.

Table 11. Superhump maxima of AK Cnc (2012).

E	Max*	Error	$O-C$†	N‡
0	55952.0678	0.0047	−0.0045	42
1	55952.1424	0.0007	0.0028	74
2	55952.2086	0.0007	0.0018	54
45	55955.1043	0.0016	0.0062	74
46	55955.1591	0.0011	−0.0062	69

* BJD − 2400000.
† Against max = 2455952.0723 + 0.067239E.
‡ Number of points used to determine the maximum.

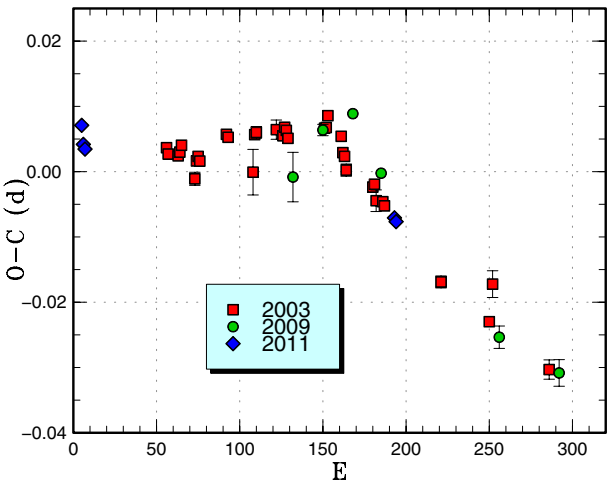

Fig. 8. Comparison of different superoutbursts of GZ Cet in the $O-C$ diagram. A period of 0.05672 d was used to draw this figure. Approximate cycle counts (E) after the start of the superoutburst were used. We assumed that the 2011 superoutburst was caught around its peak, based on the brightness and the evolution of superhumps, and that it was the start of the superoutburst.

transition. A global $P_{\rm dot}$ corresponded to $-3.8(2.6) \times 10^{-5}$.

The signal of the ordinary superhumps already became difficult to trace even before the rapid fading (BJD 2455751). However, the PDM analysis of the data during the period from BJD 2455751 to 2455754 yielded a period of 0.0814(1) d, suggesting that ordinary superhumps were still the dominant signal, rather than negative superhumps.

After BJD 2455754, large-amplitude modulations appeared again. The times of maxima were not on a smooth extension of the times of superhump maxima during the superoutburst plateau. These new signals appear to correspond to the traditional late superhumps (e.g., Vogt 1983), rather than our designation "stage-C superhumps" (table 17).

The times of superhump maxima during the 2011 October superoutburst are listed in table 16. Although the signal at epoch $E = 114$ is possibly a late superhump, as it existed in the 2011 July superoutburst, the lack of subsequent observations prevented identification of its late superhumps. We list a global $P_{\rm orb}$ and $P_{\rm dot}$ in table 2. A period derived from $E \leq 27$ (stage B) was 0.08151(8) d.

We were not able to detect a signal of negative superhumps during the fading stage and the subsequent quiescence, and the signal was dominated by positive superhumps. The situation was thus different from that in ER UMa (Ohshima et al. 2012). The mean period of (traditional late) superhumps during the post-superoutburst stage was 0.08032(3) d (PDM method), 3.4% longer than $P_{\rm orb}$, and was significantly shorter than that of ordinary superhumps. Although the superhump signal persisted in the quiescent state after the superoutburst, the signal became dominated by $P_{\rm orb}$ after the next normal outburst. The $P_{\rm orb}$ determined from all of the observations during the period from BJD 2455744 to 2455802 was 0.077773(2) d. This period is in agreement with the results based on an analysis of the data set restricted to the phase when the object did not show superhumps within their respective errors. The period is also in agreement with that obtained from the 2010 observations (Pavlenko et al. 2012b). We list this refined $P_{\rm orb}$ in table 2.

The lack of negative superhumps during these observations is in clear contrast to the observation by Harvey et al. (1995). V503 Cyg is known to display a highly variable number of normal outbursts among superoutbursts (Kato et al. 2002), and normal outbursts were very infrequent (every $\sim$30 d) during the period of the observation by Harvey et al. (1995), while the current observations showed much more frequent normal outbursts (every $\sim$10 d). Kato, Ishioka, and Uemura (2002) suggested that mechanisms of the suppressing of normal outbursts may have worked when normal outbursts were very infrequent. As discussed by various authors (Cannizzo et al. 2010; Kato et al. 2012a; Ohshima et al. 2012), the state with negative superhumps prevents the disk-instability from occurring. The condition to produce negative superhumps (likely a disk tilt) seems to naturally explain the association of the presence of negative superhumps with the reduced number of normal outbursts in V503 Cyg.

3.14. V1454 Cygni

This SU UMa-type dwarf nova undergoes outbursts relatively rarely, and the last outburst was in 2009 (Kato et al. 2010). The new observation during the 2012 superoutburst confirmed the period selection, as stated in Kato et al. (2010). The times of superhump maxima are listed in table 18. A. Henden reported that there is a $V \sim 20.5$ mag blue quiescent counterpart (cf. vsnet-alert 14568), whose position is in agreement with the astrometry ($19^{\rm h}53^{\rm m}38\overset{\rm s}{.}47$, $+35°21'45\overset{''}{.}8$)

Table 12. Superhump maxima of CC Cnc (2011).

E	Max*	Error	$O-C^{\dagger}$	$N^{\ddagger}$
0	55910.1871	0.0006	−0.0065	155
26	55912.1601	0.0011	0.0028	91
27	55912.2360	0.0006	0.0031	154
42	55913.3697	0.0002	0.0038	200
88	55916.8407	0.0004	0.0003	77
89	55916.9144	0.0009	−0.0015	37
90	55916.9918	0.0007	0.0003	73
101	55917.8222	0.0006	−0.0001	79
102	55917.8948	0.0008	−0.0031	77
103	55917.9741	0.0005	0.0008	79

* BJD − 2400000.
† Against max = 2455910.1935 + 0.075532E.
‡ Number of points used to determine the maximum.

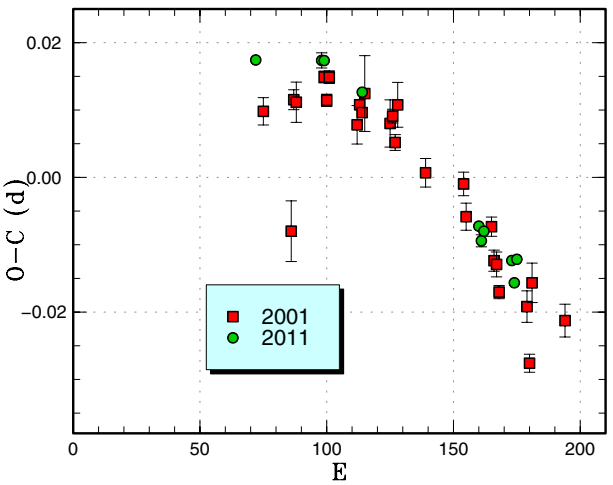

Fig. 9. Comparison of different superoutbursts of CC Cnc in the $O-C$ diagram. A period of 0.07589 d was used to draw this figure. Approximate cycle counts (E) after the start of the superoutburst were used. Since the start of the 2001 superoutburst was not well constrained, we so shifted the $O-C$ diagrams that they are best fitted to the best-recorded 2011 one.

measured during the outburst (vsnet-alert 14566).

3.15. *AQ Eridani*

The 2011 superoutburst of AQ Eri was observed only in its early and late stages. Although well-developed superhumps were observed on the first night, we were not able to measure the superhump period precisely. The late stage of the superoutburst and the post-superoutburst stage were well observed. Superhumps apparently persisted after the rapid decline. The times of superhump maxima are listed in table 19. By using the PDM analysis, the signal of the superhumps was detected until BJD 2455586. The signal was, however, not significantly detected after this epoch. The present case appears to be different from the long-persisting stage-C superhumps in many short-$P_{\rm orb}$ dwarf novae, such as QZ Vir (Ohshima et al. 2011).

Table 13. Superhump maxima of GO Com (2012).

E	Max*	Error	$O-C^{\dagger}$	$N^{\ddagger}$
0	55983.5944	0.0002	0.0015	63
1	55983.6575	0.0003	0.0017	61
2	55983.7221	0.0003	0.0032	65
11	55984.2863	0.0003	0.0006	107
25	55985.1654	0.0002	−0.0022	130
26	55985.2284	0.0003	−0.0023	128
57	55987.1766	0.0003	−0.0067	145
62	55987.4973	0.0009	−0.0009	54
64	55987.6193	0.0008	−0.0049	53
109	55990.4632	0.0005	0.0045	129
110	55990.5289	0.0011	0.0072	92
125	55991.4696	0.0004	0.0030	128
126	55991.5306	0.0005	0.0011	131
127	55991.5936	0.0005	0.0010	122
128	55991.6615	0.0008	0.0060	71
142	55992.5337	0.0010	−0.0037	55
143	55992.5976	0.0009	−0.0028	48
144	55992.6570	0.0015	−0.0063	45

* BJD − 2400000.
† Against max = 2455983.5929 + 0.062990E.
‡ Number of points used to determine the maximum.

3.16. *UV Geminorum*

We observed the middle part of the 2011 superoutburst. The times of superhump maxima are listed in table 20. A comparison of different superoutbursts in the $O-C$ diagram is shown in figure 12. Despite the large variation of the superhump period, the periods during the middle stage of different superoutbursts were almost the same.

3.17. *NY Herculis*

NY Her was discovered by Hoffmeister (1949) to be a Mira-type variable with a photographic magnitude range of 15.0 to fainter than 16.5. Gessner (1966) classified this object as a Cepheid (likely a W Vir-type variable) with a period of 6.3146 d. Pastukhova (1988), however, did not confirm this classification. Pastukhova (1988) identified the object as an 18 mag blue object on POSS plates, and obtained a mean period of 67.7067 d. In addition to this mean period, short outbursts were irregularly observed. The object varied at a rate of up to 2 mag d^{-1}, and Pastukhova (1988) classified the object as a blue irregular variable.

On 2011 June 10, CRTS (Catalina Real-Time Survey) detected an outburst of this object. T. Kato suggested that this object resembles ER UMa in behavior (cf. vsnet-alert 13410). A follow-up observation indicated the presence of superhumps (vsnet-alert 13418). The best superhump period, found by the PDM method, was 0.07602(14) d (figure 13).

The times of superhump maxima are listed in table 21. The CRTS data suggest a supercycle of 80–90 d. Judging from the relatively long superhump period, the object may be similar to V503 Cyg (Harvey et al. 1995), rather than ER UMa. Further intensive observations are particularly needed to determine the true cycle length for such a rare variety of SU UMa-type

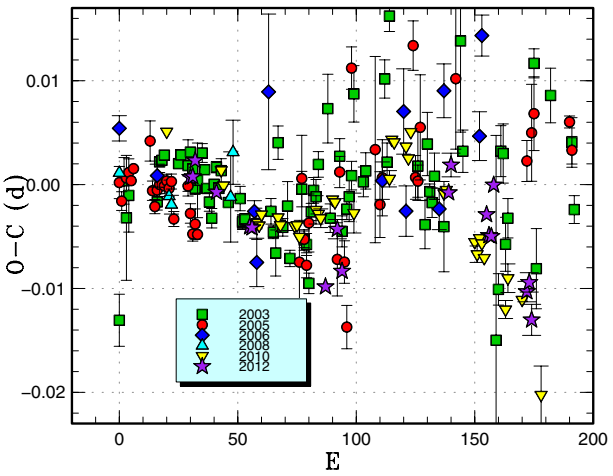

Fig. 10. Comparison of different superoutbursts of GO Com in the $O-C$ diagram. A period of 0.06303 d was used to draw this figure. Approximate cycle counts (E) after the start of the superoutburst were used.

dwarf novae.

3.18. *PR Herculis*

PR Her was discovered to be a dwarf nova (S 4247) by Hoffmeister (1951) with a photographic magnitude range of 14.0 to fainter than 17.5. Although this star was monitored by amateur observers since the early 1990s, no outburst was recorded. In the meantime, A. Henden identified the object as a $V = 21$ mag blue star in 1999 (vsnet-chat 1800).[2] The large outburst amplitude increased the possibility that the object is a WZ Sge-type dwarf nova.

On 2011 November 21, W. MacDonald II reported a very bright outburst at a magnitude of $V = 12.84$ (cf. cvnet-outburst 4406). Subsequent observations confirmed the presence of typical double-wave early superhumps (figure 14). Due to an unfavorable location, the object soon got hard to access in the low evening sky. Ordinary superhumps were detected despite this unfavorable condition (vsnet-alert 13932; figure 15). The times of superhump maxima are listed in table 22. The large outburst amplitude, the low frequency of outbursts, and the existence of prominent early superhumps qualify PR Her as a WZ Sge-type dwarf nova.

3.19. *V611 Herculis*

Little was known about this dwarf nova since its discovery (Hoffmeister 1968). CRTS detected four past outbursts. An analysis of the SDSS (Sloan Digital Sky Survey) colors of the quiescent counterpart suggested an object below the period gap (Kato et al. 2012b). A new outburst was detected by CRTS on 2012 June 8 (cf. vsnet-alert 14647). Subsequent observations detected superhumps (vsnet-alert 14648; figure 16). We detected two superhump maxima at BJD 2456087.4232(5) ($N = 62$) and 2456087.4877(6) ($N = 27$). The best period determined by the PDM method was 0.0636(4) d.

[2] See also ⟨ftp://ftp.aavso.org/upload/chartteam/MISC/seq/Her%20PR.txt⟩.

Table 14. Superhump maxima of TU Crt (2011).

E	Max*	Error	$O-C$†	N‡
0	55925.2955	0.0003	0.0004	151
69	55931.1543	0.0017	−0.0033	99
70	55931.2437	0.0005	0.0011	151
82	55932.2639	0.0007	0.0018	151

* BJD − 2400000.
† Against max = 2455925.2952 + 0.084962E.
‡ Number of points used to determine the maximum.

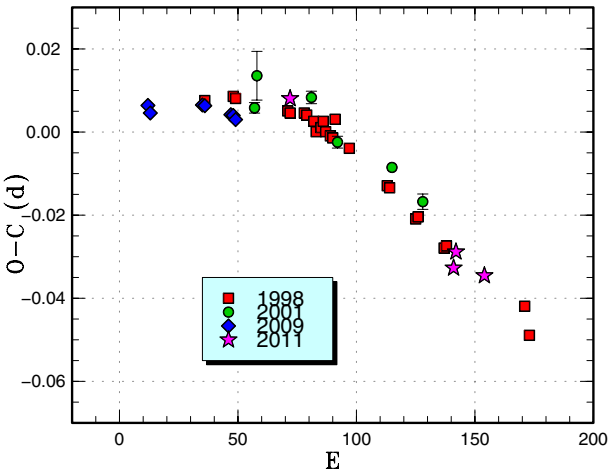

Fig. 11. Comparison of different superoutbursts of TU Crt in the $O-C$ diagram. A period of 0.08550 d was used to draw this figure. Approximate cycle counts (E) after the start of the superoutburst were used.

3.20. *V844 Herculis*

The well-known SU UMa-type dwarf nova V844 Her underwent a superoutburst in 2012 May (vsnet-alert 14525). After the period of frequent outbursts in 2009–2011, the object again entered a relatively inactive phase in 2011–2012; the present superoutburst occurred ~ 370 d after the 2011 superoutburst. The times of superhump maxima are listed in table 23. Although a clear pattern of stages A–C was observed, the period of stage A was not determined due to limited observations during this stage. The $P_{\rm dot}$ during stage B was clearly positive, as seen in other superoutbursts of this object.

Figure 17 illustrates a comparison of different superoutbursts in the $O-C$ diagram. As noted in Kato et al. (2012a), epochs of the stage B–C transition are different in each superoutburst. The B–C transition in the 2012 superoutburst appears to have occurred earlier than those in other superoutbursts.

3.21. *MM Hydrae*

We observed the early and late stages of the 2012 superoutburst of this object. The times of superhump maxima are listed in table 24. The $O-C$ diagram indicates that we missed the middle-to-end part of stage B, and it was thus impossible to determine $P_{\rm dot}$. Although a comparison of $O-C$ diagrams

Table 15. Superhump maxima of V503 Cyg (2011 July).

E	Max*	Error	$O-C^{\dagger}$	$N^{\ddagger}$
0	55744.5173	0.0005	−0.0041	89
1	55744.6008	0.0008	−0.0017	47
10	55745.3315	0.0016	−0.0007	21
12	55745.4959	0.0009	0.0016	31
24	55746.4683	0.0008	0.0010	92
25	55746.5524	0.0009	0.0039	82
35	55747.3620	0.0023	0.0027	16
36	55747.4410	0.0006	0.0006	75
37	55747.5227	0.0008	0.0012	75
39	55747.6836	0.0004	−0.0000	129
40	55747.7639	0.0005	−0.0008	150
41	55747.8465	0.0005	0.0007	133
47	55748.3339	0.0014	0.0016	30
61	55749.4612	0.0024	−0.0063	30
73	55750.4418	0.0186	0.0013	101
74	55750.5206	0.0021	−0.0010	126
77	55750.7689	0.0011	0.0041	136
78	55750.8419	0.0026	−0.0040	116

* BJD − 2400000.
† Against max = 2455744.5214 + 0.081084E.
‡ Number of points used to determine the maximum.

Table 16. Superhump maxima of V503 Cyg (2011 October).

E	Max*	Error	$O-C^{\dagger}$	$N^{\ddagger}$
0	55831.1911	0.0014	−0.0055	33
1	55831.2718	0.0004	−0.0059	58
2	55831.3537	0.0004	−0.0049	59
3	55831.4366	0.0005	−0.0030	58
4	55831.5186	0.0007	−0.0020	36
25	55833.2234	0.0012	0.0018	24
26	55833.3128	0.0020	0.0101	28
27	55833.3946	0.0019	0.0110	29
87	55838.2578	0.0016	0.0142	45
114	55840.4147	0.0042	−0.0159	45

* BJD − 2400000.
† Against max = 2455831.1966 + 0.081000E.
‡ Number of points used to determine the maximum.

Table 17. Superhump maxima of V503 Cyg (2011 July) (late superhumps).

E	Max*	Error	$O-C^{\dagger}$	$N^{\ddagger}$
0	55753.4128	0.0018	−0.0076	30
1	55753.4995	0.0019	−0.0015	30
10	55754.2291	0.0006	0.0041	82
16	55754.7127	0.0018	0.0050	60
17	55754.7878	0.0008	−0.0003	145
24	55755.3518	0.0012	0.0006	30
25	55755.4300	0.0021	−0.0017	30
26	55755.5117	0.0010	−0.0004	29
38	55756.4835	0.0016	0.0060	30
42	55756.8034	0.0007	0.0040	144
43	55756.8821	0.0008	0.0023	75
47	55757.2020	0.0006	0.0004	146
48	55757.2768	0.0008	−0.0052	148
60	55758.2381	0.0010	−0.0094	74
66	55758.7351	0.0010	0.0050	136
67	55758.8125	0.0008	0.0019	141
70	55759.0506	0.0008	−0.0013	65
71	55759.1311	0.0007	−0.0013	160
72	55759.2122	0.0010	−0.0007	179

* BJD − 2400000.
† Against max = 2455753.4205 + 0.080450E.
‡ Number of points used to determine the maximum.

can be drawn (figure 18), the middle-to-late part of stage B has not yet been well recorded for this object.

3.22. VW Hydri

Although this object is one of the best and oldest known prototypical SU UMa-type dwarf novae, no high-quality photometric data for superhumps have been publicly available. The present observation (Hambsch 2012) recorded the 2011 November–December superoutburst and two normal outbursts in 2011 December and 2012 January. Although the data were not as uninterrupted as the Kepler observation, they provide an opportunity to analyze observations of this well-known object in a modern way and with modern knowledge.

The times of the superhump maxima during the superoutburst are listed in table 25.

The outburst started with a precursor (figure 19, lower panel), after a stage of a short fading branch, and then entered the plateau phase. During the plateau phase, stage A and two segments of almost constant periods, which we attribute to stages B and C, were observed. The stage B–C transition occurred during the period between $E = 68$ and $E = 77$, and was apparently relatively smooth compared with that of short-$P_{\rm orb}$ systems (cf. Kato et al. 2009 figure 4).

During the rapid fading stage of the superoutburst, a phase reversal occurred, which is described as "traditional" late superhumps (Schoembs & Vogt 1980; Vogt 1983). This signal persisted during the quiescent period after the superoutburst (figure 19). The times of the maxima of these superhumps are listed in table 26. In contrast to V344 Lyr (Wood et al. 2011; Kato et al. 2012a), there was no prominent signal of "secondary maxima" during the late plateau stage of the superoutburst, and it appears that the phase suddenly jumped by $\sim 0.5\,P_{\rm SH}$. Although "traditional" late superhumps were usually considered to arise from an ordinary stream-impact hot spot,[3] the apparent absence of a corresponding signal before the rapid fading, as recorded in V344 Lyr, would make this traditional explanation worth reconsideration. The unavoidable gap between BJD 2455904.9 and 2455905.4 made it difficult to examine how this phase jump occurred.

The times of the late superhumps, measured after subtracting the mean orbital variation, are listed in table 26. These late

[3] See also a discussion in Hessman et al. (1992), who reported that the traditional model of late superhumps by Vogt (1983) did not trivially explain the observed eclipse depths in OY Car.

Table 18. Superhump maxima of V1454 Cyg (2012).

E	Max*	Error	$O-C^{\dagger}$	$N^{\ddagger}$
0	56059.5294	0.0005	−0.0001	60
1	56059.5872	0.0006	0.0002	58
17	56060.5067	0.0006	−0.0002	60
18	56060.5647	0.0004	0.0002	61

* BJD − 2400000.
† Against max = 2456059.5296 + 0.057494E.
‡ Number of points used to determine the maximum.

Table 19. Superhump maxima of AQ Eri (2011).

E	Max*	Error	$O-C^{\dagger}$	$N^{\ddagger}$
0	55875.8290	0.0005	−0.0016	121
1	55875.8930	0.0003	0.0001	103
143	55884.7372	0.0006	0.0079	77
144	55884.7964	0.0007	0.0049	98
145	55884.8561	0.0009	0.0024	80
159	55885.7152	0.0013	−0.0098	24
160	55885.7813	0.0029	−0.0059	22
161	55885.8513	0.0008	0.0019	15

* BJD − 2400000.
† Against max = 2455875.8306 + 0.062228E.
‡ Number of points used to determine the maximum.

Table 20. Superhump maxima of UV Gem (2011).

E	Max*	Error	$O-C^{\dagger}$	$N^{\ddagger}$
0	55892.6080	0.0004	0.0006	62
1	55892.6996	0.0005	−0.0007	80
10	55893.5351	0.0005	−0.0005	84
11	55893.6284	0.0004	−0.0001	83
12	55893.7231	0.0007	0.0019	51
13	55893.8129	0.0004	−0.0012	60

* BJD − 2400000.
† Against max = 2455892.6074 + 0.092822E.
‡ Number of points used to determine the maximum.

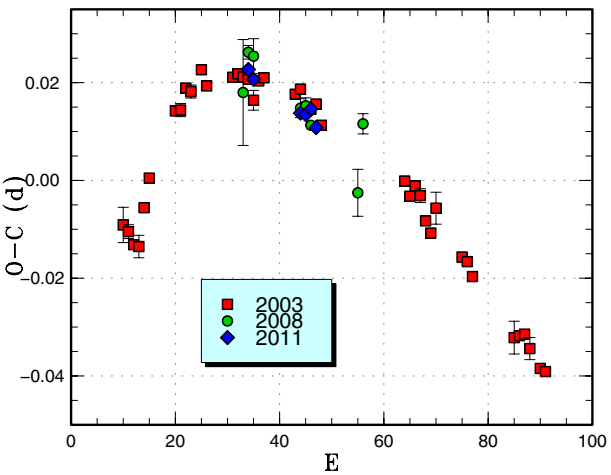

Fig. 12. Comparison of different superoutbursts of UV Gem in the $O-C$ diagram. A period of 0.0936 d was used to draw this figure. Approximate cycle counts (E) after the start of the superoutburst were used.

superhumps persisted until the next second normal outburst, as observed in V344 Lyr (Wood et al. 2011; Kato et al. 2012a). After this second normal outburst, superhumps still persisted with a shorter period [0.075333(4) d], and there was a well-recognizable signal through the PDM analysis (figure 20).

3.23. RZ Leonis Minoris

We analyzed three superoutbursts in 2012 based on the AAVSO data (tables 27, 28, 29). The first two superoutbursts were observed for their later parts, and the third superoutburst was mainly observed for its earlier part. In measuring $P_{\rm dot}$, we did not use $E \geq 176$ for the first outburst, which was obtained during the fading stage, and identfying the phases was ambiguous. A comparison of $O-C$ diagrams is shown in figure 21. Although a combined $O-C$ analysis of Olech et al. (2008) in Kato et al. (2009) was suggestive of a positive $P_{\rm dot}$, the current analysis of the new data more strongly supports a positive $P_{\rm dot}$ in this very unusual object. Although there was a hint of the emergence of double-wave modulations during the fading stage, we could not detect secure stage-C superhumps. It is well worth noting that the epochs of the superhump maxima for these three superoutbursts can be reasonably well (within 0.005 d) expressed by a single period of 0.059432(2) d, which might strengthen the finding by Olech et al. (2008) that there was no phase shift between different superhumps. A direct analysis of the photometric data (PDM method, figure 22), however, strongly preferred a period of 0.059585(1) d with larger (0.010 d) and systematically variable $O-C$ values. Since the $O-C$ analysis of individual superoutbursts gives only small residuals for the period of 0.05940 d, this preference for a different period over 0.05940 d is an unnatural behavior. This suggests that the apparent coherence of the superhumps in the $O-C$ analysis combined with a period of 0.059432(2) d may be simply superficial, and that the true underlying period may be different. This possibility should be clarified by a larger set of data.

While most of the weak signal in figure 22 corresponds to aliases of the main superhump signal, as it is evident from the window function, a period of 0.059053(2) d does not arise from an alias. Since ϵ for objects around these $P_{\rm SH}$ is usually 1.0%, or slightly less (cf. Kato et al. 2012a), we regard this period as a candidate orbital period. The waveform of this periodicity is shown in figure 23. If this is the true orbital period, ϵ for stage-B superhumps is 0.6%. Further testing concerning the stability of this signal needs to be confirmed.

3.24. BK Lyncis

BK Lyn has been a well-known permanent superhumper below the period gap (Skillman & Patterson 1993). However, it has recently been demonstrated that the object shows dwarf nova-type outbursts, and that the pattern of outbursts is quite

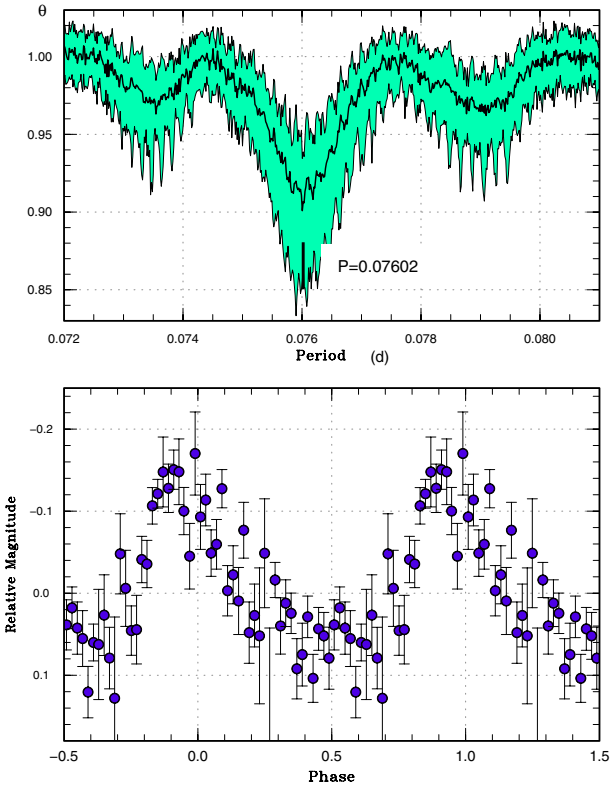

Fig. 13. Superhumps in NY Her (2011). Upper: PDM analysis. Lower: Phase-averaged profile.

Table 21. Superhump maxima of NY Her (2011).

E	Max*	Error	$O-C^{\dagger}$	$N^{\ddagger}$
0	55724.6932	0.0013	−0.0023	77
1	55724.7690	0.0009	−0.0022	79
2	55724.8466	0.0009	−0.0005	78
3	55724.9220	0.0006	−0.0009	78
13	55725.6829	0.0014	0.0020	78
14	55725.7585	0.0072	0.0018	40
26	55726.6702	0.0027	0.0039	65
27	55726.7455	0.0031	0.0034	34
29	55726.8994	0.0040	0.0057	77
37	55727.4892	0.0044	−0.0109	28

* BJD − 2400000.
† Against max = 2455724.6955 + 0.075802E.
‡ Number of points used to determine the maximum.

similar to those of ER UMa stars (E. de Miguel, see also Kemp et al. 2012). According to the Northern Sky Variability Survey (NSVS), the object was still in the novalike (NL)-type state in 2002.[4] The CRTS data indicate that the object already entered a DN state in 2005. The outburst-like variations were also recorded in AAVSO observations in 2005–2006. We here analyze observations in 2012, mostly from the AAVSO database.

As seen in recent ER UMa (Ohshima et al. 2012), the object showed negative superhumps during most of its outburst cycle, and showed positive superhumps during the $\sim$ 10 d initial part of superoutbursts. We first identified the period of positive superhumps using the best-observed superoutburst in 2012 April. The period was identified as 0.07859(1) d (figure 24). With the help of this period, we could identify the times of the superhump maxima during the less-observed 2012 February–March superoutburst (table 30). Although the maxima for $E \leq 3$ were those of negative superhumps [$P = 0.071(2)$ d], we included these epochs to illustrate the smooth transition from negative superhumps to positive superhumps in phase, as recorded in ER UMa (Ohshima et al. 2012). The times of the superhump maxima during the 2012 April superoutburst are given in table 32. Since the epochs $E = 1,2$ were obtained before the maximum of the superoutburst, we did not use them for calculating the period and $P_{\rm dot}$. During the later stage ($E \geq 114$), the structure of the superhumps became complex, and both negative and positive superhumps appeared to coexist. Although the superhump period during the superoutburst was not very different from those recorded during its NL-type state (Skillman & Patterson 1993), the amplitudes of superhumps were much larger than those in its former NL-type state, implying that the 3:1 resonance is more strongly excited during a superoutburst.

A comparison of different superhumps of positive superhumps in the $O-C$ diagram is shown in figure 25. The disagreement in the $O-C$ diagram was slightly wider than that in other SU UMa-type dwarf novae, which may be a result of remnant, overlapping negative superhumps. Particularly, the relatively large scatter in the $O-C$ diagram in the later part of this figure was caused by profile variations, due to evolving negative superhumps.

The behavior of the negative superhumps was very similar to that of ER UMa (figure 26; cf. figure 2 of Ohshima et al. 2012). The mean period of the negative superhumps during the superoutburst was 0.072793(7) d ($0 \leq E \leq 280$). The period slightly lengthened later, and stabilized at a slightly longer period during the phase showing normal outbursts [mean period 0.072922(6) d for $280 \leq E \leq 544$] (table 31). It is noteworthy that there was no jump in the phase when superhumps switched from negative to positive. The same phenomenon was observed in ER UMa (Ohshima et al. 2012). The amplitudes of the negative superhumps were well correlated with the system magnitude, and the amplitudes became larger when the system became fainter. This relation was also observed in V344 Lyr (cf. figure 79 of Kato et al. 2012a), V503 Cyg (Harvey et al. 1995), MN Dra (Pavlenko et al. 2010a), and ER UMa, although Ohshima et al. (2012) did not present the corresponding figure.

Kemp et al. (2012) proposed that a transition from a permanent superhumper to a dwarf nova may be a result of cooling of the white dwarf following a nova eruption. The time-scale (several years) of this transition, however, appears to be too short when compared with the proposed duration ($\sim$ 1900 yr) of the post-nova state. The change of state may also be the result of a variable mass-transfer rate, as recorded in the other ER UMa-type dwarf novae, such as V1159 Ori (Kato 2001), rather than secular evolution.

[4] ⟨http://skydot.lanl.gov/nsvs/star.php?num=7454712&mask=32004⟩.

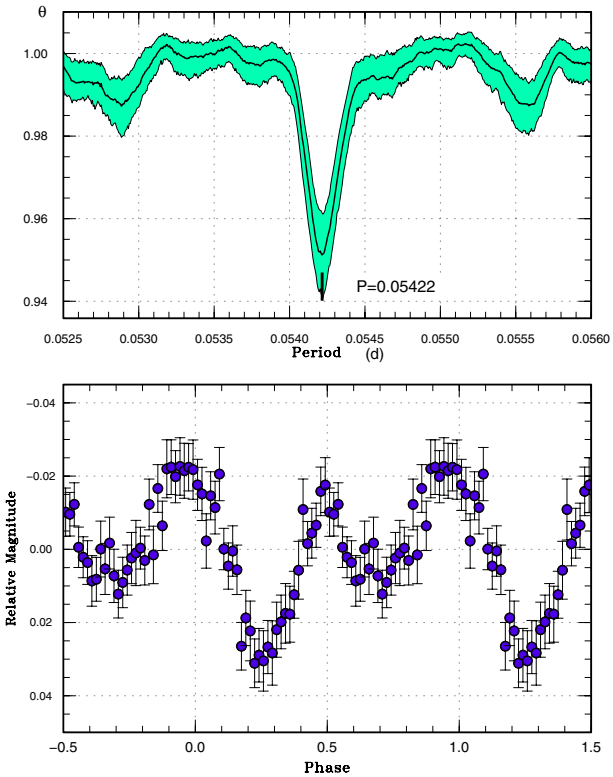

Fig. 14. Early superhumps in PR Her (2011). Upper: PDM analysis. Lower: Phase-averaged profile.

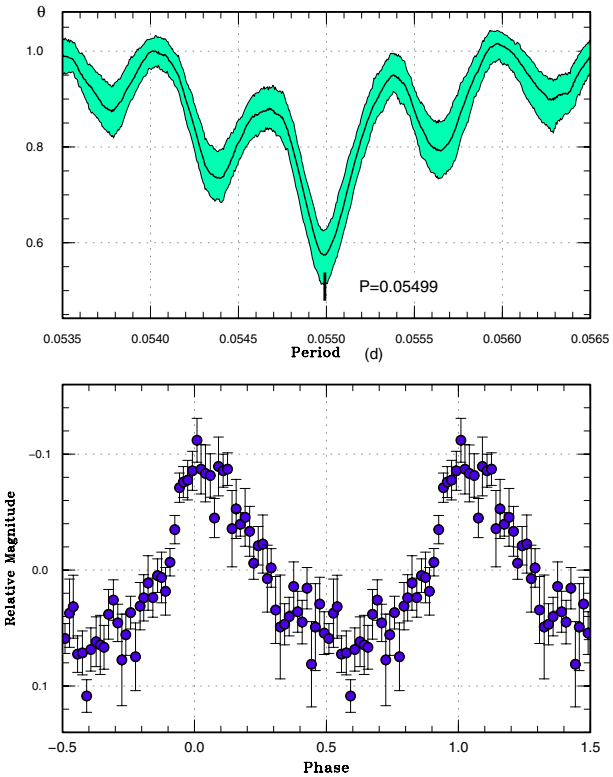

Fig. 15. Ordinary superhumps in PR Her (2011). Upper: PDM analysis. Lower: Phase-averaged profile.

3.25. *V585 Lyrae*

Although the object was extensively observed during the 2003 superoutburst (cf. Kato et al. 2009), no secure record of an outburst was recorded until 2012. The 2012 superoutburst was detected by P. A. Dubovsky (vsnet-alert 14494). We obtained two nights of observations, and listed the times of the maxima (table 33). The period given in table 2 was obtained by the PDM method.

3.26. *FQ Monocerotis*

Only a fragment of the 2011 superoutburst was observed. The times of superhump maxima are listed in table 34. Since the object quickly faded three days after the observation, it is likely that we only observed stage-C superhumps.

3.27. *V1032 Ophiuchi*

This object is an eclipsing SU UMa-type dwarf nova (Kato et al. 2010). By applying the Markov-chain Monte Carlo (MCMC) method to the phased data using the period and epoch as trial variables (see the Appendix), we obtained an updated orbital ephemeris of

$$\mathrm{Min(BJD)} = 2455286.68256(7) + 0.081055386(10)E, \quad (1)$$

based on 2010 and 2012 observations. The times of superhump maxima are listed in table 35. The PDM analysis yielded a consistent result of 0.08599(5) d.

Table 22. Superhump maxima of PR Her (2011).

E	Max*	Error	$O-C$†	N‡
0	55900.2456	0.0006	0.0008	74
1	55900.3034	0.0006	0.0035	54
11	55900.8507	0.0015	0.0006	31
12	55900.9020	0.0021	−0.0031	51
19	55901.2905	0.0005	0.0002	43
37	55902.2771	0.0008	−0.0036	51
91	55905.2512	0.0004	−0.0008	114
92	55905.3094	0.0011	0.0025	58

* BJD − 2400000.
† Against max = 2455900.2449 + 0.055022E.
‡ Number of points used to determine the maximum.

3.28. *V2051 Ophiuchi*

Only one superhump was recorded during the 2012 February superoutburst: BJD 2455985.3378(2) ($N = 157$).

3.29. *V1159 Orionis*

V1159 Ori is one member of the ER UMa stars (Robertson et al. 1995; Nogami et al. 1995; Patterson et al. 1995). Although the object generally follows the ER UMa-type pattern with a short supercycle (Kato & Kunjaya 1995), it is known to show variations of supercycles with a range of

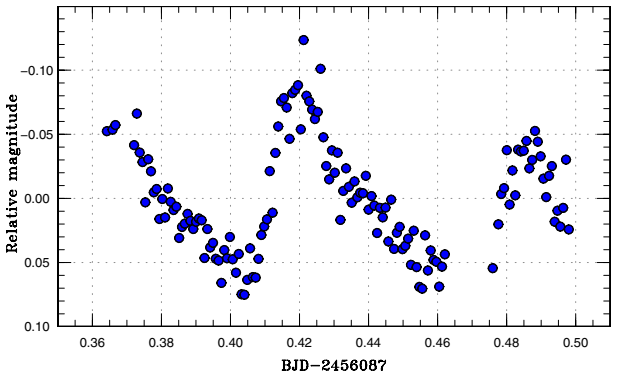

Fig. 16. Superhumps in V611 Her.

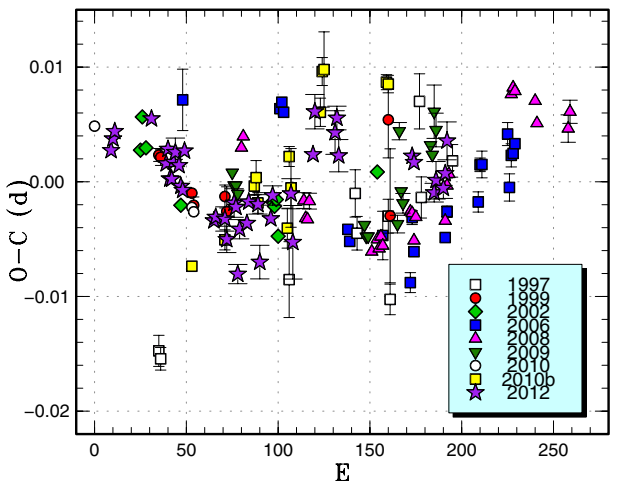

Fig. 17. Comparison of different superoutbursts of V844 Her in the $O-C$ diagram. A period of 0.05590 d was used to draw this figure. Approximate cycle counts (E) after the start of the superoutburst were used. For descriptions of the 2009, 2010, and 2010b superoutbursts, see Kato et al. (2012a).

44.6–53.3 d (Kato 2001). Since it has been demonstrated that the prototype ER UMa has recently been in a state of "negative superhumps" (Ohshima et al. 2012), it would be worth examining the current state of superhumps in V1159 Ori.

The observations were taken during its 2012 March superoutburst (the data were mainly from the AAVSO). The times of superhump maxima are listed in table 36. There was an $\sim$0.5-phase shift between $E = 31$ and $E = 77$, as can be seen in ER UMa in its "positive superhump" state (Kato et al. 2003a). A period analysis for $E \geq 61$ yielded a period of 0.06430(5) d, indicating that the period after the phase shift was that of positive superhumps, and not that of negative superhumps. The behavior well reproduced ER UMa in its "positive superhump" state (in the 1990s). V1159 Ori is currently the best target to investigate the ER UMa-type phenomena in the "positive superhump" state; further detailed observations are required.

Table 23. Superhump maxima of V844 Her (2012).

E	Max*	Error	$O-C$†	N‡
0	56050.3428	0.0002	0.0028	108
1	56050.3997	0.0001	0.0038	117
2	56050.4563	0.0001	0.0044	71
22	56051.5754	0.0004	0.0055	51
30	56052.0187	0.0004	0.0016	91
31	56052.0758	0.0003	0.0029	92
32	56052.1291	0.0003	0.0003	93
33	56052.1850	0.0003	0.0002	81
34	56052.2424	0.0008	0.0017	23
35	56052.2992	0.0012	0.0026	22
37	56052.4098	0.0002	0.0014	68
38	56052.4639	0.0002	−0.0004	75
39	56052.5194	0.0003	−0.0007	61
40	56052.5788	0.0004	0.0027	41
56	56053.4671	0.0003	−0.0034	76
57	56053.5233	0.0002	−0.0031	76
62	56053.8026	0.0011	−0.0032	11
63	56053.8568	0.0011	−0.0050	12
67	56054.0835	0.0012	−0.0018	67
68	56054.1391	0.0005	−0.0022	92
69	56054.1891	0.0008	−0.0080	108
70	56054.2490	0.0008	−0.0041	57
74	56054.4731	0.0003	−0.0036	74
75	56054.5308	0.0003	−0.0018	76
80	56054.8101	0.0008	−0.0020	12
81	56054.8610	0.0015	−0.0070	12
87	56055.2002	0.0007	−0.0032	61
88	56055.2581	0.0008	−0.0012	62
98	56055.8172	0.0013	−0.0010	12
99	56055.8689	0.0032	−0.0053	12
110	56056.4915	0.0006	0.0024	75
111	56056.5511	0.0015	0.0061	69
122	56057.1642	0.0019	0.0043	35
123	56057.2213	0.0010	0.0055	40
124	56057.2740	0.0014	0.0023	38
164	56059.5099	0.0007	0.0022	46
165	56059.5653	0.0004	0.0017	42
176	56060.1775	0.0008	−0.0010	42
177	56060.2345	0.0016	0.0001	40
181	56060.4574	0.0009	−0.0006	59
182	56060.5146	0.0008	0.0007	62
183	56060.5734	0.0017	0.0035	62

* BJD − 2400000.
† Against max = 2456050.3401 + 0.055900E.
‡ Number of points used to determine the maximum.

3.30. AR Pictoris

We observed the 2011 superoutburst of this object (= CTCV J0549−4921, Imada et al. 2008a). Kato et al. (2009) identified this object having a large negative $P_{\rm dot}$. The times of superhump maxima are listed in table 37. We observed only the terminal portion of the superoutburst, and the mean superhump period [0.08315(15) d] was much shorter than the value

Table 24. Superhump maxima of MM Hya (2012).

E	Max*	Error	$O-C$†	N‡
0	55993.5863	0.0008	0.0008	12
1	55993.6431	0.0009	−0.0012	17
2	55993.7015	0.0008	−0.0016	18
3	55993.7580	0.0023	−0.0040	20
104	55999.6983	0.0025	−0.0078	9
105	55999.7591	0.0026	−0.0058	14
119	56000.5967	0.0017	0.0078	16
120	56000.6488	0.0020	0.0011	19
121	56000.7086	0.0017	0.0021	14
122	56000.7681	0.0019	0.0027	10
135	56001.5303	0.0005	−0.0002	44
136	56001.5987	0.0009	0.0094	23
137	56001.6485	0.0013	0.0003	18
138	56001.7135	0.0022	0.0065	6
139	56001.7670	0.0011	0.0011	15
144	56002.0616	0.0009	0.0014	122
145	56002.1193	0.0008	0.0003	99
152	56002.5325	0.0007	0.0015	40
153	56002.5928	0.0011	0.0029	23
154	56002.6484	0.0012	−0.0003	18
201	56005.3977	0.0019	−0.0170	61

* BJD − 2400000.
† Against max = 2455993.5854 + 0.058852E.
‡ Number of points used to determine the maximum.

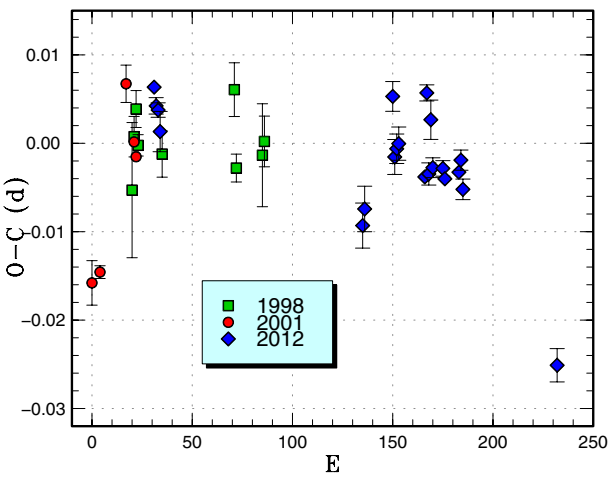

Fig. 18. Comparison of different superoutbursts of MM Hya in the $O-C$ diagram. A period of 0.05892 d was used to draw this figure. Approximate cycle counts (E) after the start of the superoutburst were used.

Table 25. Superhump maxima of VW Hyi (2011).

E	Max*	Error	$O-C$†	N‡
0	55892.5748	0.0007	−0.0202	840
3	55892.8124	0.0024	−0.0128	26
12	55893.5120	0.0006	−0.0041	33
13	55893.5865	0.0004	−0.0064	42
14	55893.6647	0.0005	−0.0050	24
15	55893.7424	0.0004	−0.0040	22
16	55893.8190	0.0005	−0.0042	25
25	55894.5140	0.0001	−0.0001	721
26	55894.5919	0.0001	0.0011	834
27	55894.6701	0.0003	0.0025	371
28	55894.7459	0.0007	0.0016	19
29	55894.8231	0.0013	0.0020	21
31	55894.9762	0.0002	0.0016	180
38	55895.5102	0.0015	−0.0018	28
39	55895.5896	0.0008	0.0009	42
40	55895.6670	0.0012	0.0015	29
41	55895.7415	0.0012	−0.0008	21
42	55895.8203	0.0014	0.0013	22
51	55896.5134	0.0004	0.0034	647
52	55896.5924	0.0002	0.0057	839
53	55896.6712	0.0004	0.0078	353
54	55896.7447	0.0011	0.0045	20
55	55896.8205	0.0024	0.0035	22
64	55897.5133	0.0010	0.0054	32
65	55897.5926	0.0013	0.0079	42
66	55897.6672	0.0014	0.0058	21
67	55897.7454	0.0017	0.0072	22
68	55897.8205	0.0010	0.0056	22
77	55898.5086	0.0013	0.0028	26
78	55898.5903	0.0009	0.0077	42
79	55898.6630	0.0008	0.0036	30
80	55898.7420	0.0011	0.0058	31
81	55898.8203	0.0017	0.0074	34
90	55899.5028	0.0038	−0.0010	25
91	55899.5842	0.0007	0.0036	42
92	55899.6586	0.0006	0.0013	30
93	55899.7368	0.0014	0.0027	31
94	55899.8123	0.0010	0.0015	33
103	55900.5017	0.0022	−0.0000	25
104	55900.5804	0.0013	0.0019	21
105	55900.6553	0.0015	0.0000	30
106	55900.7322	0.0011	0.0002	30
107	55900.8089	0.0012	0.0001	34
130	55902.5656	0.0020	−0.0088	25
131	55902.6465	0.0038	−0.0046	30
132	55902.7214	0.0016	−0.0066	30
133	55902.7957	0.0015	−0.0090	34
145	55903.7186	0.0016	−0.0073	30
146	55903.7915	0.0015	−0.0112	34

* BJD − 2400000.
† Against max = 2455892.5949 + 0.076765E.
‡ Number of points used to determine the maximum.

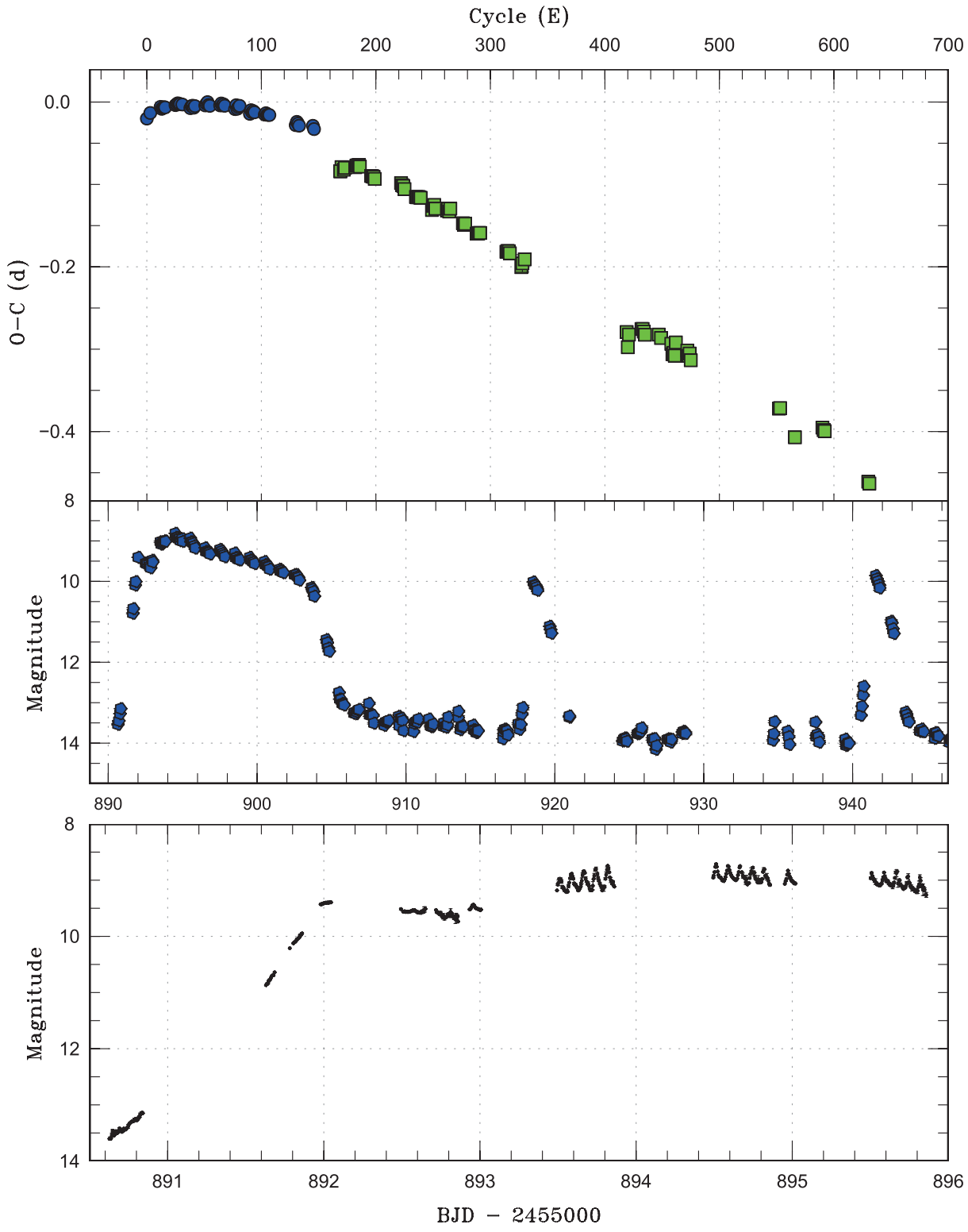

Fig. 19. $O-C$ diagram of superhumps in VW Hyi (2011). Upper: $O-C$. Filled circles and filled squares represent superhumps and late superhumps after the rapid fading. We used a period of 0.076914 d for calculating the $O-C$ residual. Middle: Light curve. Lower: Enlarged light curve of showing the precursor and evolution of superhumps.

Table 26. Late superhumps in VW Hyi (2011).

E	Max*	Error	$O-C^{\dagger}$	$N^{\ddagger}$	E	Max*	Error	$O-C^{\dagger}$	$N^{\ddagger}$
0	55905.5093	0.0016	−0.0199	32	121	55914.7410	0.0019	0.0039	27
1	55905.5913	0.0018	−0.0140	21	122	55914.8180	0.0014	0.0048	26
0	55905.5093	0.0015	−0.0199	30	145	55916.5642	0.0016	0.0007	15
3	55905.7420	0.0014	−0.0155	32	146	55916.6421	0.0019	0.0025	21
4	55905.8211	0.0019	−0.0124	33	147	55916.7187	0.0015	0.0030	26
13	55906.5142	0.0015	−0.0042	33	148	55916.7930	0.0020	0.0012	26
14	55906.5930	0.0015	−0.0015	19	158	55917.5454	0.0023	−0.0074	28
15	55906.6703	0.0014	−0.0004	28	159	55917.6268	0.0105	−0.0021	13
16	55906.7476	0.0012	0.0009	34	161	55917.7855	0.0047	0.0044	19
17	55906.8225	0.0021	−0.0003	33	250	55924.5427	0.0012	−0.0112	46
27	55907.5803	0.0011	−0.0035	21	251	55924.6012	0.0035	−0.0288	22
28	55907.6569	0.0013	−0.0030	30	252	55924.6934	0.0016	−0.0126	25
29	55907.7331	0.0009	−0.0029	33	263	55925.5463	0.0011	0.0031	41
30	55907.8075	0.0025	−0.0046	34	264	55925.6232	0.0026	0.0039	23
53	55909.5714	0.0009	0.0090	22	265	55925.6969	0.0017	0.0016	26
54	55909.6458	0.0010	0.0073	28	266	55925.7700	0.0022	−0.0015	32
55	55909.7218	0.0015	0.0072	31	278	55926.6932	0.0046	0.0085	13
56	55909.7949	0.0014	0.0042	32	280	55926.8429	0.0028	0.0060	9
66	55910.5545	0.0008	0.0029	20	289	55927.5281	0.0021	0.0063	23
67	55910.6310	0.0010	0.0032	21	290	55927.5923	0.0015	−0.0056	18
68	55910.7084	0.0008	0.0045	22	291	55927.6709	0.0013	−0.0031	19
69	55910.7847	0.0010	0.0048	27	292	55927.7444	0.0025	−0.0056	21
70	55910.8612	0.0023	0.0051	14	293	55927.8374	0.0021	0.0112	14
80	55911.6155	0.0027	−0.0016	15	303	55928.5967	0.0027	0.0095	17
81	55911.6975	0.0007	0.0044	24	304	55928.6673	0.0010	0.0040	18
82	55911.7755	0.0007	0.0062	27	305	55928.7469	0.0010	0.0075	22
83	55911.8477	0.0016	0.0024	20	306	55928.8156	0.0025	0.0002	13
93	55912.6148	0.0021	0.0085	16	383	55934.6792	0.0017	0.0042	17
94	55912.6937	0.0012	0.0113	20	384	55934.7569	0.0012	0.0057	14
95	55912.7673	0.0019	0.0088	26	397	55935.7212	0.0034	−0.0192	18
96	55912.8477	0.0009	0.0130	18	421	55937.5789	0.0010	0.0121	16
107	55913.6761	0.0015	0.0043	20	422	55937.6529	0.0007	0.0099	18
108	55913.7510	0.0010	0.0031	25	423	55937.7285	0.0014	0.0095	18
109	55913.8291	0.0016	0.0052	26	461	55940.5898	0.0008	−0.0210	19
119	55914.5864	0.0022	0.0015	15	462	55940.6646	0.0015	−0.0223	22
120	55914.6634	0.0008	0.0024	20					

* BJD − 2400000.
† Against max = 2455905.5291 + 0.076099E.
‡ Number of points used to determine the maximum.

obtained during the 2006 superoutburst (Kato et al. 2009). During the post-superoutburst phase, we were able to detect a superhump period of 0.08225(9) d (PDM method). The Lasso analysis yielded a combination of the superhump period and a period of 0.0801(1) d, which is potentially the orbital period. If this is indeed $P_{\rm orb}$, the ϵ values for the 2006 and 2011 superoutbursts were 5.4% (average) and 3.7% (2011). A comparison of $O-C$ diagrams (figure 27) indicates that the $O-C$ diagram in 2011 is a smooth extension of that in 2006, which was obtained only during the early stage.

3.31. GV Piscium

The 2011 superoutburst of this object was detected by CRTS on October 17. Subsequent observations confirmed the presence of superhumps (vsnet-alert 13768). The times of superhump maxima are listed in table 38. There was little hint as to a period variation, and the mean period was close to that obtained during the 2008 superoutburst (Kato et al. 2009). Since the object faded relatively soon after outburst detection, it is likely that we also observed only stage-C superhumps, as in 2008.

3.32. BW Sculptoris

This object (= HE 2350−3908, RX J2353.0−3852) was initially discovered in the Hamburg/ESO quasar survey (Augusteijn & Wisotzki 1997), and also selected as a ROSAT CV (Abbott et al. 1997). Its remarkable similarity with WZ Sge was already noted at its very early history

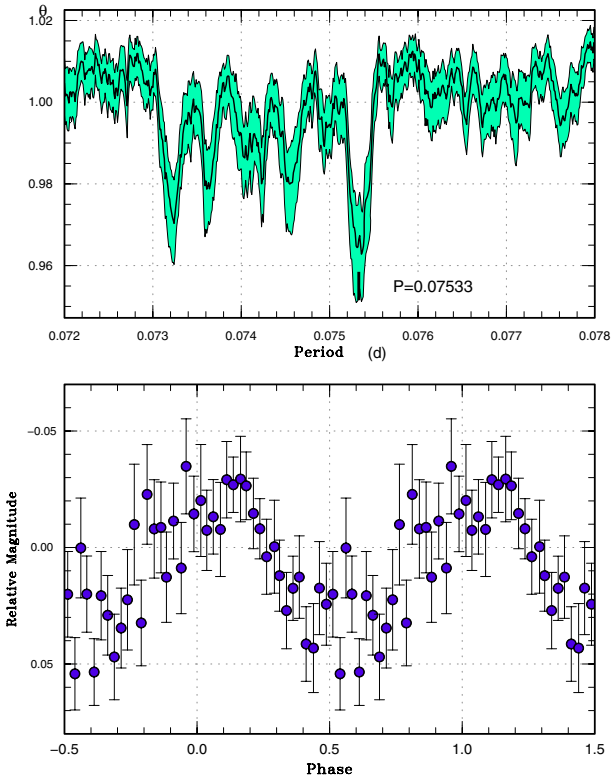

Fig. 20. Late superhumps in VW Hyi after a normal outburst. Upper: PDM analysis after removing the mean orbital variation. The rejection rate for bootstrapping was reduced to 0.2 for better visualization. Lower: Phase-averaged profile.

Table 27. Superhump maxima of RZ LMi (2012 February–March).

E	Max*	Error	$O-C^{\dagger}$	$N^{\ddagger}$
0	55985.8946	0.0016	0.0046	10
1	55985.9531	0.0014	0.0036	7
11	55986.5476	0.0011	0.0027	18
12	55986.6056	0.0012	0.0011	14
13	55986.6690	0.0017	0.0050	14
14	55986.7253	0.0014	0.0017	15
15	55986.7866	0.0057	0.0035	13
26	55987.4366	0.0004	−0.0014	40
28	55987.5568	0.0031	−0.0003	12
29	55987.6183	0.0019	0.0016	14
30	55987.6743	0.0011	−0.0019	14
31	55987.7325	0.0019	−0.0032	13
42	55988.3877	0.0011	−0.0030	38
43	55988.4431	0.0017	−0.0071	34
44	55988.5117	0.0033	0.0020	44
45	55988.5717	0.0014	0.0024	57
46	55988.6243	0.0007	−0.0045	55
61	55989.5188	0.0015	−0.0032	42
62	55989.5808	0.0011	−0.0007	42
63	55989.6342	0.0008	−0.0068	41
126	55993.3849	0.0022	−0.0071	38
176	55996.3719	0.0012	0.0030	35
177	55996.4281	0.0040	−0.0004	35
178	55996.4921	0.0011	0.0040	43
179	55996.5485	0.0008	0.0009	43
180	55996.6107	0.0011	0.0036	43

* BJD − 2400000.
† Against max = 2455985.8900 + 0.059540E.
‡ Number of points used to determine the maximum.

(Augusteijn & Wisotzki 1997). Despite monitoring, there was no outburst until 2011. Uthas et al. (2012) reported on the ZZ Cet-type pulsation of the white dwarf and the presence of quiescent superhumps 11% longer than $P_{\rm orb}$.

The 2011 outburst was detected by M. Linnolt on October 21 at a visual magnitude of 9.6 (posting to AAVSO discussion); a subsequent observation soon confirmed early superhumps (vsnet-alert 13786; figure 28). The last observation before this outburst was carried out on October 15 (by J. Hambsch; see also Hambsch 2012) when the object was still in quiescence. On October 31, ordinary superhumps developed (vsnet-alert 13815, 13819; figure 29). The object entered the rapid fading stage on November 12 (vsnet-alert 13847, 13850). The times of the maxima of ordinary superhumps are listed in table 39. Following a period of stage A ($E \leq 25$), there was stage B with $P_{\rm dot} = +4.3(0.3) \times 10^{-5}$. Although there was a suggestion of a sudden shortening of the superhump period after $E = 210$, as seen in other WZ Sge-type dwarf novae [e.g., GW Lib and V455 And (Kato et al. 2009); OT J012059.6+325545 and SDSS J080434.20+510349.2 = EZ Lyn (Kato et al. 2012a)], a discontinuity in the observation made identifying hump phasing uncertain. We list the times of the hump maxima after this rapid fading in table 40, which were measured after subtracting the mean orbital variation (figure 30). The overall behavior of the outburst and the $O-C$ diagram were very similar to those of GW Lib and V455 And. The period of early superhumps was 0.054308(2) d, 0.03% shorter than $P_{\rm orb}$. The ϵ value for stage-B superhumps was 1.3%.

A full analysis will be presented by T. Ohshima et al. (in preparation).

3.33. CC Sculptoris

CC Scl was discovered to be a ROSAT-selected CV (Schwope et al. 2000). During its 2000 October outburst (the second known), Ishioka et al. (2001a) detected likely superhumps with a period of 0.078 d and amplitudes of $\sim$0.3 mag. In 2000, however, Augusteijn et al. (vsnet-campaign 544) reported the detection of a photometric period of 0.058 d, which was considered to be the orbital period. Based on a discrepancy between the apparent period of the superhumps and the orbital period, Ishioka et al. (2001a) suggested that the object may be an intermediate polar. The unusual short duration of the superoutburst was also noted. It was later confirmed that the 0.058 d period is the orbital one (Chen et al. 2001; Tappert et al. 2004). Although there have been several outbursts from then on, no confirmatory observations of superhumps have been reported.

The 2011 superoutburst was detected by CRTS Siding Spring Survey (SSS), and subsequent observations indicated the presence of low-amplitude (up to 0.1 mag) variations similar to superhumps with a period of 0.0603 d (vsnet-alert

Table 28. Superhump maxima of RZ LMi (2012 March–April).

E	Max*	Error	$O-C^{\dagger}$	$N^{\ddagger}$
0	56013.6575	0.0013	0.0032	48
1	56013.7157	0.0011	0.0019	48
2	56013.7722	0.0011	−0.0011	47
17	56014.6658	0.0009	0.0004	47
18	56014.7193	0.0040	−0.0055	61
19	56014.7888	0.0022	0.0045	72
20	56014.8436	0.0026	−0.0002	25
34	56015.6745	0.0016	−0.0018	47
35	56015.7329	0.0016	−0.0029	49
36	56015.7914	0.0027	−0.0040	47
50	56016.6273	0.0017	−0.0006	64
51	56016.6882	0.0006	0.0008	63
52	56016.7519	0.0020	0.0051	91
53	56016.8072	0.0011	0.0009	76
54	56016.8649	0.0021	−0.0009	20
67	56017.6371	0.0009	−0.0018	62
68	56017.6986	0.0010	0.0002	62
69	56017.7581	0.0010	0.0002	63
84	56018.6517	0.0017	0.0017	60

* BJD − 2400000.
† Against max = 2456013.6543 + 0.059472E.
‡ Number of points used to determine the maximum.

Table 29. Superhump maxima of RZ LMi (2012 April).

E	Max*	Error	$O-C^{\dagger}$	$N^{\ddagger}$
0	56030.8288	0.0004	0.0026	18
15	56031.7195	0.0015	0.0022	37
16	56031.7776	0.0005	0.0009	32
47	56033.6196	0.0011	0.0012	34
48	56033.6779	0.0004	0.0001	81
49	56033.7354	0.0003	−0.0018	88
50	56033.7953	0.0010	−0.0013	21
64	56034.6275	0.0005	−0.0009	63
65	56034.6854	0.0005	−0.0023	99
66	56034.7453	0.0005	−0.0018	96
81	56035.6371	0.0004	−0.0012	67
82	56035.6959	0.0005	−0.0018	94
83	56035.7560	0.0006	−0.0011	74
98	56036.6480	0.0007	−0.0002	62
131	56038.6100	0.0025	0.0013	44
132	56038.6712	0.0013	0.0031	63
133	56038.7287	0.0009	0.0012	61

* BJD − 2400000.
† Against max = 2456030.8262 + 0.059408E.
‡ Number of points used to determine the maximum.

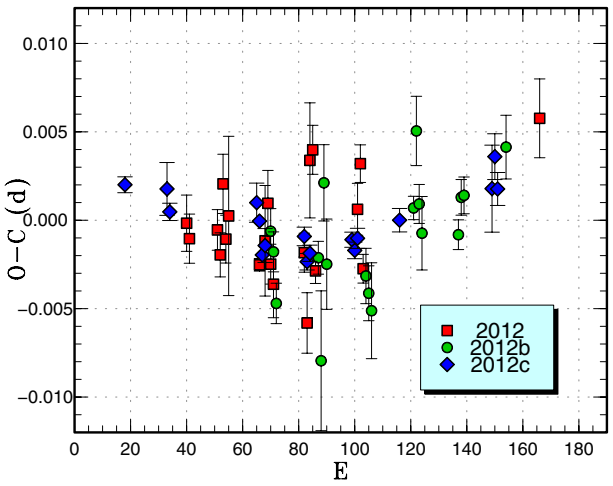

Fig. 21. Comparison of different superoutbursts of RZ LMi in the $O-C$ diagram. A period of 0.05940 d was used to draw this figure. Approximate cycle counts (E) after the start of the superoutburst were used.

13832). Although the observed variations had definite underlying periodicity (vsnet-alert 13841, 13846), individual waveforms were rather irregular (vsnet-alert 13840; see also actual observations in figure 34), unlike most SU UMa-type dwarf novae. Even after the object faded, the superhump signal persisted for at least eight days.

The PDM analysis yielded a stronger superhump signal and a weaker orbital signal (figure 32, upper panel). A Lasso analysis, which is less affected by aliasing, also indicated the presence of both signals (figure 32, lower panel). We adopted a refined orbital period of 0.0585845(10) d. We decomposed the observations into these two periods (figure 33), and tried to reproduce the observed light curve by combining these waves (figure 34). Although the result was not as remarkable as in OT J173516.9+154708, as we mention later (subsection 3.78), a part of the complex structure in the light curve appears to be understood as an effect of the orbital signal. We therefore subtracted the orbital variation, and determined the times of the superhump maxima (table 41). The relatively large scatter in the $O-C$ residual suggests the presence of irregularities not attributable to the orbital variation. Despite these irregularities, the $O-C$ residual, itself, did not show a strong trend of variation. Considering it was likely that we missed the initial part of the outburst, we probably observed only the stage-C superhumps. In table 2, we list the values based on this interpretation.

The unusual behavior of superhumps, as well as the strong presence of orbital signals in this system, might have led to the detection of the different period (Ishioka et al. 2001a). Such behavior may be related to a likely high orbital inclination (Tappert et al. 2004). The ϵ value, however, was 2.4%, a normal value for this $P_{\rm orb}$. Future dense monitoring to detect the early stage of a superoutburst is desired.

Woudt et al. (2012) recently established that this object is an intermediate polar similar to HT Cam. Since HT Cam has not yet shown superoutbursts (Ishioka et al. 2002), CC Scl is an

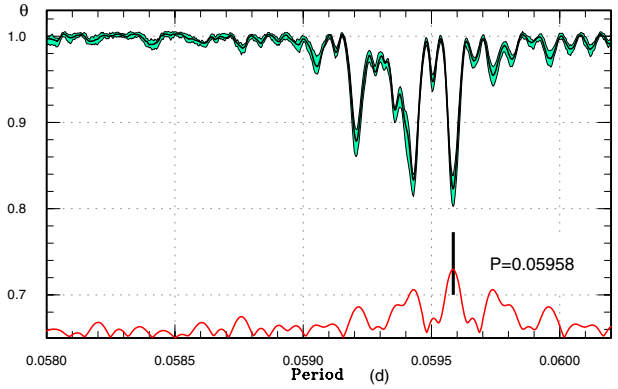

Fig. 22. Period analysis of plateau phases of three subsequent superoutbursts of RZ LMi. The curve at the bottom of the figure represents the window function.

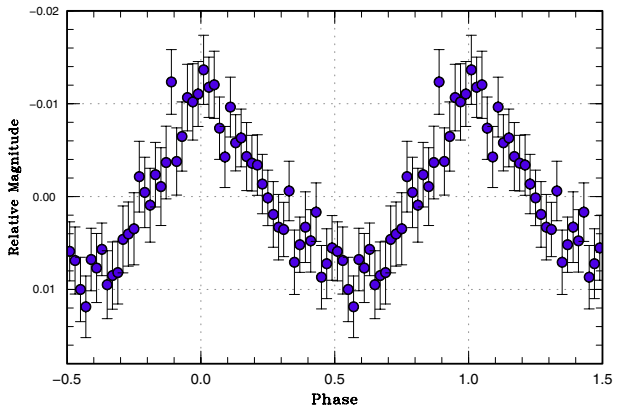

Fig. 23. Waveform of a candidate orbital period (0.059053 d) of RZ LMi.

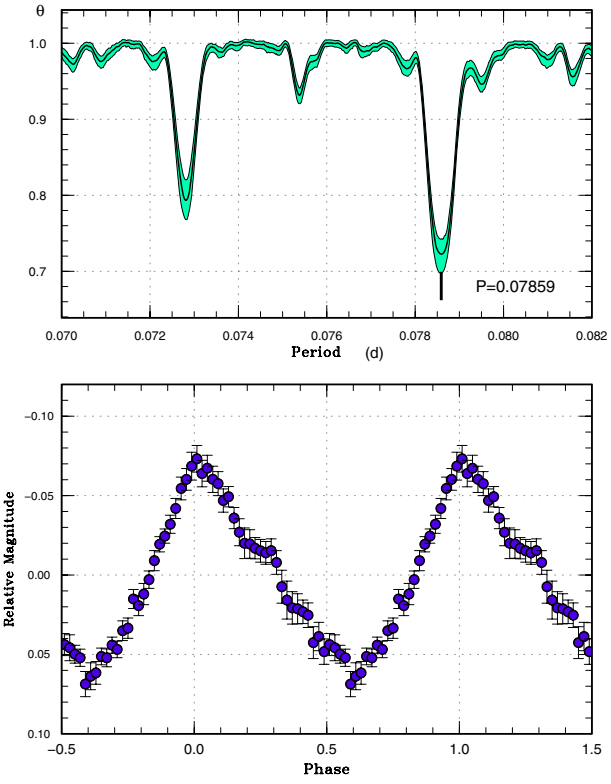

Fig. 24. Positive superhumps in BK Lyn (2012 April). Upper: PDM analysis. A period at 0.0728 d is a one-day alias of the superhump period. This period coincided with that of negative superhumps by chance. Lower: Phase-averaged profile.

intriguing case. The unusual behavior of superhumps in CC Scl may be related to the magnetism of the white dwarf.

3.34. V1208 Tauri

We observed the 2011 December superoutburst of this object, but it is likely that we missed the initial part of the outburst. The times of superhump maxima are listed in table 42. The $O - C$ values were close to zero, which strengthens the identification of these superhumps with stage-C superhumps. It is likely that both 2000 and 2002 observations (Kato et al. 2009) also recorded stage-C superhumps, which was not labeled as such in table 2 of Kato et al. (2009).

3.35. V1212 Tauri

Although the object underwent a superoutburst in 2011 January–February, it again did another in September–October. The times of superhump maxima are listed in table 43. The period given in table 2 was determined by the PDM method. The value of the period suggests that we observed either the very start of stage B or stage C. The supercycle length of this object is ~ 240 d.

Table 30. Superhump maxma of BK Lyn (2012 February–March).

E	Max*	Error	$O - C$†	N‡
0	55971.6983	0.0012	0.0155	69
1	55971.7771	0.0012	0.0159	75
2	55971.8456	0.0011	0.0061	76
3	55971.9115	0.0015	−0.0062	71
9	55972.3785	0.0006	−0.0088	39
10	55972.4569	0.0005	−0.0087	41
21	55973.3168	0.0021	−0.0099	21
22	55973.3992	0.0008	−0.0059	40
23	55973.4779	0.0012	−0.0054	40
24	55973.5590	0.0008	−0.0026	39
25	55973.6400	0.0009	0.0001	39
26	55973.7193	0.0010	0.0012	20
73	55977.3967	0.0015	−0.0006	72
74	55977.4807	0.0049	0.0051	43
76	55977.6363	0.0027	0.0041	71

* BJD − 2400000.
† Against max = 2455971.6828 + 0.078280E.
‡ Number of points used to determine the maximum.

Table 31. Times of negative superhumps in BK Lyn.

E	Max*	Error	$O-C^{\dagger}$	$N^{\ddagger}$	E	Max*	Error	$O-C^{\dagger}$	$N^{\ddagger}$
0	55980.3754	0.0007	0.0147	38	274	56000.3215	0.0007	−0.0043	59
1	55980.4487	0.0017	0.0153	38	275	56000.3944	0.0005	−0.0043	94
3	55980.5802	0.0018	0.0010	37	276	56000.4666	0.0004	−0.0049	96
4	55980.6492	0.0011	−0.0028	38	277	56000.5342	0.0008	−0.0102	74
7	55980.8787	0.0011	0.0080	33	278	56000.6064	0.0006	−0.0109	118
8	55980.9500	0.0028	0.0065	35	279	56000.6762	0.0006	−0.0139	144
14	55981.3926	0.0006	0.0118	39	280	56000.7488	0.0003	−0.0142	169
15	55981.4669	0.0007	0.0133	37	281	56000.8213	0.0004	−0.0146	159
16	55981.5455	0.0014	0.0191	37	282	56000.9008	0.0010	−0.0079	65
17	55981.6180	0.0020	0.0186	38	288	56001.3384	0.0004	−0.0076	90
21	55981.8987	0.0005	0.0079	33	289	56001.4108	0.0003	−0.0080	165
22	55981.9707	0.0020	0.0071	35	290	56001.4818	0.0003	−0.0099	164
35	55982.9136	0.0006	0.0027	37	291	56001.5541	0.0004	−0.0104	138
36	55982.9856	0.0014	0.0018	35	292	56001.6257	0.0004	−0.0117	160
83	55986.4151	0.0016	0.0066	38	293	56001.6982	0.0005	−0.0120	154
84	55986.4814	0.0014	0.0001	33	294	56001.7739	0.0004	−0.0092	118
85	55986.5601	0.0013	0.0059	34	295	56001.8487	0.0003	−0.0073	127
86	55986.6320	0.0009	0.0050	37	302	56002.3597	0.0005	−0.0064	52
96	55987.3671	0.0016	0.0114	34	303	56002.4311	0.0005	−0.0078	60
97	55987.4377	0.0017	0.0091	37	304	56002.5064	0.0005	−0.0054	61
98	55987.5104	0.0029	0.0089	20	305	56002.5792	0.0006	−0.0054	60
99	55987.5807	0.0010	0.0064	37	307	56002.7236	0.0004	−0.0068	70
100	55987.6514	0.0012	0.0042	74	308	56002.7958	0.0006	−0.0074	70
114	55988.6707	0.0007	0.0034	70	316	56003.3838	0.0005	−0.0024	67
115	55988.7376	0.0010	−0.0026	70	319	56003.6021	0.0007	−0.0026	77
128	55989.6868	0.0011	−0.0006	107	320	56003.6714	0.0004	−0.0062	96
129	55989.7556	0.0009	−0.0047	109	321	56003.7420	0.0008	−0.0085	70
130	55989.8273	0.0006	−0.0059	76	322	56003.8161	0.0006	−0.0073	61
131	55989.9025	0.0008	−0.0036	38	334	56004.6958	0.0008	−0.0020	71
132	55989.9795	0.0006	0.0006	27	335	56004.7690	0.0007	−0.0016	70
142	55990.7038	0.0018	−0.0037	29	343	56005.3553	0.0007	0.0018	52
143	55990.7704	0.0006	−0.0100	28	346	56005.5768	0.0005	0.0047	31
144	55990.8470	0.0009	−0.0063	37	347	56005.6492	0.0006	0.0041	58
145	55990.9213	0.0009	−0.0049	36	349	56005.7955	0.0019	0.0048	40
146	55990.9992	0.0013	0.0002	32	357	56006.3766	0.0006	0.0030	150
205	55995.2980	0.0015	−0.0001	37	358	56006.4429	0.0005	−0.0036	161
206	55995.3687	0.0010	−0.0022	105	359	56006.5174	0.0005	−0.0020	150
207	55995.4409	0.0019	−0.0029	61	360	56006.5887	0.0007	−0.0036	119
208	55995.5085	0.0016	−0.0082	30	370	56007.3278	0.0005	0.0069	38
220	55996.3870	0.0015	−0.0040	37	384	56008.3424	0.0005	0.0014	99
233	55997.3443	0.0015	0.0060	28	385	56008.4199	0.0003	0.0060	99
234	55997.4104	0.0020	−0.0008	37	386	56008.4893	0.0006	0.0025	90
235	55997.4785	0.0015	−0.0056	36	387	56008.5628	0.0007	0.0032	132
237	55997.6176	0.0013	−0.0122	37	388	56008.6355	0.0005	0.0030	82
238	55997.6893	0.0015	−0.0134	26	390	56008.7829	0.0007	0.0047	64
247	55998.3545	0.0010	−0.0039	33	398	56009.3636	0.0008	0.0025	67
248	55998.4217	0.0017	−0.0096	36	399	56009.4342	0.0006	0.0002	67
249	55998.4863	0.0012	−0.0179	37	400	56009.5119	0.0008	0.0051	66
261	55999.3772	0.0008	−0.0014	149	402	56009.6606	0.0008	0.0080	65
262	55999.4466	0.0006	−0.0049	155	403	56009.7327	0.0013	0.0072	70
263	55999.5109	0.0006	−0.0134	85	404	56009.7992	0.0014	0.0008	66
264	55999.5829	0.0004	−0.0142	83	425	56011.3411	0.0003	0.0125	162
265	55999.6572	0.0009	−0.0128	80	426	56011.4104	0.0004	0.0090	233
266	55999.7331	0.0010	−0.0098	76	427	56011.4817	0.0003	0.0074	238
267	55999.8042	0.0010	−0.0115	69	428	56011.5444	0.0005	−0.0027	136

Table 31. (Continued)

E	Max*	Error	$O-C^{\dagger}$	$N^{\ddagger}$	E	Max*	Error	$O-C^{\dagger}$	$N^{\ddagger}$
431	56011.7727	0.0005	0.0069	48	482	56015.4887	0.0007	0.0068	201
439	56012.3546	0.0003	0.0059	220	483	56015.5588	0.0006	0.0041	162
440	56012.4247	0.0003	0.0031	212	484	56015.6340	0.0005	0.0064	50
441	56012.5003	0.0003	0.0059	124	494	56016.3649	0.0006	0.0086	211
444	56012.7173	0.0008	0.0043	70	495	56016.4368	0.0006	0.0077	182
445	56012.7888	0.0006	0.0029	61	496	56016.5051	0.0005	0.0031	125
453	56013.3721	0.0002	0.0033	213	498	56016.6493	0.0007	0.0016	46
454	56013.4456	0.0003	0.0040	215	508	56017.3803	0.0005	0.0039	71
455	56013.5206	0.0003	0.0061	111	509	56017.4536	0.0007	0.0044	108
467	56014.3951	0.0004	0.0062	196	510	56017.5283	0.0008	0.0062	74
468	56014.4673	0.0004	0.0056	163	522	56018.3972	0.0005	0.0007	60
469	56014.5387	0.0004	0.0041	131	523	56018.4714	0.0003	0.0020	62
470	56014.6154	0.0011	0.0080	23	524	56018.5430	0.0004	0.0008	61
471	56014.6861	0.0008	0.0057	56	530	56018.9824	0.0006	0.0030	129
472	56014.7585	0.0008	0.0053	56	540	56019.7023	0.0011	−0.0058	71
480	56015.3382	0.0010	0.0020	299	544	56020.0010	0.0010	0.0015	150
481	56015.4170	0.0006	0.0080	281					

* BJD − 2400000.
† Against max = 2455980.3606 + 0.072866E.
‡ Number of points used to determine the maximum.

3.36. *DI Ursae Majoris*

Since the online data for Rutkowski et al. (2009) are available, we extracted the times of superhump maxima for two superoutbursts in 2007 using our method (tables 44 and 45). The resultant values of $P_{\rm dot}$ were not very different from those obtained through an analysis by Rutkowski et al. (2009). Although we listed the times of maxima before the superoutburst ($E \leq 2$) and after the superoutburst ($E \geq 216$) for the first superoutburst, these maxima may not be equivalent to stage-A and stage-C superhumps in other SU UMa-type dwarf novae. Although there may be either a discontinuous period change or a phase shift during the period between $E = 182$ and $E = 216$, we were not able to make the distinction using the available data. The second superoutburst was less observed, and the resultant $P_{\rm dot}$ was less reliable. We also analyzed the entire 2007 light curve to determine the orbital period. We detected a strong signal with a period of 0.0545665(8) d. This period is closer to the spectroscopic period of 0.054564(2) d obtained by Thorstensen et al. (2002b) than that obtained by Rutkowski et al. (2009), and it is likely to represent the correct orbital period. The better-determined ϵ of the first superoutburst was 1.4%, and there was no need for modification of the ϵ given by Rutkowski et al. (2009). This ϵ is fairly common among such short-$P_{\rm orb}$ objects, and we cannot discriminate DI UMa from other SU UMa-type dwarf novae by ϵ only.

3.37. *IY Ursae Majoris*

We observed a superoutburst in 2011 June. Only two superhump maxima were recorded: BJD 2455717.0312(4) ($N = 60$) and BJD 2455718.0930(17) ($N = 68$).

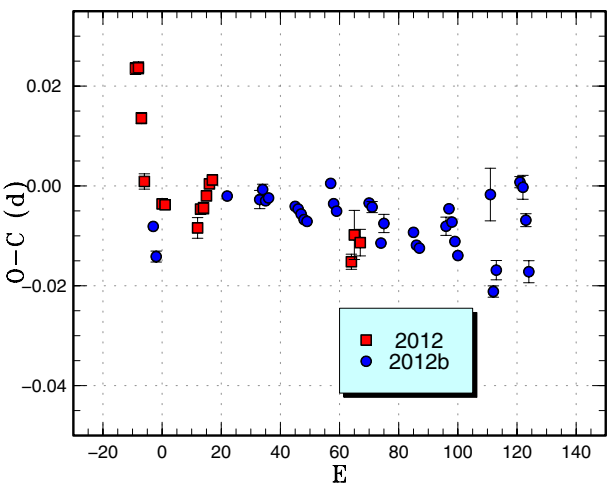

Fig. 25. Comparison of different superoutbursts of positive superhumps of BK Lyn in the $O-C$ diagram. The abbreviation for the 2012 February–March superoutburst is 2012 and the 2012 April one is 2012b. A period of 0.07859 d was used to draw this figure. Approximate cycle counts (E) after the appearance of positive superhumps were used. The maxima for $E < 0$ are negative superhumps. As known in ER UMa (Ohshima et al. 2012), there were relatively large intranight $O-C$ variations against the mean period of positive superhumps, which can be interpreted as being a result of the coexistence of negative superhumps.

3.38. *KS Ursae Majoris*

We observed a superoutburst in 2012 May. Only two superhump maxima were recorded: BJD 2456052.0468(13) ($N = 52$) and BJD 2456052.1159(18) ($N = 50$).

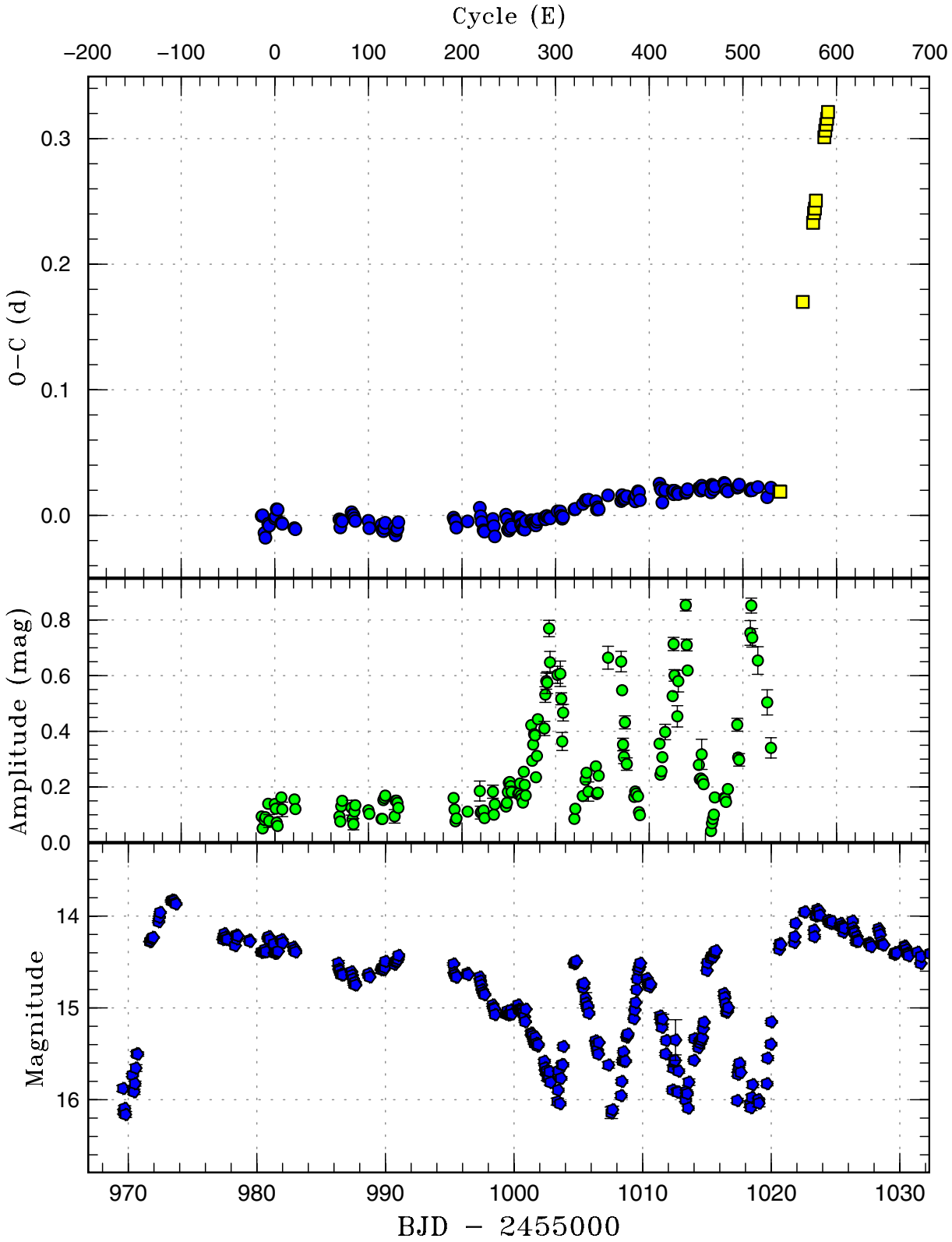

Fig. 26. $O - C$ diagram of negative superhumps in BK Lyn (2012). Upper: $O - C$. Filled circles and filled squares represent negative and positive superhumps, respectively. The positive superhumps appeared when the next superoutburst started, and the phase of the hump maximum was continuous with that of the preceding negative superhumps. The maxima of positive superhumps during the first superoutburst are not shown. We used a period of 0.07280 d for calculating the $O - C$ residuals. Middle: Amplitudes of negative superhumps. The amplitudes become larger when the system fades. Lower: Light curve. The supercycle is $\sim$ 50 d, and there were three normal outbursts between the two superoutbursts.

Table 32. Superhump maxima of BK Lyn (2012 April).

E	Max*	Error	$O-C^\dagger$	$N^\ddagger$
0	56020.6533	0.0009	−0.0043	67
1	56020.7259	0.0011	−0.0102	66
25	56022.6242	0.0004	0.0029	142
36	56023.4880	0.0018	0.0027	62
37	56023.5685	0.0011	0.0047	95
38	56023.6449	0.0005	0.0025	71
39	56023.7240	0.0006	0.0031	70
48	56024.4297	0.0005	0.0018	66
49	56024.5077	0.0006	0.0013	73
50	56024.5853	0.0006	0.0003	94
51	56024.6628	0.0004	−0.0007	146
52	56024.7410	0.0005	−0.0011	139
60	56025.3774	0.0005	0.0069	82
61	56025.4519	0.0005	0.0029	82
62	56025.5290	0.0005	0.0014	90
73	56026.3951	0.0008	0.0035	75
74	56026.4729	0.0011	0.0027	75
77	56026.7014	0.0009	−0.0043	76
78	56026.7839	0.0018	−0.0004	43
88	56027.5681	0.0009	−0.0017	43
89	56027.6441	0.0005	−0.0043	70
90	56027.7221	0.0005	−0.0048	66
99	56028.4338	0.0018	−0.0000	88
100	56028.5159	0.0008	0.0035	50
101	56028.5918	0.0007	0.0009	74
102	56028.6665	0.0006	−0.0030	69
103	56028.7423	0.0008	−0.0057	63
114	56029.6190	0.0053	0.0069	51
115	56029.6781	0.0011	−0.0124	66
116	56029.7610	0.0019	−0.0081	40
124	56030.4074	0.0011	0.0098	153
125	56030.4849	0.0024	0.0089	104
126	56030.5569	0.0013	0.0023	69
127	56030.6252	0.0022	−0.0080	91

* BJD − 2400000.
† Against max = 2456020.6576 + 0.078548E.
‡ Number of points used to determine the maximum.

Table 33. Superhump maxima of V585 Lyr (2012).

E	Max*	Error	$O-C^\dagger$	$N^\ddagger$
0	56045.1580	0.0005	−0.0005	123
1	56045.2195	0.0006	0.0006	71
18	56046.2441	0.0008	−0.0025	124
19	56046.3094	0.0023	0.0023	68

* BJD − 2400000.
† Against max = 2456045.1584 + 0.060454E.
‡ Number of points used to determine the maximum.

Table 34. Superhump maxima of FQ Mon (2011).

E	Max*	Error	$O-C^\dagger$	$N^\ddagger$
0	55922.0918	0.0011	−0.0015	130
1	55922.1676	0.0033	0.0015	67
13	55923.0405	0.0020	0.0018	91
14	55923.1096	0.0015	−0.0018	130

* BJD − 2400000.
† Against max = 2455922.0934 + 0.072718E.
‡ Number of points used to determine the maximum.

Table 35. Superhump maxima of V1032 Oph (2012).

E	Max*	Error	$O-C^\dagger$	Phase‡	$N^\ddagger$
0	56076.3539	0.0046	−0.0101	0.52	80
9	56077.1475	0.0015	0.0098	0.23	127
12	56077.3984	0.0009	0.0029	0.15	148
47	56080.4017	0.0012	−0.0026	0.29	150

* BJD − 2400000.
† Against max = 2456076.3640 + 0.085965E.
‡ Number of points used to determine the maximum.

3.39. MR Ursae Majoris

The times of the superhump maxima during the 2012 superoutburst are listed in table 46. Only the late stage of the outburst was observed, and we recorded typical stage-C superhumps. A comparison of different superoutbursts in the $O-C$ diagram is shown in figure 35.

3.40. PU Ursae Majoris

PU UMa (= SDSS J090103.93+480911.1) originally discovered by Szkody et al. (2003) is a deeply eclipsing CV below the period gap (Dillon et al. 2008). Three past outbursts were recorded before 2012: 2007 October (likely normal outburst), 2009 May (superoutburst; although superhumps were detected, the period under the observation was insufficient to determine the superhump period), and 2009 December (likely normal outburst).

The 2012 outburst was detected by J. Shears (BAAVSS alert 2830). Subsequent observations detected developing superhumps and eclipses (vsnet-alert 14201, 14214, 14215). The times of recorded eclipses were determined by the Kwee and van Woerden (KW) method (Kwee & van Woerden 1956; modified by the present authors, see the Appendix), after removing linearly approximated trends near eclipses in order to minimize the effect of superhumps; they are summarized in table 47. We obtained an updated ephemeris of

$$\mathrm{Min(BJD)} = 2453773.4875(3) + 0.07788054(1)E. \quad (2)$$

The times of the superhump maxima outside the eclipse are listed in table 48. Except for $E = 0$ (stage A), there is a hint as to the stage B–C transition at around $E = 48$. Its overall pattern is similar to those of relatively long P_{orb} systems, such as EG Aqr (Imada et al. 2008b) and NSV 4838 (Imada et al. 2009).

Table 36. Superhump maxima of V1159 Ori (2012).

E	Max*	Error	$O-C^{\dagger}$	$N^{\ddagger}$
0	55991.6169	0.0004	0.0065	123
1	55991.6826	0.0004	0.0074	124
16	55992.6410	0.0010	−0.0046	57
30	55993.5407	0.0012	−0.0106	42
31	55993.6059	0.0023	−0.0101	57
61	55995.5631	0.0005	0.0064	54
62	55995.6264	0.0009	0.0049	58
77	55996.5919	0.0011	0.0000	58

* BJD − 2400000.
† Against max = 2455991.6105 + 0.064694E.
‡ Number of points used to determine the maximum.

Table 37. Superhump maxima of AR Pic (2011).

E	Max*	Error	$O-C^{\dagger}$	$N^{\ddagger}$
0	55910.5774	0.0018	0.0038	20
1	55910.6570	0.0014	0.0002	25
2	55910.7425	0.0011	0.0026	29
3	55910.8225	0.0017	−0.0005	29
13	55911.6510	0.0016	−0.0036	25
24	55912.5752	0.0144	0.0059	19
25	55912.6474	0.0066	−0.0051	17
26	55912.7304	0.0022	−0.0052	23
38	55913.7164	0.0111	−0.0171	27
39	55913.8294	0.0034	0.0128	29
50	55914.7376	0.0093	0.0063	28

* BJD − 2400000.
† Against max = 2455910.5736 + 0.083154E.
‡ Number of points used to determine the maximum.

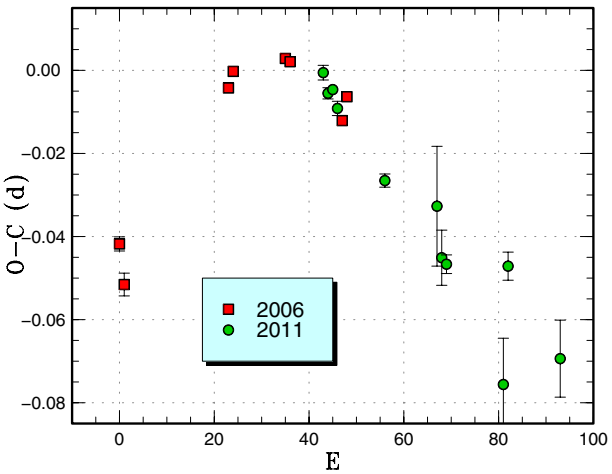

Fig. 27. Comparison of different superoutbursts of AR Pic in the $O-C$ diagram. A period of 0.08458 d was used to draw this figure. Approximate cycle counts (E) after the start of the superoutburst were used.

Table 38. Superhump maxima of GV Psc (2011).

E	Max*	Error	$O-C^{\dagger}$	$N^{\ddagger}$
0	55852.3350	0.0003	−0.0003	95
1	55852.4291	0.0003	−0.0005	86
4	55852.7127	0.0003	0.0001	94
5	55852.8055	0.0003	−0.0014	87
11	55853.3728	0.0003	−0.0000	90
12	55853.4688	0.0005	0.0016	99
25	55854.6952	0.0003	0.0020	99
26	55854.7867	0.0004	−0.0008	90
61	55858.0892	0.0008	0.0007	62
62	55858.1814	0.0007	−0.0014	61

* BJD − 2400000.
† Against max = 2455852.3354 + 0.094313E.
‡ Number of points used to determine the maximum.

The ϵ values for stage-B and stage-C superhumps were 4.1% and 3.7%, respectively, and slightly larger than typical values of SU UMa-type dwarf novae with these $P_{\rm orb}$. A mean profile of stage-B superhumps is shown in figure 36. Shears et al. (2012a) also reported on observations of the same superoutburst, although they did not distinguish between stage-B and stage-C superhumps.

3.41. SS Ursae Minoris

Olech et al. (2006) reported on observations of the 2004 superoutburst, and obtained a mean period of 0.070149(16) d with a negative (global) $P_{\rm dot}$. We observed the late stage of a superoutburst in 2012 March. As presented in Olech et al. (2006), the main peak of the superhump was already diminishing, and the secondary maximum was developing. We list the times of the maxima of these humps in table 49. At this and the following stages, the secondary humps were the dominant signal; they are listed in table 50. These secondary humps persisted during the quiescent state following the superoutburst, and the behavior is similar to the late stage of VW Hyi (subsection 3.22) and V344 Lyr (Wood et al. 2011; Kato et al. 2012a). Since SS UMi is considered to have a high mass-transfer rate, comparable to ER UMa stars (Kato et al. 2000a; Olech et al. 2006), these secondary humps are possibly "traditional" late superhumps arising from the stream impact point. The signal became less convincing after the next normal outburst. A period analysis of the entire observation (BJD 2456007–2456038) yielded a photometric orbital period of 0.067855(7) d, which is slightly longer than the spectroscopic period of 0.06778(4) d in Thorstensen et al. (1996).

3.42. 1RXS J231935.0+364705

This object (hereafter 1RXS J231935) was selected as a variable star, as a likely dwarf nova, during the course of identification of the ROSAT sources (Denisenko & Sokolovsky 2011). The two previously known outbursts occurred in 2009 November and 2010 December, and both appeared to be normal outbursts (H. Maehara detected no superhumps during the 2009 outburst). The 2011 September outburst was detected by E. Muyllaert (BAAVSS alert 2710). Subsequent observations confirmed the presence of superhumps (vsnet-

Table 39. Superhump maxima of BW Scl (2011).

E	Max*	Error	$O-C^{\dagger}$	$N^{\ddagger}$	E	Max*	Error	$O-C^{\dagger}$	$N^{\ddagger}$
0	55865.5288	0.0016	−0.0209	89	94	55870.7217	0.0003	−0.0016	44
1	55865.5827	0.0022	−0.0221	61	104	55871.2706	0.0001	−0.0030	238
2	55865.6444	0.0031	−0.0155	89	105	55871.3265	0.0002	−0.0022	237
3	55865.6992	0.0044	−0.0157	89	106	55871.3808	0.0003	−0.0029	197
8	55865.9875	0.0003	−0.0026	426	108	55871.4894	0.0006	−0.0045	24
9	55866.0407	0.0004	−0.0044	187	109	55871.5484	0.0006	−0.0004	33
10	55866.0966	0.0006	−0.0035	154	110	55871.5994	0.0003	−0.0045	40
17	55866.4844	0.0030	−0.0010	50	111	55871.6557	0.0004	−0.0033	40
18	55866.5415	0.0005	0.0011	89	112	55871.7096	0.0006	−0.0043	40
19	55866.6000	0.0004	0.0045	88	123	55872.3150	0.0003	−0.0044	219
20	55866.6558	0.0004	0.0053	89	124	55872.3748	0.0004	0.0004	237
21	55866.7103	0.0008	0.0048	89	126	55872.4877	0.0014	0.0032	222
25	55866.9339	0.0003	0.0082	279	127	55872.5363	0.0005	−0.0033	152
26	55866.9873	0.0002	0.0065	305	128	55872.5938	0.0009	−0.0007	40
27	55867.0432	0.0003	0.0074	274	129	55872.6470	0.0008	−0.0026	40
28	55867.0976	0.0004	0.0068	223	130	55872.7023	0.0008	−0.0024	41
31	55867.2628	0.0001	0.0069	238	140	55873.2540	0.0005	−0.0010	155
32	55867.3191	0.0001	0.0081	238	141	55873.3079	0.0002	−0.0022	238
33	55867.3729	0.0001	0.0069	236	142	55873.3626	0.0002	−0.0025	235
34	55867.4282	0.0003	0.0071	125	143	55873.4179	0.0002	−0.0022	240
35	55867.4830	0.0001	0.0069	281	144	55873.4718	0.0004	−0.0033	161
36	55867.5371	0.0001	0.0060	302	145	55873.5282	0.0006	−0.0021	32
37	55867.5926	0.0002	0.0065	75	146	55873.5822	0.0003	−0.0031	40
38	55867.6471	0.0002	0.0059	89	147	55873.6364	0.0004	−0.0039	41
39	55867.7022	0.0002	0.0060	89	148	55873.6916	0.0004	−0.0037	40
46	55868.0864	0.0002	0.0049	89	152	55873.9127	0.0019	−0.0027	76
47	55868.1424	0.0002	0.0058	68	153	55873.9670	0.0010	−0.0035	115
54	55868.5261	0.0004	0.0044	89	154	55874.0217	0.0010	−0.0038	114
55	55868.5816	0.0003	0.0048	88	158	55874.2507	0.0014	0.0050	133
56	55868.6357	0.0003	0.0039	89	159	55874.2986	0.0002	−0.0021	238
57	55868.6911	0.0003	0.0042	88	160	55874.3519	0.0004	−0.0039	235
58	55868.7479	0.0005	0.0059	55	161	55874.4064	0.0003	−0.0044	237
63	55869.0200	0.0002	0.0029	144	162	55874.4653	0.0004	−0.0006	237
64	55869.0756	0.0003	0.0035	182	163	55874.5174	0.0004	−0.0035	232
65	55869.1295	0.0003	0.0023	102	164	55874.5729	0.0004	−0.0030	40
72	55869.5126	0.0006	0.0001	91	165	55874.6268	0.0007	−0.0042	40
73	55869.5701	0.0012	0.0026	65	166	55874.6858	0.0007	−0.0003	40
74	55869.6238	0.0004	0.0013	89	167	55874.7388	0.0005	−0.0022	32
75	55869.6781	0.0005	0.0005	89	182	55875.5660	0.0007	−0.0006	40
76	55869.7328	0.0005	0.0002	84	183	55875.6218	0.0010	0.0001	40
80	55869.9520	0.0005	−0.0008	141	184	55875.6762	0.0016	−0.0005	40
81	55870.0068	0.0004	−0.0010	165	185	55875.7297	0.0014	−0.0020	40
82	55870.0626	0.0004	−0.0003	237	207	55876.9523	0.0010	0.0097	60
83	55870.1169	0.0002	−0.0010	93	208	55877.0060	0.0005	0.0084	50
84	55870.1713	0.0003	−0.0017	84	209	55877.0583	0.0005	0.0057	100
90	55870.5005	0.0004	−0.0026	33	210	55877.1150	0.0008	0.0074	58
91	55870.5567	0.0004	−0.0015	37	218	55877.5496	0.0019	0.0016	24
92	55870.6106	0.0003	−0.0027	44	219	55877.6102	0.0026	0.0072	25
93	55870.6659	0.0003	−0.0024	43	220	55877.6578	0.0025	−0.0003	25

* BJD − 2400000.
† Against max = 2455865.5497 + 0.055038E.
‡ Number of points used to determine the maximum.

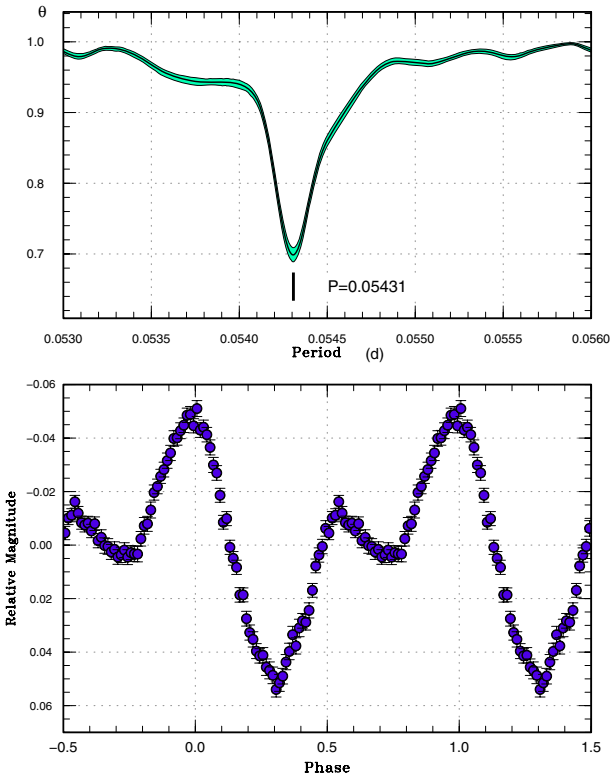

Fig. 28. Early superhumps in BW Scl (2011). Upper: PDM analysis. Lower: Phase-averaged profile.

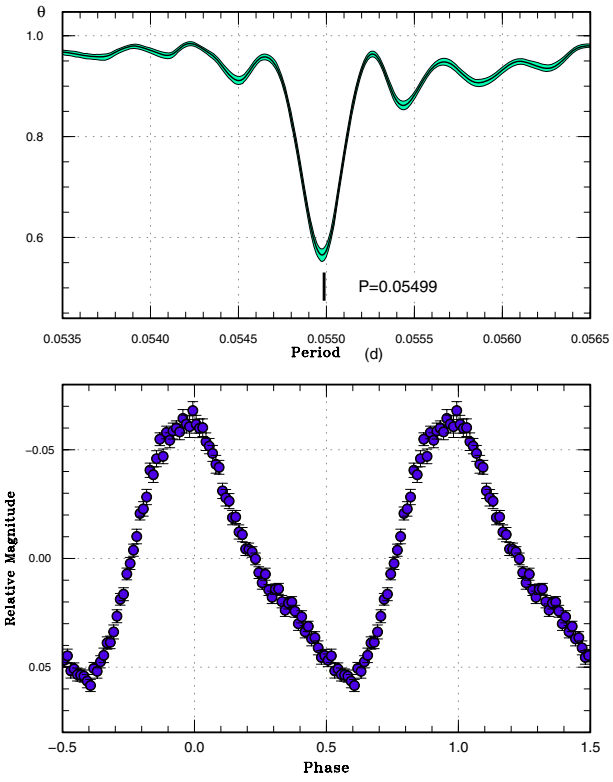

Fig. 29. Ordinary superhumps in BW Scl (2011). Upper: PDM analysis. Lower: Phase-averaged profile.

alert 13711, 13712, 13719; figure 37). The times of superhump maxima are listed in table 51. The $O - C$ diagram clearly shows the familiar pattern of stages B and C. The $P_{\rm dot}$ for stage-B superhumps was large [$+11.6(1.7) \times 10^{-5}$], typical for an object with this $P_{\rm SH}$.

3.43. ASAS J224349+0809.5

The 2011 June outburst of this object (hereafter ASAS J224349) was detected by Y. Maeda at a visual magnitude of 13.2 (vsnet-alert 13458). Due to the seasonal unfavorable conditions, we obtained only two superhump maxima: BJD 2455740.6014(5) ($N = 40$) and 2455741.5730(5) ($N = 49$).

3.44. DDE 19

DDE 19 is a CV discovered by D. Denisenko.[5] The object is located at $00^{\rm h}38^{\rm m}37\overset{\rm s}{.}40$, $+79°21'37\overset{''}{.}5$ (J2000.0). During its outburst in 2011 November, superhumps were detected (vsnet-alert 13886, 13890; figure 38). The times of superhump maxima are listed in table 52. The object faded quickly after these observations, and we observed only the late stage of this superoutburst. We attributed these superhumps to stage-C superhumps listed in table 2.

3.45. MASTER OT J072948.66+593824.4

This object (hereafter MASTER J072948) is a transient detected at an unfiltered CCD magnitude of 13.3 on 2012 February 17 (Balanutsa et al. 2012c; see also vsnet-alert 14249). Although subsequent observations detected superhump-like modulations (vsnet-alert 14252), their waveform was rather irregular, and the variation did not appear to be expressed by a single period (vsnet-alert 14253, 14258, 14263). The observed maxima cannot be expressed by any single period, and it is likely that there was a superposition of two close periods (vsnet-alert 14265).

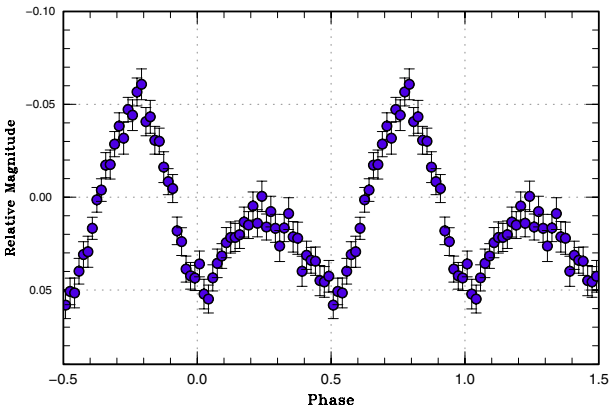

Fig. 30. Averaged orbital profile of BW Scl (2011) after the rapid decline.

PDM and Lasso analyses (see subsection 3.78 for the application of Lasso and the separation of two signals) are shown

[5] ⟨http://hea.iki.rssi.ru/∼denis/VarDDE.html⟩.

Table 40. Late-stage superhumps in BW Scl (2011).

E	Max*	Error	$O-C^{\dagger}$	$N^{\ddagger}$	E	Max*	Error	$O-C^{\dagger}$	$N^{\ddagger}$
0	55878.5682	0.0018	0.0005	25	200	55889.5946	0.0013	0.0069	59
1	55878.6229	0.0020	0.0000	25	217	55890.5255	0.0005	0.0012	58
2	55878.6792	0.0016	0.0013	25	218	55890.5817	0.0006	0.0023	59
3	55878.7354	0.0013	0.0024	22	231	55891.2933	0.0005	−0.0025	127
6	55878.9046	0.0013	0.0063	106	232	55891.3512	0.0004	0.0003	127
9	55879.0664	0.0003	0.0028	83	233	55891.4057	0.0004	−0.0003	127
10	55879.1202	0.0006	0.0014	84	235	55891.5101	0.0017	−0.0061	56
17	55879.4966	0.0079	−0.0078	12	236	55891.5659	0.0008	−0.0054	59
18	55879.5597	0.0019	0.0002	19	242	55891.8982	0.0013	−0.0037	55
19	55879.6089	0.0020	−0.0058	20	243	55891.9565	0.0010	−0.0005	68
20	55879.6700	0.0016	0.0002	19	245	55892.0659	0.0007	−0.0012	22
21	55879.7182	0.0024	−0.0067	19	246	55892.1261	0.0013	0.0039	19
27	55880.0462	0.0011	−0.0093	110	264	55893.1127	0.0049	−0.0014	29
28	55880.1026	0.0007	−0.0079	86	272	55893.5538	0.0019	−0.0010	31
35	55880.4947	0.0025	−0.0015	10	273	55893.6157	0.0029	0.0057	24
38	55880.6570	0.0008	−0.0045	19	280	55893.9866	0.0026	−0.0091	27
39	55880.7171	0.0008	0.0005	16	281	55894.0568	0.0046	0.0061	19
43	55880.9349	0.0024	−0.0021	61	285	55894.2767	0.0004	0.0055	104
45	55881.0489	0.0004	0.0016	97	287	55894.3843	0.0004	0.0030	126
49	55881.2693	0.0001	0.0016	390	288	55894.4320	0.0004	−0.0044	127
50	55881.3184	0.0002	−0.0044	476	303	55895.2698	0.0009	0.0068	90
51	55881.3792	0.0002	0.0014	474	304	55895.3173	0.0005	−0.0008	127
54	55881.5417	0.0010	−0.0014	18	305	55895.3718	0.0019	−0.0014	127
55	55881.5971	0.0009	−0.0011	19	308	55895.5409	0.0023	0.0025	30
56	55881.6483	0.0005	−0.0050	20	309	55895.6012	0.0012	0.0077	30
57	55881.7031	0.0017	−0.0054	19	310	55895.6448	0.0043	−0.0038	30
62	55881.9812	0.0012	−0.0027	76	336	55897.0768	0.0027	−0.0045	31
72	55882.5419	0.0013	0.0070	20	345	55897.5796	0.0010	0.0025	30
73	55882.5929	0.0008	0.0028	20	353	55898.0220	0.0009	0.0041	22
74	55882.6502	0.0007	0.0051	20	354	55898.0742	0.0013	0.0011	30
75	55882.7038	0.0004	0.0035	19	355	55898.1331	0.0018	0.0050	20
100	55884.0747	0.0005	−0.0030	55	362	55898.5154	0.0024	0.0015	26
108	55884.5163	0.0008	−0.0022	57	363	55898.5645	0.0028	−0.0045	30
109	55884.5752	0.0006	0.0016	59	364	55898.6223	0.0026	−0.0017	17
110	55884.6275	0.0005	−0.0013	58	372	55899.0623	0.0017	−0.0026	29
111	55884.6824	0.0010	−0.0014	58	373	55899.1255	0.0016	0.0056	28
114	55884.8482	0.0011	−0.0009	41	380	55899.5067	0.0012	0.0011	22
115	55884.9028	0.0005	−0.0014	38	381	55899.5630	0.0019	0.0022	30
116	55884.9684	0.0014	0.0091	31	382	55899.6172	0.0011	0.0014	19
117	55885.0094	0.0007	−0.0050	59	400	55900.6020	0.0022	−0.0057	15
118	55885.0703	0.0012	0.0008	37	417	55901.5496	0.0021	0.0053	20
123	55885.3416	0.0004	−0.0034	127	418	55901.5961	0.0017	−0.0033	16
124	55885.4023	0.0006	0.0021	99	436	55902.5986	0.0028	0.0074	18
126	55885.5076	0.0013	−0.0027	51	471	55904.5193	0.0017	−0.0004	30
127	55885.5614	0.0012	−0.0040	59	473	55904.6377	0.0032	0.0078	19
140	55886.2831	0.0004	0.0014	110	491	55905.6176	0.0019	−0.0041	15
141	55886.3414	0.0004	0.0046	127	527	55907.5997	0.0029	−0.0056	16
142	55886.3942	0.0007	0.0023	39	552	55908.9906	0.0015	0.0078	30
144	55886.5067	0.0004	0.0046	48	553	55909.0312	0.0025	−0.0067	30
145	55886.5594	0.0007	0.0022	59	594	55911.2995	0.0009	0.0025	126
146	55886.6157	0.0006	0.0034	44	612	55912.2892	0.0012	0.0004	102
163	55887.5493	0.0010	0.0003	59	613	55912.3463	0.0008	0.0024	126
164	55887.5986	0.0009	−0.0055	59	617	55912.5732	0.0044	0.0090	12
176	55888.2721	0.0003	0.0068	94	685	55916.2978	0.0005	−0.0133	116
177	55888.3224	0.0009	0.0020	127	726	55918.5678	0.0046	−0.0024	14
178	55888.3753	0.0004	−0.0002	108	885	55927.3339	0.0011	0.0029	126
181	55888.5423	0.0008	0.0015	59	886	55927.3744	0.0019	−0.0117	105
182	55888.5963	0.0008	0.0004	59	903	55928.3225	0.0003	−0.0003	85
199	55889.5340	0.0011	0.0014	58					

* BJD − 2400000.
† Against max = 2455878.5677 + 0.055100E.
‡ Number of points used to determine the maximum.

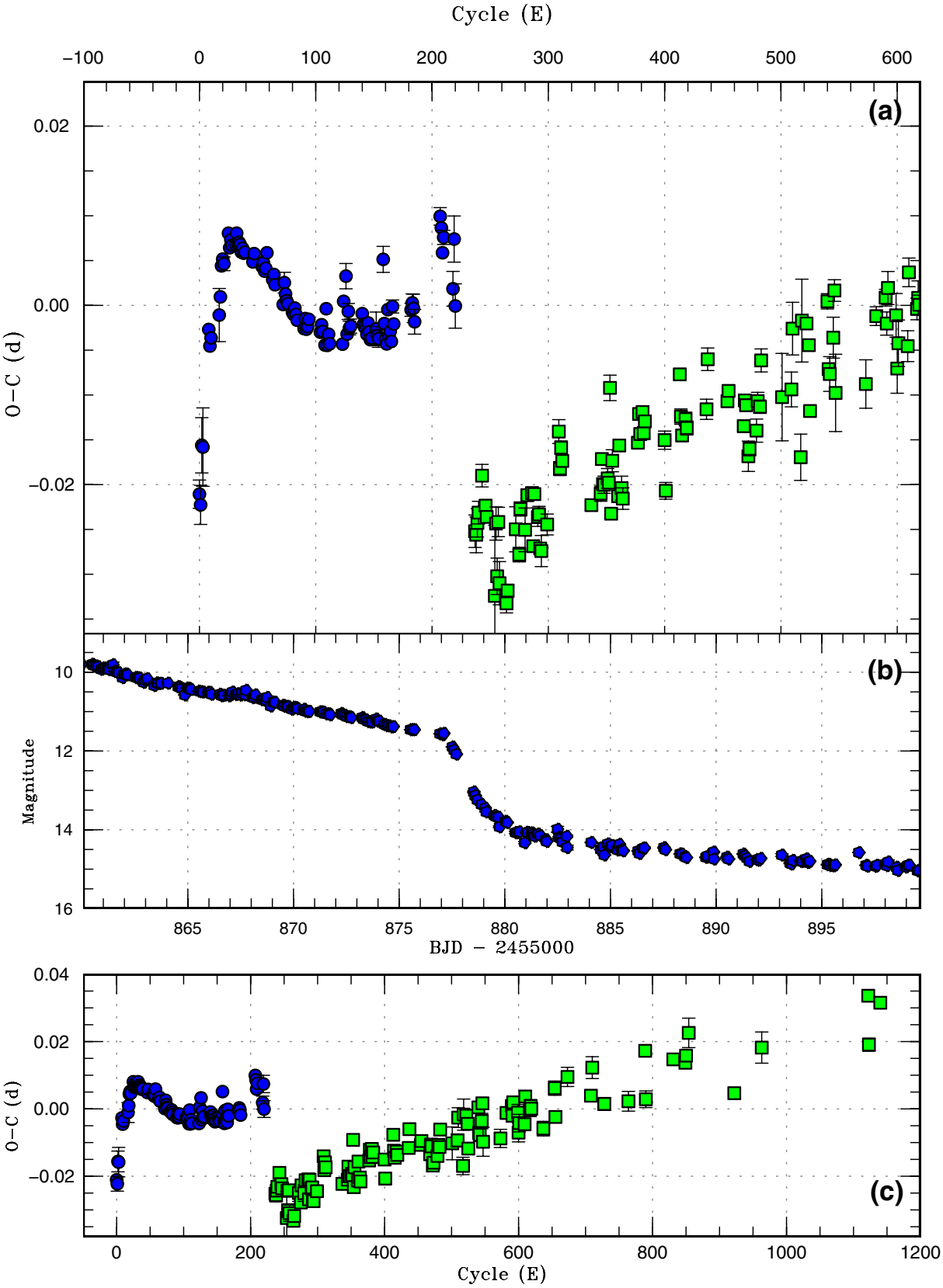

Fig. 31. $O - C$ diagram of superhumps in BW Scl (2011). (a) $O - C$. Filled circles and filled squares represent ordinary superhumps and late-stage superhumps after rapid fading. We used a period of 0.055036 d for calculating the $O - C$ residuals. (b) Light curve. (c) $O - C$ diagram of the entire observation. The global evolution of the $O - C$ diagram is remarkably similar to those of GW Lib and V455 And (Kato et al. 2009).

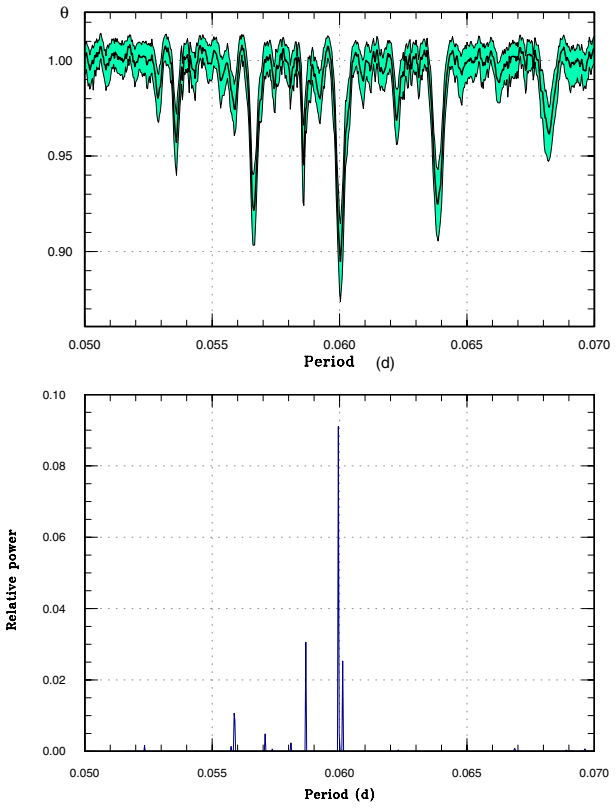

Fig. 32. Period analysis in CC Scl (2011). Upper: PDM analysis. Lower: Lasso analysis ($\log\lambda = -5.05$).

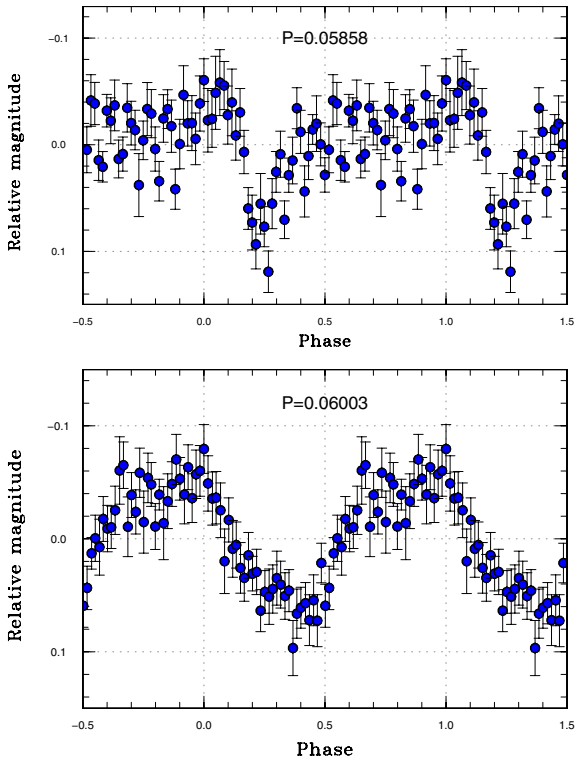

Fig. 33. Profiles of two periodicities in CC Scl (2011). Upper: Orbital variation. Lower: Superhump.

in figure 39. The Lasso analysis favored the co-existence of two periods, 0.06416(4) d and 0.06625(4) d. A period of 0.06208(3) d, a one-day alias of the 0.06625 d period, cannot be excluded instead of the 0.06625 d period. The mean profiles of these signals are shown in figure 40. While the 0.06416 d signal resembles superhumps in profile (faster rise, sharper maximum), the other signal has a sharper minimum. A combination of these signals partly reproduced the actual light curve during the plateau phase (figure 41). Based on its profile, we may identify the 0.06416 d signal as superhumps. We might then interpret the 0.06625 d period as orbital, and the 0.06416 d signal is 3.2% shorter than the orbital period. Although negative superhumps are unexpected in ordinary SU UMa-type dwarf novae, this interpretation might explain why the profile of superhumps was so unstable (as in ER UMa, cf. Ohshima et al. 2012), and why the orbital signal is so strongly visible in a non-eclipsing system. Since the object started rapidly fading only three days after the start of our observation, the base line for period analysis was insufficient to distinguish other possible periods or interpretations. Future observations in quiescence and in superoutbursts are absolutely needed.

3.46. MASTER OT J174305.70+231107.8

This object (hereafter MASTER J174305) is a transient detected at an unfiltered CCD magnitude of 15.6 on 2012 April 5 (Balanutsa et al. 2012a). Subsequent observations detected superhumps (vsnet-alert 14428; figure 42). Two superhump maxima were recorded: BJD 2456027.8604(12) ($N = 79$) and BJD 2456027.9281(9) ($N = 82$). The superhump period by the PDM method was 0.0670(5) d.

3.47. MASTER OT J182201.93+324906.7

This object (hereafter MASTER J182201) is a transient detected at an unfiltered CCD magnitude of 15.4 on 2012 April 29 (Balanutsa et al. 2012b). Subsequent observations detected superhumps (vsnet-alert 14529; figure 43). Two superhump maxima were recorded: BJD 2456050.4464(6) ($N = 33$) and 2456050.5081(4) ($N = 33$). The superhump period obtained by the PDM method was 0.0618(2) d (figure 43).

3.48. MisV 1446

MisV 1446 was detected to be a transient by the MISAO project, and it could probably be identified with the X-ray source 1RXS J074112.2−094529 (vsnet-alert 14080). The coordinates of the object are $07^{\rm h}41^{\rm m}12\overset{\rm s}{.}70$, $-09^\circ45'55\overset{''}{.}9$. Multicolor photometry by H. Sato was consistent with that of the color of a dwarf nova in outburst (vsnet-alert 14085). Subsequent observations recorded superhumps (vsnet-alert 14096, 14102, 14104; figure 44). The times of superhump maxima are listed in table 53. It appears that the observation recorded the late stage of a superoutburst, and that superhumps at the late part of stage B and at stage C were recorded. It was impossible to measure $P_{\rm dot}$ for stage B.

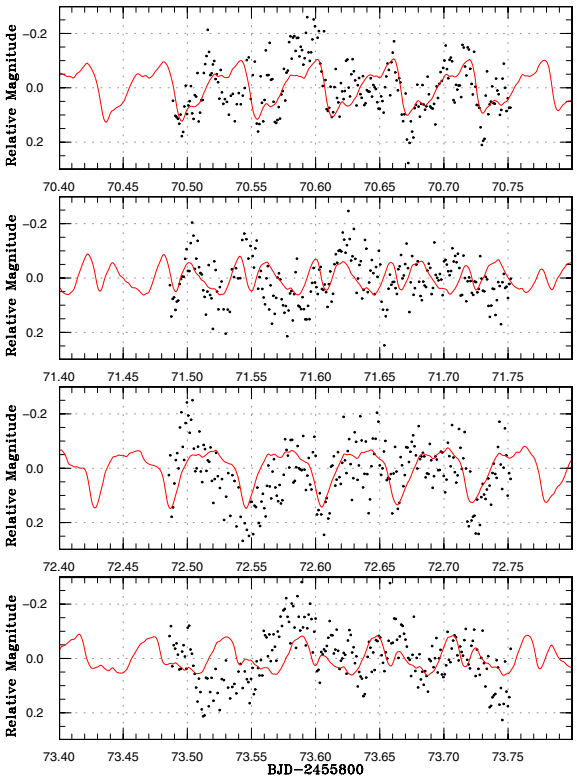

Fig. 34. Synthesized light curve of CC Scl (2011). Points represent observations. The curves represent the expected light curve by adding the two waves shown in figure 33.

Table 41. Superhump maxima of CC Scl (2011).

E	Max*	Error	$O-C^{\dagger}$	$N^{\ddagger}$
0	55870.5914	0.0009	−0.0043	47
1	55870.6551	0.0040	−0.0006	48
2	55870.7078	0.0017	−0.0079	48
15	55871.5040	0.0011	0.0082	38
16	55871.5482	0.0011	−0.0077	37
17	55871.6251	0.0014	0.0092	44
18	55871.6732	0.0023	−0.0027	44
32	55872.5019	0.0011	−0.0142	36
33	55872.5826	0.0019	0.0065	45
51	55873.6608	0.0014	0.0045	44
52	55873.7157	0.0031	−0.0006	44
66	55874.5598	0.0009	0.0033	41
67	55874.6204	0.0020	0.0039	44
69	55874.7376	0.0014	0.0011	35
82	55875.5213	0.0034	0.0046	22
83	55875.5765	0.0014	−0.0002	43
84	55875.6400	0.0014	0.0033	43
85	55875.7007	0.0037	0.0040	43
99	55876.5243	0.0047	−0.0126	24
100	55876.5904	0.0086	−0.0065	27
117	55877.6246	0.0030	0.0076	28
118	55877.6874	0.0060	0.0103	26
119	55877.7551	0.0023	0.0181	14
133	55878.5726	0.0013	−0.0046	27
134	55878.6307	0.0027	−0.0065	27
149	55879.5368	0.0016	−0.0006	20
150	55879.5937	0.0048	−0.0037	21
151	55879.6535	0.0029	−0.0040	21
152	55879.7095	0.0011	−0.0080	20

* BJD − 2400000.
† Against max = 2455870.5957 + 0.060012E.
‡ Number of points used to determine the maximum.

3.49. SBS 1108+574

This object (hereafter SBS 1108) was originally selected as an ultraviolet-excess object during the course of the Second Byurakan Survey (SBS: Markarian & Stepanian 1983). An outburst of this object was detected by CRTS on 2012 April 22 (= CSS120422:111127+571239). The very blue color ($u-g$ = −0.3) in quiescence was very notable (vsnet-alert 14475, 14483). Subsequent observations clarified that this object is an ultrashort period SU UMa-type dwarf nova showing superhumps (vsnet-alert 14480, 14484, 14493; figure 45). Although it was not initially clear whether this object belongs to AM CVn-type ones or hydrogen-rich ones, a spectroscopic observation (Garnavich et al. 2012) confirmed that it is hydrogen-rich.

The times of superhump maxima are listed in table 54. Although the epoch of the start of the outburst is unknown, the $O-C$ variation was very similar to those of ordinary short-$P_{\rm orb}$ SU UMa-type dwarf novae: consisting of stage B with a longer $P_{\rm SH}$ and a positive $P_{\rm dot}$ and stage C with a shorter $P_{\rm SH}$ having a relatively constant period (figure 46). The amplitudes of superhumps became smaller near the end of stage B, as seen in ordinary short-$P_{\rm orb}$ SU UMa-type dwarf novae (Kato et al. 2012a); they became larger at the start of stage C (figure 47). The object also slightly brightened after the stage B–C transition (figure 46). This feature is commonly seen in objects with distinct stage B–C transitions (cf. Kato et al. 2003b, 2012a). The transition from stage B to C was abrupt, as seen in ordinary short-$P_{\rm orb}$ SU UMa-type dwarf novae. The stage-C superhumps persisted after a rapid decline without a phase shift.

In addition to superhumps, we detected a stable period of 0.038449(6) d, which we identified as the orbital period (figure 48). The ϵ values for stage-B and stage-C superhumps were 1.74(2)% and 1.11(2)%, respectively. By applying the ϵ–q relation in Kato et al. (2009) to ϵ of stage-C superhumps, we obtained $q = 0.06$. This ϵ or q is larger than those of many extreme WZ Sge-type dwarf novae, which implies that the secondary is denser, or more massive, than in ordinary dwarf novae. The estimated volume radius of the Roche lobe of the secondary is located below the theoretical radius of a brown dwarf when we assume a typical mass ($0.7\,M_{\odot}$) for a white dwarf in a dwarf nova (figure 49). Only with a massive ($\geq 1.0\,M_{\odot}$) white dwarf, the secondary can be a normal lower main-sequence star. Since sustained nuclear burning is not expected for a brown dwarf, this finding suggests that this secondary is a somewhat evolved star, whose hydrogen envelope was mostly stripped during the period of the mass-exchange. The spectrum taken in

Table 42. Superhump maxima of V1208 Tau (2011).

E	Max*	Error	$O-C^\dagger$	$N^\ddagger$
0	55919.4074	0.0007	0.0021	75
1	55919.4775	0.0008	0.0016	54
9	55920.0347	0.0008	−0.0050	75
10	55920.1086	0.0006	−0.0015	58
34	55921.8064	0.0009	0.0047	73
35	55921.8728	0.0007	0.0006	73
48	55922.7901	0.0007	0.0017	73
49	55922.8548	0.0012	−0.0041	73

* BJD − 2400000.
† Against max = 2455919.4054 + 0.070481E.
‡ Number of points used to determine the maximum.

Table 43. Superhump maxima of V1212 Tau (2011b).

E	Max*	Error	$O-C^\dagger$	$N^\ddagger$
0	55834.4345	0.0034	−0.0001	21
1	55834.5065	0.0016	0.0021	63
2	55834.5735	0.0008	−0.0005	107
3	55834.6423	0.0010	−0.0016	90
15	55835.4805	0.0017	−0.0001	29
16	55835.5497	0.0019	−0.0006	66
17	55835.6201	0.0010	0.0000	35
18	55835.6906	0.0019	0.0008	19

* BJD − 2400000.
† Against max = 2455834.4346 + 0.069731E.
‡ Number of points used to determine the maximum.

quiescence (E. Pavlenko et al. in preparation), showing an enhanced abundance of helium, is consistent with this interpretation. The object may be analogous to OT J112253.3−111037 (= CSS100603:112253−111037) (Kato et al. 2010; Breedt et al. 2012; note also the unusual $u-g$ color mentioned in Kato et al. 2012b). A further detailed radial-velocity study would enable us to clarify the nature of this binary.

3.50. SDSS J073208.11+413008.7

We observed the 2012 superoutburst of this object (hereafter SDSS J073208; the object was selected by Wils et al. 2010; see a comment in Kato et al. 2010). The times of superhump maxima are listed in table 55. The period given in table 2 was determined by the PDM method. This period appears to be a global average of stage-B and stage-C superhumps.

3.51. SDSS J080303.90+251627.0

This object (hereafter SDSS J080303) was discovered to be a CV during the course of the SDSS (Szkody et al. 2005). Szkody et al. (2005) identified a spectroscopic period of 0.071 d. The object showed multiple outbursts in the CRTS data. The 2011 outburst was detected by J. Shears (BAAVSS alert 2806). The detection was sufficiently early to observe the early evolution of superhumps (vsnet-alert 14006, 14015, 14033). The object showed a large variation of the superhump period (vsnet-alert 14063). The mean superhump profile is

Table 44. Superhump maxima of DI UMa (2007).

E	Max*	Error	$O-C^\dagger$	$N^\ddagger$
0	54204.3594	0.0028	−0.0185	20
1	54204.4108	0.0015	−0.0224	24
2	54204.4641	0.0011	−0.0244	44
18	54205.3793	0.0007	0.0070	20
19	54205.4336	0.0005	0.0061	25
20	54205.4894	0.0009	0.0066	35
35	54206.3165	0.0003	0.0050	39
36	54206.3715	0.0002	0.0048	37
37	54206.4246	0.0003	0.0027	39
53	54207.3080	0.0006	0.0022	79
54	54207.3630	0.0003	0.0020	102
55	54207.4200	0.0003	0.0037	69
56	54207.4745	0.0003	0.0030	67
57	54207.5293	0.0003	0.0025	66
71	54208.3073	0.0005	0.0072	40
72	54208.3535	0.0014	−0.0020	32
91	54209.4102	0.0013	0.0051	20
127	54211.4019	0.0010	0.0081	28
128	54211.4583	0.0016	0.0093	16
143	54212.2886	0.0020	0.0110	18
144	54212.3452	0.0008	0.0123	28
182	54214.4491	0.0010	0.0170	31
216	54216.3046	0.0006	−0.0058	39
217	54216.3615	0.0005	−0.0042	46
218	54216.4143	0.0009	−0.0065	28
219	54216.4696	0.0005	−0.0065	24
235	54217.3548	0.0018	−0.0052	11
236	54217.3952	0.0035	−0.0200	11

* BJD − 2400000.
† Against max = 2454204.3779 + 0.055243E.
‡ Number of points used to determine the maximum.

Table 45. Superhump maxima of DI UMa (2007b).

E	Max*	Error	$O-C^\dagger$	$N^\ddagger$
0	54237.4668	0.0002	0.0044	29
16	54238.3514	0.0005	0.0035	36
17	54238.4042	0.0003	0.0009	39
18	54238.4571	0.0006	−0.0015	41
34	54239.3435	0.0003	−0.0005	33
35	54239.3951	0.0005	−0.0043	33
36	54239.4538	0.0004	−0.0009	30
71	54241.3914	0.0008	−0.0002	22
89	54242.3861	0.0008	−0.0016	29
90	54242.4357	0.0016	−0.0074	28
107	54243.3918	0.0007	0.0079	19
108	54243.4289	0.0018	−0.0103	26
126	54244.4451	0.0016	0.0098	27

* BJD − 2400000.
† Against max = 2454237.4624 + 0.055340E.
‡ Number of points used to determine the maximum.

Table 46. Superhump maxima of MR UMa (2012).

E	Max*	Error	$O-C^{\dagger}$	$N^{\ddagger}$
0	56094.3735	0.0005	0.0019	129
1	56094.4353	0.0006	−0.0011	135
16	56095.4070	0.0008	−0.0006	124
17	56095.4713	0.0010	−0.0010	131
31	56096.3792	0.0009	0.0004	133
32	56096.4438	0.0010	0.0003	134
47	56097.4144	0.0012	−0.0003	133
48	56097.4799	0.0020	0.0004	104

* BJD − 2400000.
† Against max = 2456094.3716 + 0.064746E.
‡ Number of points used to determine the maximum.

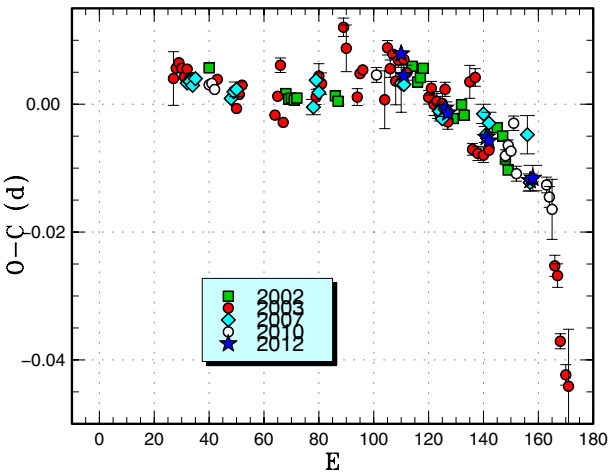

Fig. 35. Comparison of different superoutbursts of MR UMa in the $O-C$ diagram. A period of 0.06512 d was used to draw this figure. Approximate cycle counts (E) after the start of the 2007 superoutburst were used. Since the starts of the other superoutbursts were not well constrained, we so shifted the $O-C$ diagrams that they are best fitted to the 2007 one.

shown in figure 50.

The times of superhump maxima are listed in table 56. The initial stage A with growing superhumps is immediately recognizable. We considered $E = 27$–31 to be the stage B–C transition, and list the period according to these identifications in table 2.

The large negative $P_{\rm dot}$ [global value of $-79(8) \times 10^{-5}$] and the long $P_{\rm SH}$ resemble those of MN Dra (Pavlenko et al. 2010b).

3.52. SDSS J165359.06+201010.4

We observed a superoutburst in 2012 May of this SU UMa-type dwarf nova (hereafter SDSS J165359). The times of superhumps are listed in table 57. Since the object faded rapidly after our final observation, the superhumps recorded on the last three nights were most likely to be stage-C superhumps. Although the identification of the stage of earlier observations was unclear due to a long gap in the observation, a comparison between the 2010 and 2012 superoutbursts in the $O-C$ diagram suggests that we observed the earlier part of stage B (figure 51).

Table 47. Eclipse minima of PU UMa (2012).

E	Minimum*	Error	$O-C^{\dagger}$
28068	55959.43896	0.00006	0.00019
28069	55959.51692	0.00003	0.00027
28080	55960.37350	0.00005	0.00017
28081	55960.45131	0.00006	0.00010
28092	55961.30786	0.00002	−0.00004
28093	55961.38604	0.00004	0.00026
28110	55962.70976	0.00004	0.00001
28111	55962.78746	0.00004	−0.00017
28112	55962.86561	0.00003	0.00009
28118	55963.33222	0.00004	−0.00058
28119	55963.41032	0.00005	−0.00036
28173	55967.61633	0.00003	0.00010

* BJD − 2400000.
† Against equation (2).

Table 48. Superhump maxima of PU UMa (2012).

E	Max*	Error	$O-C^{\dagger}$	Phase‡	$N^{\S}$
0	55959.4659	0.0007	−0.0331	0.13	183
11	55960.3880	0.0009	−0.0029	0.16	123
12	55960.4712	0.0008	−0.0007	0.18	101
22	55961.2845	0.0012	0.0019	0.54	63
23	55961.3685	0.0006	0.0049	0.17	239
24	55961.4507	0.0015	0.0060	0.30	77
35	55962.3444	0.0011	0.0079	0.46	34
36	55962.4242	0.0011	0.0067	0.55	35
40	55962.7460	0.0005	0.0042	0.18	132
41	55962.8265	0.0008	0.0036	0.30	115
47	55963.3178	0.0014	0.0085	0.41	67
48	55963.3998	0.0011	0.0094	0.30	69
83	55966.2293	0.0045	0.0015	0.41	28
84	55966.3101	0.0015	0.0013	0.33	40
100	55967.5984	0.0006	−0.0076	0.19	96
121	55969.2966	0.0039	−0.0118	0.68	132

* BJD − 2400000.
† Against max = 2455959.4991 + 0.081068E.
‡ Orbital phase.
§ Number of points used to determine the maximum.

3.53. SDSS J170213.26+322954.1

This object (hereafter SDSS J170213) is an eclipsing SU UMa-type dwarf nova in the period gap (Boyd et al. 2006; Littlefair et al. 2006). Boyd, Oksanen, and Henden (2006) reported on an analysis of the 2005 superoutburst. Kato et al. (2009) analyzed their data, and concluded that this object showed an increase in $P_{\rm SH}$ during the middle-to-late stage of a superoutburst, contrary to most SU UMa-type dwarf novae with a similar $P_{\rm SH}$.

The 2011 superoutburst was detected by G. Poyner using an unfiltered CCD camera, at a magnitude of 13.93 (vsnet-outburst 13058). Subsequent observations confirmed the

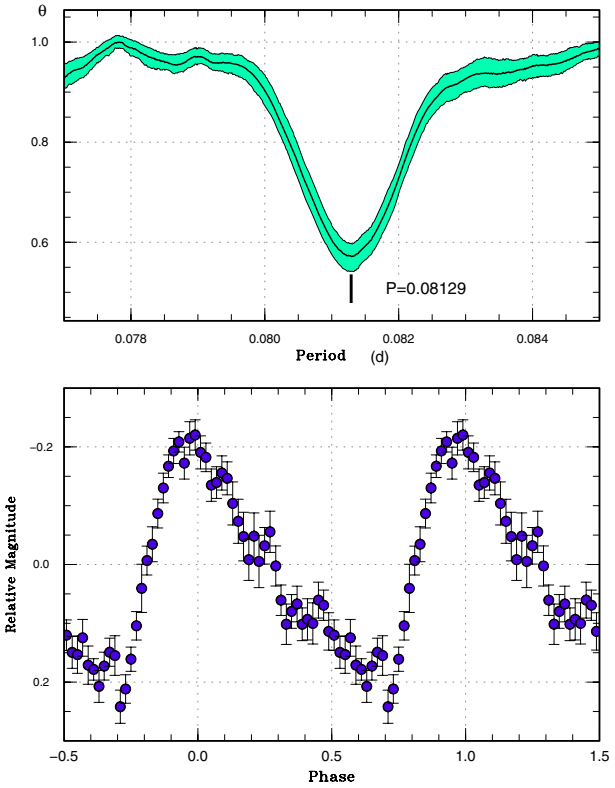

Fig. 36. Stage-B superhumps in PU UMa (2012). Upper: PDM analysis. Lower: Phase-averaged profile.

Table 49. Superhump maxima of SS UMi (2012).

E	Max*	Error	$O-C^\dagger$	$N^\ddagger$
0	56009.5129	0.0007	0.0029	53
1	56009.5786	0.0009	−0.0017	53
2	56009.6468	0.0014	−0.0039	50
5	56009.8662	0.0043	0.0044	80
6	56009.9295	0.0014	−0.0026	80
7	56010.0062	0.0020	0.0037	54
15	56010.5616	0.0015	−0.0038	52
33	56011.8328	0.0053	0.0010	80

* BJD − 2400000.
† Against max = 2456009.5100 + 0.070358E.
‡ Number of points used to determine the maximum.

Table 50. Superhump maxima of SS UMi (2012) (secondary humps).

E	Max*	Error	$O-C^\dagger$	$N^\ddagger$
0	56009.5410	0.0012	−0.0003	52
1	56009.6083	0.0007	−0.0029	52
4	56009.8206	0.0009	−0.0004	80
5	56009.8899	0.0010	−0.0010	79
6	56009.9611	0.0006	0.0002	80
14	56010.5134	0.0007	−0.0070	53
15	56010.5876	0.0009	−0.0028	52
16	56010.6528	0.0010	−0.0075	50
18	56010.7969	0.0006	−0.0033	71
19	56010.8669	0.0006	−0.0032	79
20	56010.9348	0.0009	−0.0053	79
28	56011.4990	0.0009	−0.0006	52
29	56011.5696	0.0016	0.0000	86
30	56011.6398	0.0005	0.0003	74
33	56011.8523	0.0006	0.0030	79
34	56011.9197	0.0008	0.0004	79
35	56011.9931	0.0006	0.0039	69
42	56012.4833	0.0011	0.0044	52
43	56012.5527	0.0009	0.0039	64
44	56012.6247	0.0004	0.0059	104
45	56012.6965	0.0045	0.0078	48
56	56013.4677	0.0006	0.0097	53
57	56013.5267	0.0027	−0.0013	27
58	56013.6075	0.0015	0.0096	53
59	56013.6717	0.0011	0.0038	36
71	56014.5123	0.0012	0.0051	21
72	56014.5843	0.0008	0.0071	27
73	56014.6504	0.0011	0.0033	34
78	56014.9951	0.0015	−0.0017	46
85	56015.4873	0.0017	0.0009	27
86	56015.5525	0.0007	−0.0038	53
87	56015.6182	0.0014	−0.0081	53
88	56015.6914	0.0027	−0.0048	18
92	56015.9750	0.0008	−0.0010	52
100	56016.5337	0.0012	−0.0019	20
101	56016.5996	0.0009	−0.0059	28
102	56016.6762	0.0012	0.0008	27
106	56016.9480	0.0006	−0.0072	55

* BJD − 2400000.
† Against max = 2456009.5412 + 0.069943E.
‡ Number of points used to determine the maximum.

presence of superhumps and eclipses (vsnet-alert 13524, 13526, 13528, 13532). The times of recorded eclipses, determined by the KW method, after removing linearly approximated trends near eclipses in order to minimize the effect of superhumps, are summarized in table 58. We obtained an updated ephemeris of

$$\mathrm{Min(BJD)} = 2453648.23651(31)+0.100082207(15)E. \quad (3)$$

The times of the superhump maxima determined outside the eclipse are listed in table 59. There were clear stage A ($E \leq 32$) and stage B with a positive $P_{\rm dot}$. There was no indication of a transition to stage C, despite that the observation covered the early stage of the rapid decline. The large positive $P_{\rm dot}$ confirmed the 2005 results and, as suggested in Kato et al. (2009), this object imitates a short-$P_{\rm orb}$ system both in the $O-C$ variation and in the stage transition. The value $\epsilon = 6.0\%$ is, however, much larger than those in systems with a short $P_{\rm orb}$. This object appears to show relatively infrequent outbursts [the only known outbursts were in 2005 September–October (superoutburst), 2006 July (normal outburst), 2007 September (superoutburst), 2009 February (normal outburst), 2009 October (superoutburst), and 2011 July (superoutburst)] and probably indeed resembles EF Peg (cf. Howell et al. 1993; Kato 2002b), as proposed in Kato et al. (2009), rather than an unusual system with a large $P_{\rm dot}$, GX Cas (Kato et al. 2012a).

Table 51. Superhump maxima of 1RXS J231935.

E	Max*	Error	$O-C^{\dagger}$	$N^{\ddagger}$
0	55835.4280	0.0003	−0.0040	65
1	55835.4930	0.0003	−0.0048	68
2	55835.5596	0.0002	−0.0039	102
3	55835.6240	0.0002	−0.0052	203
4	55835.6920	0.0004	−0.0030	84
14	55836.3491	0.0004	−0.0035	49
15	55836.4142	0.0003	−0.0042	213
16	55836.4793	0.0002	−0.0049	362
17	55836.5457	0.0002	−0.0043	389
18	55836.6113	0.0002	−0.0044	217
19	55836.6764	0.0003	−0.0051	132
29	55837.3357	0.0003	−0.0035	157
30	55837.4024	0.0002	−0.0025	169
31	55837.4658	0.0002	−0.0049	250
32	55837.5312	0.0003	−0.0052	267
33	55837.5978	0.0002	−0.0044	267
34	55837.6649	0.0005	−0.0031	93
44	55838.3270	0.0007	0.0014	86
45	55838.3920	0.0006	0.0006	126
46	55838.4587	0.0006	0.0015	125
47	55838.5220	0.0038	−0.0009	41
56	55839.1186	0.0011	0.0038	94
57	55839.1859	0.0006	0.0054	123
59	55839.3162	0.0006	0.0041	98
60	55839.3808	0.0007	0.0030	116
61	55839.4481	0.0006	0.0045	121
62	55839.5133	0.0006	0.0039	85
63	55839.5871	0.0025	0.0120	77
64	55839.6491	0.0015	0.0082	41
75	55840.3753	0.0005	0.0110	51
76	55840.4449	0.0014	0.0149	50
77	55840.5081	0.0007	0.0123	57
78	55840.5728	0.0006	0.0112	57
79	55840.6379	0.0006	0.0106	44
102	55842.1444	0.0006	0.0045	112
103	55842.2125	0.0005	0.0068	119
104	55842.2761	0.0008	0.0047	66
118	55843.1927	0.0005	0.0005	95
140	55844.6357	0.0010	−0.0033	31
141	55844.7006	0.0011	−0.0041	31
142	55844.7650	0.0008	−0.0054	36
143	55844.8324	0.0009	−0.0038	33
144	55844.8970	0.0009	−0.0050	35
153	55845.4853	0.0036	−0.0086	54
154	55845.5512	0.0010	−0.0084	59
155	55845.6205	0.0010	−0.0049	83
157	55845.7555	0.0039	−0.0014	34
159	55845.8803	0.0010	−0.0081	28

* BJD − 2400000.
† Against max = 2455835.4320 + 0.065764E.
‡ Number of points used to determine the maximum.

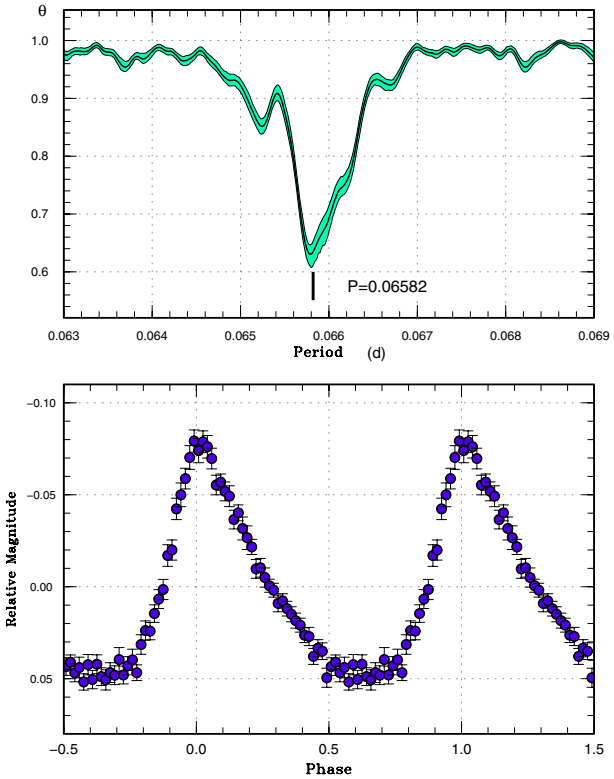

Fig. 37. Superhumps in 1RXS J231935 (2011). Upper: PDM analysis. Lower: Phase-averaged profile.

The behavior of the $O-C$ variation was similar between the 2005 and 2011 outbursts (figure 52). It is noteworthy that their stage A lasted much longer than in other systems.

3.54. SDSS J172102.48+273301.2

This object (hereafter SDSS J172102) was originally selected as a helium CV using the SDSS colors, and confirmed by spectroscopy (Rau et al. 2010). Although there had been no record of outbursts, CRTS detected this object in outburst on 2012 June 8 at an unfiltered CCD magnitude of 16.4 (CSS120608:172102+273301). A quick follow-up observation confirmed the presence of superhumps on June 9 (vsnet-alert 14653). A retrospective study indicated that the object was recorded at unfiltered CCD magnitudes of 16.0–16.2 on June 5 at MASTER-Kislovodsk (vsnet-alert 14657). The object rapidly faded to 18.9 on June 11 (W. N. Goff) and 19.1 on June 15 (CRTS). The object was thus likely to be a superoutburst of an AM CVn-type object detected during its final stage. The object underwent a short post-superoutburst rebrightening on June 20, whose peak brightness must have been brighter than 17.5 (W. N. Goff). The times of superhump maxima are listed in table 60. Note that these observations were mostly carried out during the final stage of the superoutburst and the subsequent post-superoutburst phase, and the maxima were rather difficult to identify due to their faintness. Our best estimate of the superhump period is 0.026673(8) d (figure 53). It is remarkable that both spectra shown in Rau et al. (2010) and the SDSS public archive were continuum-dominated (vsnet-alert

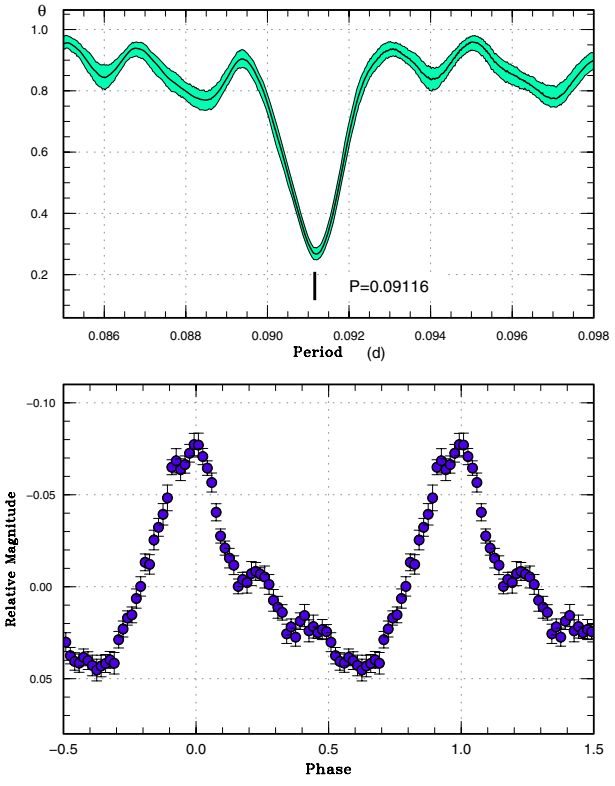

Fig. 38. Superhumps in DDE 19 (2011). Upper: PDM analysis. Lower: Phase-averaged profile.

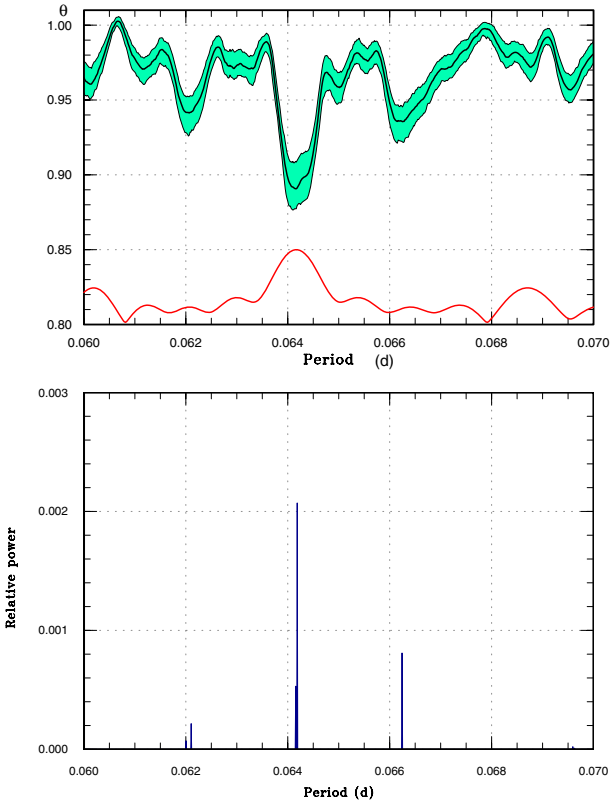

Fig. 39. Period analysis in MASTER J072948 (2012). Upper: PDM analysis. The lower curve at the bottom indicates the window function. Lower: Lasso analysis ($\log\lambda = -4.34$).

Table 52. Superhump maxima of DDE 19 (2011).

E	Max*	Error	$O-C$†	N‡
0	55888.6444	0.0004	0.0018	97
2	55888.8256	0.0004	0.0006	96
11	55889.6458	0.0009	−0.0001	87
12	55889.7356	0.0008	−0.0014	96
13	55889.8258	0.0006	−0.0025	96
33	55891.6541	0.0007	0.0017	96
34	55891.7445	0.0013	0.0008	96
35	55891.8339	0.0010	−0.0010	96

* BJD − 2400000.
† Against max = 2455888.6425 + 0.091210E.
‡ Number of points used to determine the maximum.

14650) in contrast to the quiescent state of many AM CVn-type objects showing dwarf-nova-type outbursts.

3.55. SDSS J210449.94+010545.8

This object (hereafter SDSS J210449) was discovered to be a CV during the course of the SDSS (Szkody et al. 2006). Szkody et al. (2006) recorded high and low states ranging over 17.1–20.6 mag. Southworth et al. (2007) detected a photometric period of 0.07196(8) d. CRTS recorded multiple outbursts, and at least one of them (2006 November) lasted for more than 18 d, and was most likely to be a superoutburst. During the superoutburst in 2011 September, I. Miller detected superhumps (vsnet-alert 13704). The PDM analysis yielded two equally acceptable one-day aliases (figure 54).

The times of superhump maxima are listed in table 61 The timing analysis prefers an alias of 0.0753 d, and we obtained a period of 0.07531(4) d by the PDM method, which is used in table 2. The ϵ value of 4.7% inferred from this period is likely to be too large for this $P_{\rm orb}$, and there may have been negative superhumps at the time of observations by Southworth et al. (2007). The exact orbital period needs to be determined by radial-velocity studies.

3.56. SDSS J220553.98+115553.7

This object (hereafter SDSS J220553) was detected to be a CV during the course of SDSS (Szkody et al. 2003). Szkody et al. (2003) showed the presence of the underlying white dwarf in the spectrum, suggesting a low mass-transfer rate. Warner and Woudt (2004) indicated that this system contains a ZZ Cet-type pulsating white dwarf (see also Szkody et al. 2007), also suggesting a low surface-temperature of its white dwarf (consistent with a low mass-transfer rate). Southworth et al. (2008) obtained the spectroscopic orbital period of 0.0575175(62) d, and found that the pulsation of the white dwarf ceased in 2007. Although the spectrum and the orbital period suggested an SU UMa-type, or even a WZ Sge-type, dwarf nova, no outburst was recorded until 2011.

CRTS detected an outburst on 2011 May 20 (cf. vsnet-alert

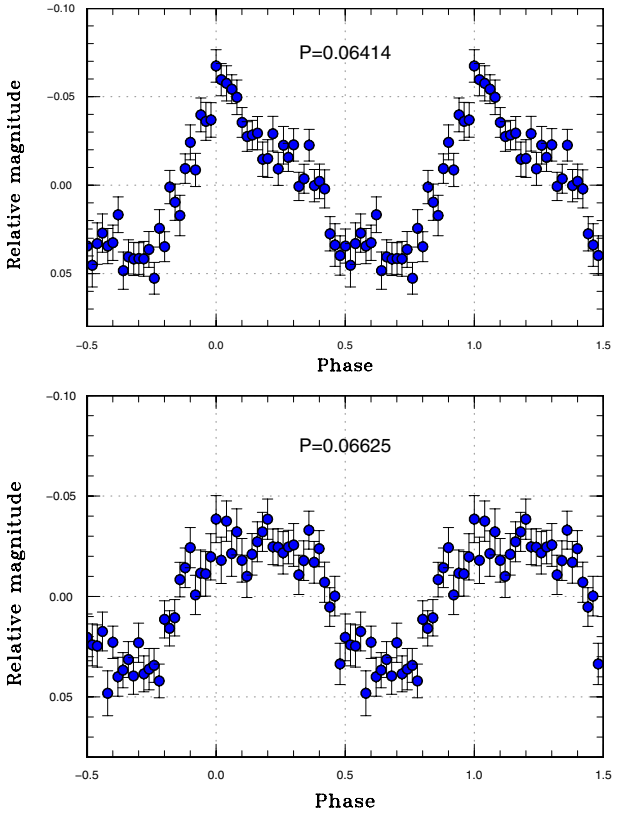

Fig. 40. Profiles of two periodicities in MASTER J072948 (2012). Upper: Superhump period. Lower: Orbital period.

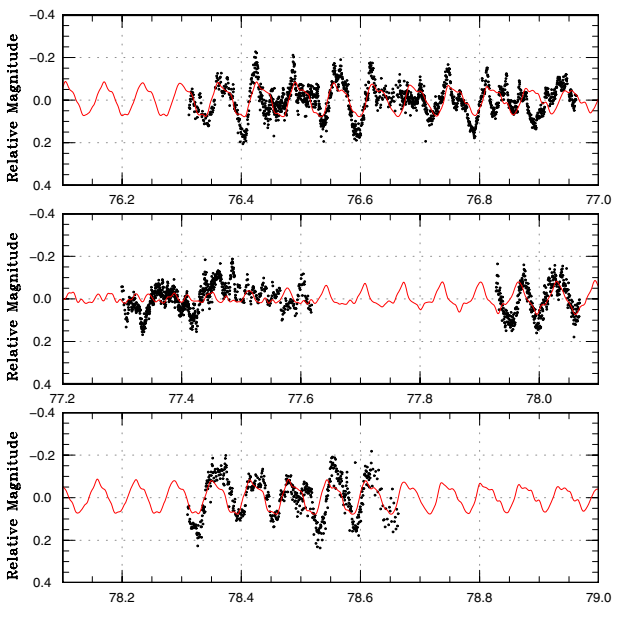

Fig. 41. Synthesized light curve of MASTER J072948 (2011). Points represent observations. The curve represents an expected light curve by adding the two waves in figure 40.

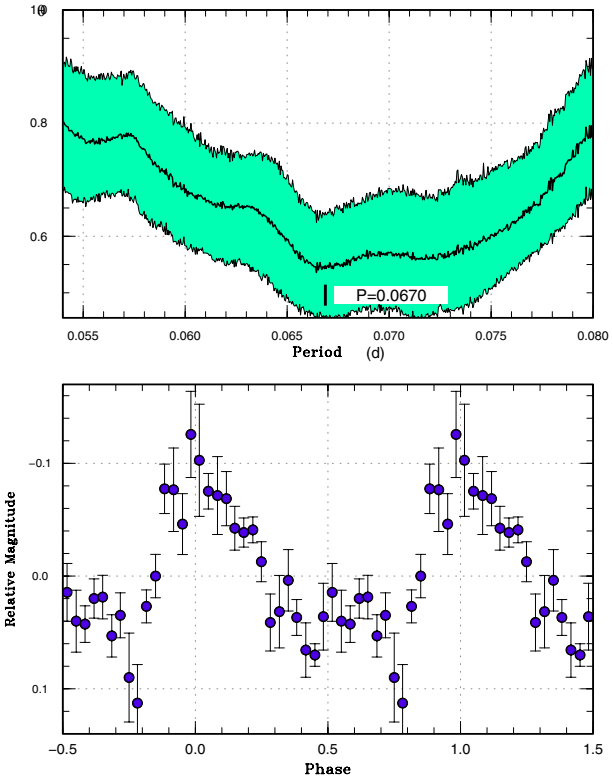

Fig. 42. Superhumps in MASTER J174305 (2012). Upper: PDM analysis. Lower: Phase-averaged profile.

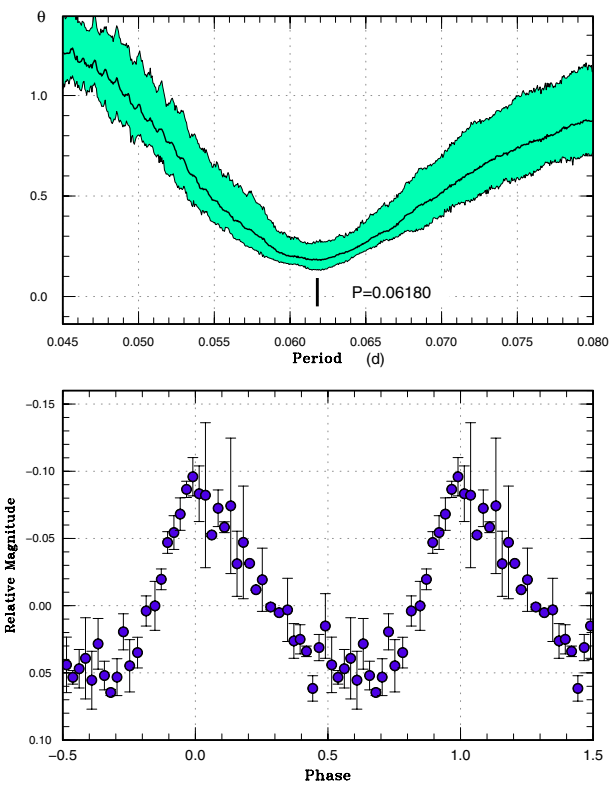

Fig. 43. Superhumps in MASTER J182201 (2012). Upper: PDM analysis. Lower: Phase-averaged profile.

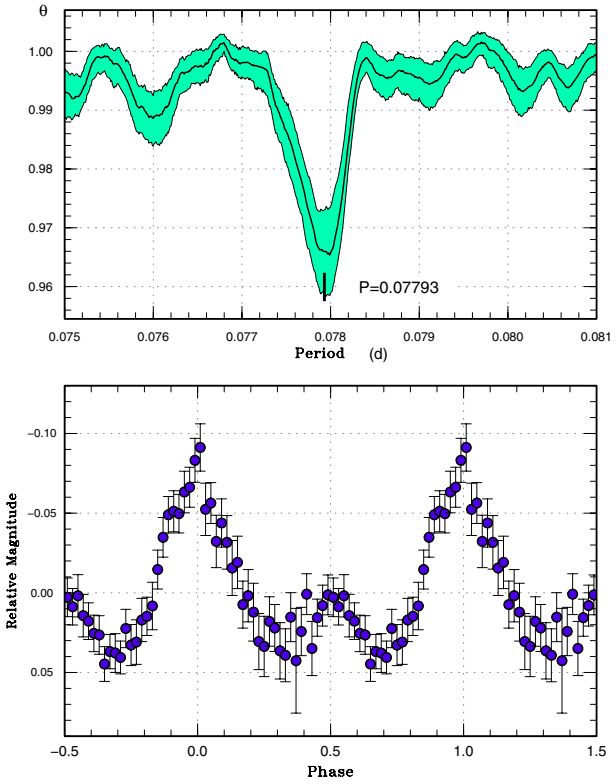

Fig. 44. Superhumps in MisV 1446 (2012). Upper: PDM analysis. Lower: Phase-averaged profile.

13325). The announcement of this detection was immediately followed by observations. Fully grown superhumps were soon detected (vsnet-alert 13329; figure 55), and the later development suggested a low ϵ value, characteristic of a WZ Sge-type dwarf nova (vsnet-alert 13332, 13336). $P_{\rm dot}$ was, however, unexpectedly large (vsnet-alert 13348).

The times of superhump maxima are listed in table 62. The resultant $P_{\rm dot}$ was $+7.7(0.9) \times 10^{-5}$. The ϵ value for the mean period of stage B superhumps was 1.1%, which is much smaller than what would be expected for this large $P_{\rm dot}$.

According to the CRTS data, the object was brighter than in the usual quiescence during the four months after the outburst. This feature, combined with the low ϵ value and the lack of previous outbursts in the CRTS data, suggests that the object is a WZ Sge-type dwarf nova. It may be that we missed the period of early superhumps, and that the true maximum was much brighter.

3.57. OT J001952.2+433901

This transient (= CSS120131:001952+433901; hereafter OT J001952) was detected by CRTS on 2012 January 31. The large outburst amplitude ($\sim$ 6.5 mag) and the lack of previous outbursts attracted the attention of observers (vsnet-alert 14182). Subsequent observations detected short-period superhumps (vsnet-alert 14189, 14202; figure 56). The times of superhump maxima are listed in table 63. The large outburst amplitude and the short superhump period suggest the possibility of a WZ Sge-type dwarf nova.

Table 53. Superhump maxima of MisV 1446 (2012).

E	Max*	Error	$O-C$†	N‡
0	55938.0155	0.0031	−0.0006	134
1	55938.0949	0.0006	0.0010	207
2	55938.1682	0.0005	−0.0034	312
3	55938.2450	0.0006	−0.0044	281
4	55938.3233	0.0006	−0.0040	279
5	55938.4019	0.0015	−0.0031	113
13	55939.0278	0.0012	0.0003	178
14	55939.1040	0.0007	−0.0013	287
15	55939.1822	0.0007	−0.0009	158
16	55939.2639	0.0012	0.0030	155
17	55939.3371	0.0008	−0.0016	124
26	55940.0351	0.0031	−0.0038	138
27	55940.1209	0.0010	0.0042	108
35	55940.7515	0.0016	0.0123	81
36	55940.8206	0.0008	0.0035	67
37	55940.9001	0.0009	0.0053	82
40	55941.1329	0.0011	0.0046	225
41	55941.2098	0.0012	0.0038	157
42	55941.2873	0.0010	0.0034	155
44	55941.4427	0.0006	0.0032	301
45	55941.5184	0.0007	0.0011	407
48	55941.7484	0.0104	−0.0023	18
49	55941.8340	0.0123	0.0055	10
56	55942.3688	0.0037	−0.0043	191
57	55942.4462	0.0025	−0.0047	408
58	55942.5173	0.0010	−0.0114	336
69	55943.3793	0.0014	−0.0053	31

* BJD − 2400000.
† Against max = 2455938.0160 + 0.077806E.
‡ Number of points used to determine the maximum.

3.58. OT J011516.5+245530

This transient (= CSS101008:011517+245530; hereafter OT J011516) was detected by CRTS on 2010 October 8. Although several outbursts have been known, the 2012 outburst was the brightest one (vsnet-alert 14142). Subsequent observations recorded superhumps (vsnet-alert 14147, 14149). Only a single-night observation with the superhump maxima of BJD 2455952.2518(7) (N = 51) and 2455952.3253(10) (N = 44) was available. The best superhump period by the PDM method was 0.0731(6) d (figure 57).

3.59. OT J050716.2+125314

This transient (= CSS081221:050716+125314; hereafter OT J050716) was detected by CRTS on 2008 December 21. The 2012 January outburst led to a detection of superhumps (vsnet-alert 14150, 14151). The times of superhump maxima are listed in table 64. Although the $O-C$ analysis favored an alias of 0.06592(8) d (adopted in table 2), an alias of 0.07055(9) d is not excluded (figure 58).

3.60. OT J055721.8−363055

This transient (= SSS111229:055722−363055; hereafter OT J055721) was detected by CRTS SSS on 2011

Table 54. Superhump maxima of SBS 1108 (2012).

E	Max*	Error	$O-C^{\dagger}$	$N^{\ddagger}$	E	Max*	Error	$O-C^{\dagger}$	$N^{\ddagger}$
0	56040.6654	0.0007	−0.0064	67	120	56045.3523	0.0007	−0.0051	19
1	56040.7056	0.0007	−0.0053	56	121	56045.3914	0.0012	−0.0050	19
3	56040.7820	0.0006	−0.0070	63	122	56045.4288	0.0004	−0.0066	20
11	56041.0923	0.0021	−0.0090	59	123	56045.4678	0.0007	−0.0067	22
12	56041.1304	0.0010	−0.0099	80	124	56045.5092	0.0016	−0.0043	38
13	56041.1755	0.0042	−0.0039	80	125	56045.5457	0.0009	−0.0068	35
14	56041.2158	0.0045	−0.0027	53	128	56045.6634	0.0020	−0.0063	27
18	56041.3662	0.0007	−0.0085	32	129	56045.7028	0.0009	−0.0060	31
19	56041.4061	0.0005	−0.0076	40	130	56045.7438	0.0011	−0.0040	35
20	56041.4448	0.0004	−0.0079	43	131	56045.7821	0.0015	−0.0048	36
21	56041.4834	0.0005	−0.0084	42	132	56045.8224	0.0008	−0.0035	35
22	56041.5227	0.0004	−0.0082	43	134	56045.8998	0.0013	−0.0042	12
23	56041.5617	0.0005	−0.0082	42	136	56045.9809	0.0017	−0.0012	72
24	56041.6002	0.0004	−0.0087	108	137	56046.0187	0.0012	−0.0024	81
25	56041.6390	0.0005	−0.0090	71	144	56046.2898	0.0011	−0.0046	14
26	56041.6778	0.0004	−0.0093	69	145	56046.3279	0.0007	−0.0056	20
27	56041.7171	0.0006	−0.0089	69	146	56046.3673	0.0010	−0.0053	20
33	56041.9475	0.0022	−0.0128	62	152	56046.6089	0.0022	0.0021	12
34	56041.9887	0.0012	−0.0107	121	153	56046.6420	0.0008	−0.0039	13
35	56042.0287	0.0010	−0.0097	122	154	56046.6783	0.0019	−0.0066	14
36	56042.0697	0.0042	−0.0078	35	155	56046.7206	0.0017	−0.0033	13
44	56042.3807	0.0006	−0.0091	42	156	56046.7576	0.0010	−0.0054	13
45	56042.4206	0.0005	−0.0083	42	157	56046.7970	0.0008	−0.0050	14
46	56042.4600	0.0005	−0.0079	42	158	56046.8373	0.0016	−0.0038	14
47	56042.4995	0.0005	−0.0075	43	159	56046.8747	0.0019	−0.0055	14
48	56042.5390	0.0004	−0.0070	43	160	56046.9123	0.0024	−0.0068	14
49	56042.5768	0.0005	−0.0083	42	170	56047.3054	0.0016	−0.0042	20
50	56042.6166	0.0007	−0.0075	37	171	56047.3472	0.0025	−0.0015	20
51	56042.6560	0.0007	−0.0072	67	172	56047.3861	0.0013	−0.0017	35
52	56042.6963	0.0005	−0.0059	69	173	56047.4238	0.0015	−0.0029	30
53	56042.7332	0.0005	−0.0081	61	174	56047.4636	0.0008	−0.0022	13
54	56042.7724	0.0004	−0.0079	14	175	56047.4987	0.0007	−0.0062	13
55	56042.8130	0.0011	−0.0064	10	176	56047.5407	0.0007	−0.0032	9
56	56042.8522	0.0011	−0.0062	14	178	56047.6210	0.0016	−0.0010	12
57	56042.8875	0.0019	−0.0099	14	179	56047.6593	0.0017	−0.0017	14
68	56043.3183	0.0006	−0.0087	26	180	56047.6971	0.0020	−0.0030	14
69	56043.3565	0.0005	−0.0095	26	181	56047.7396	0.0029	0.0005	9
70	56043.3964	0.0007	−0.0086	24	182	56047.7811	0.0043	0.0029	13
71	56043.4355	0.0008	−0.0086	26	183	56047.8170	0.0036	−0.0002	14
72	56043.4770	0.0014	−0.0061	26	184	56047.8543	0.0029	−0.0020	14
73	56043.5145	0.0009	−0.0077	26	185	56047.8944	0.0018	−0.0009	14
94	56044.3342	0.0007	−0.0080	75	195	56048.2844	0.0011	−0.0014	20
95	56044.3729	0.0006	−0.0083	98	196	56048.3227	0.0010	−0.0021	20
96	56044.4121	0.0008	−0.0081	96	197	56048.3627	0.0010	−0.0012	20
97	56044.4503	0.0024	−0.0089	21	198	56048.3996	0.0013	−0.0034	15
98	56044.4894	0.0009	−0.0089	12	199	56048.4412	0.0012	−0.0007	19
99	56044.5289	0.0012	−0.0085	12	200	56048.4785	0.0022	−0.0025	18
100	56044.5709	0.0016	−0.0055	8	201	56048.5203	0.0010	0.0003	20
101	56044.6077	0.0009	−0.0077	38	204	56048.6349	0.0018	−0.0023	14
102	56044.6465	0.0008	−0.0080	53	205	56048.6749	0.0025	−0.0014	14
103	56044.6850	0.0010	−0.0085	50	206	56048.7141	0.0025	−0.0012	14
104	56044.7266	0.0009	−0.0060	53	207	56048.7513	0.0019	−0.0031	14
105	56044.7671	0.0014	−0.0045	36	208	56048.7908	0.0014	−0.0026	13
106	56044.8053	0.0014	−0.0054	14	209	56048.8291	0.0033	−0.0033	14
107	56044.8460	0.0025	−0.0038	14	220	56049.2630	0.0047	0.0010	14
108	56044.8851	0.0014	−0.0037	14	221	56049.2994	0.0049	−0.0016	17
109	56044.9287	0.0031	0.0009	10	222	56049.3368	0.0014	−0.0033	20
118	56045.2718	0.0008	−0.0074	20	223	56049.3781	0.0048	−0.0010	20
119	56045.3110	0.0009	−0.0073	21	224	56049.4163	0.0021	−0.0018	20

Table 54. (Continued)

E	Max*	Error	$O-C^{\dagger}$	$N^{\ddagger}$	E	Max*	Error	$O-C^{\dagger}$	$N^{\ddagger}$
230	56049.6538	0.0026	0.0014	14	430	56057.4837	0.0013	0.0221	61
232	56049.7313	0.0024	0.0008	11	431	56057.5178	0.0014	0.0171	60
234	56049.8109	0.0040	0.0023	14	450	56058.2623	0.0018	0.0198	10
236	56049.8953	0.0031	0.0086	14	451	56058.3031	0.0021	0.0216	16
237	56049.9301	0.0010	0.0044	7	476	56059.2684	0.0080	0.0106	14
248	56050.3554	0.0020	0.0001	82	477	56059.3158	0.0012	0.0190	17
249	56050.4003	0.0022	0.0060	85	478	56059.3567	0.0007	0.0209	31
252	56050.5193	0.0017	0.0079	14	479	56059.3930	0.0016	0.0182	58
253	56050.5521	0.0010	0.0016	14	480	56059.4306	0.0010	0.0167	61
255	56050.6310	0.0033	0.0024	13	481	56059.4684	0.0009	0.0154	41
256	56050.6719	0.0013	0.0043	13	482	56059.5069	0.0012	0.0149	15
274	56051.3804	0.0024	0.0100	44	487	56059.7054	0.0014	0.0182	20
276	56051.4498	0.0025	0.0013	33	488	56059.7442	0.0009	0.0179	18
281	56051.6506	0.0042	0.0069	9	489	56059.7845	0.0013	0.0191	20
282	56051.7007	0.0029	0.0179	14	490	56059.8094	0.0012	0.0050	20
283	56051.7320	0.0035	0.0101	13	492	56059.9002	0.0022	0.0178	20
284	56051.7690	0.0024	0.0081	13	512	56060.6731	0.0020	0.0098	8
285	56051.8086	0.0020	0.0087	13	513	56060.7125	0.0012	0.0100	20
287	56051.8760	0.0019	−0.0020	12	514	56060.7444	0.0013	0.0029	18
306	56052.6258	0.0054	0.0059	13	515	56060.7918	0.0017	0.0113	19
307	56052.6741	0.0038	0.0151	14	516	56060.8281	0.0018	0.0085	18
308	56052.7138	0.0063	0.0158	32	517	56060.8687	0.0029	0.0101	20
309	56052.7508	0.0057	0.0137	35	518	56060.9091	0.0038	0.0114	14
310	56052.7808	0.0034	0.0047	31	528	56061.3000	0.0034	0.0118	12
311	56052.8246	0.0017	0.0094	34	531	56061.4138	0.0019	0.0086	43
312	56052.8690	0.0038	0.0148	29	533	56061.4901	0.0028	0.0068	32
313	56052.9066	0.0045	0.0134	25	540	56061.7538	0.0013	−0.0028	20
323	56053.2924	0.0029	0.0088	16	541	56061.7907	0.0050	−0.0050	18
324	56053.3230	0.0036	0.0002	16	542	56061.8396	0.0068	0.0048	19
332	56053.6286	0.0019	−0.0065	9	543	56061.8850	0.0033	0.0112	17
333	56053.6690	0.0019	−0.0052	14	556	56062.3817	0.0056	0.0003	72
334	56053.7237	0.0024	0.0105	13	558	56062.4634	0.0020	0.0039	72
335	56053.7632	0.0029	0.0110	10	559	56062.5072	0.0013	0.0087	29
338	56053.8731	0.0108	0.0038	11	564	56062.7000	0.0036	0.0062	20
352	56054.4292	0.0043	0.0132	46	565	56062.7351	0.0019	0.0023	19
354	56054.5078	0.0035	0.0137	29	566	56062.7764	0.0023	0.0046	20
357	56054.6351	0.0027	0.0239	10	582	56063.3952	0.0038	−0.0014	29
359	56054.7126	0.0010	0.0233	30	583	56063.4310	0.0020	−0.0046	28
360	56054.7527	0.0020	0.0243	28	584	56063.4683	0.0036	−0.0064	26
361	56054.7857	0.0062	0.0182	30	607	56064.3700	0.0033	−0.0028	42
362	56054.8322	0.0016	0.0257	27	608	56064.4070	0.0042	−0.0048	43
363	56054.8668	0.0067	0.0213	21	609	56064.4419	0.0022	−0.0090	42
364	56054.9069	0.0038	0.0223	17	634	56065.4115	0.0021	−0.0155	25
399	56056.2788	0.0015	0.0277	12	635	56065.4566	0.0023	−0.0094	26
402	56056.3998	0.0016	0.0315	24	657	56066.3051	0.0023	−0.0199	17
403	56056.4295	0.0015	0.0222	33	658	56066.3447	0.0008	−0.0194	29
405	56056.5165	0.0028	0.0311	23	659	56066.3833	0.0011	−0.0198	39
406	56056.5499	0.0038	0.0254	26	660	56066.4265	0.0034	−0.0157	38
410	56056.7049	0.0009	0.0242	20	662	56066.4951	0.0035	−0.0252	12
411	56056.7437	0.0026	0.0240	18	736	56069.3768	0.0026	−0.0329	9
412	56056.7791	0.0024	0.0204	20	738	56069.4499	0.0015	−0.0379	6
413	56056.8207	0.0013	0.0229	20	763	56070.4258	0.0012	−0.0382	11
414	56056.8615	0.0018	0.0247	20	770	56070.6959	0.0017	−0.0413	9
415	56056.9012	0.0017	0.0253	21	773	56070.8146	0.0013	−0.0398	8
425	56057.2882	0.0014	0.0218	16	872	56074.6617	0.0049	−0.0583	7
426	56057.3266	0.0025	0.0212	31	873	56074.7169	0.0034	−0.0421	7
427	56057.3600	0.0033	0.0155	80	875	56074.7828	0.0042	−0.0542	9
428	56057.4052	0.0009	0.0216	104	876	56074.8171	0.0018	−0.0591	9
429	56057.4426	0.0015	0.0201	88					

* BJD − 2400000.
† Against max = 2456040.6718 + 0.039046E.
‡ Number of points used to determine the maximum.

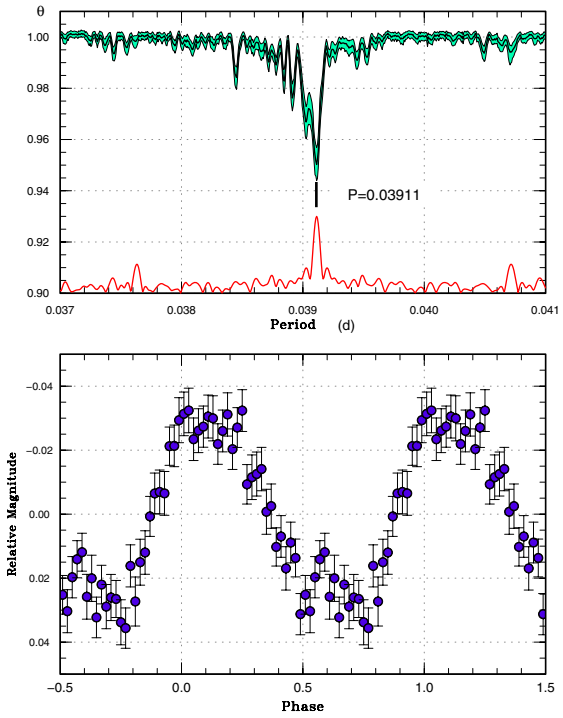

Fig. 45. Superhumps in SBS 1108 (2012). Upper: PDM analysis. The curve at the bottom of the figure represents the window function. The signal at $P = 0.038449$ d is a candidate orbital period. Lower: Phase-averaged profile.

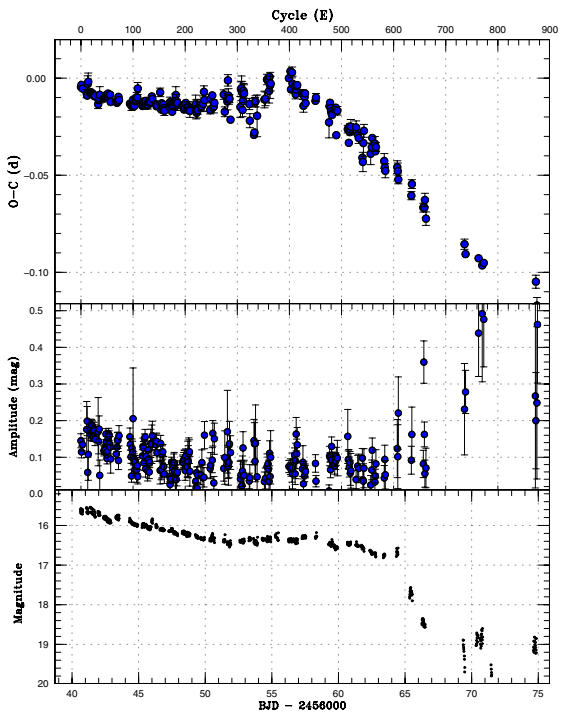

Fig. 46. $O - C$ diagram of superhumps in SBS 1108. Upper: $O - C$ diagram. We used a period of 0.03912 d for calculating the $O - C$ residual. Middle: Amplitudes of superhumps. There was a slight tendency to regrowth of superhumps near the stage B–C transition. Lower: Light curve. The object slightly brightened after the stage B–C transition.

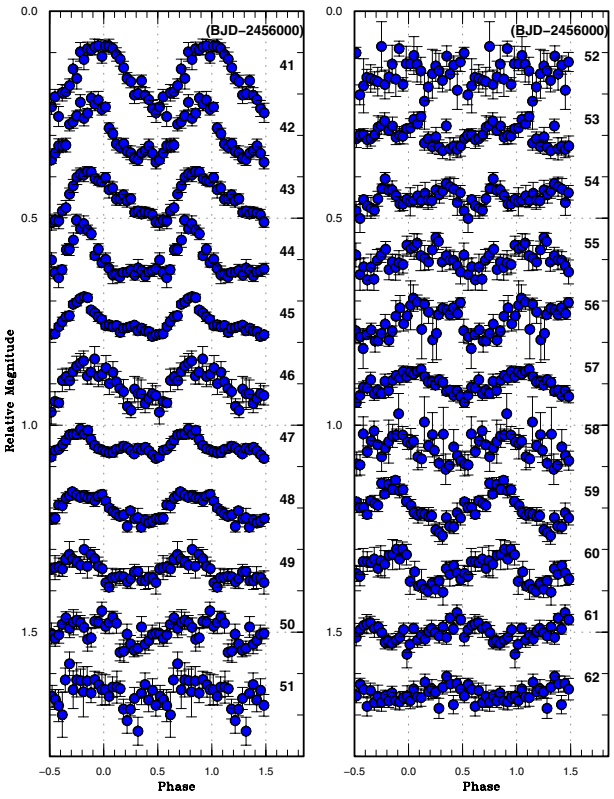

Fig. 47. Variation of superhump profiles in SBS 1108 (2012). A period of 0.039111 d was assumed in phase-averaging. Although the amplitude of superhumps decreased during the period (BJD 2456050–2456056), it increased again (BJD 2456057–2456060).

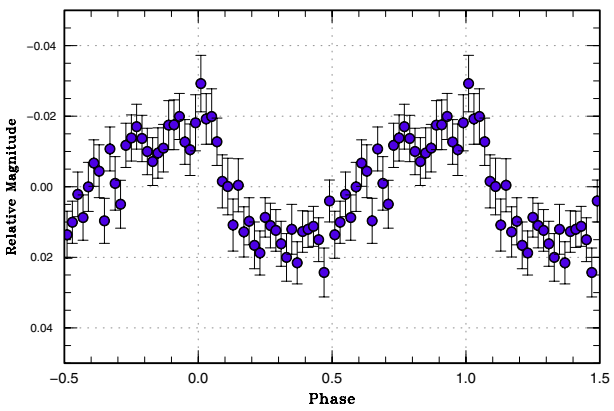

Fig. 48. Waveform of a candidate orbital period (0.038449 d) of SBS 1108.

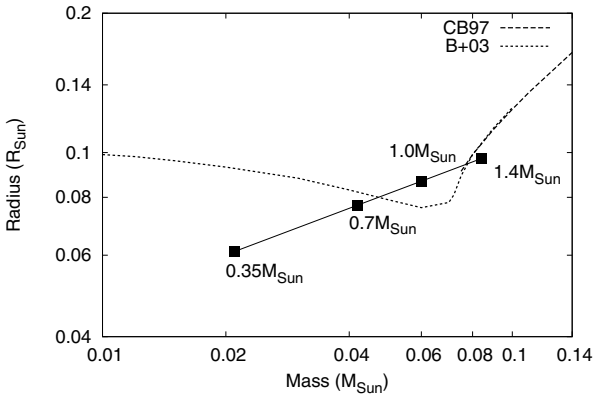

Fig. 49. Mass–radius relation of the secondary of SBS 1108. Volume radii of the Roche lobe of the secondary for various masses of the primary are plotted against the mass–radius relationship of 10 Gyr brown dwarfs and low-mass main-sequence stars by Baraffe et al. (2003) (B03) and Chabrier and Baraffe (1997) (CB97).

Table 55. Superhump maxima of SDSS J073208 (2012).

E	Max*	Error	$O-C^{\dagger}$	$N^{\ddagger}$
0	55977.6385	0.0015	−0.0009	41
1	55977.7190	0.0008	0.0000	51
2	55977.7994	0.0012	0.0009	53
72	55983.3671	0.0025	−0.0000	43

* BJD − 2400000.
† Against max = 2455977.6394 + 0.079552E.
‡ Number of points used to determine the maximum.

December 29. The amplitude of the large outburst suggested an SU UMa-type dwarf nova, or even a WZ Sge-type (vsnet-alert 14041). Subsequent observations detected superhumps (vsnet-alert 14052). The times of superhump maxima are listed in table 65. Although the observations in the middle of the outburst were rather sparse, it is likely that we observed stage-B superhumps with a positive $P_{\rm dot}$. The amplitudes of the superhumps (cf. figure 59) resemble those of ordinary SU UMa-type dwarf novae, rather than those of extreme WZ Sge-type dwarf novae. The object, however, underwent a post-outburst rebrightening similar to those of WZ Sge-type dwarf novae (rebrightening followed by a short "dip"; vsnet-alert 14097).

3.61. OT J064608.2+403305

This transient (= CSS 080512:064608+403305; hereafter OT J064608) was detected by CRTS on 2008 May 12. A bright outburst in 2011 December was detected by E. Muyllaert (BAAVSS alert 2808). Subsequent observations confirmed the presence of superhumps (vsnet-alert 14023, 14036, 14039; figure 60). The times of superhump maxima are listed in table 66. $P_{\rm dot}$ was $+11.1(2.6) \times 10^{-5}$, a typical value for stage-B superhumps with this $P_{\rm SH}$.

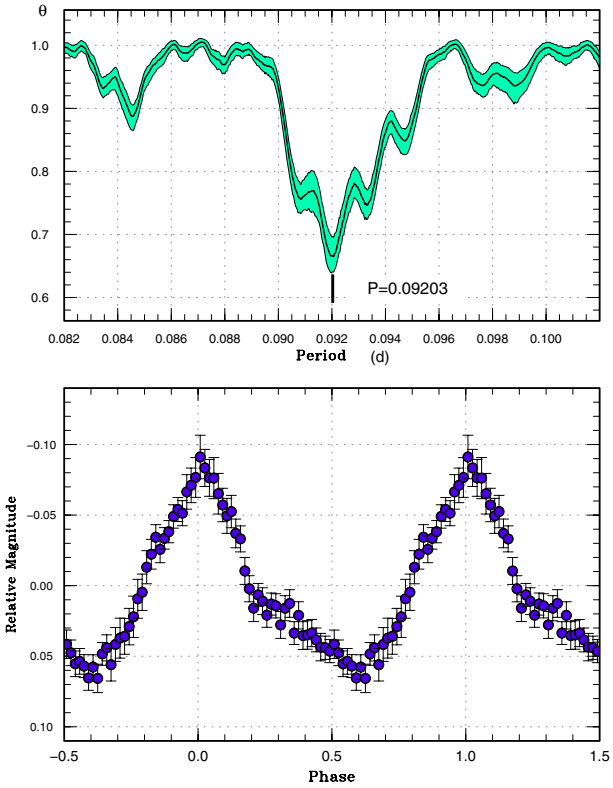

Fig. 50. Superhumps in SDSS J080303 (2011). Upper: PDM analysis. Lower: Phase-averaged profile.

Table 56. Superhump maxima of SDSS J080303 (2011).

E	Max*	Error	$O-C^{\dagger}$	$N^{\ddagger}$
0	55921.6801	0.0015	−0.0524	96
1	55921.7738	0.0026	−0.0499	56
10	55922.6375	0.0004	−0.0071	187
11	55922.7343	0.0005	−0.0016	137
17	55923.2981	0.0008	0.0150	104
21	55923.6649	0.0003	0.0169	99
22	55923.7573	0.0005	0.0181	75
27	55924.2195	0.0005	0.0243	101
28	55924.3112	0.0009	0.0247	100
30	55924.4919	0.0006	0.0230	59
31	55924.5842	0.0006	0.0240	59
43	55925.6680	0.0006	0.0133	99
87	55929.6462	0.0020	−0.0220	97
88	55929.7332	0.0022	−0.0262	98

* BJD − 2400000.
† Against max = 2455921.7325 + 0.091215E.
‡ Number of points used to determine the maximum.

Table 57. Superhump maxima of SDSS J165359 (2012).

E	Max*	Error	$O-C$†	N‡
0	56062.5903	0.0004	0.0011	67
1	56062.6574	0.0004	0.0031	52
13	56063.4328	0.0004	−0.0025	105
14	56063.4999	0.0004	−0.0005	116
23	56064.0889	0.0009	0.0027	70
24	56064.1505	0.0011	−0.0008	52
28	56064.4077	0.0008	−0.0040	47
91	56068.5137	0.0007	0.0015	64
106	56069.4898	0.0009	0.0013	57
107	56069.5505	0.0007	−0.0032	55
115	56070.0719	0.0022	−0.0025	132
121	56070.4688	0.0013	0.0039	48

* BJD − 2400000.
† Against max = 2456062.5892 + 0.065089E.
‡ Number of points used to determine the maximum.

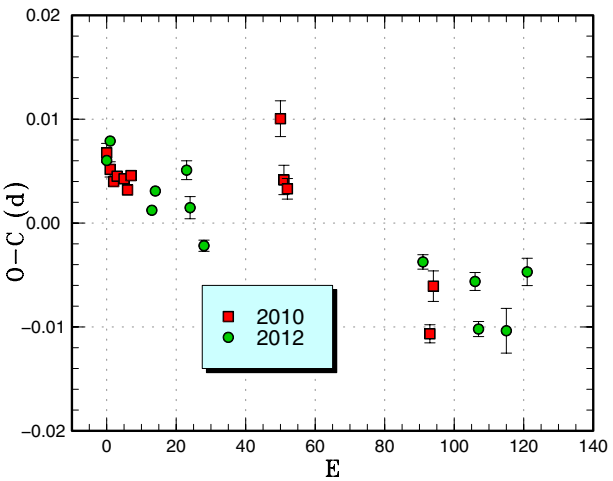

Fig. 51. Comparison of different superoutbursts of SDSS J165359 in the $O-C$ diagram. A period of 0.06520 d was used to draw this figure. Approximate cycle counts (E) after the start of the observation were used. We cannot obtain a better match even if we shifted the cycle number between these superoutbursts.

3.62. *OT J081117.1+152003*

This transient (= CSS 111030:081117+152003; hereafter OT J081117) was detected by CRTS on 2011 October 30. The object had a large (∼ 6 mag) amplitude of the outburst, and was considered to be a likely candidate for the SU UMa-type dwarf nova. As expected, short-period superhumps were detected (vsnet-alert 13816; figure 61). Due to the insufficient observation, we were not able to measure $P_{\rm SH}$ precisely. The times of superhump maxima are listed in table 67. We list the most likely alias determined by the PDM method in table 2.

3.63. *OT J084127.4+210053*

This transient (= CSS 090525:084127+210054; hereafter OT J084127) was detected by CRTS on 2009 May 25. There were other known outbursts (CRTS detections) in 2007 September, 2010 January, and 2010 May. Kato, Maehara, and Uemura (2012b) suggested $P_{\rm orb} = 0.10$ d derived from the SDSS colors. The 2012 March outburst was observed and its superhumps were immediately detected (vsnet-alert 14391, 14392, 14396; figure 62). The times of superhump maxima are listed in table 68.

Table 58. Eclipse minima of SDSS J170213 (2011).

E	Minimum*	Error	$O-C$†
21165	55766.47660	0.00003	0.00018
21195	55769.47798	0.00004	−0.00091
21196	55769.57867	0.00004	−0.00029
21205	55770.48023	0.00004	0.00052
21214	55771.38036	0.00012	−0.00009
21215	55771.48107	0.00009	0.00054
21224	55772.38128	0.00003	0.00001
21225	55772.48149	0.00005	0.00013
21234	55773.38194	0.00003	−0.00015
21235	55773.48223	0.00003	0.00005
21245	55774.48296	0.00004	−0.00004
21248	55774.78356	0.00013	0.00032
21254	55775.38378	0.00003	0.00004
21255	55775.48378	0.00003	−0.00004
21264	55776.38464	0.00003	0.00008
21265	55776.48473	0.00005	0.00009
21270	55776.98509	0.00005	0.00004
21271	55777.08517	0.00006	0.00003
21274	55777.38503	0.00003	−0.00035
21280	55777.98583	0.00011	−0.00005
21281	55778.08560	0.00005	−0.00036
21284	55778.38640	0.00014	0.00020

* BJD − 2400000.
† Against equation (3).

3.64. *OT J094854.0+014911*

This transient (= CSS 120315:094854+014911; hereafter OT J094854) was detected by CRTS on 2012 March 15. There were no previous outbursts detected by CRTS. Immediately following this discovery, superhumps were detected (vsnet-alert 14326, 14327; figure 63). The SDSS colors of the quiescent counterpart resemble those of ordinary SU UMa-type dwarf novae, rather than those of extreme WZ Sge-type dwarf novae (vsnet-alert 14328; see also Kato et al. 2012b). S. Yoshida pointed out that the object was already in outburst on March 11 (vsnet-alert 14330). The times of superhump maxima are listed in table 69. It is likely that there was a stage B–C transition at around $E = 77$. We missed the early part of stage B, and the observations were not sufficient to determine the period of stage-C superhumps.

3.65. *OT J102842.9−081927*

This object (= CSS 090331:102843−081927; hereafter OT J102842) was originally discovered by CRTS. Kato et al. (2009) indicated that this object has a very short [0.038147(14) d] superhump period, suggesting an unusual evolutionary state similar to EI Psc (Thorstensen et al. 2002a;

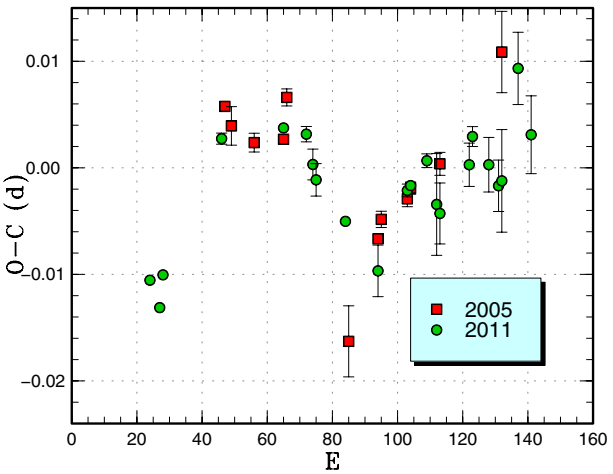

Fig. 52. Comparison of different superoutbursts of SDSS J170213 in the $O-C$ diagram. A period of 0.10510 d was used to draw this figure. Approximate cycle counts (E) after the start of the superoutburst were used.

Uemura et al. 2002) or V485 Cen (Augusteijn et al. 1993, 1996; Olech 1997). The 2012 superoutburst, detected by CRTS, was also observed. The times of superhump maxima are listed in table 70. Contrary to Kato et al. (2009), the present observation gave a longer superhump period, particularly during the first half of the observation. It is difficult to reconcile disagreement between two superhump periods unless we assume that the first half of the 2012 observation recorded stage-A superhumps (since CRTS observations were typically made with an interval of 10 d, it is difficult to determine the starting date of outbursts). In table 2 and figure 64 we gave values and a comparison of $O-C$ diagrams based on this identification. A problem with this interpretation is, however, that it cannot explain the large amplitude of superhumps at the initial stage of the 2012 observation. It may be either that the evolution of the superhumps in this system is unusual, or that the period of the superhumps greatly varies from superoutburst to superoutburst. Further observations, particularly regular monitoring to record the start of outbursts and the superhumps during the full course of the outbursts, are needed.

3.66. OT J105122.8+672528

This transient (= CSS 120101:105123+672528; hereafter OT J105122) was detected by CRTS on 2012 January 1. There is an X-ray counterpart, 1RXS J105120.5+672550. D. Denisenko reported that this object was recorded bright on a Palomer Sky Survey infrared plate taken on 1999 December 12 (vsnet-alert 14060). Subsequent observations detected superhumps (vsnet-alert 14067, 14072). The MASTER team also independently detected this transient (Tiurina et al. 2012). Although it was classified as a CV (Sokolovsky et al. 2012), the authors were not able to detect any variability. Pavlenko et al. (2012a) further observed this object in quiescence, and recorded high-amplitude variations with a period of 0.0596(9) d, which was considered to be the orbital period.

The times of superhump maxima are listed in table 71.

Table 59. Superhump maxima of SDSS J170213 (2011).

E	Max*	Error	$O-C$†	Phase‡	N§
0	55766.1025	0.0004	−0.0084	0.27	125
3	55766.4152	0.0003	−0.0111	0.39	187
4	55766.5234	0.0004	−0.0081	0.47	190
22	55768.4280	0.0005	0.0041	0.50	89
32	55769.4973	0.0010	0.0221	0.19	181
33	55769.5977	0.0011	0.0174	0.19	122
41	55770.4259	0.0004	0.0045	0.46	82
48	55771.1610	0.0007	0.0037	0.81	141
50	55771.3684	0.0014	0.0008	0.88	35
51	55771.4720	0.0015	−0.0007	0.92	77
60	55772.4140	0.0005	−0.0048	0.33	87
70	55773.4604	0.0024	−0.0098	0.78	96
79	55774.4138	0.0006	−0.0025	0.31	120
80	55774.5194	0.0005	−0.0021	0.37	110
85	55775.0472	0.0006	0.0001	0.64	169
88	55775.3584	0.0048	−0.0041	0.75	53
89	55775.4627	0.0029	−0.0050	0.79	100
98	55776.4132	0.0020	−0.0007	0.29	157
99	55776.5209	0.0009	0.0019	0.36	106
104	55777.0438	0.0026	−0.0009	0.59	231
107	55777.3571	0.0024	−0.0030	0.72	82
108	55777.4626	0.0048	−0.0026	0.77	79
113	55777.9987	0.0034	0.0078	0.13	148
117	55778.4129	0.0037	0.0015	0.27	138

* BJD − 2400000.
† Against max = 2455766.1110 + 0.105132E.
‡ Orbital phase.
§ Number of points used to determine the maximum.

During these observations, the amplitudes of superhumps were small (figure 65), and not triangular, as typically seen in early stage superhumps. Although it is likely that these superhumps were recorded when their amplitudes become smaller (particularly before the stage B–C transition, cf. subsection 4.7 of Kato et al. 2012a), it was impossible to identify the stages in which they were observed.

3.67. OT J125905.8+242634

This transient (= CSS 120424:125906+242634; hereafter OT J125905) was detected by CRTS on 2012 April 24. There was a previous outburst in 2009 February. Subsequent observations detected superhumps (vsnet-alert 14500, 14501). The two superhump maxima were BJD 2456045.3135(17) ($N = 28$) and 2456045.3795(14) ($N = 35$). We adopted a period of 0.0660(2) d shown by this timing analysis. The profile of the superhumps is shown in figure 66.

3.68. OT J131625.7−151313

This transient (= CSS 080427:131626−151313; hereafter OT J131625) was detected by CRTS on 2008 April 27. Two more outbursts were detected by CRTS in 2010 February and 2011 April. The 2012 March outburst was also detected by CRTS. The subsequent observation clarified the presence of superhumps (vsnet-alert 14376, 14377). Since the observation was carried out only on one night, we obtained a single

Table 60. Superhump maxima of SDSS J172102 (2012).

E	Max*	Error	$O-C^{\dagger}$	$N^{\ddagger}$
0	56087.5334	0.0007	0.0035	18
1	56087.5601	0.0008	0.0036	19
82	56089.7123	0.0007	−0.0043	13
83	56089.7401	0.0007	−0.0032	14
84	56089.7687	0.0010	−0.0013	12
85	56089.7919	0.0017	−0.0047	14
86	56089.8217	0.0014	−0.0016	12
87	56089.8449	0.0008	−0.0050	10
88	56089.8753	0.0011	−0.0013	14
89	56089.9039	0.0016	0.0006	13
90	56089.9306	0.0015	0.0007	9
120	56090.7290	0.0011	−0.0010	13
122	56090.7869	0.0019	0.0036	14
123	56090.8112	0.0032	0.0012	14
124	56090.8354	0.0056	−0.0013	13
127	56090.9128	0.0041	−0.0039	13
233	56093.7449	0.0021	0.0015	13
234	56093.7751	0.0037	0.0050	14
236	56093.8200	0.0012	−0.0034	13
237	56093.8512	0.0013	0.0011	8
238	56093.8733	0.0019	−0.0035	14
239	56093.9027	0.0032	−0.0007	13
271	56094.7616	0.0007	0.0048	11
272	56094.7900	0.0030	0.0065	14
273	56094.8203	0.0050	0.0101	14
274	56094.8427	0.0012	0.0059	8
275	56094.8690	0.0033	0.0055	13
345	56096.7276	0.0019	−0.0026	11
346	56096.7560	0.0020	−0.0009	10
347	56096.7784	0.0019	−0.0051	14
350	56096.8612	0.0021	−0.0023	13
384	56097.7699	0.0025	−0.0004	11
387	56097.8535	0.0022	0.0033	11
388	56097.8736	0.0057	−0.0033	13
389	56097.9032	0.0033	−0.0004	14
390	56097.9289	0.0016	−0.0013	12
457	56099.7196	0.0050	0.0026	13
460	56099.8005	0.0044	0.0035	13
461	56099.8212	0.0034	−0.0025	9
462	56099.8486	0.0024	−0.0017	12
463	56099.8699	0.0050	−0.0071	14

* BJD − 2400000.
† Against max = 2456087.5299 + 0.026668E.
‡ Number of points used to determine the maximum.

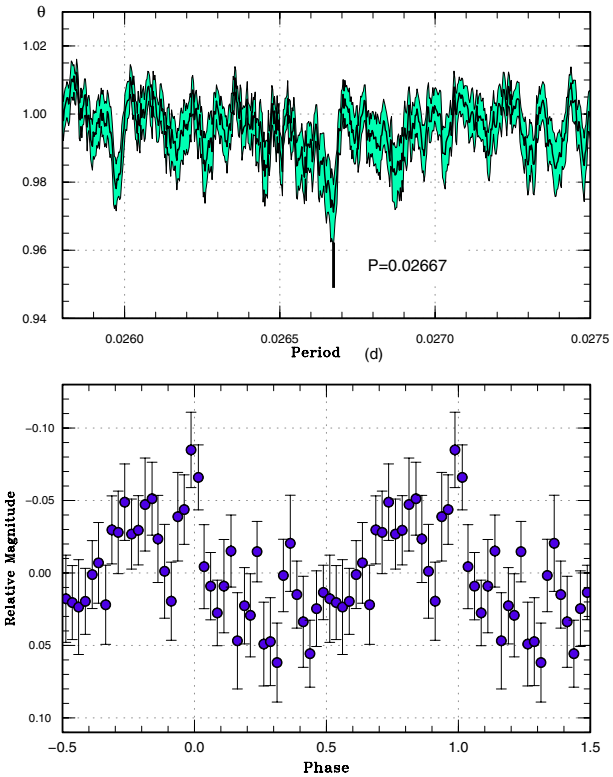

Fig. 53. Superhumps in SDSS J172102 (2012). Upper: PDM analysis. The rejection rate for bootstrapping was reduced to 0.2 for better visualization. Lower: Phase-averaged profile.

superhump maximum of BJD 2456012.5086(9) ($N = 71$). The best-superhump period is 0.0955(8) d (PDM method).

3.69. OT J142548.1+151502

This transient (= CSS 110628:142548+151502; hereafter OT J142548) was detected by CRTS on 2011 June 28. Only a single-night observation was available, and it clearly showed superhumps (vsnet-alert 13474). The best-superhump period (PDM method) was 0.0984(10) d, and we obtained only two superhump maxima: BJD 2455742.3565(9) ($N = 34$) and 2455742.4548(14) ($N = 27$).

3.70. OT J144252.0−225040

This transient (= CSS 120417:144252−225040; hereafter OT J144252) was detected by CRTS on 2012 April 17. The large outburst amplitude attracted attention (vsnet-alert 14448). Subsequent observations detected superhumps (vsnet-alert 14455, 14457; figure 67). The times of superhump maxima are listed in table 72. A clear pattern of stages B and C can be recognized. Despite the large outburst amplitude and the lack of past outbursts in the CRTS data, the $O-C$ diagram resembles those of ordinary SU UMa-type dwarf novae, rather than those of extreme WZ Sge-type dwarf novae.

3.71. OT J144453.1−131118

This transient (= CSS 120424:144453−131118; hereafter OT J144453) was detected by CRTS on 2012 April 24. There was a past outburst in 2005 December. Although there was a hint of superhumps in the first observation (vsnet-alert 14491), confirmatory observations became available four days after (vsnet-alert 14507). Later observations well characterized the superhumps (vsnet-alert 14516, 14522, 14530; figure 68). The times of superhump maxima are listed in table 73. There was no hint of any period variation. By taking the long initial gap of the observation into account, we are likely to have observed stage-C superhumps. However, it is not

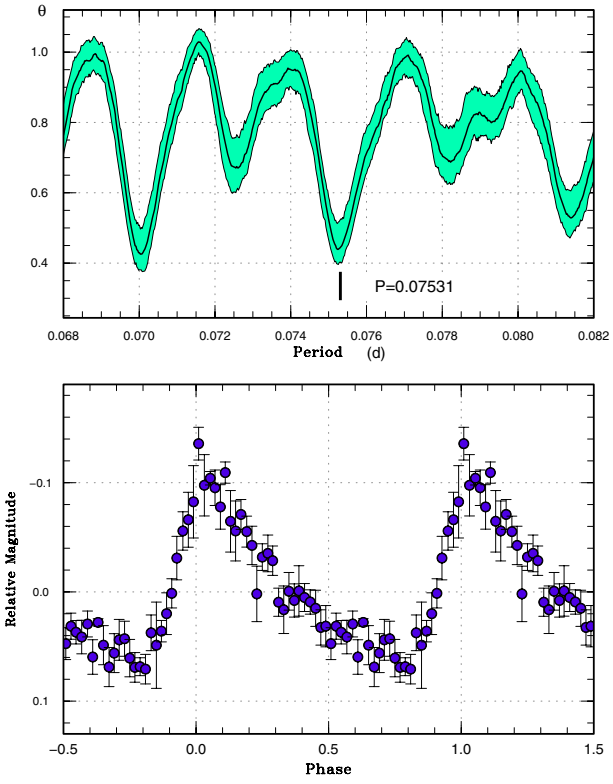

Fig. 54. Superhumps in SDSS J210449 (2011). Upper: PDM analysis. The alias selection was based on the superhump timing analysis. Lower: Phase-averaged profile.

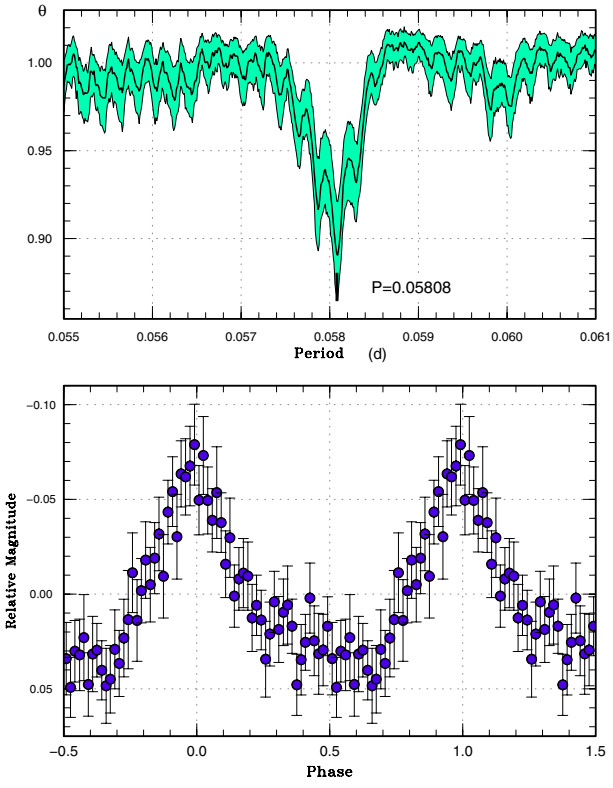

Fig. 55. Superhumps in SDSS J220553 (2011). Upper: PDM analysis. Lower: Phase-averaged profile.

Table 61. Superhump maxima of SDSS J210449 (2011).

E	Max*	Error	$O-C$†	N‡
0	55834.4629	0.0008	−0.0000	79
26	55836.4217	0.0015	0.0000	69
27	55836.4970	0.0011	−0.0000	55

* BJD − 2400000.
† Against max = 2455834.4629 + 0.075338E.
‡ Number of points used to determine the maximum.

excluded that this object has a virtually zero $P_{\rm dot}$, as seen in some long-$P_{\rm orb}$ systems.

3.72. OT J145921.8+354806

This transient (= CSS 110613:145922+354806; hereafter OT J145921) was detected by CRTS on 2011 June 13. There was an earlier outburst in 2008 April. Subsequent observations detected superhumps (vsnet-alert 13427; figure 69). The times of superhump maxima are listed in table 74. The large amplitudes of the superhumps suggest that the outburst was detected at a relatively early stage. The resultant $P_{\rm dot}$ was less likely to be negative, as expected for an object with this $P_{\rm SH}$, and may even be positive. The object may be analogous to GX Cas (cf. Kato et al. 2012a), which showed a large positive $P_{\rm dot}$ despite its long $P_{\rm SH}$.

3.73. OT J155631.0−080440

The object was detected to be a transient (= CSS 090321:155631−080440; hereafter OT J155631) by CRTS on 2009 March 21. Although several outbursts have been recorded since then, the 2012 March outburst was the brightest (15.3 mag) in its history. Superhumps were soon detected (vsnet-alert 14406, 14416; figure 70). The times of superhump maxima are listed in table 75.

3.74. OT J160410.6+145618

The object was detected to be a transient (= CSS 120326:160411+145618; hereafter OT J160410) by CRTS on 2012 March 26. There was another outburst in 2010 July (CRTS data). A large (> 5 mag) amplitude of the outburst was noted (vsnet-alert 14384). Although there was only a single-night observation, two superhump maxima were recorded: BJD 2456014.5194(8) (N = 35) and BJD 2456014.5841(11) (N = 34). The superhump period obtained by the PDM method is 0.0656(5) d.

3.75. OT J162806.2+065316

The object was detected to be a transient (= CSS 110611:162806+065316; hereafter OT J162806) by CRTS on 2011 June 11. The object was selected as a candidate for QSO based on the SDSS colors (Richards et al. 2009). The existence of two previous outbursts in the CRTS data confirmed the DN-type nature (vsnet-alert 13413). The observations soon confirmed that the object shows superhumps

Table 62. Superhump maxima of SDSS J220553 (2011).

E	Max*	Error	$O-C^{\dagger}$	$N^{\ddagger}$
0	55702.2039	0.0015	0.0042	109
1	55702.2618	0.0008	0.0039	119
12	55702.8979	0.0004	0.0003	60
13	55702.9551	0.0004	−0.0006	53
29	55703.8834	0.0004	−0.0028	87
30	55703.9436	0.0003	−0.0007	86
40	55704.5235	0.0010	−0.0024	31
46	55704.8715	0.0009	−0.0032	87
47	55704.9297	0.0005	−0.0032	86
63	55705.8626	0.0008	−0.0007	60
64	55705.9204	0.0005	−0.0010	61
97	55707.8427	0.0028	0.0023	36
98	55707.9006	0.0007	0.0021	60
99	55707.9586	0.0007	0.0018	43

* BJD − 2400000.
† Against max = 2455702.1998 + 0.058151E.
‡ Number of points used to determine the maximum.

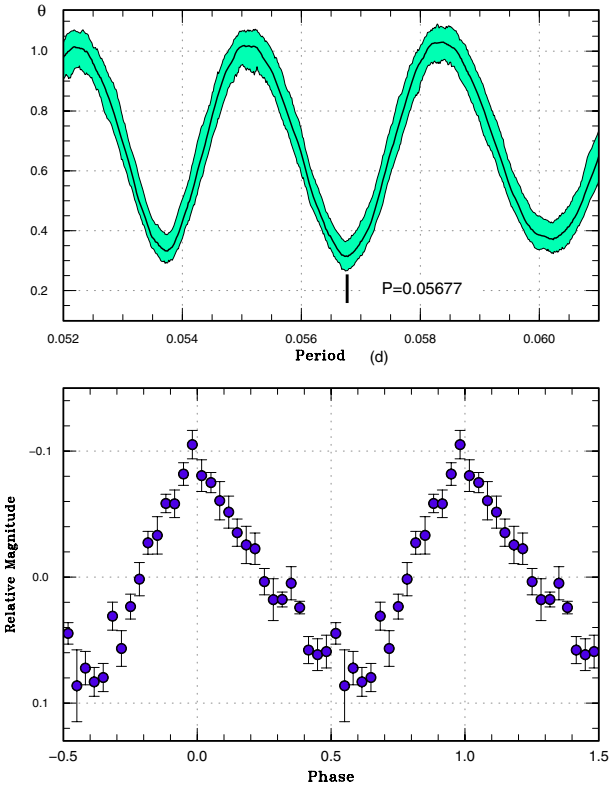

Fig. 56. Superhumps in OT J001952 (2012). Upper: PDM analysis. The alias selection was based on a continuous single-night observation. Lower: Phase-averaged profile.

(vsnet-alert 13416; figure 71). The times of superhump maxima are listed in table 76.

3.76. OT J163942.7+122414

The object was originally detected to be a transient (= CSS 080131:163943+122414; hereafter OT J163942) by CRTS on 2008 January 31. We observed the 2012 April outburst detected by CRTS. The observations confirmed the presence of superhumps (vsnet-alert 14474; figure 72). The times of superhump maxima are listed in table 77. The period given in table 2 refers to the result of the PDM analysis. The object appears to be a long-$P_{\rm orb}$ system with frequent outbursts, based on numerous detections of its outbursts by CRTS.

3.77. OT J170609.7+143452

The object was originally detected to be a transient (= CSS 090205:170610+143452; hereafter OT J170609) by CRTS on 2009 February 5. Although superhumps were detected during the 2009 outburst (vsnet-alert 11061), their period was not well determined because the object faded quickly after this observation.

The object underwent another outburst in 2011 June (CRTS detection, see also vsnet-alert 13456). Although it once faded (vsnet-alert 13464), it showed a rebrightening in July (vsnet-alert 13481). The outburst turned out to be a superoutburst preceded by a precursor. Observations on two nights yielded a likely superhump period of 0.05946(8) d (PDM analysis; figure 73), although one-day aliases cannot be perfectly excluded. The selection of the alias appears to be justified by an independently determined spectroscopic period of 0.0582 d (Thorstensen & Skinner 2012), yielding an ϵ value of 2.2%. The times of superhump maxima are listed in table 78.

Table 63. Superhump maxima of OT J001952.

E	Max*	Error	$O-C^{\dagger}$	$N^{\ddagger}$
0	55958.3297	0.0005	0.0005	61
1	55958.3856	0.0007	−0.0005	42
17	55959.2959	0.0006	0.0005	50
18	55959.3517	0.0008	−0.0005	60

* BJD − 2400000.
† Against max = 2455958.3292 + 0.056827E.
‡ Number of points used to determine the maximum.

3.78. OT J173516.9+154708

The object was detected to be a transient (= CSS 110623:173517+154708; hereafter OT J173516) by CRTS on 2011 June 23. The object was also in outburst in GSC 1.2. Although early observations already recorded superhump-like modulations (vsnet-alert 13465, 13468, 13470), the times of the maxima cannot be well expressed by any trial period (vsnet-alert 13473, 13482). Although the main power of the periodicity was recorded in the range of 0.05–0.06 d, we were not able to sort out a single superhump period at the time of the observation. On July 9, the object entered a rapid decline phase.

When the best part (June 26–29) of our observation before

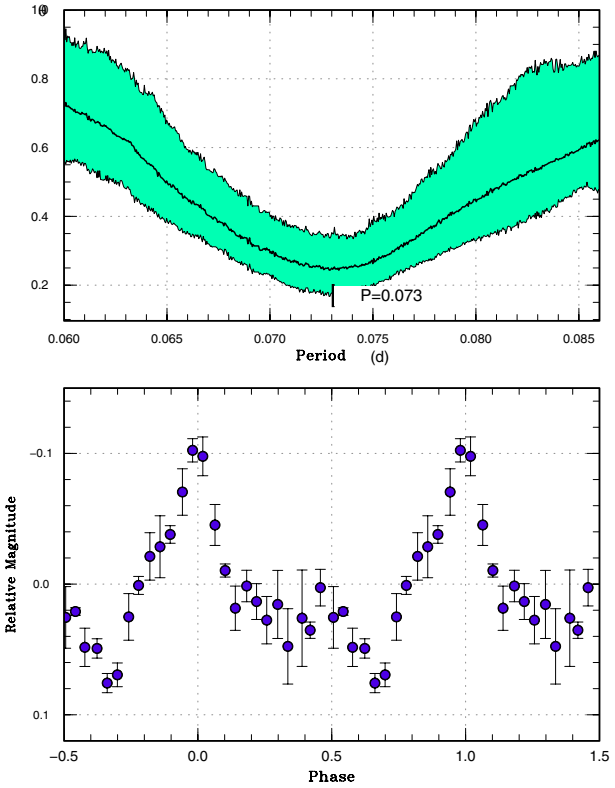

Fig. 57. Superhumps in OT J011516 (2012). Upper: PDM analysis. Lower: Phase-averaged profile.

the rapid decline is used, there appeared to be two strong signals at around 0.05436 d and 0.05827 d based on the PDM analysis. The Lasso analysis, which is less affected by the window function, yielded two same signals (figure 74). By partially subtracting the mean profiles from the observations folded by individual periods, we have been able to decompose the light curve into the two periods (figure 75). It is shown that a simple superposition of these two waves expresses the observed light curve fairly well (figure 76).

The exact identification of these periods are still unclear. It might be that the shorter period is $P_{\rm orb}$, and the longer period is $P_{\rm SH}$. In this case, however, the ϵ value is 7.2%, extremely too large for this $P_{\rm orb}$, and none of non-eclipsing SU UMa-type dwarf novae have yet shown similar amplitudes of orbital humps and superhumps at the same time. We put an alternative interpretation on the periodicity; the longer period is $P_{\rm orb}$ and the shorter period represents negative superhumps. The small amplitude of superhumps, when compared with that of orbital humps, may be reconciled if negative superhumps were indeed excited. The exact identification of the periods should await future observations.

3.79. OT J184228.1+483742

This object (hereafter OT J184228) was discovered by H. Nishimura on 2011 September 5.5293 UT at an unfiltered CCD magnitude of 11.8 (= PNV J18422792+4837425; Nakano et al. 2011). S. Kiyota's early multicolor photometry has already suggested a dwarf-nova-type nature (vsnet-

Table 64. Superhump maxima of OT J050716.

E	Max*	Error	$O-C^\dagger$	$N^\ddagger$
0	55952.4395	0.0009	−0.0012	31
1	55952.5075	0.0024	0.0015	19
14	55953.3518	0.0055	−0.0033	28
15	55953.4234	0.0018	0.0030	36

* BJD − 2400000.
† Against max = 2455952.4407 + 0.065317E.
‡ Number of points used to determine the maximum.

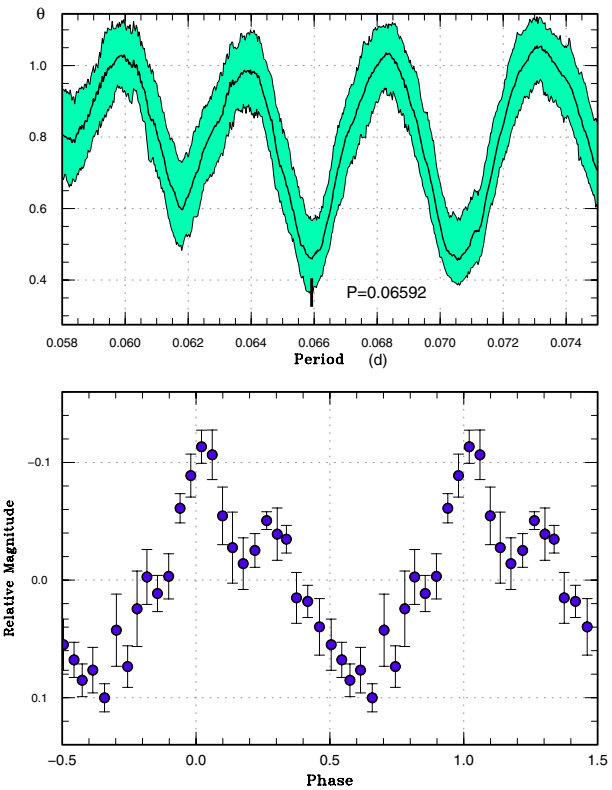

Fig. 58. Superhumps in OT OT J050716 (2012). Upper: PDM analysis. Lower: Phase-averaged profile.

alert 13645). M. Fujii, A. Ayani, C. Buil (vsnet-alert 13650, 13651, 13655), and A. Arai[6] reported spectra, all of which indicated Balmer lines in absorption with emission cores for Hα and Hβ, indicating that the object is indeed a dwarf nova in outburst. The relatively narrow absorption suggested a low inclination of this object. U. Munari also reported on its spectrum (Nakano et al. 2011). Although there were small-amplitude variations, the object started rapidly fading on September 25 before developing superhumps (we call this outburst the "first plateau phase"; vsnet-alert 13703). The object brightened again on October 3 (vsnet-alert 13713), and its brightness reached the second plateau phase. During

[6] ⟨http://www.cbat.eps.harvard.edu/unconf/followups/J18422792+4837425.html⟩.

Table 65. Superhump maxima of OT J055721 (2011).

E	Max*	Error	$O-C$†	N‡
0	55926.5487	0.0010	0.0008	22
1	55926.6101	0.0006	0.0024	14
2	55926.6685	0.0005	0.0010	10
3	55926.7283	0.0015	0.0010	15
4	55926.7898	0.0011	0.0028	20
17	55927.5657	0.0006	0.0019	17
18	55927.6250	0.0012	0.0014	14
19	55927.6836	0.0006	0.0002	13
20	55927.7438	0.0005	0.0008	17
21	55927.8028	0.0007	0.0000	20
33	55928.5184	0.0024	−0.0015	17
34	55928.5806	0.0010	0.0010	15
35	55928.6376	0.0009	−0.0018	14
36	55928.6967	0.0008	−0.0024	16
37	55928.7549	0.0005	−0.0040	17
38	55928.8170	0.0006	−0.0016	19
94	55932.1550	0.0068	−0.0100	100
152	55935.6360	0.0036	0.0051	14
153	55935.6934	0.0029	0.0029	17

* BJD − 2400000.
† Against max = 2455926.5480 + 0.059756E.
‡ Number of points used to determine the maximum.

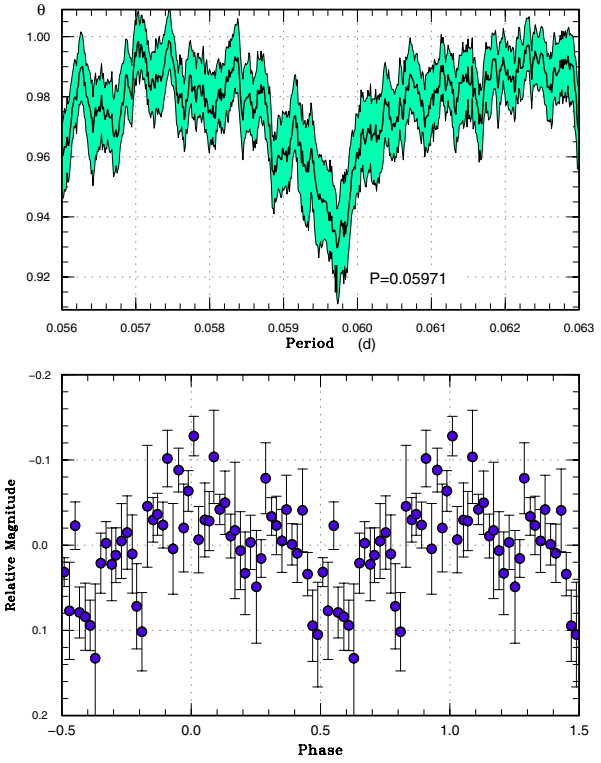

Fig. 59. Superhumps in OT J055721 (2011). Upper: PDM analysis. The rejection rate for bootstrapping was reduced to 0.2 for better visualization. Lower: Phase-averaged profile.

this plateau phase, ordinary superhumps finally developed (vsnet-alert 13726, 13728, 13729). Such development of the outburst was unprecedented in dwarf novae. On October 18, the object entered a rapid fading stage (vsnet-alert 13775). It remained above quiescence, even following the rapid decline, and there was another rebrightening following the second plateau phase (N. Katysheva et al. in preparation).

The times of the superhump maxima during the second plateau phase and the post-superoutburst stage are listed in table 79. The epochs $E = 0$, 1 were recorded during the rise in brightness to the second plateau phase. The times for $E > 206$ were recorded during the post-superoutburst stage. Although the humps were clearly detected, the cycle counts for the latter maxima were slightly uncertain. As can be seen from $E = 413$ and $E = 428$, there appeared to have been double maxima during one superhump cycle. The low visibility in the evening during this stage hindered us from unambiguously identifying the nature of these maxima. We identified $E \leq 64$ as stage-A superhumps, because they evolved during this stage, and subsequent superhumps as stage B. However, these stages may be inadequate, considering the peculiar evolution of the entire outburst. In determining the period of stage-A superhumps, we disregarded $E = 0$, 1. The period of stage-B superhumps was very stable, and $P_{\rm dot}$ was almost zero (figure 77). Although these superhumps bore more characteristics of stage-C superhumps in ordinary SU UMa-type dwarf novae, identification of the nature should await the fruits of future research. The amplitudes of superhumps were small (0.045 mag in full amplitude in average), suggesting a weak manifestation of tidal instability.

During the first plateau phase, there was a possible signal of early superhumps with a period of 0.07168(1) d (figure 78). Since the signal had only a small amplitude, exact identification of the orbital period should await future observations. Assuming that this period is close to the orbital period, we obtained an ϵ value of 0.9%, comparable to those of short-$P_{\rm orb}$ WZ Sge-type dwarf novae, but this value is unusually small for a $P_{\rm orb} = 0.07168$ d object. This might suggest the presence of an anomalously undermassive secondary, and this object could be a likely candidate for a period bouncer.

The unique feature of the outburst evolution might also be understood if the mass-ratio is anomalously low, as explained in the following scenario: (1) The disk was initially expanded enough to trigger the 2:1 resonance; (2) The disk started to cool down before the 3:1 resonance governs as seen in ordinary WZ Sge-type dwarf novae, and the object made a temporary excursion into a quiescent state; then (3) the 3:1 resonance started to grow slowly and triggered a second thermal instability, and the outburst entered the second plateau phase. The second plateau phase apparently started from an inside-out type outburst, as suggested by the slow rise. The small amplitude probably reflects weak tidal torque resulting from a low mass-ratio.

The object has features of long $P_{\rm orb}$ and apparently low mass-ratio, which suggests a brown-dwarf secondary, the famous CV GD 552 (Hessman & Hopp 1990; Unda-Sanzana et al. 2008), which has never been observed to undergo an outburst (cf. Richter 1990). If GD 552 were to undergo an outburst, we might expect a phenomenon similar

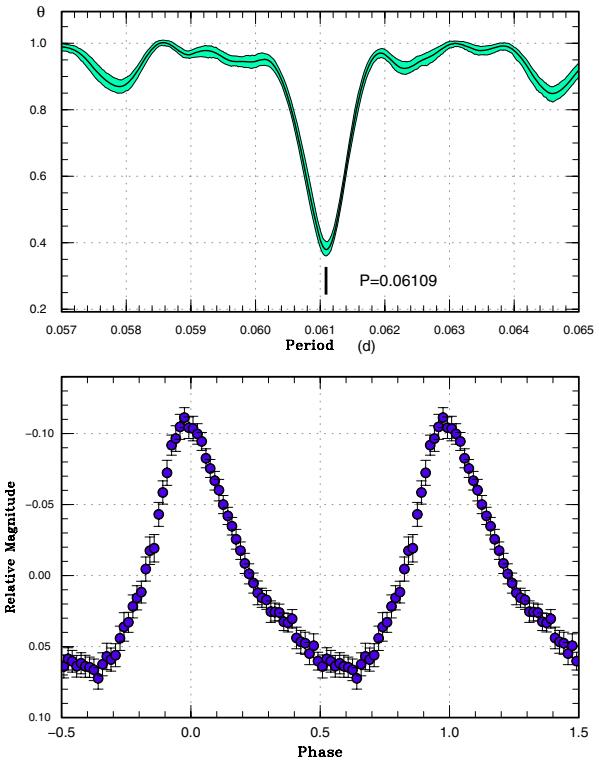

Fig. 60. Superhumps in OT J064608 (2011). Upper: PDM analysis. Lower: Phase-averaged profile.

Table 66. Superhump maxima of OT J064608 (2011).

E	Max*	Error	$O-C$†	N‡
0	55923.3629	0.0006	−0.0018	36
1	55923.4269	0.0002	0.0010	64
2	55923.4884	0.0002	0.0014	79
3	55923.5492	0.0002	0.0011	54
4	55923.6111	0.0002	0.0019	54
7	55923.7948	0.0002	0.0023	63
8	55923.8553	0.0002	0.0017	63
9	55923.9152	0.0006	0.0005	63
10	55923.9751	0.0003	−0.0007	64
17	55924.4049	0.0003	0.0013	64
18	55924.4661	0.0003	0.0015	64
23	55924.7705	0.0002	0.0004	64
24	55924.8319	0.0003	0.0006	64
25	55924.8923	0.0002	−0.0001	65
26	55924.9527	0.0003	−0.0007	64
27	55925.0124	0.0005	−0.0022	55
39	55925.7448	0.0008	−0.0031	36
40	55925.8078	0.0003	−0.0012	64
41	55925.8668	0.0003	−0.0032	64
42	55925.9280	0.0004	−0.0031	64
43	55925.9880	0.0005	−0.0043	63
56	55926.7855	0.0004	−0.0011	64
57	55926.8473	0.0003	−0.0004	64
58	55926.9074	0.0003	−0.0014	64
59	55926.9667	0.0008	−0.0032	63
60	55927.0366	0.0016	0.0055	34
82	55928.3828	0.0008	0.0075	65

* BJD − 2400000.
† Against max = 2455923.3648 + 0.061105E.
‡ Number of points used to determine the maximum.

to OT J184228.

A more detailed analysis will be reported in T. Ohshima et al. (in preparation).

3.80. OT J210950.5+134840

This object (hereafter OT J210950) was discovered to be a possible nova (= PNV J21095047+1348396) by K. Itagaki at a magnitude of 11.5 (unfiltered CCD) (Yamaoka et al. 2011). Although an initial announcement of discovery suggested the absence of a quiescent counterpart, independent examinations of plate archives indicated the presence of an 18–19 mag counterpart (S. Korotkiy, vsnet-alert 13342; E. Guido and G. Sostero, Yamaoka et al. 2011, vsnet-alert 13344). It was already suggested to be a WZ Sge-type dwarf nova with an amplitude exceeding 7 mag (vsnet-alert 13341). D. Denisenko also noted the presence of an M dwarf having a common proper motion and the detection of this object in GALEX UV data (vsnet-alert 13343). Although only low-amplitude variations were detected soon after its discovery, superhumps appeared on May 30, 6 d after the discovery (vsnet-alert 13359). The obtained period was not suggestive of an extreme WZ Sge-type dwarf nova. There was a hint of evolving (double wave) superhumps on May 28 (vsnet-alert 13363). The object was spectroscopically confirmed as a dwarf nova (Yamaoka et al. 2011).

The times of superhump maxima are listed in table 80. Distinct stages of A–C are present. Although the last two epochs were measured after a rapid fading, the times of maxima were well on the extension curve of the timings of stage-C superhumps recorded before the rapid fading, and we consider them to be persisting stage-C superhumps, as we already reported in the earlier papers (Kato et al. 2009, 2010, 2012a). The resultant $P_{\rm dot}$ for stage B was +8.5(0.6) $\times 10^{-5}$, whose large value is consistent with the idea that this object is not an extreme WZ Sge-type dwarf nova. No post-superoutburst rebrightening was recorded. The CRTS data[7] did not record a prior outburst, and the data indicated that the object remained brighter than quiescence during five months after the outburst. These features suggest that the outburst frequency is low, and the presence of a long-fading tail looks like those of WZ Sge-type dwarf novae (e.g., GW Lib, figure 33 in Kato et al. 2009). The object may be a WZ Sge-type dwarf nova with non-extreme properties, and showed a type-D superoutburst in terms of the lack of a post-superoutburst rebrightening. The $P_{\rm dot}$–ϵ relation [equation (6) in Kato et al. 2009] suggests an ϵ value of 2.6%.

In the PDM analysis (figure 79) there seems to be a slightly enhanced signal shorter than $P_{\rm SH}$; we employed the Lasso analysis to detect the possible $P_{\rm orb}$. The obtained candidate period was 0.05865(1) d, suggesting that the ϵ value for stage-B superhumps is 2.4%. Although this period is close to what

[7] ⟨http://nesssi.cacr.caltech.edu/catalina/20110606/1106061121124182967p.html⟩.

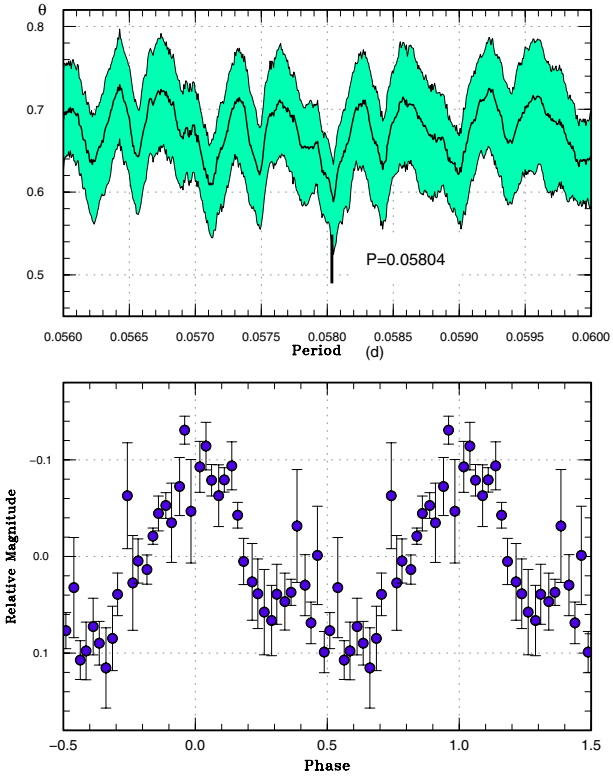

Fig. 61. Superhumps in OT J081117 (2011). Upper: PDM analysis. The rejection rate for bootstrapping was reduced to 0.2 for better visualization. Lower: Phase-averaged profile.

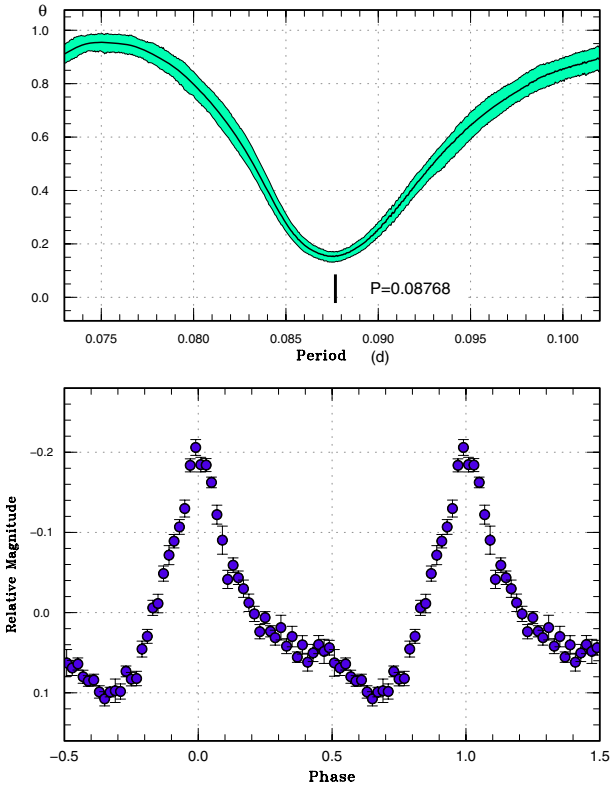

Fig. 62. Superhumps in OT J084127 (2012). Upper: PDM analysis. Lower: Phase-averaged profile.

Table 67. Superhump maxima of OT J081117 (2011).

E	Max*	Error	$O-C^{\dagger}$	$N^{\ddagger}$
0	55865.6525	0.0003	−0.0003	55
1	55865.7111	0.0004	0.0003	36
63	55869.3040	0.0031	−0.0000	20

* BJD − 2400000.
† Against max = 2455865.6529 + 0.057955E.
‡ Number of points used to determine the maximum.

Table 68. Superhump maxima of OT J084127 (2012).

E	Max*	Error	$O-C^{\dagger}$	$N^{\ddagger}$
0	56014.1263	0.0005	−0.0004	131
2	56014.3029	0.0004	0.0007	84
3	56014.3901	0.0004	0.0003	177
4	56014.4769	0.0007	−0.0006	91

* BJD − 2400000.
† Against max = 2456014.1268 + 0.087686E.
‡ Number of points used to determine the maximum.

was expected from the $P_{\rm dot}$–ϵ relation, it needs to be tested by future observations.

3.81. OT J214738.4+244553

The object was detected to be a transient (= CSS 111004:214738+244554; hereafter OT J214738) by CRTS on 2011 October 4. ASAS-3 (Pojmański 2002) recorded three additional outbursts. Subsequent observations recorded superhumps (vsnet-alert 13720, 13721; figure 80). The times of superhump maxima are listed in table 81. Although it is unclear whether we indeed observed the early stage of the outburst, the superhumps for $E \leq 20$ appear to be stage-A superhumps. There was no clear transition to stage C, and $P_{\rm dot}$ for $E \leq 20$ was $+8.8(1.0) \times 10^{-5}$, which is anomalously high for a long-$P_{\rm SH}$ system. The behavior resembles those of SDSS J170213 (subsection 3.53) and GX Cas (Kato et al. 2012a). There is a strong signal at 0.09273(3) d (see figure 80), which we interpret as being the orbital period. Assuming this period to be orbital, the ϵ value for the mean $P_{\rm SH}$ is 4.9%.

3.82. OT J215818.5+241925

This object (hereafter OT J215818) is an object reported by G. Sun and X. Gao to Central Bureau for Astronomical Telegrams (CBAT) Transient Objects Confirmation Page (TOCP), originally suspected to be a nova (= PNV J21581852+2419246). Soon after its discovery, R. Koff [8] detected modulations similar to superhumps. This

[8] ⟨http://www.cbat.eps.harvard.edu/unconf/followups/J21581852+2419246.html⟩.

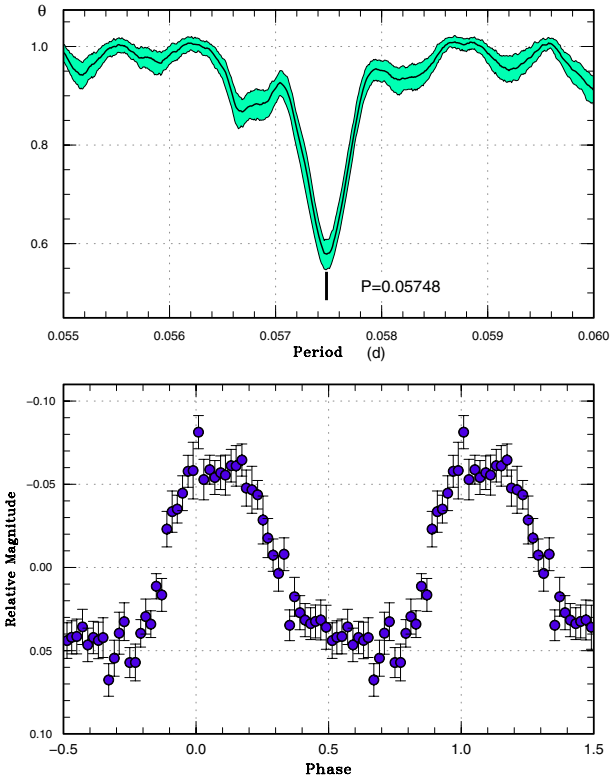

Fig. 63. Superhumps in OT J094854 (2012). Upper: PDM analysis. Lower: Phase-averaged profile.

finding was confirmed by subsequent observations (vsnet-alert 13803, 13805, 13807; figure 81), and the dwarf nova-type nature was confirmed. The times of superhump maxima are listed in table 82. The $O-C$ diagram shows typical stage-B and stage-C superhumps. $P_{\rm dot}$ for stage-B superhumps was not meaningfully determined, because the outburst was apparently observed only during its late course. Shears et al. (2012b) reported a $P_{\rm dot}$ of 0.06728(21) d using a slightly different data set, and obtained a similar pattern of the $O-C$ variation to this analysis. Shears et al. (2012b) also reported the possible presence of an orbital signal at 0.06606(35) d. Our analysis yielded only a very weak signal (see figure 81), and it appears to be still inconclusive. Using the Lasso method, we obtained a period of 0.06607(5) d, assuming that it is real periodicity.

3.83. OT J221232.0+160140

The object was detected to be a transient (= CSS 090911:221232+160140; hereafter OT J221232) by CRTS on 2009 September 11. A bright outburst was detected on 2011 December 23 by E. Muyllaert (BAAVSS alert 2804). Subsequent observations confirmed the presence of superhumps (vsnet-alert 14017, 14018, 14020; figure 82). The times of superhump maxima are listed in table 83. The early stage of the outburst was not observed. It is likely that there was a stage B–C transition at around $E = 29$.

Table 69. Superhump maxima of OT J094854 (2012).

E	Max*	Error	$O-C$†	N‡
0	56002.2812	0.0013	0.0024	24
1	56002.3383	0.0005	0.0019	40
2	56002.3946	0.0005	0.0007	31
18	56003.3141	0.0010	0.0002	40
19	56003.3720	0.0008	0.0007	40
22	56003.5445	0.0013	0.0006	20
23	56003.6031	0.0015	0.0018	16
24	56003.6583	0.0012	−0.0005	13
25	56003.7166	0.0005	0.0003	74
26	56003.7748	0.0016	0.0010	21
28	56003.8899	0.0009	0.0011	30
35	56004.2905	0.0007	−0.0008	31
36	56004.3477	0.0007	−0.0011	31
39	56004.5197	0.0008	−0.0017	26
40	56004.5798	0.0010	0.0010	19
41	56004.6341	0.0018	−0.0022	14
42	56004.6889	0.0010	−0.0049	13
43	56004.7467	0.0018	−0.0046	15
57	56005.5512	0.0016	−0.0051	14
58	56005.6125	0.0018	−0.0013	10
59	56005.6712	0.0009	−0.0001	9
60	56005.7287	0.0033	−0.0001	9
74	56006.5347	0.0040	0.0009	14
75	56006.5936	0.0016	0.0023	13
76	56006.6552	0.0017	0.0064	9
77	56006.7073	0.0025	0.0010	9
78	56006.7620	0.0016	−0.0017	9
91	56007.5118	0.0024	0.0006	17
92	56007.5717	0.0026	0.0030	14
93	56007.6220	0.0022	−0.0042	9
94	56007.6851	0.0027	0.0014	58
95	56007.7428	0.0013	0.0016	70
96	56007.7971	0.0013	−0.0016	60
97	56007.8572	0.0019	0.0010	60

* BJD − 2400000.
† Against max = 2456002.2789 + 0.057498E.
‡ Number of points used to determine the maximum.

3.84. OT J224736.4+250436

This object (= CSS 120616:224736+250436; hereafter OT J224736) is a transient detected by CRTS on 2012 June 16. There was a previous outburst in 2006 November (CRTS data). An analysis of the SDSS colors using the neural network (Kato et al. 2012b) suggested an object below the period gap (vsnet-alert 14682). Subsequent observation detected superhumps (vsnet-alert 14684; figure 83). The times of superhump maxima are listed in table 84. Due to a gap in the observations, the other 2 d aliases are still viable. We used a period that gave the smallest residual to the superhump maxima on individual nights.

Table 70. Superhump maxima of OT J102842 (2012).

E	Max*	Error	$O-C$†	N‡
0	55958.0498	0.0042	−0.0053	41
1	55958.0876	0.0007	−0.0058	64
2	55958.1250	0.0005	−0.0068	65
3	55958.1687	0.0007	−0.0013	60
14	55958.5897	0.0004	−0.0015	37
15	55958.6277	0.0004	−0.0018	36
16	55958.6663	0.0004	−0.0015	37
17	55958.7048	0.0008	−0.0013	31
18	55958.7423	0.0010	−0.0021	19
19	55958.7811	0.0011	−0.0016	20
20	55958.8223	0.0010	0.0013	12
21	55958.8579	0.0012	−0.0014	20
22	55958.8962	0.0008	−0.0013	11
28	55959.1281	0.0008	0.0008	68
29	55959.1672	0.0010	0.0016	68
30	55959.2048	0.0004	0.0010	123
31	55959.2437	0.0004	0.0015	113
32	55959.2811	0.0003	0.0007	113
33	55959.3183	0.0005	−0.0004	78
44	55959.7426	0.0022	0.0027	8
45	55959.7777	0.0084	−0.0005	5
46	55959.8194	0.0010	0.0029	7
47	55959.8566	0.0009	0.0018	11
48	55959.8970	0.0007	0.0040	5
70	55960.7412	0.0008	0.0058	9
73	55960.8654	0.0010	0.0151	24
74	55960.8927	0.0003	0.0041	44
75	55960.9308	0.0004	0.0039	39
76	55960.9693	0.0004	0.0041	39
77	55961.0065	0.0004	0.0031	40
122	55962.7235	0.0011	−0.0031	18
123	55962.7629	0.0008	−0.0019	15
124	55962.8019	0.0009	−0.0012	20
126	55962.8790	0.0017	−0.0007	20
148	55963.7167	0.0011	−0.0054	16
150	55963.7946	0.0016	−0.0040	20
151	55963.8312	0.0013	−0.0057	15

* BJD − 2400000.
† Against max = 2455958.0552 + 0.038290E.
‡ Number of points used to determine the maximum.

3.85. *TCP J08461690+3115554*

This object (hereafter TCP J084616) is a transient discovered by T. V. Kryachko et al. on 2012 March 19.[9] The object was soon recognized to be a deeply eclipsing SU UMa-type dwarf nova (vsnet-alert 14347, 14348, 14351). The object has an SDSS counterpart of g magnitude, 21.8. Using the MCMC method (in the Appendix), we obtained an eclipse ephemeris of

$$\mathrm{Min(BJD)} = 2456007.33870(6) + 0.091383(6)E. \quad (4)$$

The times of superhumps maxima are listed in table 85.

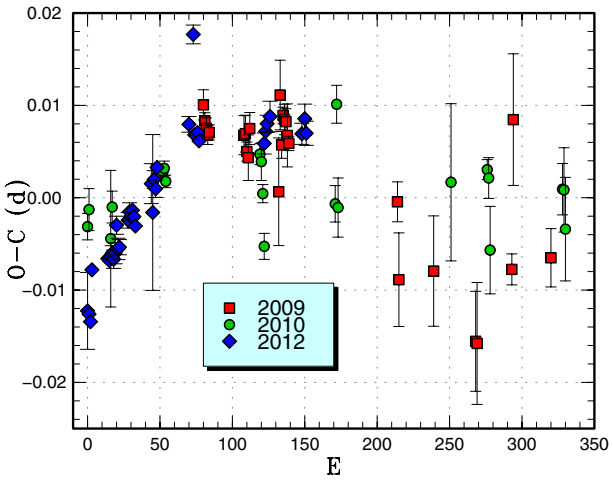

Fig. 64. Comparison of different superoutbursts of J102842 in the $O-C$ diagram. A period of 0.03816 d was used to draw this figure. Approximate cycle counts (E) after the start of the observations were used for 2009 and 2012, assuming that the observations started at the initial stage of the outbursts. The $O-C$ diagram for 2010 was shifted by 80 cycles.

The PDM analysis (figure 84) yielded a period of 0.09633(11) d, giving an ϵ value of 5.4(1)%.

3.86. *TCP J23130812+2337018*

This object (hereafter TCP J231308) was discovered by K. Itagaki and H. Kaneda to be an object of unfiltered CCD magnitude, 14.3 (TCP J23130812+2337018).[10] According to ASAS-3 data, the object underwent a brighter ($V = 13.4$) outburst in 2005 August. Subsequent observations confirmed the presence of superhumps (vsnet-alert 13438; figure 85). The times of superhump maxima are listed in table 86. The $O-C$ value clearly showed a stage B–C transition. The period during the observation of stage B was not long enough to determine P_{dot}.

4. Discussion

4.1. *Period Derivatives during Stage B*

In the same manner as presented in Kato et al. (2012a), we compared period derivatives during stage B (figure 86). The newly obtained P_{dot} for the object of $P_{\mathrm{orb}} < 0.076$ d followed the trend obtained in previous research. There were also two $P_{\mathrm{dot}} > 0$ systems (SDSS J170213 and OT J145921) for $P_{\mathrm{orb}} > 0.080$ d, as noted in Kato et al. (2012a). The former, SDSS J170213, showed infrequent outbursts, and indeed resembles EF Peg, the representative $P_{\mathrm{dot}} \sim 0$ object with a long P_{orb} (cf. Kato et al. 2009). The latter, OT J145921, showed more frequent outbursts, and may resemble GX Cas that shows $P_{\mathrm{dot}} > 0$ with the typical SU UMa-type outburst behavior, despite its long P_{SH}. There may be two classes of objects with $P_{\mathrm{dot}} > 0$ among SU UMa-type dwarf novae with a long P_{orb}.

[9] ⟨http://www.cbat.eps.harvard.edu/unconf/followups/J08461690+3115554.html⟩.

[10] ⟨http://www.cbat.eps.harvard.edu/unconf/followups/J23130812+2337018.html⟩.

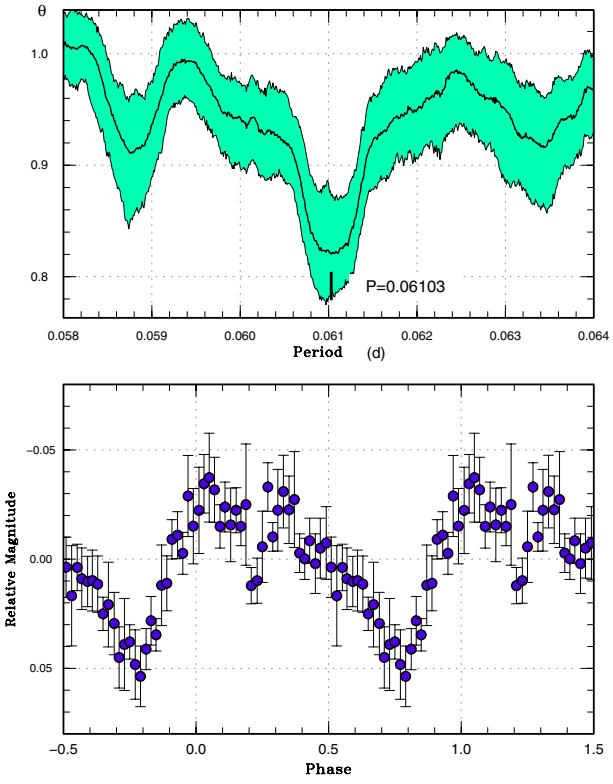

Fig. 65. Superhumps in OT J105122 (2012). Upper: PDM analysis. Lower: Phase-averaged profile.

Table 71. Superhump maxima of OT J105122 (2012).

E	Max*	Error	$O-C$†	N‡
0	55929.7466	0.0019	0.0007	64
1	55929.8069	0.0015	−0.0001	63
2	55929.8626	0.0009	−0.0055	63
3	55929.9291	0.0014	−0.0001	63
4	55929.9894	0.0009	−0.0008	57
12	55930.4884	0.0023	0.0098	16
26	55931.3292	0.0033	−0.0041	16
27	55931.3949	0.0024	0.0005	20
29	55931.5163	0.0072	−0.0003	23
30	55931.5776	0.0038	−0.0000	23

* BJD − 2400000.
† Against max = 2455929.7460 + 0.061054E.
‡ Number of points used to determine the maximum.

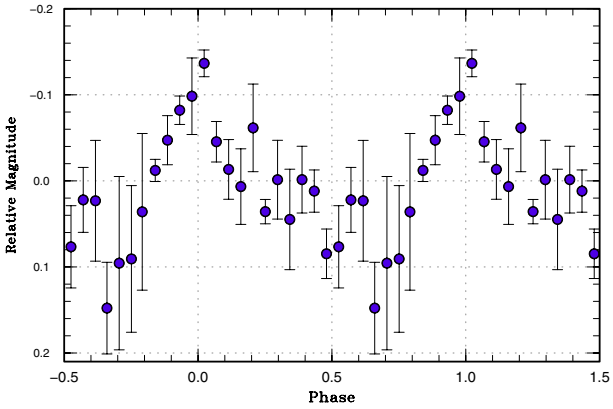

Fig. 66. Superhumps in OT J125905 (2012). A period of 0.0660 d was assumed in the process of phase-averaging.

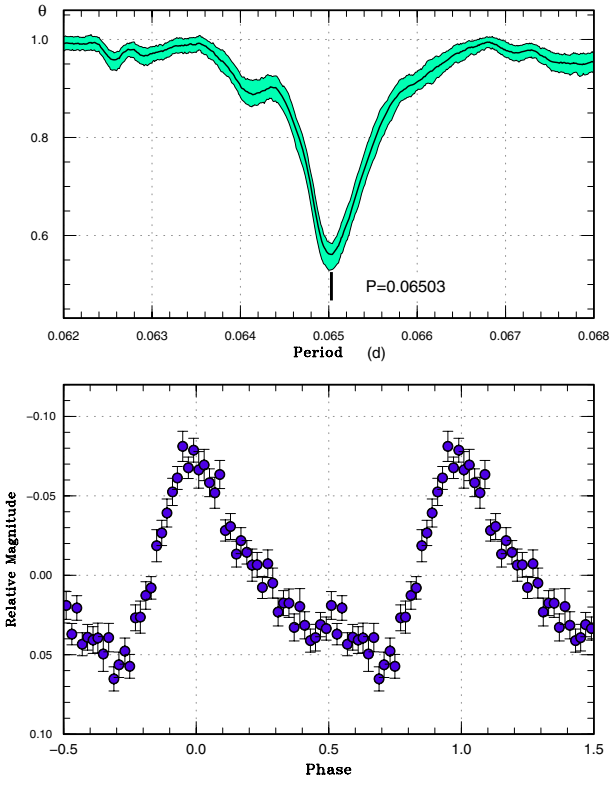

Fig. 67. Superhumps in OT J144252 (2012). Upper: PDM analysis. Lower: Phase-averaged profile.

4.2. *Periods of Stage-A Superhumps*

Stage-A superhumps recorded in the present study are listed in table 87. Although most of the objects in this study followed the trend obtained in the previous study, one object (SDSS J170213) has a substantially smaller fractional excess for stage-A superhumps. This may have been either due to small number of observations (insufficient coverage for stage A), to a systematic effect of overlapping eclipses, or to the unusual period evolution of this object for this $P_{\rm orb}$ (cf. subsection 4.1). Although the object may also resemble short-$P_{\rm orb}$ objects in its small fractional excess for stage-A superhumps, this needs to be confirmed by further observations.

4.3. *WZ Sge-Type Stars*

New WZ Sge-type dwarf novae and candidates are listed in table 88. Three out of them, PR Her, BW Scl, and OT J184228, were well characterized. SV Ari was observed only in the late stage of its superoutburst, and SDSS J220553 and OT J210950 are given in this table, because their post-superoutburst behaviors have a resemblance to WZ Sge-type

Table 72. Superhump maxima of OT J144252 (2012).

E	Max*	Error	$O-C^{\dagger}$	$N^{\ddagger}$
0	56035.6984	0.0015	−0.0041	78
1	56035.7648	0.0010	−0.0027	89
2	56035.8322	0.0007	−0.0003	14
3	56035.8949	0.0006	−0.0025	18
12	56036.4809	0.0004	−0.0013	140
13	56036.5455	0.0006	−0.0017	152
14	56036.6126	0.0010	0.0004	75
15	56036.6742	0.0011	−0.0030	12
18	56036.8697	0.0009	−0.0024	18
27	56037.4552	0.0007	−0.0017	150
28	56037.5212	0.0008	−0.0006	133
29	56037.5855	0.0011	−0.0014	13
30	56037.6543	0.0016	0.0024	14
33	56037.8448	0.0014	−0.0020	17
34	56037.9103	0.0021	−0.0014	13
44	56038.5666	0.0031	0.0051	13
45	56038.6260	0.0017	−0.0004	13
48	56038.8248	0.0013	0.0034	14
49	56038.8921	0.0032	0.0057	18
59	56039.5453	0.0018	0.0092	12
60	56039.6056	0.0015	0.0045	13
61	56039.6725	0.0012	0.0064	11
64	56039.8669	0.0013	0.0059	19
75	56040.5781	0.0013	0.0023	13
76	56040.6422	0.0017	0.0014	13
79	56040.8370	0.0012	0.0013	18
80	56040.9001	0.0021	−0.0006	17
90	56041.5552	0.0069	0.0048	9
91	56041.6086	0.0013	−0.0068	13
106	56042.5791	0.0034	−0.0109	13
107	56042.6463	0.0026	−0.0087	13

* BJD − 2400000.
† Against max = 2456035.7025 + 0.064977E.
‡ Number of points used to determine the maximum.

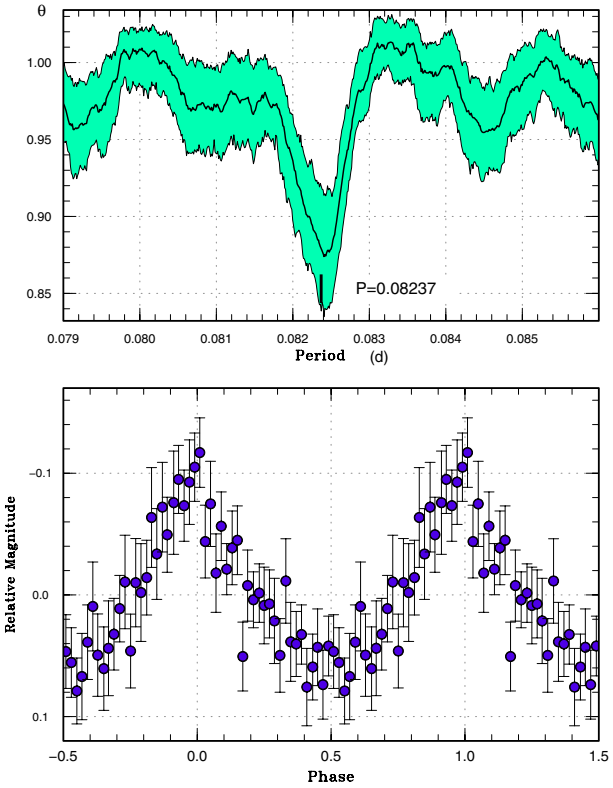

Fig. 68. Superhumps in OT J144453 (2011). Upper: PDM analysis. Lower: Phase-averaged profile.

Table 73. Superhump maxima of OT J144453 (2012).

E	Max*	Error	$O-C^{\dagger}$	$N^{\ddagger}$
0	56046.1078	0.0009	0.0001	170
17	56047.5119	0.0020	0.0053	13
18	56047.5888	0.0015	−0.0001	14
20	56047.7561	0.0009	0.0026	10
21	56047.8346	0.0010	−0.0011	25
32	56048.7402	0.0010	−0.0007	12
33	56048.8242	0.0012	0.0010	24
34	56048.9017	0.0016	−0.0039	19
42	56049.5541	0.0030	−0.0098	15
43	56049.6493	0.0045	0.0031	15
44	56049.7259	0.0205	−0.0025	12
45	56049.8057	0.0010	−0.0050	21
46	56049.8926	0.0020	−0.0004	22
55	56050.6386	0.0041	0.0050	14
56	56050.7191	0.0029	0.0032	12
57	56050.7967	0.0050	−0.0015	18
58	56050.8849	0.0028	0.0044	26

* BJD − 2400000.
† Against max = 2456046.1077 + 0.082289E.
‡ Number of points used to determine the maximum.

objects. Concerning OT J001952 and OT J055721 we have only very limited information; these objects were included due to their large outburst amplitudes.

The relation between $P_{\rm dot}$ and ϵ for WZ Sge-type dwarf novae is shown in figure 88. Although there is a tendency of increasing $P_{\rm dot}$ for objects with larger ϵ, as stated in Kato et al. (2009), several objects lie well above this relation, as discussed in Kato et al. (2012a). Although we may add two additional examples in the present study, these objects, SDSS J220553 and PR Her, were not very well sampled, and it is not certain whether they are on the outside of this relation. In the reverse case, OT J184228 is remarkable in that it showed almost zero $P_{\rm dot}$. It was indeed unusual for this object to show the "double plateau" superoutburst. The unusually small $P_{\rm dot}$ may be related to the unusual binary parameters (long $P_{\rm orb}$ and small expected q), and probably to its evolutionary stage as a candidate period bouncer.

Figure 89 indicates an updated relation between $P_{\rm dot}$ and $P_{\rm orb}$ and its relation to the type of post-superoutburst

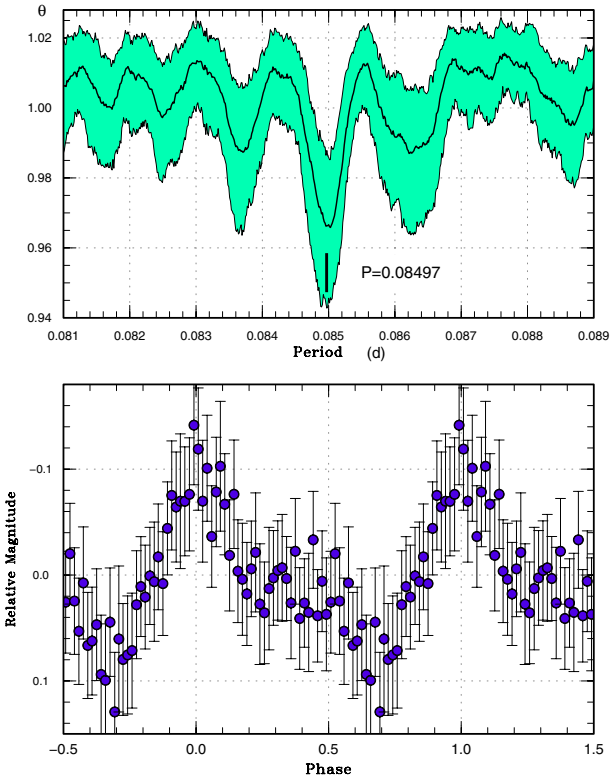

Fig. 69. Superhumps in OT J145921 (2011). Upper: PDM analysis. Lower: Phase-averaged profile.

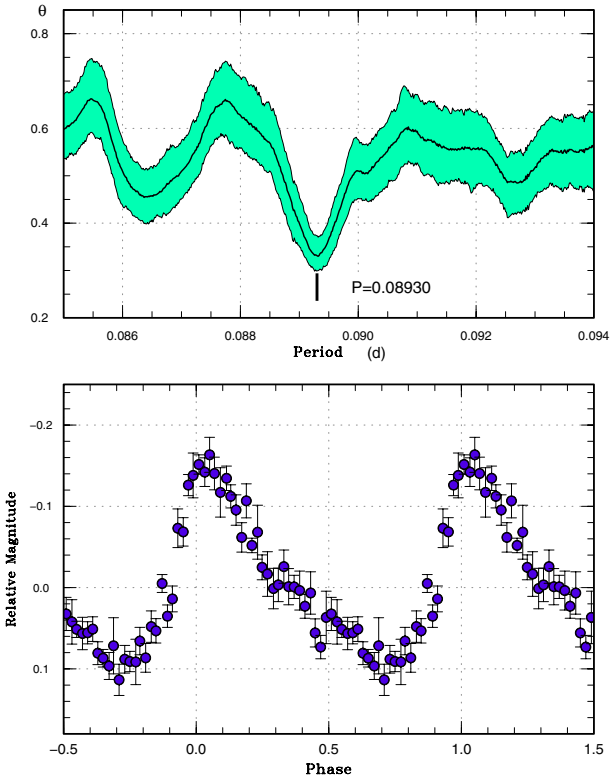

Fig. 70. Superhumps in OT J155631 (2012). Upper: PDM analysis. Lower: Phase-averaged profile.

Table 74. Superhump maxima of OT J145921 (2011).

E	Max*	Error	$O-C^{\dagger}$	$N^{\ddagger}$
0	55728.4160	0.0011	0.0033	69
11	55729.3516	0.0003	0.0027	50
12	55729.4362	0.0005	0.0022	59
24	55730.4490	0.0023	−0.0064	30
25	55730.5413	0.0015	0.0008	33
35	55731.3891	0.0006	−0.0026	43
36	55731.4725	0.0007	−0.0043	36
58	55733.3492	0.0016	−0.0001	36
59	55733.4357	0.0011	0.0013	46
62	55733.6885	0.0018	−0.0013	125
63	55733.7754	0.0016	0.0005	126
71	55734.4462	0.0018	−0.0096	37
73	55734.6391	0.0082	0.0131	78
74	55734.7113	0.0032	0.0002	128

* BJD − 2400000.
† Against max = 2455728.4126 + 0.085114E.
‡ Number of points used to determine the maximum.

Table 75. Superhump maxima of OT J155631 (2012).

E	Max*	Error	$O-C^{\dagger}$	$N^{\ddagger}$
0	56017.2322	0.0007	−0.0021	92
1	56017.3236	0.0005	−0.0000	95
18	56018.8443	0.0013	0.0024	13
29	56019.8257	0.0020	0.0015	10
30	56019.9149	0.0019	0.0013	14
40	56020.8067	0.0025	0.0001	9
41	56020.8928	0.0029	−0.0032	21

* BJD − 2400000.
† Against max = 2456017.2343 + 0.089309E.
‡ Number of points used to determine the maximum.

rebrightening phenomenon: type-A (long-lasting post-outburst rebrightening), type-B (multiple discrete rebrightenings), type-C (single rebrightening), and type-D (no rebrightening) (cf. Kato et al. 2009). In the present study, type-C and type-D superoutbursts followed the same trend as in past studies. There is a noteworthy presence of a new type-B superoutburst (OT J184228) with an exceptionally long $P_{\rm orb}$ and small $P_{\rm dot}$. This presence seems to support an earlier suggestion (Kato et al. 2009, 2012a) that type-B superoutbursts are associated with low-q systems, and that they are likely to be period bouncers.

4.4. *VW Hydri — Revisiting the Prototype of SU UMa-Type Dwarf Novae*

In discussing superoutbursts and superhumps, we often refer to the historical observations of bright southern SU UMa-type dwarf novae (VW Hyi, Z Cha, and OY Car), from which our early knowledge concerning the phenomenology of superhumps was established. These early findings were also summa-

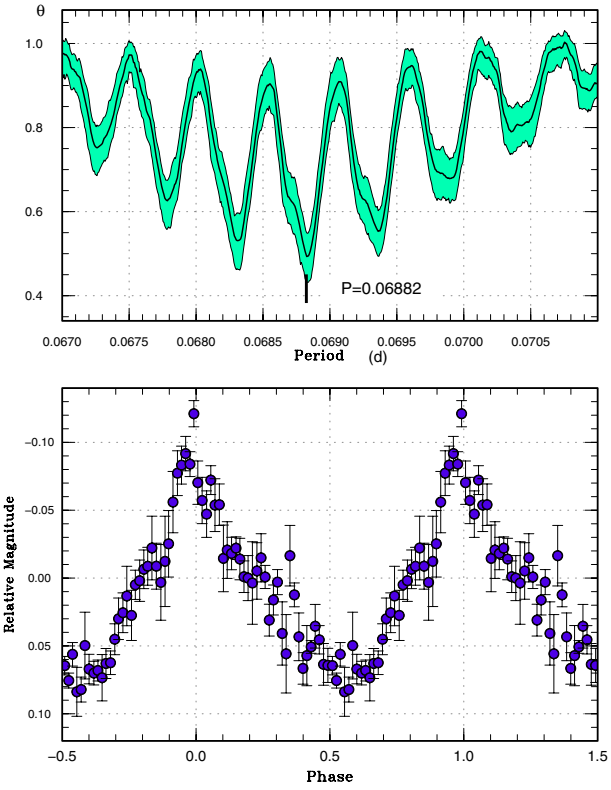

Fig. 71. Superhumps in OT J162806 (2011). Upper: PDM analysis. Lower: Phase-averaged profile.

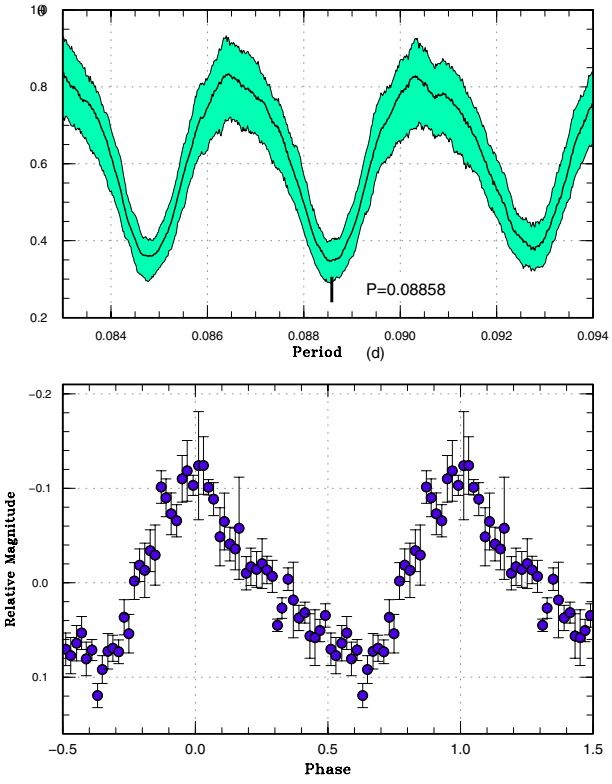

Fig. 72. Superhumps in OT J163942 (2012). Upper: PDM analysis. The alias was selected by the $O-C$ analysis of a continuous run on a single night. Lower: Phase-averaged profile.

Table 76. Superhump maxima of OT J162806 (2011).

E	Max*	Error	$O-C^{\dagger}$	$N^{\ddagger}$
0	55724.4545	0.0003	0.0009	67
13	55725.3473	0.0005	−0.0013	38
14	55725.4175	0.0003	0.0000	64
15	55725.4866	0.0003	0.0003	55
139	55734.0220	0.0012	−0.0013	105
140	55734.0935	0.0022	0.0014	99

* BJD − 2400000.
† Against max = 2455724.4536 + 0.068847E.
‡ Number of points used to determine the maximum.

Table 77. Superhump maxima of OT J163942 (2012).

E	Max*	Error	$O-C^{\dagger}$	$N^{\ddagger}$
0	56039.5603	0.0007	−0.0000	88
22	56041.5094	0.0024	0.0009	33
23	56041.5962	0.0011	−0.0008	39

* BJD − 2400000.
† Against max = 2456039.5603 + 0.088554E.
‡ Number of points used to determine the maximum.

rized in textbooks, such as Warner (1995)'s. These early observations were, however, based on photoelectric photometry, and only part of the entire observation was published in figure form; these observations are not accessible in electronic form. This has constituted an obstacle to comparing the results of CCD observations in modern days with historical knowledge. Although Kepler observations of V344 Lyr and V1504 Cyg (Kato et al. 2012a; Wood et al. 2011) partly filled this gap, a direct comparison in the "prototype" object VW Hyi was wanted. We have fortunately been able to obtain the entire course of the 2011 November–December superoutburst and two subsequent normal outbursts as well as the intervening quiescent phase, although they were obtained only at a single observing location, and suffered from unavoidable gaps in the coverage. These data are available from the AAVSO database.

The results of these observations (subsection 3.22) can be summarized as follows:

1. The superoutburst started with a precursor outburst.
2. There was no hint as to superhumps during the rising and early phases of the precursor outburst.
3. During the later stage of the precursor outburst, superhumps started to grow and the object brightened.
4. The amplitudes of the superhumps reached a maximum when the object reached the maximum brightness.
5. The amplitudes of the superhumps decreased during the superoutburst plateau.
6. The global $P_{\rm dot}$ was negative.
7. Stage A was recognized during the evolving stage of the superhumps.

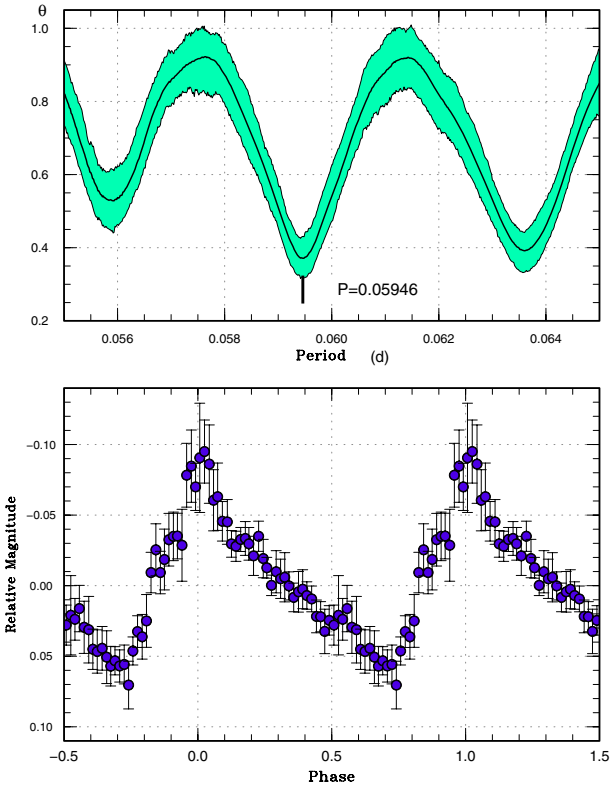

Fig. 73. Superhumps in OT J170609 (2011). Upper: PDM analysis. Lower: Phase-averaged profile.

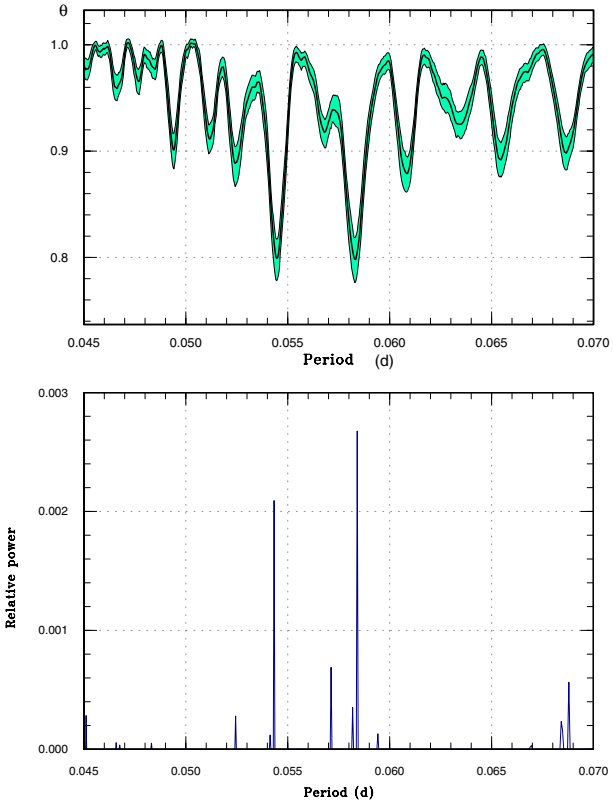

Fig. 74. Period analysis in OT J173516 (2011). Upper: PDM analysis. Lower: Lasso analysis ($\log\lambda = -6.42$).

Table 78. Superhump maxima of OT J170609 (2011).

E	Max*	Error	$O-C^{\dagger}$	$N^{\ddagger}$
0	55745.5333	0.0006	−0.0017	59
1	55745.5963	0.0015	0.0018	31
15	55746.4283	0.0004	−0.0003	57
16	55746.4884	0.0004	0.0002	60

* BJD − 2400000.
† Against max = 2455745.5350 + 0.059578E.
‡ Number of points used to determine the maximum.

8. It is likely that there was a stage B with an almost constant period, followed by a likely stage C with a shorter period.
9. The transition from stage B to C was smoother than in short-$P_{\rm orb}$ systems. This feature is similar to those in the Kepler data for V344 Lyr and V1504 Cyg.
10. Superhumps having phases of $\sim$0.5 offset appeared during the late stage of the superoutburst. These superhumps indeed appear to be "traditional" late superhumps, rather than a simple extension of stage-C superhumps, as seen in short-$P_{\rm orb}$ systems.
11. The late superhumps persisted during the quiescent period before the next normal outburst, and they were still detected even after this normal outburst. The signal became undetectable after the second normal outburst.

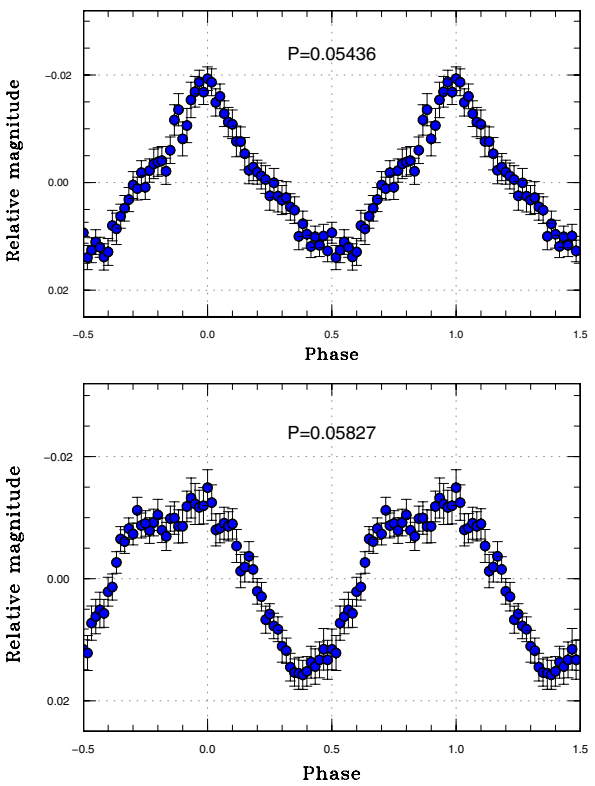

Fig. 75. Profiles of two periods in OT J173516 (2011).

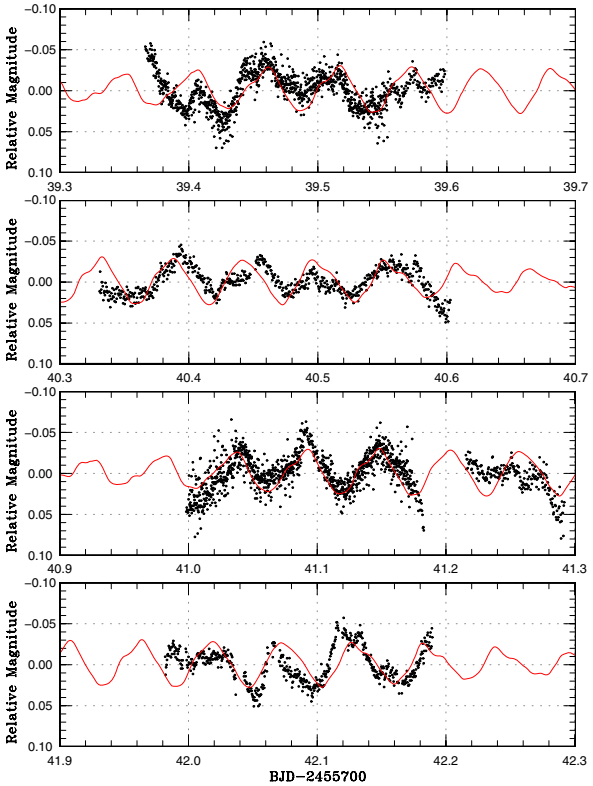

Fig. 76. Synthesized light curve of OT J173516 (2011). The points represent observations. The curves represent the expected light curve by adding the two waves shown in figure 75.

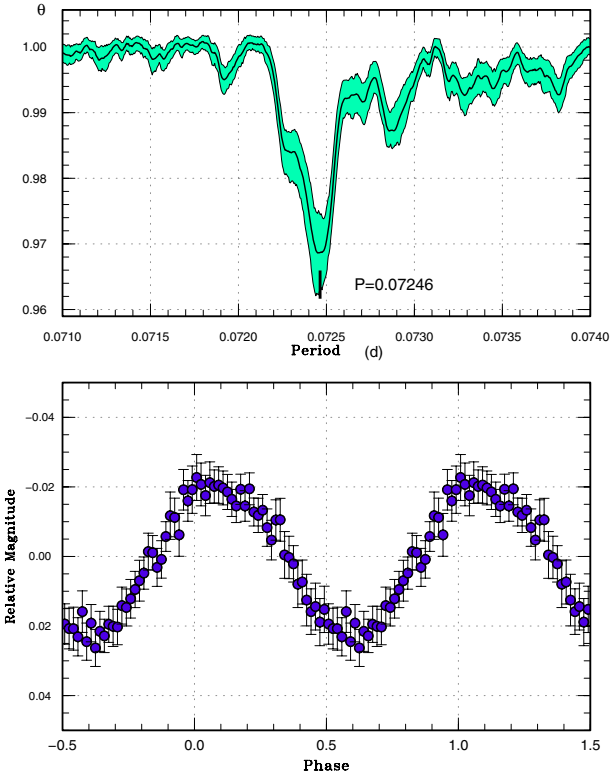

Fig. 77. Superhumps in OT J184228 (2011). Upper: PDM analysis. Lower: Phase-averaged profile.

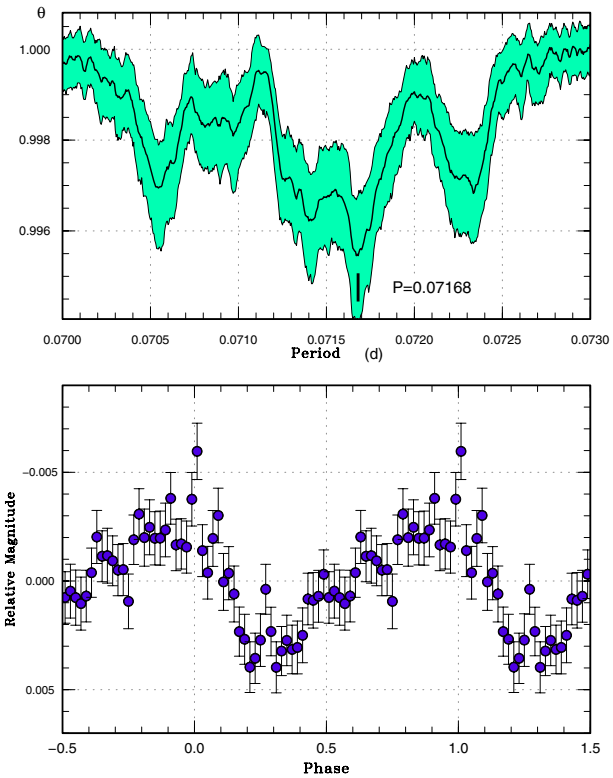

Fig. 78. Possible early superhumps in OT J184228 (2011). Upper: PDM analysis. Lower: Phase-averaged profile.

The situation was very similar to the Kepler result for V344 Lyr.

12. In contrast to V344 Lyr, secondary maxima of superhumps were not prominent.

We thus confirmed most of the classical superhump phenomenology, including the "traditional" late superhumps, whose presence has been questioned in most of recently observed objects (Kato et al. 2009, 2010, 2012a). Combined with knowledge concerning V344 Lyr, the traditional descriptions about the development of superhumps and the appearance of late superhumps seem to be common among relatively long-$P_{\rm orb}$ and high mass-transfer systems, and VW Hyi can indeed be regarded as a prototype of these systems. Things in shorter-$P_{\rm orb}$ and lower mass-transfer systems are, however, somewhat different: the clear presence of stages B and C, and no clear signature of "traditional" late superhumps. Although the systematics of the superhumps in VW Hyi would be adequate for describing long-$P_{\rm orb}$ systems, we regard it as dangerous to describe the phenomena seen in shorter-$P_{\rm orb}$ systems in the same manner. This will be particularly true of the term "late superhumps," which has been the main cause of confusion in describing stage-C superhumps. Although some authors refer to superhumps seen in the late stages of a superoutburst as late superhumps, this causes confusion; because the original term "late superhumps" implies an $\sim$0.5 phase shift, and stage-C superhumps do not show such a phase shift. This ambiguity in terminology could introduce confusion into

Table 79. Superhump maxima of OT J184228 (2011).

E	Max*	Error	$O-C^{\dagger}$	$N^{\ddagger}$	E	Max*	Error	$O-C^{\dagger}$	$N^{\ddagger}$
0	55838.9637	0.0022	−0.0366	172	89	55845.4512	0.0022	0.0016	64
1	55839.0387	0.0005	−0.0341	83	100	55846.2521	0.0009	0.0054	157
17	55840.2225	0.0011	−0.0097	164	101	55846.3275	0.0005	0.0083	254
18	55840.2982	0.0009	−0.0065	322	102	55846.4008	0.0008	0.0092	283
19	55840.3668	0.0007	−0.0104	270	103	55846.4745	0.0024	0.0103	46
22	55840.5828	0.0017	−0.0117	51	109	55846.9046	0.0013	0.0057	74
31	55841.2434	0.0017	−0.0033	104	114	55847.2699	0.0015	0.0087	226
32	55841.3122	0.0009	−0.0070	76	115	55847.3359	0.0017	0.0022	280
33	55841.3884	0.0003	−0.0032	211	128	55848.2806	0.0014	0.0049	70
34	55841.4617	0.0008	−0.0024	134	129	55848.3479	0.0012	−0.0002	144
35	55841.5395	0.0019	0.0029	91	130	55848.4222	0.0020	0.0015	145
36	55841.6068	0.0005	−0.0023	154	141	55849.2102	0.0164	−0.0075	109
37	55841.6791	0.0008	−0.0024	113	142	55849.2933	0.0024	0.0030	257
41	55841.9707	0.0011	−0.0007	221	143	55849.3628	0.0013	0.0001	216
42	55842.0431	0.0015	−0.0007	355	144	55849.4368	0.0021	0.0016	141
43	55842.1302	0.0046	0.0139	36	156	55850.3115	0.0015	0.0068	156
45	55842.2669	0.0011	0.0057	76	157	55850.3759	0.0013	−0.0013	138
46	55842.3374	0.0019	0.0037	76	158	55850.4445	0.0018	−0.0051	138
49	55842.5624	0.0008	0.0113	118	165	55850.9518	0.0014	−0.0051	150
50	55842.6314	0.0006	0.0079	131	170	55851.3083	0.0032	−0.0109	54
56	55843.0700	0.0024	0.0117	87	171	55851.3874	0.0041	−0.0043	71
58	55843.1943	0.0071	−0.0090	56	183	55852.2622	0.0018	0.0009	187
59	55843.2815	0.0018	0.0058	76	184	55852.3280	0.0007	−0.0057	271
60	55843.3504	0.0022	0.0022	75	185	55852.4003	0.0010	−0.0059	272
63	55843.5736	0.0010	0.0080	164	186	55852.4717	0.0010	−0.0069	126
64	55843.6538	0.0017	0.0158	124	192	55852.9039	0.0011	−0.0095	167
65	55843.7276	0.0020	0.0171	65	193	55852.9774	0.0014	−0.0085	251
68	55843.9248	0.0013	−0.0030	172	194	55853.0539	0.0018	−0.0044	150
69	55843.9854	0.0023	−0.0149	165	198	55853.3424	0.0045	−0.0058	65
73	55844.3040	0.0008	0.0139	60	199	55853.4125	0.0026	−0.0082	55
74	55844.3727	0.0011	0.0100	74	198	55853.3424	0.0045	−0.0058	65
75	55844.4453	0.0010	0.0102	72	206	55853.9201	0.0018	−0.0078	110
76	55844.5252	0.0010	0.0176	47	226	55855.3771	0.0010	−0.0001	56
77	55844.5898	0.0011	0.0098	47	321	55862.2628	0.0015	0.0016	27
82	55844.9495	0.0010	0.0072	114	377	55866.3262	0.0018	0.0070	19
84	55845.0895	0.0020	0.0022	104	413	55868.9431	0.0010	0.0152	79
87	55845.3107	0.0012	0.0060	73	428	55869.9909	0.0009	−0.0241	91
88	55845.3790	0.0015	0.0019	72	472	55873.2097	0.0053	0.0064	9

* BJD − 2400000.
† Against max = 2455839.0003 + 0.072464E.
‡ Number of points used to determine the maximum.

interpreting the mechanism [see, e.g., Hessman et al. (1992), a work before the clarification on difference between "traditional" superhumps and stage-C ones, analyzed stage-C superhumps with a term of "late superhumps" and an assumption of an $\sim$0.5 phase shift]. We propose that we should not use the term "late superhumps" unless they show an $\sim$0.5 phase shift.

Schreiber, Hameury, and Lasota (2004) recently compared calculations of the pure thermal-tidal-instability (TTI) model and the enhanced mass-transfer (EMT) model for VW Hyi. Although both models (TTI and EMT) well explain most of the observed characteristics, the authors claimed an advantage for the EMT model in that it can explain a variety of observed light curves of single systems, such as VW Hyi. Although we do not intend to validate or invalidate their claim here, we must be specially careful in interpreting observations. They referred to the variaty of light curves based on historical visual observations, and these observations may not have been very sensitive to subtle signatures of the light curves. For example, while the present superoutburst showed a clear signature of a precursor, the visual observation of the same superoutburst reported to the AAVSO did not contain this feature. Considering that all superoutbursts (six of V344 Lyr and six of V1504 Cyg) showed precursors in the Kepler data (Cannizzo et al. 2012), and considering that these light curves are very similar to the

Table 80. Superhump maxima of OT J210950 (2011).

E	Max*	Error	$O-C$†	N‡
0	55710.5319	0.0009	−0.0188	168
1	55710.5897	0.0008	−0.0211	168
27	55712.1758	0.0006	0.0044	96
28	55712.2356	0.0003	0.0042	92
34	55712.5982	0.0002	0.0066	104
37	55712.7804	0.0003	0.0088	87
38	55712.8401	0.0002	0.0084	104
39	55712.9005	0.0002	0.0088	122
54	55713.7970	0.0002	0.0049	170
55	55713.8564	0.0003	0.0043	87
71	55714.8117	0.0004	−0.0008	86
72	55714.8706	0.0004	−0.0019	86
77	55715.1733	0.0008	0.0006	38
78	55715.2326	0.0004	−0.0001	48
84	55715.5900	0.0003	−0.0028	115
87	55715.7693	0.0004	−0.0036	61
88	55715.8315	0.0004	−0.0015	74
89	55715.8904	0.0004	−0.0026	75
104	55716.7890	0.0004	−0.0043	72
105	55716.8497	0.0002	−0.0036	146
106	55716.9099	0.0004	−0.0035	142
117	55717.5703	0.0003	−0.0033	168
117	55717.5703	0.0003	−0.0034	167
121	55717.8098	0.0006	−0.0040	106
122	55717.8708	0.0008	−0.0030	82
128	55718.2312	0.0005	−0.0027	101
148	55719.4352	0.0008	0.0008	120
165	55720.4667	0.0013	0.0119	122
166	55720.5259	0.0010	0.0110	133
187	55721.7886	0.0020	0.0132	68
188	55721.8463	0.0010	0.0109	69
220	55723.7585	0.0029	0.0023	35
221	55723.8227	0.0008	0.0064	48
222	55723.8818	0.0013	0.0055	49
288	55727.8236	0.0018	−0.0143	82
289	55727.8802	0.0019	−0.0178	93

* BJD − 2400000.
† Against max = 55710.5507 + 0.060025E.
‡ Number of points used to determine the maximum.

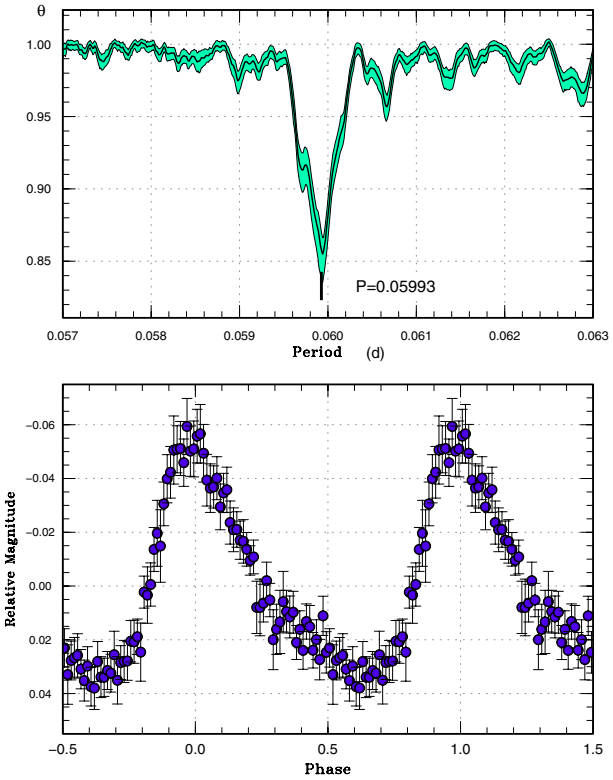

Fig. 79. Superhumps in OT J210950 (2011). Upper: PDM analysis. Lower: Phase-averaged profile.

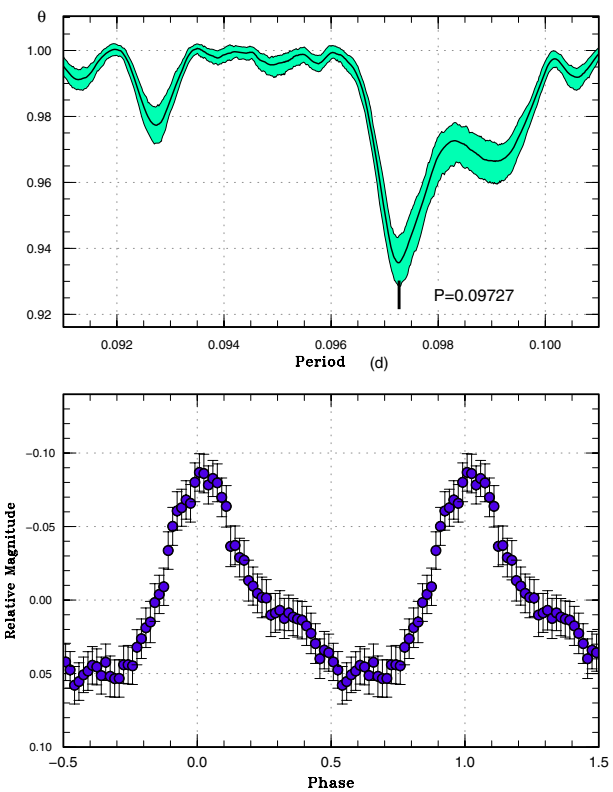

Fig. 80. Superhumps in OT J214738 (2011). Upper: PDM analysis. Lower: Phase-averaged profile.

present ones of VW Hyi (figure 19, lower panel), we may postulate that precursors in the superoutburst of these systems are more common than that assumed in Schreiber, Hameury, and Lasota (2004), and that variations within the single system are less pronounced. This stability of the appearance of precursors might in turn favor the pure TTI model, and it needs to be examined further.

4.5. ER UMa Stars

Early years from the discovery of ER UMa-type stars (Kato & Kunjaya 1995; Robertson et al. 1995; Patterson et al. 1995), it was not possible to fully analyze period variations and $O-C$ diagrams in these systems (Kato et al. 1996b, 2003a). Only recently, superhumps in DI UMa (Rutkowski et al. 2009;

Table 81. Superhump maxima of OT J214738 (2011).

E	Max*	Error	$O-C^{\dagger}$	$N^{\ddagger}$
0	55839.3213	0.0002	−0.0289	244
1	55839.4206	0.0002	−0.0270	250
10	55840.3196	0.0002	−0.0038	253
11	55840.4178	0.0003	−0.0029	297
12	55840.5161	0.0003	−0.0019	252
13	55840.6173	0.0005	0.0020	260
14	55840.7175	0.0004	0.0049	140
21	55841.4019	0.0002	0.0081	408
22	55841.5001	0.0003	0.0090	237
24	55841.6948	0.0003	0.0090	175
25	55841.7914	0.0002	0.0083	186
27	55841.9864	0.0002	0.0087	160
28	55842.0864	0.0003	0.0114	88
31	55842.3748	0.0005	0.0078	152
32	55842.4717	0.0003	0.0074	327
33	55842.5686	0.0003	0.0070	135
34	55842.6645	0.0003	0.0056	237
35	55842.7619	0.0006	0.0057	64
44	55843.6347	0.0006	0.0027	60
45	55843.7323	0.0004	0.0030	69
51	55844.3131	0.0006	−0.0001	110
52	55844.4106	0.0007	0.0001	137
53	55844.5068	0.0008	−0.0011	96
55	55844.7015	0.0002	−0.0009	251
56	55844.7976	0.0002	−0.0022	212
65	55845.6732	0.0006	−0.0024	142
66	55845.7686	0.0003	−0.0043	186
71	55846.2559	0.0004	−0.0036	163
72	55846.3539	0.0003	−0.0029	381
73	55846.4503	0.0003	−0.0038	403
75	55846.6462	0.0051	−0.0026	94
76	55846.7457	0.0004	−0.0004	183
82	55847.3285	0.0003	−0.0015	180
86	55847.7168	0.0004	−0.0024	183
87	55847.8098	0.0007	−0.0067	166
96	55848.6900	0.0007	−0.0024	101
97	55848.7888	0.0007	−0.0009	102
107	55849.7643	0.0017	0.0015	24

* BJD − 2400000.
† Against max = 2455839.3502 + 0.097313E.
‡ Number of points used to determine the maximum.

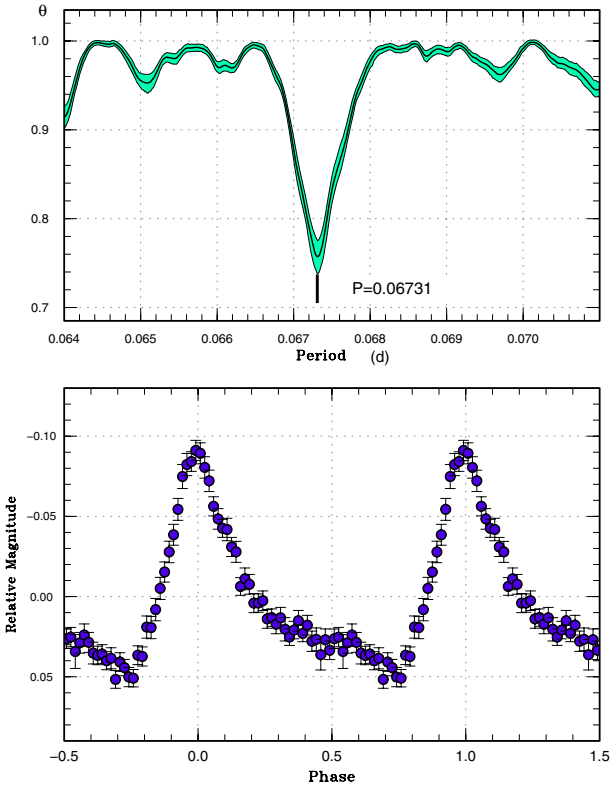

Fig. 81. Superhumps in OT J215818 (2011). Upper: PDM analysis. Lower: Phase-averaged profile.

subsection 3.36) and RZ LMi (Olech et al. 2008) have been studied systematically. Although ER UMa showed positive superhumps at least until 2007 (our unpublished observations) and 2008 (AAVSO data),[11] the object now predominantly shows negative superhumps, even during superoutbursts, at least since 2011 (Ohshima et al. 2012) and in quiescence in 2008 (Kjurkchieva & Marchev 2010) [there was also a possible signature of negative superhumps in 1998 (Gao et al. 1999)]; it is now impossible to follow the evolution of positive superhumps during the entire course of a superoutburst of ER UMa, as in the 1990s.

V1159 Ori, on the other hand, still shows positive superhumps (subsection 3.29), and it would be very desirable to study this object in detail. A recently recognized member of this family, BK Lyn, now shows almost the same behavior as ER UMa during its "negative superhump" (present) state.

We also studied RZ LMi, and found some evidence of period variation (subsection 3.23). We also suggested a candidate orbital period from photometry, and this needs to be tested by further observations.

We list currently known ER UMa stars and their periods in table 89. Orbital periods were taken from Thorstensen et al. (1997) (ER UMa, V1159 Ori), Thorstensen et al. (2002b) (DI UMa), and Ringwald et al. (1996) (BK Lyn). The superhump periods were from Kato and Kunjaya (1995) and Ohshima et al. (2012) (ER UMa), Rutkowski et al. (2009) (DI UMa), Olech et al. (2004) (IX Dra), and this work (V1159 Ori, RZ LMi, BK Lyn). Although Olech et al. (2004) suggested a possible orbital period, we did not include it because it is less likely to detect an orbital signal having a period close to the superhump period (as they claimed) from such a limited coverage. Since the behavior of IX Dra is very similar to that of ER UMa in the 1990s (Ishioka et al. 2001b), we would expect an ϵ value similar to that of ER UMa. A search for a definite orbital period is still needed. It would

[11] We do not completely rule out that negative superhumps may have appeared during the later course of superoutbursts in 2007 and 2008, since we do not have data during the late course of the superoutbursts.

Table 82. Superhump maxima of OT J215818 (2011).

E	Max*	Error	$O-C^{\dagger}$	$N^{\ddagger}$
0	55863.2398	0.0003	−0.0043	134
1	55863.3048	0.0002	−0.0064	231
2	55863.3696	0.0004	−0.0088	277
3	55863.4404	0.0002	−0.0051	438
4	55863.5061	0.0003	−0.0065	185
17	55864.3810	0.0005	−0.0039	78
18	55864.4489	0.0002	−0.0031	209
19	55864.5162	0.0003	−0.0029	201
20	55864.5814	0.0006	−0.0048	204
21	55864.6512	0.0003	−0.0021	318
22	55864.7198	0.0004	−0.0006	259
23	55864.7865	0.0009	−0.0010	99
30	55865.2517	0.0023	−0.0056	31
31	55865.3245	0.0007	0.0002	112
32	55865.3927	0.0004	0.0012	193
33	55865.4587	0.0004	0.0002	195
34	55865.5280	0.0005	0.0023	155
36	55865.6653	0.0004	0.0054	175
37	55865.7313	0.0004	0.0044	175
40	55865.9351	0.0005	0.0068	119
41	55865.9970	0.0009	0.0016	114
50	55866.6093	0.0004	0.0100	179
51	55866.6757	0.0003	0.0093	226
52	55866.7436	0.0004	0.0101	176
55	55866.9400	0.0008	0.0052	116
56	55867.0100	0.0005	0.0081	74
61	55867.3408	0.0008	0.0034	147
62	55867.4088	0.0005	0.0042	193
63	55867.4778	0.0006	0.0061	143
80	55868.6185	0.0009	0.0061	91
81	55868.6812	0.0010	0.0017	93
125	55871.6216	0.0008	−0.0105	127
126	55871.6902	0.0008	−0.0090	176
127	55871.7544	0.0018	−0.0119	148

* BJD − 2400000.
† Against max = 2455863.2441 + 0.067104E.
‡ Number of points used to determine the maximum.

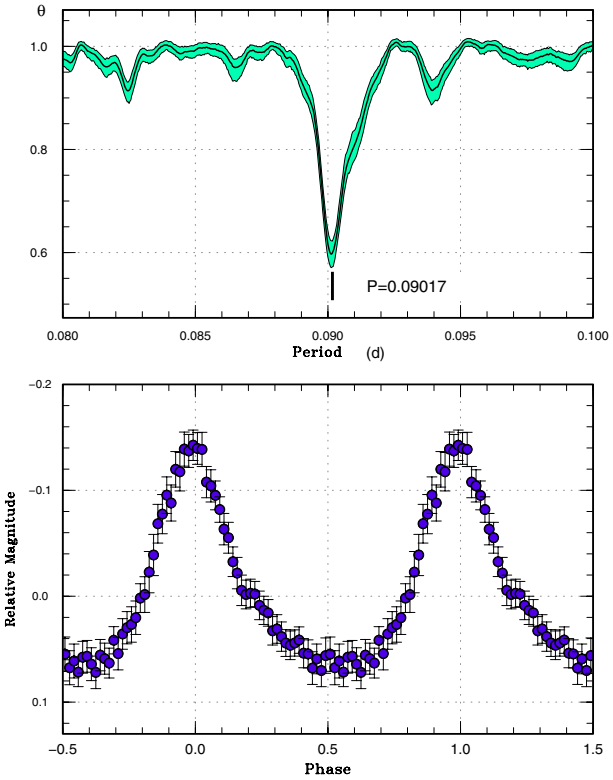

Fig. 82. Superhumps in OT J221232 (2011). Upper: PDM analysis. Lower: Phase-averaged profile.

Table 83. Superhump maxima of OT J221232 (2011).

E	Max*	Error	$O-C^{\dagger}$	$N^{\ddagger}$
0	55921.6566	0.0004	−0.0069	93
6	55922.2042	0.0003	−0.0000	116
7	55922.2925	0.0004	−0.0019	122
11	55922.6537	0.0005	−0.0012	91
14	55922.9302	0.0018	0.0050	45
17	55923.1942	0.0005	−0.0015	48
18	55923.2872	0.0005	0.0014	96
22	55923.6480	0.0005	0.0018	91
28	55924.1862	0.0023	−0.0008	84
29	55924.2797	0.0007	0.0026	221
33	55924.6417	0.0008	0.0040	90
55	55926.6221	0.0006	0.0017	82
73	55928.2400	0.0004	−0.0026	91
106	55931.2153	0.0024	−0.0016	30

* BJD − 2400000.
† Against max = 2455921.6635 + 0.090126E.
‡ Number of points used to determine the maximum.

be also interesting to see whether this object currently shows positive or negative superhumps.

4.6. Superoutbursts of AM CVn Stars

We analyzed the superhumps in a dwarf nova (CR Boo) belonging to AM CVn-type objects (subsection 3.5). CR Boo recently showed a regular pattern of superoutbursts similar to that of ER UMa (as noted in Kato et al. 2000b). We recorded a stage B–C transition similar to hydrogen-rich SU UMa-type dwarf novae. This is the first indication that superhumps in helium dwarf novae evolve in a similar way to hydrogen-rich SU UMa-type dwarf novae. Since this pattern of the stage B–C transition was also recorded in the black-hole X-ray transient KV UMa (Kato et al. 2009), the presence of stages B and C appears to be ubiquitous in all low-q systems. Theoretical studies concerning the origin of the superhump stage are required. Although the early stage of the superoutburst was not observed, SDSS J172102 underwent a superoutburst, followed by a short post-superoutburst rebrightening, resembling that of short-$P_{\rm orb}$ hydrogen-rich SU UMa-type dwarf novae. This also strengthens the similarity in phenomenology between helium-rich and hydrogen-rich SU UMa-type dwarf novae.

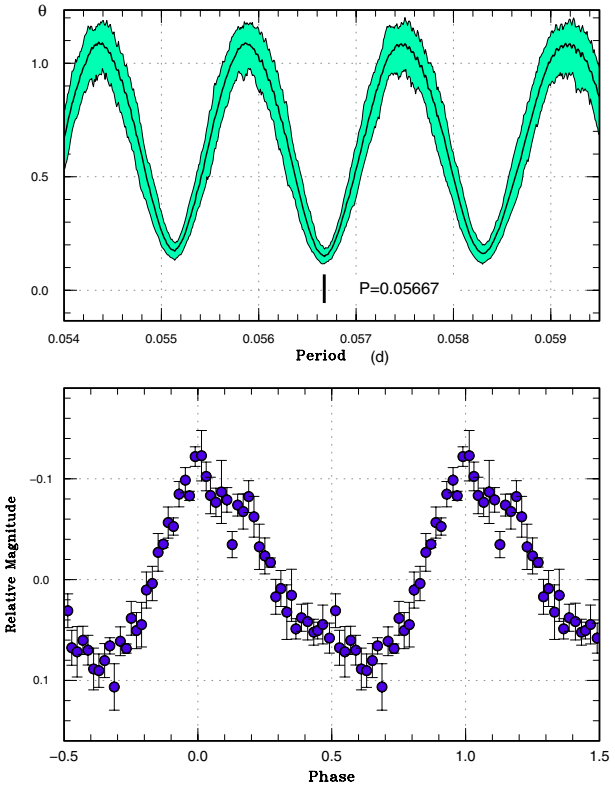

Fig. 83. Superhumps in OT J224736 (2012). Upper: PDM analysis. Lower: Phase-averaged profile.

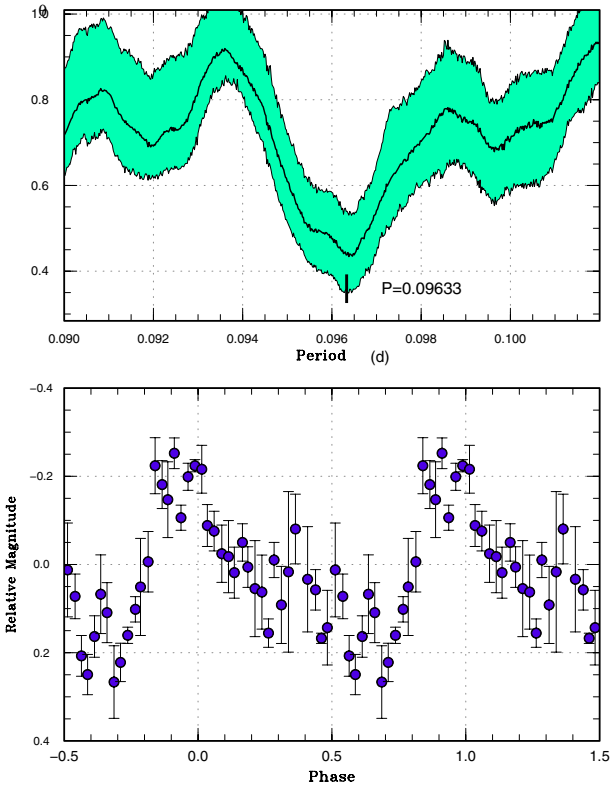

Fig. 84. Superhumps in TCP J084616 (2012). Upper: PDM analysis. Lower: Phase-averaged profile.

Table 84. Superhump maxima of OT J224736 (2012).

E	Max*	Error	$O-C^{\dagger}$	$N^{\ddagger}$
0	56095.4674	0.0005	−0.0005	27
1	56095.5251	0.0004	0.0005	28
36	56097.5076	0.0007	−0.0006	30
37	56097.5653	0.0005	0.0005	29

* BJD − 2400000.
† Against max = 2456095.4679 + 0.056673E.
‡ Number of points used to determine the maximum.

Table 85. Superhump maxima of TCP J084616 (2012).

E	Max*	Error	$O-C^{\dagger}$	Phase‡	$N^{\S}$
0	56007.2977	0.0006	−0.0009	0.35	32
1	56007.3955	0.0014	0.0006	0.33	27
11	56008.3626	0.0046	0.0046	0.62	35
12	56008.4500	0.0028	−0.0043	0.59	40

* BJD − 2400000.
† Against max = 2456007.2986 + 0.096303E.
‡ Orbital phase.
§ Number of points used to determine the maximum.

The peculiar object SBS 1108+574, a hydrogen-rich CV below the period minimum, also showed distinct stages B and C, as shown in ordinary short-$P_{\rm orb}$ SU UMa-type dwarf novae (subsection 3.49). Although the system parameters of this object are similar to those of AM CVn-type stars, its superoutburst was much longer than those of AM CVn-type superoutbursts, and there were no "dip"-like fadings during the superoutburst plateau (cf. Kotko et al. 2012). Such a difference in the behavior between pure-helium and hydrogen-rich accretion disks may be a result of their different properties, and warrants further study.

4.7. Double Periodic Superhumps?

In the present work, we encountered three unusual objects (CC Scl, MASTER J072948, and OT J173516), which showed superoutbursts similar to other SU UMa-type dwarf novae, but with only low-amplitude and rather irregular superhumps. The light curves of these systems appear to be expressed by a combination of closely separated two periods. In CC Scl, these periods are almost certainly $P_{\rm orb}$ and positive superhumps, while the situation for MASTER J072948 and OT J173516 is unclear: either positive superhumps with an unusual ϵ or negative superhumps. Although these objects comprise only a minority of known SU UMa-type dwarf novae, there may have been "overlooked" systems, since the amplitudes of the variations are very small. We cannot explain the unusual behavior of these systems. If negative superhumps (or a tilted disk) were excited as in the present-day ER UMa, the co-existence of both signals of $P_{\rm orb}$ and negative superhumps, and the rather irregular waveform may be easier to reconcile.

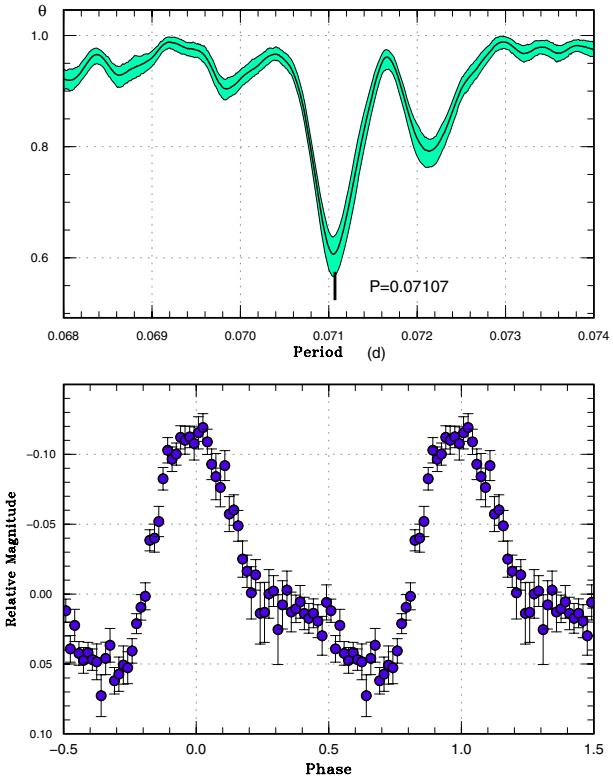

Fig. 85. Superhumps in TCP J231308 (2011). Upper: PDM analysis. Lower: Phase-averaged profile.

Table 86. Superhump maxima of TCP J231308 (2011).

E	Max*	Error	$O-C$†	N‡
0	55732.5371	0.0003	−0.0036	188
1	55732.6077	0.0002	−0.0041	212
14	55733.5369	0.0003	0.0015	91
15	55733.6066	0.0003	0.0001	59
19	55733.8916	0.0003	0.0009	94
23	55734.1796	0.0013	0.0047	176
24	55734.2488	0.0014	0.0029	118
28	55734.5318	0.0002	0.0017	78
29	55734.6024	0.0004	0.0013	50
51	55736.1610	0.0034	−0.0031	74
56	55736.5193	0.0003	−0.0001	45
57	55736.5888	0.0004	−0.0017	44
71	55737.5845	0.0003	−0.0006	176
85	55738.5799	0.0003	0.0001	199

* BJD − 2400000.
† Against max = 2455732.5407 + 0.071048E.
‡ Number of points used to determine the maximum.

5. Summary

We studied the characteristics of superhumps for 86 SU UMa-type dwarf novae whose superoutbursts were mainly observed during the 2011–2012 season. Most of the new data for systems with a short orbital period basically confirmed the earlier findings.

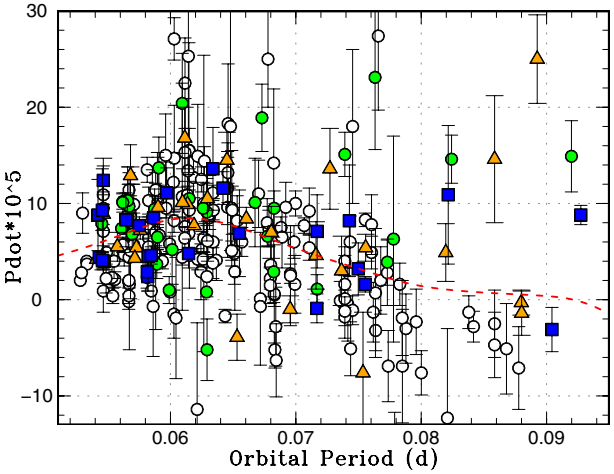

Fig. 86. $P_{\rm dot}$ during stage B versus $P_{\rm orb}$. Open circles, filled circles, filled triangles, and filled squares represent samples in Kato et al. (2009, 2010, 2012a) and this paper, respectively. The curve represents the spline-smoothed global trend.

Table 87. Superhump periods during stage A.

Object	Year	Period (d)	Error
SV Ari	2011	0.05575	0.00012
VW Hyi	2011	0.07770	0.00013
BW Scl	2011	0.05623	0.00012
PU UMa	2012	0.08382	—
SDSS J080303	2011	0.09540	0.00028
SDSS J170213	2011	0.10605	0.00011
OT J102842	2012	0.03844	0.00002
OT J184228	2011	0.07287	0.00008
OT J210950	2011	0.06087	0.00006
OT J214738	2011	0.09928	0.00022

Among WZ Sge-type dwarf novae, BW Scl showed an $O-C$ variation similar to other WZ Sge-type dwarf novae, such as V455 And and GW Lib, and this pattern of period variation appears to be common among WZ Sge-type dwarf novae with the shortest orbital periods. The WZ Sge-type object OT J184228.1+483742 showed an unusual pattern of double outbursts composed of an outburst with early superhumps and another with ordinary superhumps, separated by a temporary fading. We propose an interpretation that a very small growth rate of the 3:1 resonance due to an extremely low mass-ratio led to quenching the superoutburst before ordinary superhumps appeared. We suspect that this object is a likely candidate for a period bouncer.

We studied VW Hyi during its superoutburst in 2011 November–December and two subsequent normal outbursts. We confirmed the presence of "traditional" late superhumps with an $\sim$0.5 phase shift. These late superhumps persisted until the next second normal outburst. The behavior was very similar to the results obtained from Kepler observations of V344 Lyr, and it is likely that these late superhumps

Table 88. Parameters of WZ Sge-type superoutbursts.

Object	Year	$P_{\rm SH}$	$P_{\rm orb}$	$P_{\rm dot}$*	Error*	ϵ	Type†	$N_{\rm reb}$‡	Delay§	Max	Min
SV Ari	2011	0.055524	—	4.0	0.2	—	D	0	—	]15.0‖	22.1
PR Her	2011	0.055022	0.05422	8.8	3.7	0.015	—	—	13	12.8	21.0
BW Scl	2011	0.055000	0.054323	4.4	0.3	0.012	D	0	10	9.0	16.4
SDSS J220553	2011	0.058151	0.05752	7.7	0.9	0.011	—	—	—	]14.4	20.1
OT J001952	2012	0.056770	—	—	—	—	—	—	—	]15.6	21.5:
OT J055721	2011	0.059756	—	4.6	0.9	—	C	1	—	]14.7	21.0:
OT J184228	2011	0.072342	0.07168	−0.9	1.5	0.009	B	]2	]29	]11.8	20.6
OT J210950	2011	0.060045	0.05865	8.5	0.6	0.024	D	0	]6	]11.5	18.7

* In units of 10^{-5}.
† A, long-lasting rebrightening; B, multiple rebegitehnings; C, single rebrightening; D, no rebrightening.
‡ Number of rebrightenings.
§ Number of days before ordinary superhumps appeared.
‖ "]" represents the lower limit.

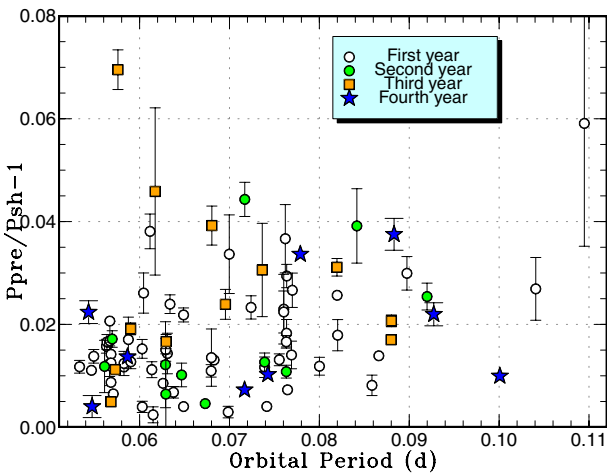

Fig. 87. Superhump periods during stage A. Superhumps in this stage have a period of typically 1.0%–1.5% longer than that during stage B. There is a slight tendency of increasing fractional period excess for longer-$P_{\rm orb}$ systems. The symbols for the first, second, third and fourth years represent data in Kato et al. (2009, 2010, 2012a) and this paper.

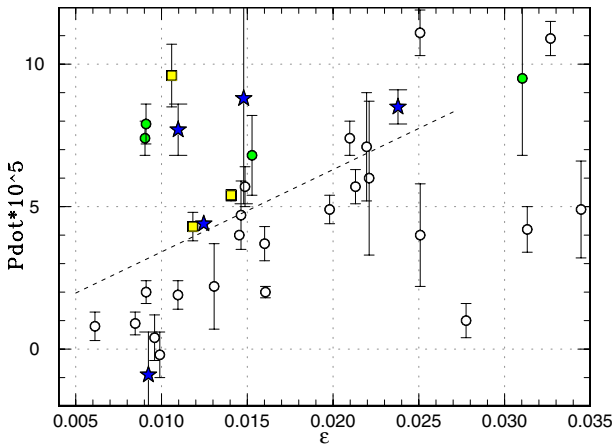

Fig. 88. $P_{\rm dot}$ versus ϵ for WZ Sge-type dwarf novae. Open circles, filled circles, filled squares and filled stars represent outbursts reported in Kato et al. (2009, 2010, 2012a) and this paper, respectively. The dashed line represents a linear regression for points with $\epsilon < 0.026$ as shown in figure 35 of Kato et al. (2009).

seem to be common among relatively long-$P_{\rm orb}$ and high mass-transfer systems.

We extended our research to the analysis of positive and negative superhumps in ER UMa-type dwarf novae, and found that the current V1159 Ori shows positive superhumps similar to ER UMa in the 1990s. In two extreme ER UMa stars (DI UMa and RZ LMi), there is an indication of positive period derivatives. We identified likely orbital periods for these objects, and both objects are likely to have a small mass-ratio. The recently identified ER UMa-type object BK Lyn has been in a dwarf nova-type state at least since 2005, and its current variation is dominated by negative superhumps, as observed in ER UMa, at least since 2011.

We further examined superhumps in AM CVn-type objects, and for the first time established the pattern of period variations to be very similar to short-period hydrogen-rich SU UMa-type dwarf novae; these objects are indeed a helium analogue of hydrogen-rich SU UMa-type dwarf novae.

We also studied a peculiar object, SBS 1108+574, a hydrogen-rich dwarf nova below the period minimum, which showed a very similar period variation to those of short-period SU UMa-type dwarf novae. We detected a likely orbital period in this system, and estimated the mass-ratio to be $q = 0.06$. This finding suggests that this secondary is a somewhat evolved star whose hydrogen envelope was mostly stripped during the mass-exchange.

We identified a new group of SU UMa-type dwarf novae (CC Scl, MASTER J072948, and OT J173516.9+154708) with low-amplitude superhumps having complex profiles. The complex profile in CC Scl is likely to be a result of the combination of orbital humps and positive superhumps. In the cases of MASTER J072948 and OT J173516.9+154708, their complex profiles are less clear, and their second signals may be negative superhumps.

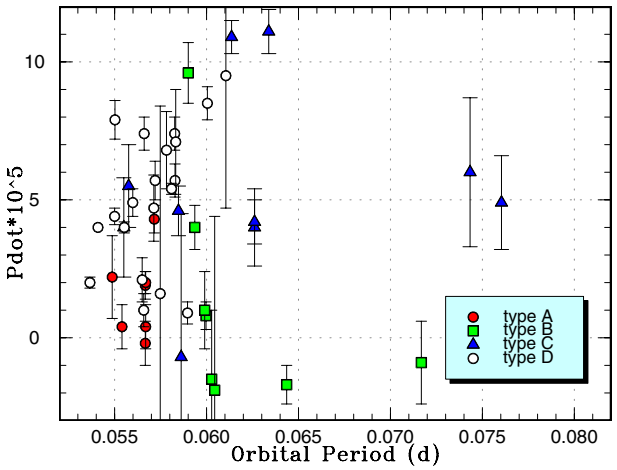

Fig. 89. $P_{\rm dot}$ versus $P_{\rm orb}$ for WZ Sge-type dwarf novae. Symbols represent the type (cf. Kato et al. 2009) of outbursts: type-A (filled circles), type-B (filled squares), type-C (filled triangles), and type-D (open circles).

Table 89. List of ER UMa-type stars.

Object	$P_{\rm orb}$ (d)	$P_{\rm SH}$ (d)*	State†
ER UMa (1995–2008)	0.06366	0.0657	+
ER UMa (2011–)		0.06226	−
V1159 Ori	0.062178	0.0643	+
RZ LMi	(0.059053)	0.05944	+
DI UMa	0.054567	0.05531	+
IX Dra	—	0.06697	+
BK Lyn (2005–)	0.07498	0.07279	−

* The period of dominant periodicty is given.
† Positive (+) and negative (−) superhumps.

This work was supported by a Grant-in-Aid for the Global COE Program, "The Next Generation of Physics, Spun from Universality and Emergence", from the Ministry of Education, Culture, Sports, Science and Technology (MEXT) of Japan. The authors are grateful to observers of the VSNET Collaboration and VSOLJ observers, who supplied vital data. We acknowledge with thanks the variable-star observations from the AAVSO International Database, contributed by observers worldwide and used in this research. This work is deeply indebted to outburst detections and announcements by a number of variable-star observers worldwide, including participants of CVNET, BAA VSS alert, and AVSON networks. We are grateful to the Catalina Real-time Transient Survey team for making their real-time detection of transient objects available to the public.

Appendix. MCMC Analysis of Eclipses

The KW method is widely used to determine the mid-eclipse time of eclipsing binaries. Although this method is useful for densely sampled light curves, it is difficult to determine the period of eclipsing binaries with a sparse number of samples.

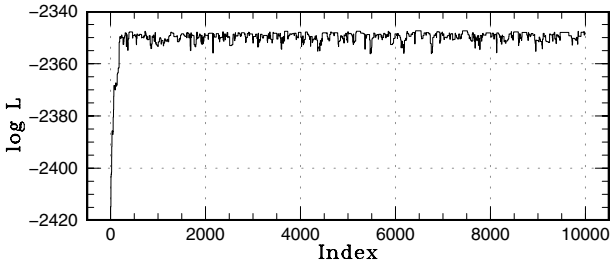

Fig. 90. MCMC analysis of TCP J084616. Behavior of the likelihood function.

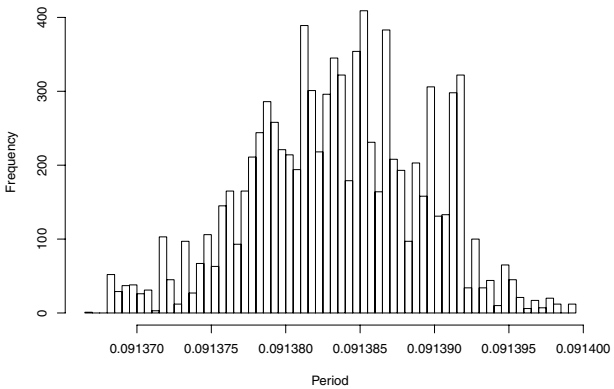

Fig. 91. Posterior probablistic function of the period of TCP J084616.

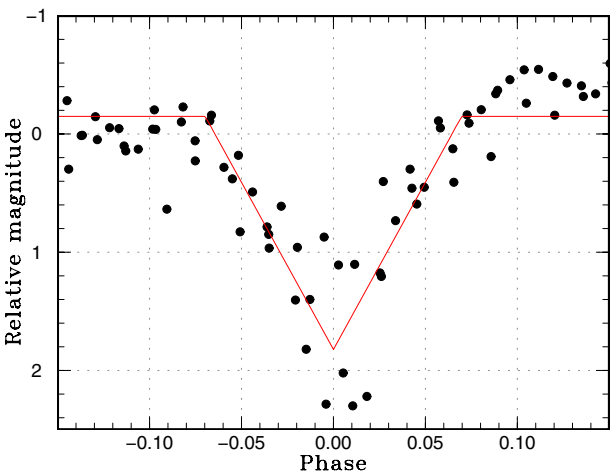

Fig. 92. Best-fit model for TCP J084616. Points are observations and the line is the model.

This is particularly applicable to the case of TCP J084616, in which each eclipse was observed with low time-resolution and with a large photometric error, due to the faintness of the object. In such cases, a usual approach to measuring the mid-eclipse times by the KW method, and then making a linear regression, does not lead to good results. We solved this problem by extending the application of the MCMC analysis introduced in Kato et al. (2010).

In this problem, $D = \{y_{\rm obs}(t_i)\}$ is the observed magnitude (corrected for trends if necessary) for the epoch $\{t_i\}$. The parameter space is $\theta = \{P, E_0, a, b, c\}$, defined by the model ($y_{\rm model}$):

$$\begin{aligned} \phi_i &= (1/2) - |(t_i - E_0)/P \bmod 1 - (1/2)| \\ y_{\rm model}(\phi_i) &= b + c(a - \phi_i) \qquad (\phi_i < a), \\ y_{\rm model}(\phi_i) &= b \qquad\qquad\quad (\phi_i \geq a), \end{aligned} \tag{A1}$$

where P and E_0 are the period and the epoch, respectively, and mod1 means the fractional part. The other parameters define the shape of the light curve. Assuming that $\epsilon_i = y_{\rm obs}(t_i) - y_{\rm model}(t_i)$ follows a normal distribution, $N(0, \sigma_i^2)$, the likelihood function can be written as

$$\mathcal{L}(\theta) = \prod_i \frac{1}{\sqrt{2\pi\sigma_i^2}} \exp\left[-\frac{\{y_{\rm obs}(t_i) - y_{\rm model}(t_i)\}^2}{2\sigma_i^2}\right]; \tag{A2}$$

the MCMC algorithm is then applied to this $\mathcal{L}(\theta)$. A sample of results is shown in figures 90, 91, and 92. We used the resultant P and E_0 in subsection 3.85. This method is also applicable to the usual determination of the minima of eclipsing binaries by appropriately defining the shape of the light curve. This method is more effective than the classical KW method owing to its plain formulation, robustness of the solution for noisy data, and easy incorporation of errors in individual measurements.

References

Abbott, T. M. C., Fleming, T. A., & Pasquini, L. 1997, A&A, 318, 134
Augusteijn, T., van der Hooft, F., de Jong, J. A., & van Paradijs, J. 1996, A&A, 311, 889
Augusteijn, T., van Kerkwijk, M. H., & van Paradijs, J. 1993, A&A, 267, L55
Augusteijn, T., & Wisotzki, L. 1997, A&A, 324, L57
Balanutsa, P., et al. 2012a, Astron. Telegram, 4022
Balanutsa, P., et al. 2012b, Astron. Telegram, 4084
Balanutsa, P., et al. 2012c, Astron. Telegram, 3935
Baraffe, I., Chabrier, G., Barman, T. S., Allard, F., & Hauschildt, P. H. 2003, A&A, 402, 701
Boyd, D., Oksanen, A., & Henden, A. 2006, J. Br. Astron. Assoc., 116, 187
Breedt, E., Gänsicke, B. T., Marsh, T. R., Steeghs, D., Drake, A. J., & Copperwheat, C. M. 2012, MNRAS, 425, 2548
Cannizzo, J. K., Smale, A. P., Wood, M. A., Still, M. D., & Howell, S. B. 2012, ApJ, 747, 117
Cannizzo, J. K., Still, M. D., Howell, S. B., Wood, M. A., & Smale, A. P. 2010, ApJ, 725, 1393
Chabrier, G., & Baraffe, I. 1997, A&A, 327, 1039
Chen, A., O'Donoghue, D., Stobie, R. S., Kilkenny, D., & Warner, B. 2001, MNRAS, 325, 89
Denisenko, D. V., & Sokolovsky, K. V. 2011, Astron. Lett., 37, 91
Dillon, M., et al. 2008, MNRAS, 386, 1568
Duerbeck, H. W. 1987, Space Sci. Rev., 45, 1
Gao, W., Li, Z., Wu, X., Zhang, Z., & Li, Y. 1999, ApJ, 527, L55
Garnavich, P., Littlefield, C., Marion, G. H., Irwin, J., Kirshner, R. P., & Vinko, J. 2012, Astron. Telegram, 4112
Gessner, H. 1966, Veröff. Sternw. Sonneberg, 7, 61
Hambsch, F.-J. 2012, J. Am. Assoc. Variable Star Obs., 40, 1003
Harvey, D., Skillman, D. R., Patterson, J., & Ringwald, F. A. 1995, PASP, 107, 551
Hessman, F. V., & Hopp, U. 1990, A&A, 228, 387
Hessman, F. V., Mantel, K.-H., Barwig, H., & Schoembs, R. 1992, A&A, 263, 147
Hoffmeister, C. 1949, Astron. Abh. Ergänzungshefte Astron. Nachr., 12, 12
Hoffmeister, C. 1951, Astron. Abh. Ergänzungshefte Astron. Nachr., 12, 14
Hoffmeister, C. 1968, Astron. Nachr., 290, 277
Howell, S. B., Schmidt, R., DeYoung, J. A., Fried, R., Schmeer, P., & Gritz, L. 1993, PASP, 105, 579
Imada, A., et al. 2006, PASJ, 58, 143
Imada, A., et al. 2008b, PASJ, 60, 1151
Imada, A., et al. 2009, PASJ, 61, 535
Imada, A., Kato, T., Monard, L. A. G. B., Stubbings, R., Uemura, M., Ishioka, R., & Nogami, D. 2008a, PASJ, 60, 267
Ishioka, R., et al. 2002, PASJ, 54, 581
Ishioka, R., Kato, T., Matsumoto, K., Uemura, M., Iwamatsu, H., & Stubbings, R. 2001a, IBVS, 5023
Ishioka, R., Kato, T., Uemura, M., Iwamatsu, H., Matsumoto, K., Martin, B. E., Billings, G. W., & Novak, R. 2001b, PASJ, 53, L51
Ishioka, R., Sekiguchi, K., & Maehara, H. 2007, PASJ, 59, 929
Kato, T. 2001, PASJ, 53, L17
Kato, T. 2002a, PASJ, 54, L11
Kato, T. 2002b, PASJ, 54, 87
Kato, T., et al. 2009, PASJ, 61, S395
Kato, T., et al. 2010, PASJ, 62, 1525
Kato, T., et al. 2012a, PASJ, 64, 21
Kato, T., Hanson, G., Poyner, G., Muyllaert, E., Reszelski, M., & Dubovsky, P. A. 2000a, IBVS, 4932
Kato, T., Ishioka, R., & Uemura, M. 2002, PASJ, 54, 1029
Kato, T., & Kunjaya, C. 1995, PASJ, 47, 163
Kato, T., Maehara, H., & Uemura, M. 2012b, PASJ, 64, 63
Kato, T., Nogami, D., Baba, H., Hanson, G., & Poyner, G. 2000b, MNRAS, 315, 140
Kato, T., Nogami, D., Baba, H., Matsumoto, K., Arimoto, J., Tanabe, K., & Ishikawa, K. 1996a, PASJ, 48, L21
Kato, T., Nogami, D., & Masuda, S. 1996b, PASJ, 48, L5
Kato, T., Nogami, D., & Masuda, S. 2003a, PASJ, 55, L7
Kato, T., Nogami, D., Moilanen, M., & Yamaoka, H. 2003b, PASJ, 55, 989
Kato, T., Stubbings, R., Monard, B., Butterworth, N. D., Bolt, G., & Richards, T. 2004a, PASJ, 56, S89
Kato, T., & Uemura, M. 2012, 64, 122
Kato, T., Uemura, M., Ishioka, R., Nogami, D., Kunjaya, C., Baba, H., & Yamaoka, H. 2004b, PASJ, 56, S1
Kemp, J., et al. 2012, in Proc. 31st Annu. Conf., Symp. on Telescope Science, ed. B. D. Warner et al. (Rancho Cucamonga, CA: Society for Astronomical Sciences), 7
Kjurkchieva, D., & Marchev, D. 2010, Publ. Astron. Obs. Belgr., 90, 147
Kotko, I., Lasota, J.-P., Dubus, G., & Hameury, J.-M. 2012, A&A, 544, A13
Kwee, K. K., & van Woerden, H. 1956, Bull. Astron. Inst. Netherlands, 12, 327
Levitan, D., et al. 2011, ApJ, 739, 68

Littlefair, S. P., Dhillon, V. S., Marsh, T. R., & Gänsicke, B. T. 2006, MNRAS, 371, 1435
Markarian, B. E., & Stepanian, D. A. 1983, Astrofizika, 19, 639
Mennickent, R. E., Patterson, J., O'Donoghue, D., Unda, E., Harvey, D., Vanmuster, T., & Bolt, G. 1998, Ap&SS, 262, 1
Nakano, S., Nishimura, H., Noguchi, T., & Munari, U. 2011, Cent. Bur. Electron. Telegrams, 2818
Nogami, D., Kato, T., Masuda, S., & Hirata, R. 1995, IBVS, 4155
Nogami, D., Monard, B., Retter, A., Liu, A., Uemura, M., Ishioka, R., Imada, A., & Kato, T. 2004, PASJ, 56, L39
Ohshima, T., et al. 2010, PASJ submitted
Ohshima, T., et al. 2012, PASJ, 64, L3
Olech, A. 1997, Acta Astron., 47, 281
Olech, A., Mularczyk, K., Kędzierski, P., Złoczewski, K., Wiśniewski, M., & Szaruga, K. 2006, A&A, 452, 933
Olech, A., Wisniewski, M., Zloczewski, K., Cook, L. M., Mularczyk, K., & Kedzierski, P. 2008, Acta Astron., 58, 131
Olech, A., Zloczewski, K., Mularczyk, K., Kedzierski, P., Wisniewski, M., & Stachowski, G. 2004, Acta Astron., 54, 57
Pastukhova, E. N. 1988, Astron. Tsirk., 1534, 17
Patterson, J., et al. 1997, PASP, 109, 1100
Patterson, J., Jablonski, F., Koen, C., O'Donoghue, D., & Skillman, D. R. 1995, PASP, 107, 1183
Pavlenko, E., et al. 2010a, in AIP Conf. Proc., 1273, 17th European White Dwarf Workshop, ed. K. Werner & T. Rauch (Maryland: AIP), 320
Pavlenko, E., Kato, T., Pit, N., Baklanov, A., Antonyuk, K., & Stein, W. 2012a, Astron. Telegram, 3889
Pavlenko, E. P., et al. 2010b, Astron. Rep., 54, 6
Pavlenko, E. P., Samsonov, D. A., Antonyuk, O. I., Andreev, M. V., Baklanov, A. V., & Sosnovskij, A. A. 2012b, Astrophysics, 55, 494
Pojmański, G. 2002, Acta Astron., 52, 397
Provencal, J. L., et al. 1997, ApJ, 480, 383
Ramsay, G., Barclay, T., Steeghs, D., Wheatley, P. J., Hakala, P., Kotko, I., & Rosen, S. 2012, MNRAS, 419, 2836
Ramsay, G., Napiwotzki, R., Hakala, P., Potter, S., & Cropper, M. 2011, MNRAS, 417, 400
Rau, A., Roelofs, G. H. A., Groot, P. J., Marsh, T. R., Nelemans, G., Steeghs, D., Salvato, M., & Kasliwal, M. M. 2010, ApJ, 708, 456
Richards, G. T., et al. 2009, ApJS, 180, 67
Richter, G. A. 1990, Mitt. Veränderl. Sterne, 12, 59
Ringwald, F. A., Thorstensen, J. R., Honeycutt, R. K., & Robertson, J. W. 1996, MNRAS, 278, 125
Robertson, J. W., Honeycutt, R. K., Hillwig, T., & Jurcevic, J. 1998, in ASP Conf. Ser., 137, Wild Stars in the Old West, ed. S. Howell et al. (San Francisco: ASP), 469
Robertson, J. W., Honeycutt, R. K., Hillwig, T., Jurcevic, J. S., & Henden, A. A. 2000, AJ, 119, 1365
Robertson, J. W., Honeycutt, R. K., & Turner, G. W. 1995, PASP, 107, 443
Rutkowski, A., Olech, A., Wiśniewski, M., Pietrukowicz, P., Pala, J., & Poleski, R. 2009, A&A, 497, 437
Schoembs, R., & Vogt, N. 1980, A&A, 91, 25
Schreiber, M. R., Hameury, J.-M., & Lasota, J.-P. 2004, A&A, 427, 621
Schwope, A. D., et al. 2000, Astron. Nachr., 321, 1
Shears, J., et al. 2012b, J. Br. Astron. Assoc. in press (arXiv:1205.0898)
Shears, J., Hambsch, F.-J., Littlefield, C., Miller, I., Morelle, E., Pickard, R., Pietz, J., & Sabo, R. 2012a, J. Br. Astron. Assoc. in press (arXiv:1209.4062)
Skillman, D. R., & Patterson, J. 1993, ApJ, 417, 298
Sokolovsky, K. V., Baryshev, K. O., & Korotkiy, S. A. 2012, Astron. Telegram, 3849
Solheim, J.-E. 2010, PASP, 122, 1133
Southworth, J., et al. 2008, MNRAS, 391, 591
Southworth, J., Marsh, T. R., Gänsicke, B. T., Aungwerojwit, A., Hakala, P., de Martino, D., & Lehto, H. 2007, MNRAS, 382, 1145
Stellingwerf, R. F. 1978, ApJ, 224, 953
Szkody, P., et al. 2003, AJ, 126, 1499
Szkody, P., et al. 2005, AJ, 129, 2386
Szkody, P., et al. 2006, AJ, 131, 973
Szkody, P., et al. 2007, ApJ, 658, 1188
Tappert, C., Augusteijn, T., & Maza, J. 2004, MNRAS, 354, 321
Thorstensen, J. R., Fenton, W. H., Patterson, J. O., Kemp, J., Krajci, T., & Baraffe, I. 2002a, ApJ, 567, L49
Thorstensen, J. R., Patterson, J. O., Kemp, J., & Vennes, S. 2002b, PASP, 114, 1108
Thorstensen, J. R., Patterson, J. O., Shambrook, A., & Thomas, G. 1996, PASP, 108, 73
Thorstensen, J. R., & Skinner, J. N. 2012, AJ, 144, 81
Thorstensen, J. R., Taylor, C. J., Becker, C. M., & Remillard, R. A. 1997, PASP, 109, 477
Tiurina, N., et al. 2012, Astron. Telegram, 3845
Tsugawa, M., & Osaki, Y. 1997, PASJ, 49, 75
Uemura, M., et al. 2002, PASJ, 54, L15
Uemura, M., et al. 2005, A&A, 432, 261
Uemura, M., Kato, T., Pavlenko, E., Baklanov, A., & Pietz, J. 2001, PASJ, 53, 539
Unda-Sanzana, E., et al. 2008, MNRAS, 388, 889
Uthas, H., et al. 2012, MNRAS, 420, 379
Vogt, N. 1983, A&A, 118, 95
Warner, B. 1995, Cataclysmic Variable Stars (Cambridge: Cambridge University Press)
Warner, B., & Woudt, P. A. 2004, in ASP Conf. Ser., 310, IAU Colloq. 193, Variable Stars in the Local Group, ed. D. W. Kurtz & K. R. Pollard (San Francisco: ASP), 382
Wils, P., Gänsicke, B. T., Drake, A. J., & Southworth, J. 2010, MNRAS, 402, 436
Wolf, M., & Wolf, G. 1905, Astron. Nachr., 169, 415
Wood, M. A., Still, M. D., Howell, S. B., Cannizzo, J. K., & Smale, A. P. 2011, ApJ, 741, 105
Woudt, P. A., et al. 2012, MNRAS, 427, 1004
Yamaoka, H., et al. 2011, Cent. Bur. Electron. Telegrams, 2731, 1